Westfälische Wilhelms-Universität Münster

Zentrum für Molekularbiologie der Entzündung

Institut für Infektiologie

"In vivtro" - a 3D cell culture system to analyze the impact of probiotic *E.coli* Nissle 1917 on epithelial cells

Inaugural-Dissertation
zur Erlangung des Doktorgrades der Naturwissenschaften
im Fachbereich Biologie
der Mathematisch-Naturwissenschaftlichen Fakultät
der Westfälischen Wilhelms-Universität Münster

vorgelegt von

Jessyca González

aus Venezuela

- 2020 -

Dekanin/Dekan:	Prof. Dr. Susanne Fetzner
Erster Gutachter:	Prof. Dr. Ulrich Dobrindt
Zweite Gutachterin:	Prof. Dr. Eva Liebau
Tag der mündlichen Prüfung:	02.07.2020
Tag der Promotion:	.....

Table of contents

List of Figures

List of Tables

Abbreviations

2D	Two-dimensional
2.5D	Cells cultured on Transwell filters
3D	Three-dimensional
A/E	Attaching and effacing phenotype
AD	Adherent junctions
AF-6	Afadin-6
Akt	Protein kinase B
AMPs	Antimicrobial proteins
APS	Ammonium persulfate
ATP	Adenosine triphosphate
BSA	Bovine serum albumin
CD	Crohn's disease
cDNA	Complementary DNA
CLRs	C-type lectin receptors
Ct	Cycle threshold
DCs	Dendritic cells
DD	Death domain
DMEM	Dulbecco´s Modified Eagle Medium
DMSO	Dimethylsulfoxide
DNA	Deoxyribonucleic acid
D-PBS	Dulbecco´s Phosphate-Buffered Saline
DSS	Dextran sodium sulfate
ECL	Enhanced chemiluminescent
EcN	*E. coli* Nissle
EDTA	Ethylenediaminetetraacetic acid
EPEC	Enteropathogenic *E. coli*
ER	Endoplasmatic reticulum
ERK	Extracellular signal-regulated kinase

et al.	Et alii
etc.	Et cetera
FCS	Fetal calf serum
GALT	Gut-Associated Lymphoid Tissue
GAM	Goat anti-mouse
GAR	Goat anti-rabbit
GIT	Gastrointestinal tract
hBD-2	Human β-defensin 2
Hpi	Hours post-incubation
HPRT	Horseradish peroxidase
IBD	Inflammatory Bowel disease
ICAM-1	Intercellular adhesion molecule 1
IECs	Intestinal epithelial cells
IgA	Secretory immunoglobulin A
IgG (H+L)	Immunoglobulin G (heavy + light chains)
IKK	IκB kinase
IL	Interleukin
ILF	Isolated lymphoid follicles
IP-10	Interferon gamma-induced protein 10
IRAK	Interleukin-1 receptor-associated kinases
"*in vivtro*"	A model between *in vitro* and *in vivo*
JAM-A	Junctional Adhesion Molecule A
JAMs	Junctional Adhesion Molecules
JNK	c-Jun N-terminal kinase
kDa	Kilodalton
LB	Lysogeny broth
LEE	Locus of enterocyte effacement
LPS	Lipopolysaccharide
LRRs	Leucine-reach repeats
M cells	Microfold cells
MAMPs	Microbe-associated molecular patterns

MAPKs	Mitogen-activated protein kinase
MCP-1	Monocyte chemoattractant protein 1
miRNA	microRNAs
MLN	Mesenteric lymph node
MOI	Multiplicity of infection
mRNA	Messenger RNA
MUC	Mucin
MV	Microvilli
MyD88	Myeloid differentiation primary response
NASA	National Aeronautics and Space Administration
NF-κB	Nuclear factor kappa-light-chain-enhancer of activated B cells
NLRs	NOD-like receptors
NOD	Nucleotide oligomerization domain
OD	Optical density
OMVs	Outer membrane vesicles
PAI	Pathogenicity island
PAMPs	Pathogens-associated molecular patterns
PARD3	Partitioning defective 3 homologous
PBS	Phosphate buffered saline
PKCζ	Protein kinase C-*ζ*
PP	Peyer´s Patches
PRRS	Patterns recognition receptors
PVDF	Polyvinylidene difluoride
qRT-PCR	Quantitative Real-Time PCR
RLRs	RIG-I-like receptors
RNA	Ribonucleic acid
RWV	Rotating Wall Vessel bioreactor
SDS	Sodium dodecyl sulfate
SDS-PAGE	Sodium dodecyl sulfate-polyacrylamide gel
SEM	Standard error of the mean
T3SS	Type Three Secretion System

TBST	Tris-buffered saline and Tween 20
TCA	Trichloroacetic acid
TEM	Transmission electron microscopy
TEMED	N,N,N',N'-tetramethylethylenediamine
TIR	Toll/IL-1 receptor
TJs	Tight junctions
TLRs	Toll-like receptors
TNF	Tumor necrosis factor
UC	Ulcerative colitis
ZO-1	Zonula occludens 1

CHAPTER 1

ABSTRACT

Infectious diseases are a major cause of death worldwide. The increase in antibiotic resistance represents a significant threat in the context of global health, provoking an urgent need for the development of novel or more sophisticated therapeutic strategies (e.g., preventive probiotics). For decades, infectious diseases have been studied *in vitro* by the use of the two-dimensional (2D) cell culture system that has facilitated important discoveries of mechanisms underlying bacterial-host interactions. However, in the last decade there has been a shift from the "flat biology" to advanced three-dimensional (3D) cell culture methods of intestinal epithelia, closely mimicking the human *in vivo* microenvironment, which allows host-microbe crosstalk in a more physiological manner. The 3D cell culture system offers more precise "*in vivtro*" tools for the analysis of cellular response to bacterial infection. Thus, advanced cell culture models provide the possibility to elucidate the underlying mechanisms of the intricate crosstalk between the host´s immune system and probiotic bacteria more precisely, and to improve therapeutical treatment for gut inflammations.

E. coli Nissle (EcN) 1917 is the most commonly used Gram-negative probiotic. Since its discovery, many scientific studies have reported the probiotic effects of this strain in numerous clinical trials. On the one hand, EcN (serotype O6:K5:H1) lacks a pathogenicity island that encodes for a Type Three Secretion System (T3SS), which transmits effector proteins into the host cell to manipulate signaling pathways to its advantage. On the other hand, EcN has genes coding for fitness factors that are essential for the probiotic nature of EcN. Significant efforts have been made to investigate the influence of the probiotic EcN in the human gut. Hence, understanding the mechanisms by which EcN operates should continue to extend the full use of the potential of EcN or to improve its efficacy.

Colonic HT29, HT29-MTX-E12 and LS174T cell lines were used to compare molecular and cellular responses of intestinal epithelial cells incubated with variants of the probiotic EcN and the enteropathogenic EPEC strain E2348/69. Transwell filters, denoted as the "2.5D" cell culture system, were employed to grow polarized epithelial cells, but the cells do not mimic a complex mucosal surface. Therefore, the Rotating Wall Vessel (RWV) bioreactor (the 3D cell culture system) was also employed to study cellular and molecular crosstalk of host and microbes. The RWV bioreactor offers dynamic culture conditions for epithelial cells, such as low-fluid shear stress influencing gene regulation and cellular differentiation of cells growing on porous microcarrier beads. In the first part of this study, we focused on the impact of different EcN variants on epithelial cells, focusing on the barrier function, and on the immune response. The EPEC strain E2348/69 was also employed to compare differences in host

responses between probiotic and pathogenic bacteria. Incubation experiments were done under static and rotating or dynamic conditions. The expression and distribution of the tight junctional protein Junctional Adhesion Molecule A (JAM-A), after incubation of HT29-MTX-E12 cells with the different *E. coli* strains, were analyzed by qRT-PCR and immunofluorescence, respectively. We found that the expression of *JAM-A* differs between the 2D and 3D cell culture systems, and its expression is higher under rotating conditions.

The probiotic strain EcN restored the epithelial barrier function after damage by EPEC strain E2348/69. This pathogen did not produce "attaching-and-effacing (A/E)" lesions in the mucin-secreting HT29-MTX-E12 cell line, however, it did produce these lesions in the non-mucin-secreting HT29 cells. This indicates that the mucin layer has a potent microbe-disarming activity, and it should be considered when studying host-microbe interactions. The cellular immune response was also analyzed employing RT^2 Profiler arrays analyses. The immune response is different between static and rotating incubation conditions. EcN caused a transcriptional increase of genes encoding pro-inflammatory cytokines, like CXCL1 and CXCL2, and the expression of these cytokines was higher in the non-mucin-secreting HT29 cells in comparison to the HT29-MTX-E12 variant.

The second part of this study aimed to investigate outer membrane vesicles (OMVs) as another way to deliver bioactive components or pathogenicity factors. Epithelial cells incubated with probiotic and pathogenic OMVs or supernatants showed an increase in *JAM-A* expression and in the myeloid differentiation primary response (*MyD88*) expression. Probiotic OMVs and soluble factors present in the supernatants also induced the re-distribution of JAM-A to the cell boundaries after a moderate epithelial disruption caused by a pre-incubation with EPEC.

The present study contributes to the understanding of mechanisms governing host-microbe (probiotic) interactions, delivering more physiologically results about the signaling effect and mode of action of the probiotic EcN. Previous results from 2D cell culture experiments might not fully represent the correct *in vivo* situation. Therefore, employing cell culture models that better recapitulate the intestinal epithelia might pave the way for a more sophisticated application of probiotics and might promote the development of new or better strategies for controlling host immune responses.

CHAPTER 2

INTRODUCTION

2.1 The human gut microbiota

The human body is colonized by a vast number of microbes. To that extent, approximately 10^{13} microbial cells are present in the body and their total mass is about 0.2 kg (Sender *et al*., 2016). Especially, the human gastrointestinal tract (GIT) harbors a dense, diverse, complex, and dynamic bacterial ecosystem that influences the host homeostasis in various ways (DuPont *et al*. 2011). The microbiota offers many benefits to the host through a range of physiological functions contributing to metabolic activities, food digestion, also providing vitamins. It is involved in the absorption of nutrients and the protection of mucosal surfaces from pathogenic organisms and, furthermore, also modulates inflammation (DuPont *et al*. 2011).

The development of the microbiota starts from birth when the GIT is rapidly colonized. During the first years of life the microbial diversity increases, and the microbiota composition converges towards a distinct adult-like microbial profile. Although in adulthood, the gut microbiota is relatively stable, it is still subject to perturbations by life events such as illness, antibiotic treatment, and changes in diet all of which cause shifts in the microbiota composition (Thursby *et al*., 2017). The GIT of humans and other mammals have evolved complex mechanisms, which ensure a mutualistic relationship with the resident microbiota, and at the same time, retain the ability to trigger an immune response against pathogens (Round *et al*. 2009). Moreover, the crosstalk between the microbiota and the host at the GIT barrier results in the development of a precise GI organization and functionality (crypt-villus morphology, competent innate and acquired mucosal immune systems, epithelial renewal, barrier integrity, mucosal vascularisation, and innervation, etc.). Current understanding of these effects owes much to extensive studies of *in vivo* work employing a range of germ-free animal models, including among others, mostly mice and pigs. The small intestines of germ-free mice are characterized by reduced overall mass and surface area, thinner villi, shallower crypts with decreased cell proliferation, and reduced migration along the crypt-villus axis. This makes the intestine more susceptible to infection by certain bacteria (Figure 2.1). Similar studies with antibiotic-treated mice show antibiotic-related damage to the microbiota composition resulting in a reduction of cell proliferation. Here, crypts contain fewer cells than in conventional mice. The available evidence suggests that the presence of microbes not only promotes but is required for healthy epithelial development and turnover (Parker *et al*., 2018).

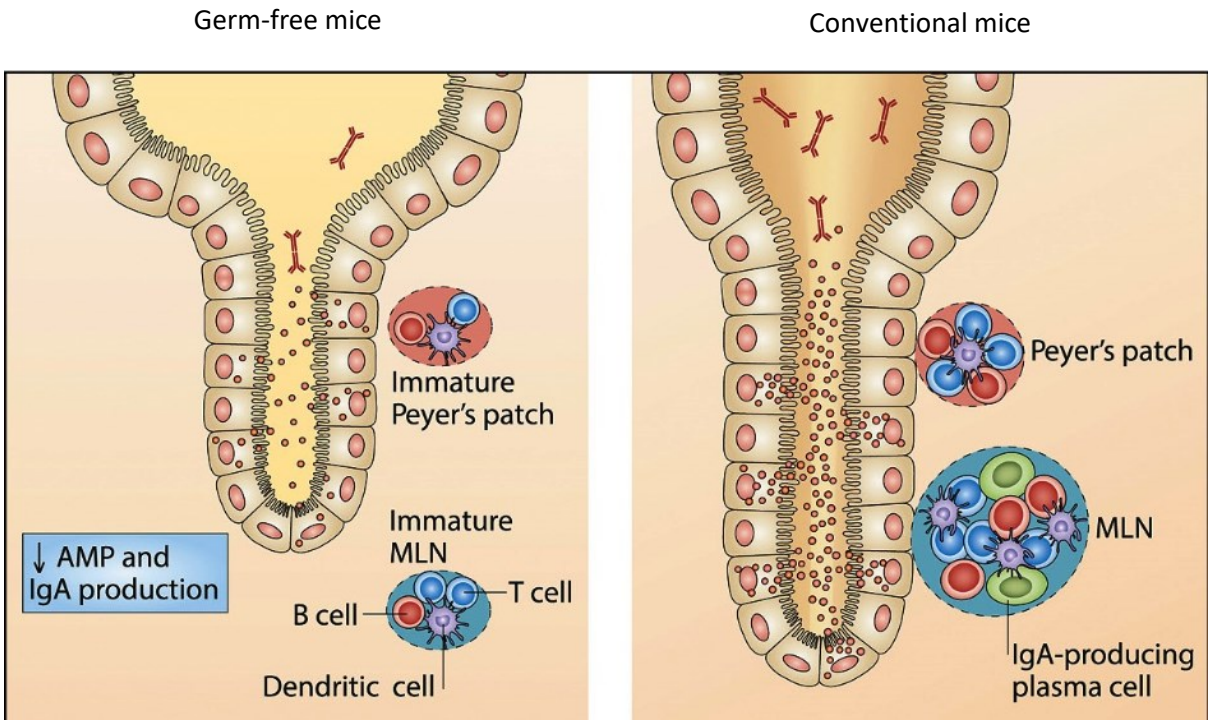

Figure 2.1. Differences in gut morphology between germ-free mice and conventional mice. The presence of the microbiota influences crypt-villus morphology, mucus composition, mucosal thickness, immune structure, and cell composition, receptor expression, and AMPs release. IgA: secretory immunoglobulin A, AMPs: antimicrobial peptides, MLN: mesenteric lymph node. Adapted from Sommer *et al*. (2013).

2.2 The biological barrier

2.2.1 The intestinal environment: structure and function

The gastrointestinal and respiratory tracts, as well as the skin, are the primary interfaces between the host and its external environment. The intestinal epithelium acts like a physical barrier separating the residential microflora and also incoming (pathogenic) microbes and other contents of the lumen from the underlying intestinal layers. The cells lining the intestine are arranged in only a single sheet of columnar intestinal epithelial cells (IECs), immersed in nutrients, commensal bacteria, immunoglobulins, and covered by mucus. IECs are also interconnected through tight junction (TJs) proteins, which are involved in the regulation of barrier permeability (Yu *et al*.,2012). The composition of this monolayer consists of absorptive enterocytes, mucus-producing goblet cells, hormone-producing enteroendocrine cells, and Paneth cells producing antimicrobial factors. This epithelial monolayer forms a barrier which is generally impermeable to commensal bacteria (Figure 2.2) (Moens *et al*., 2012). IECs are structurally polarized with an apical surface facing the lumen and a basolateral

surface facing the underlying lamina propria and immune cells. This polarity results in specific membrane proteins to be exclusively targeted to one or the other surface and kept apart by TJs (Abreu, 2010). IECs are also involved in immune processes, expressing various molecules implicated in antigen presentation and, furthermore, also coordinating interactions with other cells of the immune system (Peterson *et al.*, 2014).

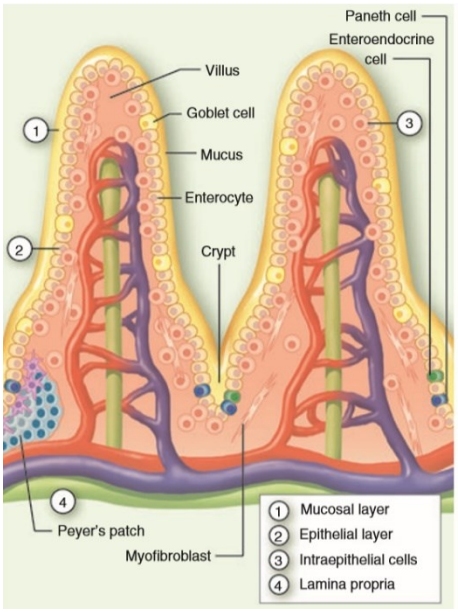

Figure 2.2. Structural organization of intestinal mucosa. (1) Mucosal layer and gradients of IgA and antimicrobial factors. **(2)** Epithelial cells made up of enterocytes, Paneth cells, goblet cells, and enteroendocrine cells. **(3)** Intraepithelial lymphocytes. **(4)** Lamina propria. In the last, secondary lymphoid structures, such as crypto patches and Peyer´s patches are present. Adapted from Moens *et al*. (2011).

2.2.2 The tight junctional complex

2.2.2.1 Junctional Adhesion Molecule A (JAM-A)

The junctional complex consists of at least 40 different proteins. Tight junctions are a part of the junctional complex consisting of adherent junctions, desmosomes, and the tight junctions itself. TJs restrict paracellular permeability, regulating the passage of a variety of molecules such as ions, water, and the entry of pathogens into the tissue to the lamina propria (Eichner *et al.*, 2017). They also play many interrelated roles in cell polarity, signaling, cell cycle, and vesicle trafficking (Fanning *et al.*, 2009). Three integral proteins build the TJs: occludin, claudins, and the JAM family. The former two constitute the backbone of TJs strands while JAMs play a role in the regulation of cell polarity, in the trafficking of T-lymphocytes, neutrophils, and dendritic cells from the lymphoid and vascular compartments to the

tissues during immune surveillance and inflammatory responses (González *et al*., 2003). The family of JAM proteins is composed of several Ig-like molecules: JAM-A, JAM-B, JAM-C, CAR, ESAM, and JAM4, all of them sharing similarities regarding their structural organization and amino acid sequences (Ebnet *et al*., 2004). Cordes *et al*. found an increase in JAM-A expression when T84 cells were incubated with the probiotic strain *E. coli* Nissle 1917 (Cordes *et al*.,2016). As JAM-A is the major protein in TJ development and barrier formation, which is regulated during bacterial infection or gastrointestinal inflammation, a central focus of the present study is the analysis of JAM-A (expression and distribution) in HT29-MTX-E12 cells when incubated with a pathogenic or probiotic bacteria.

JAM-A (approximately 37 kDa) consists of a single transmembrane domain and harbors an extracellular part with two Ig-like loops, a single membrane-spanning region, and a short cytoplasmatic tail ending in a PDZ-binding motif. This motif facilitates interactions with various scaffold proteins such as Zona occludens (ZO-1), Afadin-6 (AF-6), and Partitioning defective 3 homologous (PARD3). The PDZ-binding motif is critical in triggering a functional intracellular signaling cascade together with its dimerization. JAM-A is widely expressed in human tissues, predominantly in intracellular junctions of epithelial and endothelial cells (Figure 2.3), but also on the surface of leukocytes, lymphocytes, platelets, and erythrocytes. JAM-A controls cell-cell adhesion (aiding the formation of tight junctions), leukocyte migration, platelet activation, angiogenesis, and reovirus binding (Solimando *et al*., 2018).

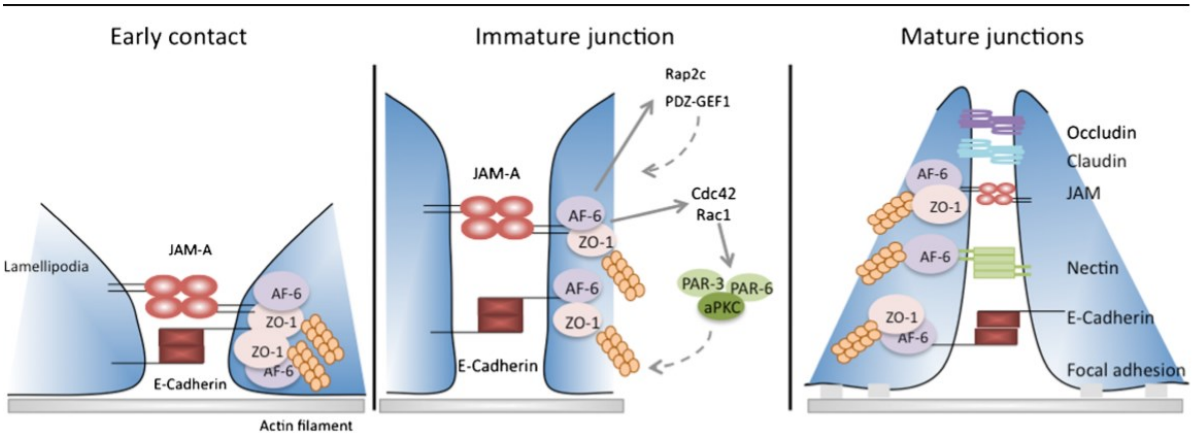

Figure 2.3. Role of JAM-A in cell polarization. JAM-A is present in the early stage of contact points between epithelial cells, along with E-cadherin. The interaction of JAM-A with ZO-1 and AF-6 allows its stabilization at the junction and, therefore, the linking to the actin cytoskeleton. Adapted from Garrido *et al*. (2014).

2.2.3 Mucus

Since trillions of microbes colonize the human body, a barrier is needed between these microbes and epithelial cells, which protects the epithelial surface but should not disrupt the normal host-microbe interactions. Mucus is a viscous substance and forms in the human body a biological hydrogel that covers every wet epithelial surface, including the lungs, eyes, and stomach. It constitutes the first line of defense in mammals and serves as a lubricant to protect epithelia against shear-induced damage from mechanical forces associated with processes such as digestion and blinking. Mucus works as a selective physicochemical barrier by excluding foreign or harmful molecules while allowing the passage of desirable compounds such as nutrients (Wagner *et al*., 2018).

Mucin is a glycoprotein that represents the primary structural component of mucus. So far, 21 mucin-type glycoproteins belonging to the *MUC* gene family have been identified. Within the mucin family, there are two distinct subgroups: **(a)** secreted mucins, which form a gel that resides outside the epithelial cell layer and **(b)** tethered, cell surface-associated mucins, that have short cytoplasmatic domains inside the cell, as well as extensive extracellular domains. Mucins are internally generated and secreted from goblet cells and mucous cells in submucosal glands throughout the epithelium. They form a complex network mediated by a series of reversible and irreversible interactions that drive mucus gel formation (Demouveaux *et al*., 2018). Native mucus is primarily composed of water (95%), mucins, salts, lipids, and proteins involved in defense, such as immunoglobulins (Wagner *et al*., 2018).

Mucus layers possess different mechanical and biochemical properties depending on their location: in the mouth, it lubricates the food and helps its transition to the stomach. In the stomach, it protects the epithelial cells against acidic gastric juices (pH ~ 1-2) during digestion. In the small intestine, a thinner semipermeable gel allows the passage of nutrients and prevents the entrance of pathogenic bacteria. In the colon, two layers of mucus are present: the outer looser layer being the ecological niche for gut bacteria and the inner layer, which is firmly attached and is impermeable to microorganisms (Demouveaux *et al*., 2018).

2.3 The immunity of the gut

The epithelial cells secrete an extensive panel of cytokines and chemokines, which attract neutrophils, macrophages, basophils, and T-cells to regulate the chemotaxis of immune cells (Chassaing *et al*., 2014). Beneath the intestinal epithelium lies a layer of mucosal tissue supporting the epithelium, known as the

lamina propria (LP). It is composed of stromal cells (mostly myofibroblasts) and immune cells, including B cells, macrophages, and dendritic cells (DCs) (Abreu, 2010).

The intestine is the primary site, which encounters foreign antigens. It is associated with several types of lymphoid organs summarized as the Gut-Associated Lymphoid Tissue (GALT). This includes Peyer´s Patches (PP) and the isolated lymphoid follicles (ILF) (Cerutti *et al*., 2011). The epithelium covering the PP contains another structurally distinct epithelial cell type, the microfold (M) cells. These cells are immune sentinels responsible for sampling intestinal microbiota and pathogens, and they pick up particles from the lumen and funnel them to the lymphoid tissues on their basolateral side. Another important component are Paneth cells. These cells have large apical defensin-rich secretory granules, which are released into epithelial crypts via exocytosis. Those granules have an important antimicrobial activity in response to various bacterial stimuli (Chassaing *et al.*, 2014).

The intact intestinal epithelial barrier does not allow the entry of commensal bacteria into the LP. This avoids excessive immune responses and ensures a balance between the gut environment and the host.

2.3.1 Host-microbe crosstalk

At the GIT interface, bacteria and their human hosts are in constant communication with each other. Various molecular signals mediate this dialogue, and its disruption is detrimental for both of them. Therefore, the epithelium employs multiple layers of regulation to ensure that this crosstalk does not go wrong. The cellular compartments comprise pathogen recognition receptors, which via complex signaling cascades coordinate the host´s immune responses and its protection against pathogens (Sabharwal, 2015). Pattern recognition receptors (PRRs) are expressed on immune and non-immune cells and are traditionally known to sense conserved pathogen-associated molecular patterns (PAMPs). However, the expression of PAMPs is not limited to pathogens but also common to the microbiota, therefore PAMPs are also referred to as microbe-associated molecular patterns (MAMPs). During normal colonization, host PRRs are exposed continuously to MAMPs, primarily provided by the resident microbiota, to promote host tissue and immune development (Chu *et al*., 2013).

Among the PRRs are Toll-like receptors (TLRs), nucleotide oligomerization domain (NOD)-like receptors (NLRs), RIG-I like receptors (RLRs), and C-type lectin receptors (CLRs) (Akira *et al*., 2004). In humans, the TLR family comprises ten members (TLR1-TLR10). They localize at the cell surface or intracellular compartments such as the endoplasmic reticulum (ER), endosomes, endolysosomes or

lysosome of dendritic cells, macrophages, as well as non-immune cells such as fibroblasts and epithelial cells. They recognize distinct or overlapping PAMPs like lipids, lipoproteins, proteins, and nucleic acid. Each TLR has an ectodomain with leucine-reach repeats (LRRs) that facilitate PAMP recognition, a transmembrane domain, and a cytoplasmic Toll/IL-1 receptor (TIR) domain that initiates downstream signaling (Kawasaki *et al*., 2014). In contrast, NLRs are localized in the cytosol and have a central nucleotide-binding and oligomerization (NOD) domain, flanked at the C-terminus by an LRR domain. They are predominantly expressed in tissues involved in immune functions (bone marrow, thymus, spleen, etc.) and in tissues that are in constant exposure to the external environment, for example, GIT and lungs (Werts *et al*., 2011).

TLR signaling regulation and its contributions to host defense have been studied intensively to understand many aspects of the innate immune responses to microbiota and given pathogens. TLRs are classified based on their location; cell surface TLRs include TLR1, TLR2, TLR4, TLR5, TLR6, and TLR10. Intracellular TLRs include TLR3, 7, 8, 9, 11, 12, and TLR13. TLR2, along with TLR1 or TLR6, recognizes lipoproteins, peptidoglycans, lipoteichoic acids, etc. TLR4 recognizes bacterial lipopolysaccharide (LPS). TLR5 recognizes bacterial flagellin, and TLR10 recognizes ligands from *Listeria* spp. and also senses influenza A virus infection in collaboration with TLR2. Intracellular TLRs recognize nucleic acid from bacteria and viruses and also its own nucleic acids under disease conditions like autoimmunity (Kawasaki *et al*., 2014).

TLRs recruit members of a set of TIR domain-containing adaptors such as myeloid differentiation primary response (MyD88), TRIF, TIRAP/MAL, or TRAM. MyD88 is a central regulator during the innate immune response and a primary adaptor protein of nearly all TLRs signaling pathways. In previous studies, Sabharwal *et al*. have shown that specific microRNAs posttranscriptionally regulate the expression of MyD88 in T84 cells incubated with probiotic bacteria (Sabharwal *et al*., 2016). Thus, the present research focuses on MyD88 gene expression and regulation during bacterial recognition in a mucin-producing cell line (HT29-MTX-E12). Most of the TLRs utilize MyD88, triggering the activation of NF- κB and mitogen-activated protein kinase (MAPKs) pathways for the induction of inflammatory cytokines genes (Kawasaki *et al*., 2014). MyD88 possesses a C-terminal TIR domain that interacts with other TIR domain-containing proteins (receptors or adaptors) and an N-terminal death domain (DD) associated with the Interleukin-1 receptor-associated kinases (IRAK) family members through homotypic DD interactions (Deguine *et al*., 2014). The association of the TLR-TIR domain with a TIR domain-containing MyD88 leads to the activation of the TLR signaling pathway. Upon stimulation with ligands, MyD88 recruits IRAK4 to TLRs through DD interactions of both molecules (Wesche *et al*., 1997). IRAK4 phosphorylates IRAK1 leading to its activation. Once IRAK4 is activated, it leaves the TLR-MyD88 complex and associates with the TNF receptor-associated factor (TRAF6), conveying its ubiquitination.

Activated TRAF6 induces the activation of TAK1, a member of the MAPK families. TAK1 associates with the enzymatic IκB kinase (IKK) complex leading to the phosphorylation and subsequent degradation of IκBα, resulting in NF- κB activation and cytokine production (Figure 2.4) (Takeda *et al*., 2005).

Since TLRs are crucial for the activation of the innate immune response, this pathway is tightly controlled to avoid the development of specific diseases and to maintain the homeostasis. The host immune response is regulated at different levels, including physical interactions, conformational changes, phosphorylation, ubiquitylation, and proteasome-mediated degradation with various participating regulatory molecules. Host cells have developed different mechanisms to regulate the microbial community. Several studies demonstrate that microRNAs (miRNA) provide a layer of regulation controlling the degree of activation of the TLR pathway and microbiota composition (Yuan *et al*., 2018). MiRNAs are small, highly conserved non-coding RNA molecules involved in the regulation of gene expression controlling diverse cellular and metabolic pathways. MiRNA bind to the 3´-UTR of their target mRNA in a sequence-specific manner. The miRNA-mRNA interaction can lead to translational repression or mRNA degradation, acting as a negative regulator (MacFarlane *et al*., 2010). Earlier studies, in T84 cells, demonstrated that miR-200c has an impact on MyD88 expression, regulating the immune signaling after incubation with probiotic bacteria (data not published).

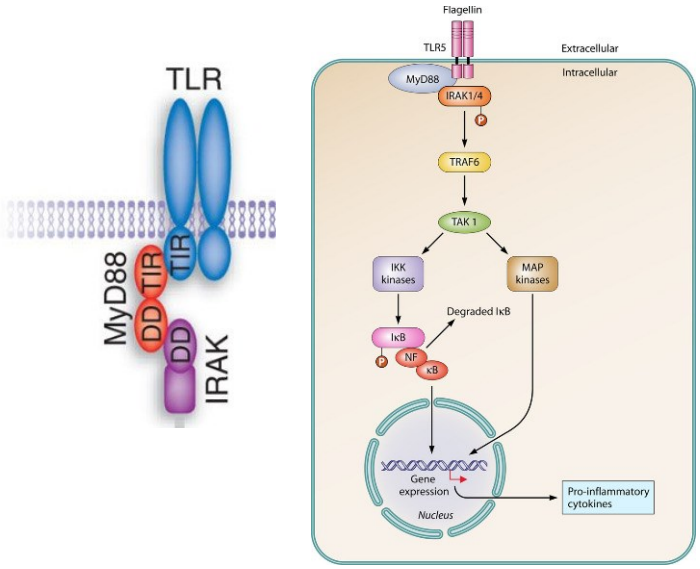

Figure 2.4. The Toll-like receptor signaling pathway. MyD88 is a central adaptor protein in the signaling path of TLRs. Its activation elicits a downstream cascade initiation of proteins involved in the NF- κB response. Adapted from Han (2006).

Even though commensals and pathogens share a lot of molecular structures and motifs, the host and its microbiota have set up a tightly regulated network of mutual control, which includes attenuation of pro-inflammatory signaling by commensals and compartmentalized expression of PRRs (Vonaesch *et al*., 2018).

2.4 Microbial imbalance: dysbiosis and disease

In the last decades, tremendous progress has been made to elucidate the mechanisms of intestinal homeostasis, dysbiosis, and disease. However, we are only beginning to understand the complexity of the gut ecosystem and the underlying interaction networks. It has already been mentioned that the human gut contains about 10^{13} bacterial cells with more than a thousand different bacterial species. These bacteria often establish a symbiotic relationship with the host providing a healthy GIT, protecting it from an overgrowth of potentially pathogenic bacteria. Nevertheless, a change in the microbial composition, that causes a drastic imbalance between the beneficial and pathogenic bacteria might result in a gut vulnerable to pathogenic microbes. The term "dysbiosis" corresponds to this imbalance in the microbial equilibrium, also described as a "disturbance of gut microbiota homeostasis due to an imbalance in the flora itself, changes in their functional composition and metabolic activities, or changes in their local distribution." (DeGruttola *et al*., 2016). Dysbiosis is categorized into three different types: **1)** loss of beneficial organisms, **2)** excessive growth of harmful microorganisms, and **3)** loss of overall microbial diversity. It is implicated in a broad range of diseases including inflammatory bowel disease (IBD), such as Chrohn´s disease (CD) and ulcerative colitis (UC), obesity, allergic disorders, Type 1 diabetes mellitus, autism, and colorectal cancer (DeGruttola *et al*., 2016). An abnormal mucin expression and mucus production also allow the proliferation of opportunistic pathogens resulting in the development of the inflammatory diseases mentioned before.

2.4.1 Enteropathogenic *Escherichia coli*

Enteropathogenic *Escherichia coli* (EPEC) represents a pathotype of the Gram-negative rod-shaped bacterium *Escherichia coli* that is able to cause watery diarrhea and is responsible for significant morbidity and mortality mostly in infants in developing countries (Kaper *et al*., 2004). To colonize the intestinal epithelium, EPEC **1)** is supposed to adhere to epithelial cells, **2)** transduces effector molecules via a Type Three Secretion System (T3SS) leading to **3)** an intimate attachment between the bacterium and the host cell (Nataro *et al*., 1998). The destruction of microvilli characterizes this close attachment,

which is described as the so-called “attaching-and-effacing (A/E)” phenotype (Moon *et al*., 1983). Furthermore, the destruction of the microvilli also reduces the ability of the cells to absorb water and nutrients, which leads to diarrhea and sometimes severe gastroenteritis. The A/E lesion is also characterized by the formation of actin-rich protruding structures right beneath the adherent bacteria, known as “pedestals,” caused by a rearrangement of the host actin cytoskeleton (Figure 2.5). To facilitate bacterial colonization, survival, and immune evasion in the infected host, EPEC translocates several virulence or effector proteins into the host via the highly conserved and specialized T3SS. The T3SS is a complex molecular machine consisting of more than 20 proteins connecting the cytoplasm of the bacteria with targeted host cells (Gaytán *et al*., 2016). On the EPEC chromosome, there is a 35-kb pathogenicity island (PAI) called “locus-of-enterocyte-effacement (LEE),” which encodes the T3SS as well as several effector proteins (Winstanley *et al*., 2001). A large number of studies provided a detailed analysis of the effector proteins of EPEC and their various functions.

Studies on EPEC and their effector proteins make the understanding of the exact mechanism of EPEC pathogenesis complex and intriguing, not only because of their central role in enteric diseases but also for their role in gut dysbiosis. The availability of genome sequences also provides more information on host-pathogen co-evolution in the context of effector-triggered immunity in the gut (Jayamani *et al*., 2014).

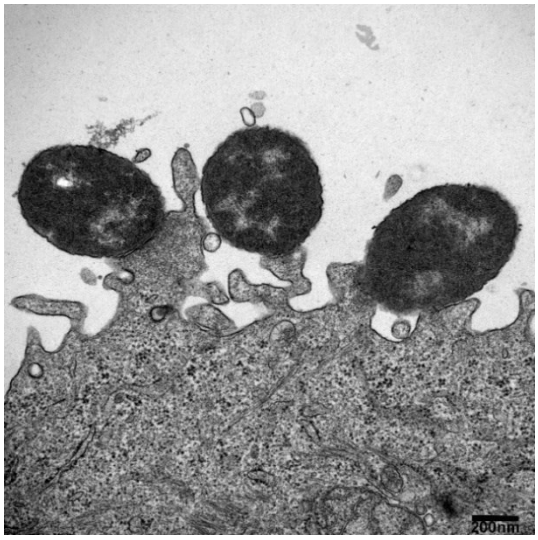

Figure 2.5. Transmission electron microscopy (TEM) of HT29 cells incubated with EPEC E2348/69 for 3 h. Bacterial attachment to the cells induces actin-rich protruding structures called pedestals (Courtesy of Lilo Greune).

2.4.2 Antibiotics: the good and bad

There is extensive use of antibiotics, not only in the medical field but also in farm animals and crops. Antibiotics offer a tremendous advantage in helping our bodies to ward off infectious diseases caused by bacteria, slowing their growth and killing many types of bacteria. They can prevent infections following surgery. The application is facilitated by oral intake. However, the human microbiota is overly exposed to them by various misuses and over-prescription. Hence, we are facing an antibiotic crisis with multiple multi-resistant bacteria spreading all over the world. Due to this fast development of antibiotic-resistant bacteria, an emerging interest focusses on a better understanding of the complex relationships between antibiotics and the human microbiome. Broad-spectrum antibiotics can affect the abundance of 30% of the bacteria in the gut community, thereby causing drops in taxonomic richness and diversity (Francino, 2016). Franzosa *et al*. summarized various "omics"-based investigations showing that antibiotic used beyond altering the taxa composition, also affects gene expression, protein activity, and metabolisms of gut microbiota (Franzosa *et al*., 2015).

Studies on antibiotic treatment in mice models showed that myeloid populations, which include macrophages, monocytes, and granulocytes, decrease in systemic sites after exposure to antibiotics. In addition to shifts in cell populations and signaling pathways, they have also demonstrated effects of the microbiota at the organ level. It is therefore not surprising to also observe upon microbial depletion changes in intestinal physiology including an enlarged mouse cecum, increased transit time, altered fecal pellet frequency and consistency, narrower villi size, decreased cellular proliferation and affected goblet cell-antigen passages in specific regions of the GIT (Kennedy *et al*., 2018). An imbalance of the microbiota caused by antibiotics, which compromises host health, can potentially generate antibiotic-induced microbiota dysbiosis.

2.5 Probiotics: a controversial issue in IBD? Benefits and importance

The use of probiotic bacteria is a promising approach aimed at impeding dysbiosis or at reestablishing the gut microbiota after antibiotic treatment. The World Health Organization defines probiotics as "live microorganisms that provide health benefits when consumed in appropriate amounts." (WHO, 2001). Even though the implementation of antibiotics and anti-inflammatory compounds has been a viable way to deal with IBD, probiotics are also proposed as a therapeutic treatment of gut inflammation since they do not negatively alter the host-microbiota. *Lactobacilli, Bifidobacterium,* lactococci, and streptococci are in the repertoire of the most frequently consumed probiotics, while yeast, bacilli, and some non-pathogenic *E. coli* strains are less often used (Lerner *et al*., 2019). Many studies examining

probiotics included patients with different diseases such as cancer, and heart, intestinal, urogenital, and immune system problems. However, many of these studies considered only small numbers of patients, were not controlled and did not include specifications about the probiotic used, leaving the application of probiotics a topic of debate. Over the last few years, better-designed studies have been conducted with modern research techniques and have thus provided relevant information about the mechanism(s) of action of probiotics (Mack, 2005).

On the one hand, studies made in the inpatient unit of the Mount Washington Pediatric Hospital, where they fed infants with chronic illnesses, aged 5-24 months, with infant formula supplemented with *Bifidobacterium* and evaluated daily for the occurrence of diarrhea and rotavirus antigen, showed that the supplementation of infant formula with this bacterial genus reduces the incidence of acute diarrhea and rotavirus shedding in infants admitted to the hospital (Mao *et al*., 2008). More recent results show prevention of functional gastrointestinal disorders in 268 healthy newborns fed with *Bifidobacterium* strains for three months in the Division of Pediatrics of the University of Piemonte Orientale "A. Avogadro." (Aloisio, *et al*., 2018).

Parker *et al*. investigated the effects of *Lactobacillus acidophilus* in mice with experimental ulcerative colitis and showed that treatment with this bacterium attenuated the severity of DSS-induce colitis. Specifically, it suppresses pro-inflammatory cytokines such as interleukin (IL)-6, IL-17, IL-1β, and tumor necrosis factor-α (TNF-α) in the colon tissues (Parker *et al*., 2018).

On the other hand, some reports suggest that not everyone may benefit equally from probiotic treatments. For example, there is no evidence that patients with Crohn´s disease will benefit from the ingestion of probiotics on any level of the disease, active stage, remission, or preventing postoperative recurrence of the disease. In the same way, some claimed little clinical experience in the use of probiotics administration to severely immunocompromised IBD patients (Mack, 2011). Further research, which includes additional meta-analysis, is necessary to further evaluate the effects of probiotics in pouchitis and mild-to-moderate ulcerative colitis. It is also essential to continue to study antibiotics *vs.* probiotics for maintaining medical remission as well as the potential cumulative beneficial effects of probiotics paired with other therapies (anti-inflammatory compounds, corticosteroids, immunomodulators, and biological agents).

2.5.1 *Escherichia coli* Nissle 1917: a candidate on the list of probiotics

E. coli Nissle (EcN) 1917, is the most commonly used Gram-negative probiotic. It was isolated by the army surgeon Alfred Nissle in 1917 during the First World War, from a soldier who did not develop infectious diarrhea during a *Shigella* outbreak. EcN (serotype O6:K5:H1) is a typical example of a non-pathogenic, commensal *E. coli* isolate. EcN contains an altered lipopolysaccharide (LPS) as a structural component of its outer cell membrane. The O6 surface antigen represents the outer part of the LPS and differs in molecular aspects from all other LPS types of *E. coli.* The O6 polysaccharide side chain is very short, with only one single "repeating unit" of the oligosaccharide building block. These particular features of the LPS of EcN may explain the immunomodulating properties without showing detrimental immunologic effects. The K5 serotype represents the extracellular capsule variant that EcN can form. In many extraintestinal pathogenic *E. coli*, the existence of a capsule protects the pathogen from attacks by non-specific defense components of the blood serum making the bacterium serum-resistant. However, EcN does not exhibit serum-resistance properties (Sonnenborn *et al*., 2009).

EcN possesses flagella that enable the microbe to move actively within the viscous intestinal mucus layer and also has important functions in bacterial crosstalk with the epithelium. EcN has three types of fimbriae: Type 1, F1C, and "curli" fimbriae, which mediate the adhesion to the mucus layer of the intestinal wall. This strain does not exhibit any virulence factors but instead carries gene clusters located on chromosomal genomic islands (GEIs) responsible for the synthesis of several "fitness factors" that enable EcN to compete with other strains in the gut and to communicate effectively with the host organism. It has also been shown that EcN produces a wide array of siderophores, which are secondary metabolites that improve the bacterial uptake of iron from the environment via specific receptors. An additional feature of this strain is the production of two microcins that contribute to the antagonistic activity of EcN against enteropathogenic microorganisms. The lack of pathogenicity islands coding for effector proteins and virulence factors such as α-hemolysin, P-fimbriae, S-fimbriae, combined with the existence of genes coding for fitness factors like microcins, iron-uptake systems, and the serum-sensitive phenotype is essential for the probiotic nature of EcN (Sonnenborn *et al*., 2009). Various studies have been performed to provide a further understanding of the probiotic effects of EcN. *In vitro* experiments done by Reissbrodt *et al*. investigating the impact of EcN when co-cultured with different enteropathogenic, uropathogenic, and other *E. coli* strains, demonstrated a decrease in the number of viable bacteria and also a dose-dependent reduction of Shiga toxin levels (Reissbrodt *et al*., 2009).

The antagonistic mode of action of this probiotic strain was also confirmed *in vivo.* Germ-free animals (rats, mice, piglets) were inoculated with EcN and different pathogenic and non-pathogenic *E. coli, Salmonella typhimurium, Candida albicans,* and *Lactobacillus johnsonii.* Either EcN and the

particular pathogen were administered simultaneously or the tested strain was fed first followed by the EcN several days later. These studies did not detect pathogenic strains in the fecal samples of the animals suggesting a complete eradication of these pathogens in the intestines (Lorenz *et al.*, 1996; Mandel *et al*., 1995). The impact of EcN on the barrier function is also an issue that matters. Guo *et al*. reported that EcN protects the intestinal barrier function by ameliorating the altered expression and localization of TJ proteins (ZO-1 and occludin) and inhibiting the NF-κβ activation (Guo *et al*., 2019). Moreover, it induces naïve and peripheral blood CD4+ T-cell clonal expansion without the activation of mucosal lamina propria T cells (Sturn *et al*., 2005). EcN is also able to attenuate the level of pro-inflammatory cytokines in Caco-2 cells, showing its anti-inflammatory effects (Huebner *et al*., 2011).

But the whole EcN panorama is not entirely white. Several hypotheses have been proposed suggesting the cancer-inducing properties of certain *E. coli* strains of the phylogenetic group B2, which can express a group of cytotoxic compounds called cyclomodulins. Colibactin is one of these compounds and it is encoded by the polyketide synthase (*pks*)-island, but to date, the active compound has not been isolated due to its instability (Homburg *et al*., 2007). It has been shown that colibactin induces DNA double-strand breaks in eukaryotic cell cultures, upon direct contact between live bacteria and epithelial cells, triggering cell death (Nougayrede *et al.*,2006). It is critical to mention that the adherent mucus layer protects the host epithelial cells from direct contact with EcN (Reuter *et al*., 2017). Genetic modifications to delete the *pks*-island of EcN have been performed, but without it, EcN loses its probiotics features (Olier *et al*., 2012; Massip *et al*., 2019). Contrary to this hypothesis, Janosch *et al*. showed by *in vitro* tests that EcN displays anti-mutagenic properties (Janosch *et al*., 2019). Some questions remain unsolved: how can colibactin pass the bacterial outer membrane and the cellular membrane, translocate through the cytoplasm encountering proteins and RNA to enter the nucleus to react with the DNA and nevertheless remain stable and active?

A significant effort has been made to investigate and characterize the probiotic EcN and its influence in the human gut. Therefore, the research in this subject should continue to extend the full use of the potential of EcN.

2.6 Outer membrane vesicles

Gram-negative bacteria do not only employ different secretion systems to deliver effector proteins but also vesicles they shed from their outer membrane as a long-distance delivery mechanism of microbial factors. These vesicles are called outer membrane vesicles (OMVs) and are involved in bacterial survival, host-microbe interactions, and competition towards other bacteria (Schwechheimer *et al*., 2015). Their size ranges from 20 to 250 nm in diameter, they contain components of the cell wall and outer membrane (OM), periplasmic proteins, some cytosolic proteins, and bacterial DNA and RNA. The content of OMVs from various species has been characterized using protein mass spectrometry. Little is known about how EcN delivers effector molecules to the host. Consequently, in the last years, researches focused as well on the analysis of EcN OMVs to better understand its beneficial effects on the intestinal barrier. Aguilera *et al*. performed the first global OMV proteome of a probiotic strain. In the analysis of EcN OMVs, they identified 313 unique proteins and selected 192 for further analysis. The results show that EcN OMVs were almost devoid of inner membrane proteins, but OM proteins were significantly present. Cytoplasmic proteins were under-represented. However, the authors suggest that these proteins may be relevant in probiotic and pathogen-derived OMVs. To estimate the extent to which each subcellular group of proteins was represented in the isolated OMVs, the investigators used the complete *E*. *coli* proteome database since the EcN-specific proteome was not available. They also evaluated the functional classification of EcN-vesicular proteins according to UniProt and GenProtectEC where approximately 40% of the proteins mediate cellular processes such as cell adhesion, macromolecule degradation, motility, cell wall biogenesis, etc. 30% are related to metabolism: inorganic iron transport and metabolism, carbohydrate and amino acid transport and metabolism. 20% mediate information transfer like DNA replication, repair, and recombination and translation, and 10% of the proteins had an unknown function (Aguilera *et al*., 2014).

The discovery of the OMVs initiated the question of whether it is necessary to have live microbes to generate effects on gut epithelia. Several studies have investigated the effect of the EcN OMVs on the barrier function. Fábrega *et al*. showed anti-inflammatory effects of EcN OMVs dextran sodium sulfate (DSS)-experimental colitis in mice: EcN OMVs decreased the expression of pro-inflammatory cytokines such as IL-1β, TNF-α, IL-6, and INFγ and increased the appearance of the anti-inflammatory cytokine IL-10 in tested animals (Fábrega *et al*., 2017). Alvarez *et al*. found an upregulation of ZO-1 and claudin-14 in T-84 and Caco-2 polarized monolayers after the addition of EcN OMVs to epithelial cells, contributing to the reinforcement of the epithelial barrier (Alvarez *et al*., 2016). In a similar way, EcN OMVs activate NOD1- mediated immune responses in intestinal epithelial cells. NODs (NOD1 and NOD2) are intracellular immune receptors essential in host defense against bacterial

infections. They are also fundamental in maintaining gut homeostasis and microbiota balance (Cañas *et al*., 2018). The application of EcN OMVs might provide new insights into the treatment of gastrointestinal diseases.

2.7 2D *vs.* 3D a new shift in the biological dimension

The interest in the comprehension of host-microbe interactions has brought major challenges in tissue engineering for infectious disease research. A better model of the *in vivo* spatiotemporal properties is necessary to mimic more closely the gut environment. Infectious diseases have been studied *in vitro* by the use of a single host cell type, that grows as a flat 2D monolayer. Even though this approach has led to important discoveries of mechanisms that underlie infection and disease, 2D cell culture models lack many essential features present in the host microenvironment, e.g., three-dimensional (3D) architecture, commensal microbiota, multicellular complexity, nutrient gradients, gas exchange, and physiologically biochemical forces like fluid shear, stretch, and compression (Barrila *et al*., 2018). Understanding the mechanisms of action of probiotics under incubation conditions, closer to the *in vivo* situation might pave the way for novel therapeutics or new preventive strategies to fight the severe and increasing problems of antibiotic resistance. Thus, new *in vitro* cell culture models that bridge the gap between cell culture base research and more sophisticated *in vivo* animal models are necessary to increase the knowledge about probiotic-host crosstalk.

In the past decades, there has been a shift from the original “flat biology” approach (2D) to 3D models of human intestinal epithelia, which offer a more precise “*in vivtro*” possibility to imitate the *in vivo* host-microbe interactions and crosstalk.

2.7.1 Rotating Wall Vessel- derived 3D models

Barrila *et al*. defined the Rotating Wall Vessel (RWV) bioreactor as an “optimized form of suspension culture that facilitates the formation of self-organizing 3D tissue-like aggregates by allowing cells the spatial freedom to colocalize and self-assemble based on natural affinities within a low-fluid-shear environment.” (Barrila *et al*., 2018) . The RWV was designed by NASA (National Aeronautics and Space Administration) and is based on a cylindrical, rotating bioreactor with a central core consisting of a gas-permeable membrane that provides adequate gas exchange. On the top part, there is a filling port where the bioreactor can be filled with cell culture medium. The rotating fluid offsets the sedimentation of the cells in the vessel, creating a gentle fall of cells through the medium under physiological fluid

shear conditions, similar to that encountered by microbes in the gut. In this cell culture system, the cells are cultured on porous collagen-coated microcarrier beads (or other scaffoldings) for attachment. The porosity of the beads allows the cells to respond to chemical and molecular gradients similarly to the response of the tissue *in vivo.* The RWV design allows easy manipulation of culture conditions, including the addition of cells for co-culture purposes, removal of cellular aggregates for analysis, and replacement of media at different time points (Barrila *et al.*, 2010). Cells cultured in the RWV can recapitulate the 3D spatial organization and polarity (Figure 2.6), cellular differentiation, multicellular complexity, and functionality, features that cannot be seen in the 2D cell culture models.

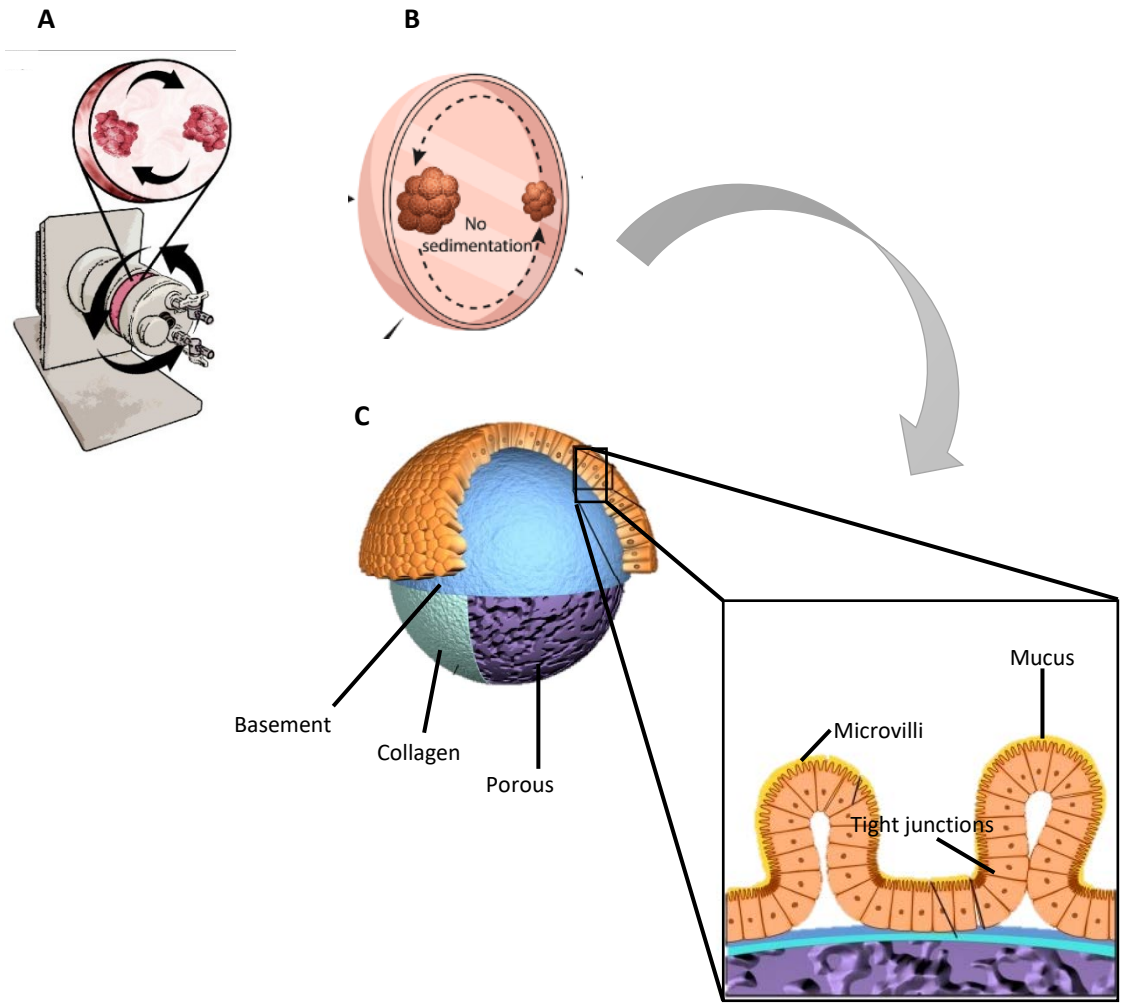

Figure 2.6. Representation and operation of the RWV cell culture system. A) RWV bioreactor containing cell culture media, cells, and porous microcarrier beads. **B)** The rotating fluid offsets the sedimentation of the cells within the vessel, allowing the formation of 3D aggregates. **C)** Attachment of the intestinal epithelial cells to the microcarrier beads. After the adhesion of the intestinal epithelial cells to the beads, they begin to differentiate and display *in vivo*-like characteristics: polarity, in which the basolateral side faces the beads, and the apical side is in contact with the cell culture medium, microvilli formation on the apical side, cell-cell connection through tight junction formation and mucus production. Adapted from Barrila *et al*. (2010)

2.8 Aim of the study

Complex mechanisms involved in host-microbe interactions, including how the intestinal epithelial cells mount an appropriate immune response to pathogenic microorganisms and, at the same time, avoid the damage of the resident microbiota is poorly understood. Hence, the implementation of cell culture models that improve the simulation of functional live tissues with complex cellular environments, like in an *in vivo* situation, is crucial to unravel the pathophysiology of a bacterial infection or inflammation like inflammatory bowel diseases. This should pave the way for developing more efficient therapies that target the disturbed biological process in the gut.

In this study, we wanted to investigate host-microbe interactions in an experimental setup that is closely related to *in vivo* conditions. For this, the RWV bioreactor was used as a cell culture model to grow HT29-MTX-E12 cells. This epithelial cell line expresses high proportions of mucin-secreted goblet cells, which is an essential feature to mimic the gut environment. Besides mucin secretion, this cell line is also characterized by junctional complex formation, including tight junction, adherent junction, and desmosomes. As explained before, cells cultured in the RWV bioreactor grow under low physiological fluid shear, which is involved in cellular differentiation, metabolism, and cellular functions. Fluid shear plays a fundamental role in growth, mucin adhesion, metabolites production, and DNA profiles of the gut microbial community. With this closely *in vivo*-like setup, we were interested in investigating the impact of the probiotic EcN (serotype 06:K5:H1) on the barrier function of host cells represented by JAM-A expression and distribution, and on the immune response represented by *MyD88*, *TLR5* and cytokines responses. We also wanted to compare molecular and cellular responses of cells grown in different cell culture systems and incubated with EcN under different conditions. The enteropathogenic EPEC strain E2348/69 (serotype O127:H6) was also employed as a reference to compare the differences in host responses between probiotic and pathogenic bacteria.

The importance of using a mucin-producing cell line, indicating its proximity to the *in vivo*-like features, is that the presence of mucus not only serves as a physical barrier that traps bacteria and viruses, but it can also disarm pathogens and prevent them for causing infections (Wheeler *et al*., 2019). Wagner *et al*. have shown that mucus can also interfere with bacterial behavior, preventing not only the attachment of microorganisms to epithelial surfaces but the communication with one another as well (Wagner *et al*., 2018). This microbe-disarming activity has powerful consequences on the ability of the bacteria to establish infections. This regulatory function is likely dependent on glycan complexity, as monosaccharides do no attenuate virulence. Therefore, “mucin glycans are potent host signals that tame microorganisms, rendering them less harmful to the host.” (Wheeler *et al*., 2019). To that extent,

we were interested in studying the behavior and effect of probiotic and pathogenic bacteria when incubated with a mucin-producing cell line.

Epithelial cells face biomechanical forces generated by a flowing liquid acting at the surface of a cell, called fluid shear stress. Fluid shear stress may have profound effects on changes in cellular gene expression. Therefore, we also compared cellular responses under rotating and static co-incubation conditions. Cells and bacteria were co-incubated in the RWV bioreactor and brought under rotating movements during the incubation times. This type of incubation was called “rotating infections.” Contrarily, co-incubations of cells and bacteria outside the RWV bioreactor but on a 24-well plate were called “static infections.” The presence of fluid shear stress during infections, besides the mucin layer on top of the host cells, is also an important aspect related to an *in vivo*-like situation.

CHAPTER 3

MATERIALS

3.1 Bacterial strains

Bacterial strains used in this study are listed in Table 3.1. Probiotic and pathogenic strains from *E. coli* were used to perform infection experiments. Cukrowska *et al*. colonized thirty-four newborn babies with EcN to analyze the influence of oral administration of EcN on the systemic humoral and cellular immunity in premature infants. Stool samples of the infants were analyzed repeatedly after 3, 5, 7, 14, 21, and 28 days to evaluate the presence of the administered probiotic strain. The analysis of the stool samples showed the presence of different variants of EcN (Cukrowska *et al*., 2002). The EcN variants we received were variants that were still present in these infants two years after inoculation with EcN. In Table 3.2 the different EcN variants are described, with their respective spontaneous mutation, we obtained from the Institute of Hygiene in Münster, Germany.

Table 3.1. Bacterial strains, characteristics, and references.

Strain	Characteristics	Reference
E. coli strain Nissle 1917 (EcN)	Probiotic, microcins H47 and M secretions; O6:K5:H1	Mutaflor® (Ardeypharm, Herdecke, Germany)
EPEC strain E2348/69	O127:H6 serotype wild type; diarrhoeagenic strain	Courtesy of MS Donnenberg (Donnenberg *et al.,* 1993)

Table 3.2. Description of the different EcN variants isolated from the infants' microbiota that have been investigated in the present study

Name of the variant	Type of change	Description
EcN variant 3413	An inframe deletion in *flgB*	FlgB: flagellar protein involved in bacterial motility (Kubori *et al*., 1997).
EcN variant 3414	An insertion in *opgH*	OpgH: glucans biosynthesis glucosyltransferase H. This protein is involved in the biosynthesis of osmoregulated periplasmic glucans (OPG), which is part of glycan

		metabolism (UniProtKB-Q83Z42_OPGH_XANEU).
EcN variant 3426	A mutation in *ycgR*	YcgR: a flagellar brake protein that regulates the cell motility by controlling the motor speed (UniProtKB-P76010_YCGR_ECOLI).
EcN variant 3419	A frameshift in *focD* and missense nutation in *iucC*	FocD: protein involved in the export and assembly of the F1C fimbriae subunit across the outer membrane (UniProtKB-KW). IucC: an aerobactin synthase protein involved in the aerobactin biosynthesis pathway, which is part of siderophore biosynthesis (de Lorenzo *et al.*, 1986).
EcN variant 3452	An insertion in *opgH*	OpgH: glucans biosynthesis glucosyltransferase H. This protein is involved in the biosynthesis of osmoregulated periplasmic glucans (OPG), which is part of glycan metabolism (UniProtKB-Q83Z42_OPGH_XANEU).
EcN variant 3453	A missense mutation in *rpsD*, *tdcE*, *ygiD, mutS*, alpha-ketoglutarate dehydrogenase, and *btuC*.	RpsD: assembly initiator protein involved in: transcription antitermination (Torres *et al.*, 2001), ribosomal small subunit assembly (Nowotny *et al.*, 1988), response to antibiotic (UniProtKB-KW), positive regulation of translational fidelity (Gaudet *et al.*, 2011) and negative regulation of translational initiation (Yates *et al.*, 1980). TdcE: a protein with catalytic activity. It is involved in L-threonine degradation via the propanoate pathway (Hesslinger *et al.*, 1998). YgiD: a protein involved in the cellular aromatic compound metabolic process, e.g., binding

EcN variant 3453	A missense mutation in r*psD*, t*dcE*, y*giD*, *mutS,* alpha-ketoglutarate dehydrogenase, and *btuC*.	to ferrous iron and zinc ions (UniProtKB – Q7UBJ4). MutS: a protein involved in the repair of mismatches in DNA (UniProtKB – Q56215 MUTS_THEAQ). Alpha-ketoglutarate dehydrogenase: a Krebs cycle enzyme: It catalyzes the oxidative decarboxylation of α-ketoglutarate to generate succinyl-CoA and carbon dioxide, along with the production of NADH plus H^+ (Park *et al*., 1997). BtuC: a protein involved in vitamin B12 import across the membrane (UniProtKB – B1XG18_ BTUC_ECODH).
EcN variant 3595	A missense mutation in *fliM*	FliM: one of three proteins that form the flagellar rotor-mounted switch complex, located at the base of the basal body.
EcN variant 3598	A missense mutation in *gspF* and in *rpoS*	GspF: involved in type two secretion system (T2SS), for the export of proteins (Gaudet *et al*., 2011). RpoS: initiation factor that promotes the attachment of RNA polymerase to specific initiations sites. It is a transcriptional regulator of the stationary phase and the general stress response (Kolodkin *et al*., 2009).
EcN variant PZ816		Highly flagellated (Ardeypharm, Herdecke, Germany)

3.2 Eukaryotic cell lines

The human cell line HT29-MTX-E12 (ECACC 120404019) was predominantly used in this study. This cell line is obtained from colon adenocarcinoma. Additionally, the HT29-MTX-E12 cell line is an HT29 derivative selected on the basis of tight junction formation and adherent mucus production. In particular, differentiated cells express MUC5AC, MUC1, MUC6, and MUC2, which more closely resembles the characteristics of a gastric cell (Cairns *et al.*, 2017; Reuter *et al.*, 2017). The HT29-18N2 is a non-mucin-producing cell line, which was used as well to study host-microbe interactions in the absence of a mucin layer. The LS174T cell line was a generous gift from Sören Ockvirk (Technische Universität München, Department of Microbiology and Ecology). The LS174T cells are adherent epithelial cells that were also obtained from human colorectal adenocarcinoma. These cells have abundant microvilli and intracytoplasmatic mucin vacuoles (Tom *et al.*, 1976).

3.3 Primers used for Real-Time Quantitative Reverse Transcription Polymerase Chain Reaction (qRT-PCR)

The sequences of the primers used for quantitative RT-PCR to detect and quantify RNA targets were synthesized by Eurofins MWG (Ebersberg, Germany) and are listed in Table 3.3.

Table 3.3. Sequences of oligonucleotides used for qRT-PCR.

Name	Sequence (5´-3´)
JAM-A forward	GCAGCCGTCCTTGTAACC
JAM-A reverse	GGCTGGCTGTAAATCACCTT
MyD88 forward	TTTGCAACTCAGCCTCTCTCC
MyD88 reverse	GTCGCAGACAGTGATGAACC
TLR5 forward	ACAGAAACAGCAGTATTTGAGGTG
TLR5 reverse	GAGTTTATGAAGAAACCAGCCAAC
hBD-2 forward	GGCACCAGAGACCTCATATTT
hBD-2 reverse	TCAACCTCATTCTTCTTTTTGTT
HPRT_hu forward	TGACCTTGATTTATTTTGCATACC
HPRT_hu reverse	CGAGCAAGACGTTCAGTCCT

3.4 Antibodies and immune fluorescence dyes

Primary, secondary antibodies, as well as fluorescent dyes used in this study for western blotting (Chapter 4, Section 4.4.5) and immunofluorescence (Chapter 4, Section 4.2.6), are listed in Table 3.4.

Table 3.4. Antibodies and fluorescent dyes used in this study

Antibody	Dilution from stock	Description	Company
A-tubulin (WB)	1:1,000	Monoclonal mouse AB against human α-tubulin	Sigma Aldrich (Taufkirchen, Germany)
JAM-A (CD321) (WB)	1:1,000	Polyclonal rabbit/IgG AB against human Junctional Adhesion Molecule -A (JAM-A) protein	Thermo Fisher Scientific (USA)
JAM-A phospho Y280 (PY280) (WB)	1:1,000	Polyclonal rabbit AB against human JAM-A protein phosphorylated at the tyrosine 280 location	Rockland antibodies & assays (Limerick, USA)
JAM-A (J3F.1) (IF)	1:100	Monoclonal mouse/IgG AB against human JAM-A	Santa Cruz Biotechnology, Europe
Mouse-HRP IgG (H+L)	1:10,000	Monoclonal goat AB against mouse conjugated with HRP	Dianova (Hamburg, Germany)
Rabbit-HRP IgG (H+L)	1:5,000	Monoclonal goat AB against rabbit conjugated with HRP	Dianova (Hamburg, Germany)
Mouse IgG-Cy2	1:500	Monoclonal goat AB against mouse conjugated with Cy2	Dianova (Hamburg, Germany)
Draq5™	1:500	Cy5 conjugated fluorescent dye intercalating into DNA	BioStatus Ltd (Shepshed, UK)
TRITC-phalloidin	1:500	Phalloidin-Tetramethylrhoadamine B isothiocyanate conjugated fluorescent dye binding to actin-cytoskeleton	Sigma-Aldrich (Taufkirchen, Germany)

AB: antibody; HRP: horseradich peroxidase; IF: immunofluorescence; WB: western blotting.

3.5 Kits

Commercially available kits used in this study are summarised in Table 3.5.

Table 3.5. Kits used in this study

Kit	Description	Company
RNeasy Mini Kit	RNA extraction from eukaryotic cells	Qiagen (Hilden, Germany)
RNase-Free DNase Set	DNA digestion for RNA purified samples	Qiagen (Hilden, Germany)
QIAxcel® Advanced System	RNA quality control	Qiagen (Hilden, Germany)
miScript II RT kit	cDNA synthesis	Qiagen (Hilden, Germany)
RT^2 First Strand Kit	cDNA synthesis for use with RT^2 Profiler PCR array	Qiagen (Hilden, Germany)
RT^2 SYBR Green qPCR Mastermix	qRT-PCR substrate	Qiagen (Hilden, Germany)
RT^2 Prodiler™ PCR Array (PAHS-148ZF)	Gene expression analysis to bacterial response	Qiagen (Hilden, Germany)
Blue SYBR Green qPCR Kit	qRT-PCR substrate	Biozym (Hessisch-Oldendorf, Germany)
Pierce™ BCA Protein Assay Kit	Quantification of protein concentration	Life Technologies (Carlsbad, USA)
ECL Western Blotting Substrate	Chemiluminescence substrate	Thermo Fisher Scientific, Waltham, MA, USA

3.6 Protein size standard

To determine in SDS-PAGE gels the approximate molecular weight of target proteins, the pre-stained size marker Protein marker VI (Applichem GmbH, Darmstadt, Germany) with peptides of the following molecular weights (kDa) was used: 11, 17, 20, 25, 35, 48, 63, 75, 100, 135, 180, 245.

3.7 Culture media

3.7.1 Bacterial culture media

To culture bacteria, the following medium was used: Lysogeny broth (LB; 86mM NaCl, 5 g/l yeast extract, 10 g/l tryptone; all from AppliChem GmbH, Darmstadt, Germany). To prepare agar plates from this medium, 15 g/l agar-agar (AppliChem GmbH, Darmstadt, Germany) was added before autoclaving. LB medium was stored at room temperature, and the agar plates were stored at 4 °C.

3.7.2 Culture media and supplements for eukaryotic cell lines

Media and supplements used to culture eukaryotic cells are listed in Table 3.6.

Table 3.6. Media and supplements for eukaryotic cell culture

Name	Description	Supplier
Advanced DMEM, high glucose	Dulbecco's Modified Eagle Medium with 4.5 g/l glucose, and without L-glutamine	ThermoFisher Scientific (Schwerte, Germany)
Advanced MEM, low glucose	Minimum Essential Medium without L-glutamine and HEPES	ThermoFisher Scientific (Schwerte, Germany)
GlutaMax	Improved cell culture supplement used as a direct substitute for L-glutamine	ThermoFisher Scientific (Schwerte, Germany)
FBS	Fetal bovine serum, sterile filtered and UV-treated	Sigma Aldrich (Taufkirchen, Germany)
D-PBS with/without Ca^{2+} and Mg^{2+}	Dulbecco´s phosphate-buffered saline with or without Ca^{2+} and Mg^{2+}	ThermoFisher Scientific (Schwerte, Germany)
Pen/Strep (100x)	Penicillin/Streptomycin	ThermoFisher Scientific (Schwerte, Germany)
Trypsin/EDTA (10x)	0.5 %/0.2 % (w/v) in D-PBS without Ca^{2+} and Mg^{2+}	ThermoFisher Scientific (Schwerte, Germany)
Fibronectin Bovine Protein, Plasma (1 mg)	Extracellular matrix protein used as a coating for cell attachment	Sigma Aldrich (Saint Louis, USA)

3.8 3D cell culture equipment

To develop a 3D *in vivo*-like architecture of the epithelial cells (HT29-MTX-E12 and LS174T) dextran Cytodex® 3 microcarrier beads, >175µm particle size (spherical), in 0.9 % NaCl solution (Sigma-Aldrich, Taufkirchen, Germany) were employed to grow the cells on the beads. The Rotating Wall Vessel (RWV) bioreactor was used to culture the cells on the microcarrier beads. In this study, the employed RWV bioreactor was the following:

RCCS-4H (4 Vessel Rotary Cell Culture System) with reusable vessels "STLV-55" or disposable 10 ml bottles "D-410".

Built by: Synthecon Inc., Houston, Texas, USA.

3.9 Common buffers and solutions

All buffers and solutions were prepared in ultrapure water type 1 (Milli-Q) and are listed below.

10 x PBS

NaCl	1.37 M
KCl	27 mM
Na2HPO4	101 mM
KH_2PO_4	15 mM
pH 7.4, autoclaved, stored at RT	

Tris-HCl (1 M)

Tris	30.275 g
H_2O	ad 1l
pH 6.8, adjusted with HCl	

10 x TBS

Tris	250 mM
NaCl	1.37 M
ddH_2O	ad 1 l
pH 7.4	

TBS-Tween 20 (TBST)

10 x TBS	10% (v/v)
Tween 20	0.2% (v/v)

Resolving gel solution

Tris-HCl	1.5 M
EDTA	0.01 M
SDS	0.5% (w/v)
pH 8.8	

Stacking gel solution

Tris-HCl	1.0 M
EDTA	0.01 M
SDS	0.5% (w/v)
pH 6.8	

10 x Running buffer

Tris-HCl	25 mM
Glycine	192 mM
SDS	0.1% (w/v)
pH 8.8	

4x Loading buffer

Tris-HCl	62.5 mM
SDS	3% (w/v)
Glycerol	10% (v/v)
2-mercaptoethanol	8% (w/v)
Bromophenol blue	*spatula* point
pH 6.8	

Coomasie Brilliant Blue staining

Coomasie Brilliant Blue R-250	3.3 mM
Ethanol	50% (v/v)
Acetic acid	10% (v/v)

Destaining solution

Ethanol	10% (v/v)
Acetic acid	7% (v/v)

PFA 8 % (v/v)

1 x PBS	8 ml
PFA	0.8 g
Heat to 60 °C	
1 M NaOH (added dropwise until the solution was clear)	
Cooled down	
pH adjusted to 6.9	25% HCl
ddH_2O	ad 10 ml
filtered	
aliquoted and stored at -20 °C	

PFA 4%

8 % PFA	50% (v/v)
1 x PBS	50% (v/v)
prepare fresh	

CHAPTER 4

METHODS

4.1 Microbiological methods

4.1.1 Cultivation of bacterial strains

All work with bacterial strains was carried out in a laminar flow hood under sterile conditions. Bacterial cultures were prepared by inoculation of Lysogeny Broth (LB) medium with a single colony from an agar plate and incubated overnight at 37 °C, 180 rpm. The overnight cultures were used for sub-culturing by inoculating fresh medium for infection experiments.

4.1.2 Storage of bacterial strains

For long-term storage, bacterial glycerol stocks were prepared. Bacteria were cultured until they reached the exponential phase and then transferred to LB medium containing 30% glycerol (v/v) to prevent ice crystal formation. The aliquots were stored at -80 °C (strain collection of the Institute of Infectiology – ZMBE). For short-term storage (4-5 weeks), bacteria were spread on agar plates without antibiotics and incubated overnight at 37 °C. The agar plates with bacterial colonies were stored at 4 °C.

4.1.3 Outer membrane vesicles isolation

Outer membrane vesicles (OMVs) from EPEC strain E2348/69, EcN, and EcN variant 3595 were isolated. Isolation of OMVs was performed by ultracentrifugation. Two days before ultracentrifugation, bacteria were grown in 10 ml LB medium and incubated overnight at 37 °C and 180 rpm (Incubator shaker Innova™ 4300, New Brunswick Scientific GmbH, Nürtingen, Germany). After 24 h, 500 ml of fresh LB medium were inoculated in a ratio of 1:50 from the overnight bacterial culture. The bacteria were cultured at 37 °C, 180 rpm for 16 h. Afterward, the culture was centrifuged at 4 °C, 14,000 x g for 15 min. The supernatant was filtered with a 0.22 µm filter (Millipore) and then, the filtrate was ultracentrifuge at 4 °C, 188,000 x g for 4 h. The pellet containing the OMVs was resuspended in 100 µl of 20 mM Tris-HCl, pH 7.4, including protease inhibitor (20 µl/ ml buffer) and stored at -20 °C.

The quality of the OMVs was confirmed by SDS-PAGE (Section 4.4.3). Protein concentration was determined by the Pierce™ BCA (bicinchoninic acid) Protein Assay Kit (Life Technologies, Carlsbad, USA) according to the manufacturer's instructions.

4.1.4 Supernatant preparation

A single colony of EPEC strain E2348/69, EcN WT, and EcN variant 3595 was isolated and cultured overnight aerobically (about 13 h) at 37 °C. Cell-free supernatants of the different strains were prepared by centrifugation of the bacterial cultured at 16,000 rpm (Centrifuge Eppendorf 5424 R; Eppendorf, Hanau, Germany) for 1 min. The resulting supernatant was collected, and the pellet was discarded. The protein concentration of each different supernatant was determined by the Pierce™ BCA Protein Assay Kit according to the manufacturer´s instructions. Cell-free supernatants were stored at -20 °C. The supernatant of the highly flagellated EcN strain PZ816 was obtained from Ardeypharm, Herdecke, Germany.

4.2 Cell biology methods

4.2.1 Culture of eukaryotic cell lines

Eukaryotic cell lines were incubated at 37 °C under 5% CO_2 in a humid atmosphere. Cell lines were grown in Corning coated cell culture flasks (75 cm^2) and cultured in the respective medium containing 100 U/ml penicillin/streptomycin (Pen/Strep). The medium was exchanged every other day. In this study, we employed the human epithelial cell lines HT29-18N2, HT29-MTX-E12, and LS174T derived from human colon adenocarcinoma. In Table 4.1, their culture media are summarised.

Table 4.1. Eukaryotic cell culture media

Cell line	Culture medium	FCS (%)	Supplements
HT29-18N2	Advanced DMEM (high glucose)	5	1% Pen/Strep 2% GlutaMax
HT29-MTX-E12	Advanced DMEM (high glucose)	5	1% Pen/Strep 2% GlutaMax
LS174T	Advanced MEM (low glucose)	5	1% Pen/Strep 2% GlutaMax

Low glucose: 1 g/l; high glucose: 4.5 g/l; DMEM: Dulbecco's Modified Eagle Medium; MEM: Minimal Essential Medium; Pen/Strep: penicillin/Streptomycin.

The eukaryotic cells were split upon reaching a confluence of 80-90%. To split the cells, the medium was first removed, and the cells were washed twice with D-PBS (without Ca^{+2}/Mg^{+2}). Afterward, cells were incubated with 10 ml D-PBS (without Ca^{+2}/Mg^{+2}) at 37 °C for 10 min to facilitate cells´ detachment. Then, the D-PBS solution was removed, and cells were incubated with 2 ml of 1x trypsin/EDTA solution at 37 °C until they detached from the flask. Cells were resuspended in fresh medium and transferred to a new sterile flask in the desired dilutions, or they were seeded on coated 24-wells at a density of 2 x 10^5 cells/ml. Generally, experiments were carried out between passages 10-20. Every month cells were routinely tested for mycoplasma contamination.

4.2.2 Freezing, storage and thawing of eukaryotic cells

For long-term storage, the cell lines were cryopreserved. For this, cells were detached from the cell culture flask as explained above, and the cell suspension was centrifuged at 300 x g for 5 min. The pellet was resuspended in fresh medium with its respective supplements (Table 4.2.1) and 10% dimethylsulfoxide (DMSO) was additionally added into the medium. The suspension was dispensed in 1 ml cryotubes and cooled slowly (~ 1 °C/min) to -80 °C in a Mr. Frosty™ Freezing Container (Thermo Fisher Scientific GmbH, Schwerte, Germany) for 24 h. After this time, cells were transferred to a liquid nitrogen tank.

To defrost these cryopreserved cells, aliquots were thawed quickly in a 37 °C water bath. The cells were immediately transferred to a sterile 25 cm^2 cell culture flask containing 5 ml of the appropriate cell culture medium, and the medium was exchanged on the following day.

4.2.3 Quantification of eukaryotic cell concentration

To quantify the number of cell per ml cell culture medium, the Neubauer cell counting chamber was employed. Cells in four big squares were counted, and the concentration was calculated using the following formula:

$$c\left(\frac{cells}{\mu l}\right) = \frac{counted\ cells * 1{,}250 * DF}{4}$$

1,250: chamber factor; DF: dilution factor

4.2.4 Culturing of eukaryotic cells on permeable membrane supports

Human epithelial cells can be polarized, mimicking the physiological features, when cultured on permeable membrane supports, also called transwell filters. Figure 4.1 shows a schematic representation of a transwell filter inserted in a well of a 24-well plate. Cells grown on transwell filters differentiate into apical (luminal) and basolateral (abluminal) sides facing the upper and lower compartments, respectively, of the two-chambered filter support system.

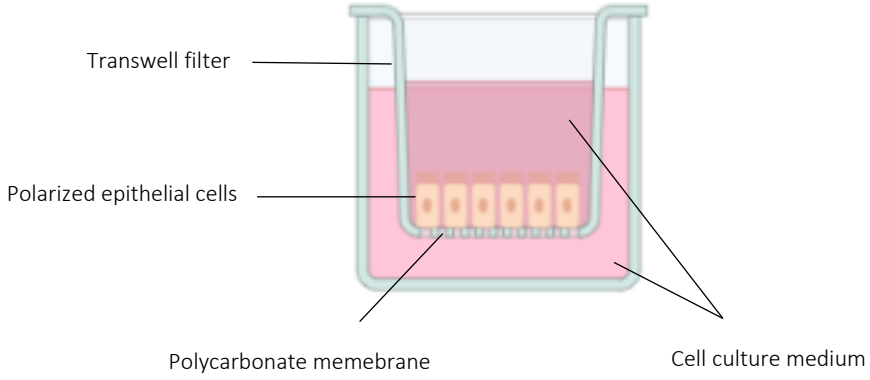

Figure 4.1. Schematic representation of epithelial cells grown on a transwell filter. The transwell filter allows polarization of the epithelial cells similar to those found in an *in vivo* state. Figure was made using the online illustrator program biorender.

Before seeding the cells on the transwell filters (Thincerts™ Cell Culture Inserts, Greiner Bio-One, Frickenhusen, Germany), these were placed in a 24-well plate and coated with extracellular matrix proteins (ECM). The ECM stock solution (Harbor Bio-Products, Norwood, MA, USA) was diluted in D-PBS (1:1000) to achieve a concentration of 0.1%. Approximately 150 µl of the diluted ECM was added onto the filters to cover the permeable membrane for 2 h at room temperature (RT). Afterward, the suspension was removed, and we let the membrane dry for 1 h more. Once the membrane was dried, 300 µl of the appropriate fresh cell culture medium was added to the apical side and 500 µl to the basolateral side. Filters were stored at 37 °C under 5% CO_2 while splitting and counting the cells. The epithelial cells were seeded on the permeable membrane in the upper compartment at a density of 1 x 10^5 cells/ml. The cells were culture for 7 days, until reaching confluency and the cell monolayer was fully polarized, and the medium was exchanged every other day.

4.2.5 Culturing of eukaryotic cells on dextran microcarrier beads

The Rotating Wall Vessel (RWV) bioreactor was employed to recapitulate the 3D spatial organization and polarity of the cells, as well as cellular differentiation, cellular complexity, and functionality. A complete description of the RWV bioreactor can be found in Chapter 1 (Introduction) in Section 1.7.1 (Rotating Wall Vessel-derived 3D models). Dextran Cytodex® 3 microcarrier beads (powder), previously coated, by the manufacturer, with denatured porcine-skin collagen, were employed to culture the epithelial cells on the beads. 50 mg of beads were hydrated by resuspending in 8 ml D-PBS (without Ca^{+2}/Mg^{+2}). The suspension was gently agitated on a roller for 3 h at RT. Then, the hydrated beads were sterilized according to the manufacturer´s instructions. After that, PBS (without Ca^{+2}/Mg^{+2}) was replaced for D-PBS (with Ca^{+2}/Mg^{+2}), and the beads were let in the washing medium until use. To culture the epithelial cells on the beads, an additional coating step was performed with 0.25 mg/ml fibronectin bovine protein (Sigma Aldrich Saint Louis, USA). The D-PBS (with Ca^{+2}/Mg^{+2}) solution was sucked off, and 1 ml of fibronectin, at the final concentration before mentioned, was added to the 50 mg hydrated porous beads. The beads were gently agitated on a roller for 1 h at 37 °C. The rest of the fibronectin was removed, and the beads were washed 3 times with fresh cell culture medium and transferred to the RWV bioreactor, previously filled with fresh cell culture medium. The bioreactor was placed inside the cell culture incubator at 37 °C under 5% CO_2 for 1 h to warm the beads and medium before seeding the cells inside the RWV bioreactor. Epithelial cells were seeded on the beads at a density of 5 x 10^6 cells/ 50 mg porous microcarrier beads. Cells and beads were cultured under rotating movements (10 rpm as a starting point) until the beads were completely covered by the cells. Confluency of the cells on the beads was controlled every 2-3 days by light microscopy.

4.2.6 Immunofluorescence microscopy

The analysis of the localization of the JAM-A within cells was conducted via fluorescence microscopy. Draq5 (Life Technologies, Carlsbad, USA) was used to label nuclear DNA in fixed cells. Draq5 is a DNA-detecting far-red-fluorescing dye, which permeates the cell membrane and binds the DNA with high affinity and selectivity (Smith *et al.*, 2004). To label the actin cytoskeleton, a phalloidin staining was performed. TRICT Phalloidin (Sigma-Aldrich, Taufkirchen, Germany) is a fungal toxin that binds to filamentous actin (Strickland *et al.*, 2004). The protein of interest was detected by a specific primary antibody (JAM-A J3F.1, Santa Cruz Biotechnology, Europe). The primary antibody was detected via species-specific secondary antibody labeled with Cy2 dye.

4.2.6.1 Immunofluorescence of cells grown on coverslips or transwell filters

Epithelial cells (HT29, HT29-MTX-E12 and LS174T) grown on coated coverslips or transwell filters were incubated with living bacteria after reaching confluency. After the incubation time, cells were fixed with 4% PFA in PBS (without Ca^{+2}/Mg^{+2}) at RT for 20 min. Next, cells were washed 3 times (5 min each) with PBS (without Ca^{+2}/Mg^{+2}) and incubated with 0,2% glycine for 20 min for quenching. The glycine is usually used to block unreacted aldehydes, which can increase the fluorescence background. Cells were again washed 3 times and incubated with 0.1% triton in PBS for 10 min. Blocking buffer (1% BSA in PBS without Ca^{+2}/Mg^{+2}) was added to the cells for 30 min at RT. Then, cells were incubated with the primary antibody, which was diluted 1:100, from the stock solution, in 0.1% blocking buffer, for 1:30 h at RT and then washed 3 times. The secondary antibody and TRICT Phalloidin were both diluted 1:500, from the stock solution, in 0.1% blocking buffer. The mixture was applied, and cells were incubated for 1 h at RT and then washed. Therefore, cells were incubated for 20 min with Draq5, which was diluted 1:500, from the stock solution, in PBS (without Ca^{+2}/Mg^{+2}). Cells were washed twice, and finally, were mounted with the Fluorescence Mounting Medium (DAKO Deutschland GmbH, Hamburg, Germany).

Samples were analyzed with the confocal CFSM LSM510 microscope (Carl Zeiss, Oberkochen, Germany). Co-localization analyses were determined with the BioImageXD software (University of Jyväskylä and Turka, Finland).

4.2.6.2 Immunofluorescence of cells grown in the RWV bioreactor

Epithelial cells (HT29-MTX-E12 and LS174T) grown on porous Cytodex® 3 microcarrier beads and cultured in the RWV bioreactor were incubated with either living bacteria or secreted proteins, present in the OMVs or supernatants, after cells became confluent on the beads. The same procedure, as explained in the Section 4.2.6.1, was followed only with few changes on the following incubation times: **1)** fixation and quenching, 30 min; **2)** blocking, 1 h; and **3)** primary and secondary antibodies, 1 h. Once finalized the immunostaining procedure described above, cells on beads were washed twice, and mounted with DAKO mounting medium. The same procedure, as described above for sample analysis, was followed.

4.2.7 Electron microscopy

The electron microscopy is used to study objects with up to 500,000 x magnification. In this study, this technique was employed to investigate the phenotypical features of the HT29-MTX-E12 cells, the formation of pedestals after infection of the epithelial cells with the pathogenic EPEC strain E2348/69 strain, and the content of the bacterial supernatants.

To analyze cell polarity, the junctional complex, microvilli formation, and secretion of mucin blebs, Transmission Electron Microscopy (TEM) was performed. HT29-MTX-E12 cells were cultured in the RWV bioreactor (5 x 10^6 cells/ml) or on transwell filters (1 x 10^5 cells/ml). Two samples were left untreated, and others were incubated with pathogenic or probiotic bacteria for a certain interval of time. After bacterial incubation, fixation, treatment, and analysis were performed by Lilo Greune (Institute of Infectiology, ZMBE, Münster). Cells were fixed with 2.5% PFA and 2.5% glutaraldehyde in D-PBS, pH 7.2 for 2 h at RT. Samples were further processed with 1% osmium tetroxide in D-PBS and afterward, with increasing concentrations of ethanol. 100% Epon 812 (Serva, Heidelberg, Germany) was used for morphological studies. 60 nm ultrathin sections were cut with the UC6 ultramicrotome (Leica, Viena, Austria). Cells were analyzed with the electron microscope Tecnai G^2 Spirit Twin (Fei, Eindhoven, Netherlands).

Negative staining was also performed to investigate the content of bacterial supernatants. Cell-free supernatants were prepared as described in Section 4.1.4. Phosphotungstic acid (PTA) in distilled water, pH 7.0, was used for contrasting staining. The negative staining procedure was performed by Lilo Greune (Institute of Infectiology, ZMBE, Münster).

4.3 Molecular Biology methods

4.3.1 RNA isolation from eukaryotic cells

The preparation of cellular RNA from cells was carried out using the RNeasy® Mini Kit (Qiagen, Hilden, Germany) according to the manufacturer´s instructions. Epithelial cells (HT29, HT29-MTX-E12 and LS174T) cultured on 24-wells, transwell filters or RWV bioreactor were incubated with bacteria or secreted proteins, and after infection, cells were lysed with 500 µl TRIzol® reagent. This reagent is a monophasic solution of phenol and guanidine isothiocyanate that facilitates the isolation of RNA, maintaining its integrity due to highly inhibition of RNase activity. After cell lysis with TRIzol®, 100 µl of chloroform were added, and the homogenate separates into a clear upper aqueous layer (containing RNA), interphase, and a red lower organic layer (containing the DNA and proteins) by centrifugation.

The upper, aqueous face was collected and mixed with 1.5 volume of 100% ethanol. The sample was then loaded to a spin column with a silica-based membrane, which allows the binding of the total RNA. The membrane was washed with RWT buffer, followed by a DNA digestion step and afterward, the membrane was washed with RPE buffer that eliminates contaminants. Finally, 18 µl of RNase-free water were added to the membrane to elute the RNA into a clean tube. The isolated RNA was stored at -80 °C.

4.3.2 RNA quality control

Quality control of RNA samples was performed using the QIAxcel® Advanced system (Qiagen). The system provides information about the size distribution, concentration, quality, and integrity of RNA by reporting the 28S/18S ratio and the RNA Integrity Score (RIS) number for analyzed samples. The quality control of the RNA samples was performed according to the manufacturer´s instructions. Before performing denaturation, the RNA concentration of each sample was adjusted to 50-300 ng/µl. The ScreenGel software version 1.6 was used to analyze the RNA samples.

4.3.3 Reverse transcription

By reverse transcription, RNA is converted into cDNA, thus creating a template for real-time PCR (qRT-PCR). The miScript II reverse transcription kit (Qiagen) was employed to reverse transcribe efficiently mRNA into cDNA. The procedure was followed according to the manufacturer´s instructions. The Transcriptase mix consists of a poly (A) polymerase and of a reverse transcriptase. Total mRNA is used as a starting material for reverse transcription reactions. The procedure includes incubation of the reaction at 37 °C for 1 h, followed by inactivation of the reaction by briefly incubating at 95 °C. Table 4.2 describes the pipetting scheme that was used to prepare the reverse transcription-polymerase chain reaction (RT-PCR).

Table 4.2. Reverse transcription reaction

Component	Volume/reaction
HiFlex Buffer	2 µl
10x Nucleics mix	1µl
Transcriptase mix	1µl
RNase-free water	4 µl
Template RNA	1 µl
Total volume	**10 µl**

The preparation of the cDNA for the RT^2 Profiler array includes a different protocol. The RT^2 First Strand Kit (50) (Qiagen, Hilden, Germany) was employed for cDNA synthesis prior to real-time PCR. This kit, together with the RT^2 Profiler PCR array, helps to monitor reverse transcription efficiency and tests for enzyme inhibitors contaminating RNA samples through a built-in external RNA control. Before cDNA synthesis, a genomic DNA elimination step was performed for each RNA sample according to Table 4.3. 10 µl reaction volume from Table 4.3 were added to a 10 µl reaction volume of Table 4.4. The procedure was followed according to the manufacturer´s instructions. For the reverse-transcription mix, the reaction was prepared as described in Table 4.4, and the procedure was followed according to the manufacturer´s instructions.

Table 4.3. Genomic DNA elimination mix

Component	Amount
RNA	25 ng – 5 µg (potential range)
Buffer GE	2 µl
RNase-free water	variable
Total volume	**10 µl**

Table 4.4. Reverse-transcription mix

Component	Volume/reaction
5 x Buffer BC3	4 µL
Control P2	1 µl
RE3 Reverse Transcriptase mix	2 µl
RNase-free water	3 µl
Total volume	**10 µl**

4.3.4 Quantitative real-time PCR

Quantitative real-time PCR (qPCR) enables reliable detection and measurement of products generated during each cycle of the PCR process. The intercalation of double-stranded DNA-binding dyes, such as SYBR Green, is used to monitor the progress of the PCR reaction. SYBR Green binds to newly synthesized DNA and the fluorescence signal of this dye increases when increasing the number of gene copies. In this study, qRT-PCR was used to quantify the relative gene expression in HT29, HT29-MTX-E12 and LS174T cells under different infection conditions. The cDNA obtained in the reverse transcriptase reaction (Section 4.3.3) was used as a template for qPCR, which was performed using a Light Cycler® 480 (Roche Diagnostics GmbH, Mannheim, Germany). Before amplification, the cDNA was diluted 1:10, 1:100 and 1:1,000 for the standard curve. Table 4.5 shows the reaction mixture for the qPCR. For the RT^2 Profiler PCR Array, the synthesized cDNA (Section 4.3.3) was mixed with the PCR components as described in Table 4.6, and 25 µl of the PCR components mix were added to each well of the RT^2 Profiler PCR Array. Before initiating the run, PCR plates were always centrifuged for 2 min at 500 g at RT to remove bubbles.

Table 4.5. qPCR pipetting scheme for mRNA amplification

Component	Volume/reaction
SYBR Green Buffer	5 µl
Primer A (diluted 1:20)	1 µl (5 pmol)
Primer B (diluted 1:20)	1 µl (5 pmol)
Distilled water	1 µl
cDNA template	2 µl
Total volume	**10 µl**

Table 4.6. PCR components mix for RT^2 Profiler PCR array

Component	96-well
Blue SYBR Green qPCR Kit	1350 µl
cDNA synthesis reaction	102 µl
RNase-free water	1248 µl
Total volume	**2700 µl**

The PCR cycler was programmed according to the conditions listed in Table 4.7 and Table 4.8

Table 4.7. Cycling conditions for real-time qPCR

Step		real-time qPCR		No. of cycles
Amplification	Initial denaturation	95 °C	5 s	1
	Denaturation	95 °C	5 s	40
	Annealing and elongation	60 °C	30 s	
Melting curve	Denaturation	95 °C	5 s	1
	Annealing	60 °C	1 min	
	Denaturation, melting	95 °C	continuos	
Cooling		50 °C	30 s	

Table 4.8. Cycling conditions for RT^2 Profiler PCR array

Step		RT^2 Profiler PCR Array		No. of cycles
Amplification	Initial denaturation	95 °C	10 min	1
	Denaturation	95 °C	15 s	45
	Annealing and elongation	60 °C	1 min	
Melting curve	Denaturation	95 °C	1 min	1
	Annealing	65 °C	2 min	
	Denaturation, melting	95 °C	continuos	
Cooling		50 °C	30 s	

4.4 Protein methods

4.4.1 Precipitation with trichloroacetic acid

Trichloroacetic acid (TCA) precipitates protein, DNA and RNA. This method was employed to precipitate the protein content in the supernatant of the probiotic EcN WT. TCA stock solution was diluted at a final volume of 10% in the sample solution and incubated 20 min on ice. Next, samples were centrifuged at 12,000 x g for 20 min, and the supernatant was discarded. Afterward, 300 µl of ice-cold acetone (previously store at -20 °C) were added, and samples were again centrifuged at 12,000 x g for 20 min. The supernatant was discarded and the pellet was air-dried and then suspended in 10 µl of 1x SDS-PAGE sample buffer. If the color after adding the SDS-PAGE sample buffer turned from blue to yellow, a few drops of NaOH were added to increase the pH.

4.4.2 Preparation of eukaryotic cell lysates

Epithelial cells grown on transwell filters or on porous beads in the RWV bioreactor were infected under different specific conditions. Cells were lysed after infection experiments to detect specific proteins in the eukaryotic homogenate. For that, cells were suspended in 4x SDS-PAGE sample buffer (62.5 mM Tris-HCl, pH 6.8; 3% SDS; 10% glycerol; 8% β-mercaptoethanol; spatula point bromophenol blue), and the mixture was very well vortexed. Afterward, DNA within the lysate sample were shredded using a syringe needle, briefly centrifuged, and subsequently, proteins in the sample were heat-denatured at 95 °C for 10 min. Samples were placed on ice for 2 min and centrifuged at 10,000 g for 5 min at 4 °C to clear the lysates. This last step was always performed before loading the lysates on an SDS-PAGE gel (Chapter 4, Section 4.4.3) for Western blotting analyses. Cells´ lysates were stored at -20 °C.

4.4.3 Sodium dodecyl sulfate-polyacrylamide gel electrophoresis

The sodium dodecyl sulfate-polyacrylamide gel electrophoresis (SDS-PAGE) is an analytical technique to separate proteins based on their molecular weight and was performed according to Laemmli, 1970. Polyacrylamide gels were prepared in a multiple gel caster (Hoefer Inc., Holliston, USA). First, the resolving gel was prepared according to the recipe in Table 4.9 and pored into the caste. Then, a thin layer of pure isopropanol was added to the gel to avoid air bubbles and allowed to polymerize. Once the gel was polymerized, the isopropanol was discarded, and the stacking gel was poured on top of the resolving gel.

Table 4.9. Polyacrylamide SDS-PAGE gel mixtures for five mini gels

Stock solutions	12.5% Resolving gel	5% Stacking gel
30% acrylamide	15 ml	3 ml
Resolving gel solution	7.5 ml	-
Stacking gel solution	-	3 ml
10% APS	330 µl	180 µl
10% SDS	150 µl	100 µl
Distilled water	13.5 ml	11.9 ml
TEMED	18 µl	9 µl

APS: ammonium persulfate; TEMED: N,N,N´,N´-tetramethylethylethylendiamine

Protein samples from cell lysates were prepared as described in Section 4.4.2. 5 µl of the protein sample were mixed with 5 µl of 1x SDS-PAGE sample buffer before loading onto the polyacrylamide gel. Polyacrylamide electrophoresis was performed using the running buffer (25 mM Tris-HCl, pH 8.8; 192 mM glycine; 0.1% SDS w/v) and allowed to run at 15 mA per gel. Once the protein marker VI started to be separated, the current was increased to 50 mA.

4.4.4 SDS-PAGE gel staining with Coomasie

Coomasie brilliant blue R-250 is a dye that has been used to stain SDS-PAGE gels (Section 4.4.3) in order to visualize protein bands. After electrophoresis, the SDS-PAGE gel was incubated in a Coomasie brilliant blue R-250 solution (3.3 mM Coomasie brilliant Blue R-250; 50% v/v ethanol; 10% v/v acetic acid) for 20 min under gentle agitation. Next, the gel was destained using a destaining solution (10% v/v ethanol; 7% v/v acetic acid) until the protein bands could be visualized. Finally, the gel was washed in distilled water before the acquisition of a picture.

4.4.5 Western blotting

Semi-dry Western blotting was employed to detect the protein of interest within a cell lysate using specific antibodies. The SDS-PAGE gel (Section 4.4.3) was soaked in a cathode buffer (25 mM Tris-HCl; 40 mM glycine; 10% methanol; pH 9.4) and then transferred to a polyvinylidene difluoride membrane (PVDF Western Blotting Membrane, Roche Diagnostics GmbH, Mannheim, Germany) activated in methanol before usage. Gel and membrane were placed between 6 pieces of Whatman paper (Figure

4.2). Three of the paper pieces were soaked in the cathode buffer, one of them in anode buffer II (25 mM Tris-HCl; 10% methanol; pH 10.4), and two of them in anode buffer I (0.3 mM Tris-HCl; 10% methanol; pH 10.4). Once the pieces were placed, a pipet was rolled over the surface of the paper (like rolling) to exclude all air bubbles. Blotting of the proteins was performed in a (peqLab HEP-1 Semidry, Thermo Fischer Scientific). Proteins were transferred for 75 min at 25 V.

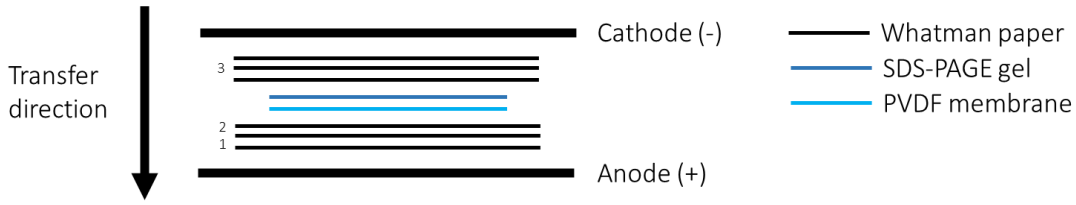

Figure 4.2. The semi-dry Western blot transfer system. 1: two paper pieces in anode buffer I; 2: one paper piece in anode buffer II; 3: three paper pieces in cathode buffer.

Upon transferring the proteins on to the PVDF membrane, this was dried for 5 min and again activated in methanol. The methanol was washed away with water, and the blocking buffer (5% non-fat milk powder in 1 x TBS-Tween 20) was poured onto the membrane and incubated for 1 h at RT with gentle agitation. Next, the primary antibody (Chapter 3, Section 3.4, Table 3.4) was diluted 1:1,000, from the stock solution, in blocking buffer containing only 0.5% non-fat milk powder, and the membrane was incubated overnight at 4 °C. The membrane was washed 3 times with TBST for 5 min and then incubated for 1 h at RT with the secondary antibody (conjugated with horseradish peroxidase; Table 3.4) diluted 1:5,000, from the stock solution, in blocking buffer. The membrane was washed as described above, including an additional washing step with 1x TBS for 5 min. Finally, the blot was developed using the enhanced chemiluminescent (ECL) Western Blotting Substrate (Pierce Biotechnology, Rockford, USA) and detected with LI-COR imager (LI-COR Biosciences GmbH, Germany). The relative protein quantification was performed using the LI-COR imager as well.

To detect another antigen, the previous antibodies were removed boiling the membrane briefly in stripping buffer (0.2M glycine in PBS, pH 2.0) and subsequently washing the membrane 3 times extensively with TBST before blocking. The next antigen was detected following the steps described previously.

4.5 Experimental procedures and sample analysis

4.5.1 Infection of eukaryotic cells with living bacteria

For infection experiments, HT29-MTX-E12 cells and LS174T cells grown on transwell filters or on porous beads were cultured with fresh Pen/Strep-free medium containing 5% FCS and 2% GlutaMax. Approximately 24 h before infection, cells were washed 3 times with D-PBS (with $Ca^{+2}/Mg^{+}2$) to remove the antibiotic within the cell culture medium, and new fresh Pen/Strep-free medium was added. Before infection, cells on the beads were divided into similar amounts and then transferred to a 24-well plate. A sample was used to count the cells grown on the beads. For that, beads were incubated with 300 ml of 1x trypsin/EDTA solution at 37 °C until they detached from the beads (~ 30 min). This sample was used only to count cells; therefore, after counting, the sample was discarded. Overnight bacterial cultures were diluted 1:10 in LB medium to measure the optical density at 600 nm (OD_{600}). An appropriate volume for a final infection of 20, 50, or 100 bacteria per host cell, also denoted as a multiplicity of infection (MOI), was added to the cells for different time intervals. In the case of cells grown on the transwell filters, the bacteria were inoculated at the apical side. Beads on the 24-well plate were infected under static conditions.

4.5.2 Infection of eukaryotic cells with OMVs and cell-free supernatants

Cells grown in the RWV bioreactor were incubated with OMVs or cell-free supernatants at different concentrations. Before infection, cells were manipulated as described in Section 4.2.6. Next, cells were inoculated with 20 µg/ml, 25 µg/ml, 30 µg/ml, and 35 µg/ml of protein from bacterial OMVs or cell-free supernatants for 4 h under static conditions.

4.5.3 Pre-infection of eukaryotic cells with EPEC strain E2348/69

Epithelial cells that were grown on coated wells, transwell filters, or porous Cytodex® 3 beads were washed 3 times with D-PBS (with $Ca^{+2}/Mg^{+}2$), and culture with fresh Pen/Strep-free medium containing 5% FCS and 2% GlutaMax 1 day before infection with the living bacteria EPEC E2348/69. Cells were infected with EPEC at an MOI of 20 or 50 for a certain time (2 h or 4:30 h). After the time of infection, EPEC was removed by washing the cells several times with D-PBS (with $Ca^{+2}/Mg^{+}2$) and then incubating the cells with 30 µg/ml or 250 µg/ml of gentamicin for 1 h at 37 °C to kill all the bacteria that could be left. Next, cells were again washed several times, carefully, to remove the antibiotic, and fresh

Pen/Strep-free cell culture medium was added to the cells. Then, cells were incubated with either probiotic bacteria at MOI 20 or 50, or with 30 µg/ml of protein of bacterial OMVs or with 20 µg/ml of protein of bacteria-free supernatant for a specific time.

4.5.4 Rotating infection

The HT29-MTX-E12 and LS174T epithelial cells were infected under the presence of low-fluid shear stress. For that, cells grown in the RWV bioreactor were washed 3 times with D-PBS (with Ca^{+2}/$Mg^{+}2$), and transferred to disposable 10 ml chambers ("D-410", Synthecon Inc., Houston, Texas, USA) with Pen/Strep-free medium containing 5% FCS and 2% GlutaMax, 24 h before infection. As explained before, overnight bacterial cultures were diluted 1:10 in LB medium, and OD_{600} was measured. An appropriate volume for a final MOI of 50 was added to the cells into the disposable chambers, and the infection was performed under dynamic conditions (14 rpm) for different intervals of time.

4.6 Bioinformatic analysis

4.6.1 Data presentation

Data are presented as the standard error of the mean (SEM) using the Prism 8 software (GraphPad Software Inc., La Jolla, USA).

4.6.2 Calculation of statistic significances

Statistical significances were calculated with the Prism 8 software, using the one-tailed, unpaired nonparametric Student´s *t-test* function. The following symbols were used to indicate calculated *p* values: * = 0.05; ** = 0.01; *** = 0.001.

4.6.3 Calculation of mRNA expression

The primer pairs for the real-time qPCR were designed with the Primer-BLAST tool of the National Center for Biotechnology Information (NCBI) and synthesized by Eurofins MWG Operon (Ebersberg, Germany). The HPRT primers (Chapter 3, Table 3.3) were used as reference (house-keeping genes) for the mRNA quantification. The relative quantification of the mRNA expression was calculated according to the calibration curve obtained from the HPRT dilutions. The RT^2 Profiler PCR Array (PAHS-148ZF) was

purchase from Qiagen, and the mRNA expression was quantified using the delta-delta Ct method. Data analysis for the Array was conducted at the Qiagen´s GeneGlobe Data Analysis Center using a software-based tool.

CHAPTER 5

RESULTS

It has been reported that the probiotic EcN may exhibit part of its beneficial activities through the modulation of the epithelial barrier function (Ukena *et al*., 2007). To further investigate the impact of EcN on the intestinal epithelial barrier function and to elucidate the underlying mechanisms of the EcN-dependent strengthening of the epithelial barrier function, we were interested in analyzing the expression and distribution of the tight junction protein Junctional Adhesion Molecule A (JAM-A). Since JAM-A is the leading protein in junctional complex formation, its phosphorylation and its subsequent delivery to the cell membrane is an important process in the regulation of intestinal permeability. Besides this, the anti-inflammatory activity of EcN was analyzed as well. The transcript levels of Myeloid differentiation primary response (MyD88), Toll-like receptor 5 (TLR5), and of different cytokines in the human mucin-producing cell line HT29-MTX-E12 were monitored after incubation of the probiotic strain with host cells.

In previous studies, Pund (2017) investigated the kinetics of *JAM-A* gene expression in HT29-MTX-E12 cells regarding the time of incubation and the multiplicity of infection (MOI) of EcN. The results showed that 4 h of incubation time and an MOI of 50, as well as the number of bacteria per cell, were the best starting point parameters to perform expression analysis of targeted genes (Pund, 2017).

5.1 Kinetics of *JAM-A* expression in HT29-MTX-E12 cells after infection with enteropathogenic *E. coli* strain E2348/69

In order to determine whether the probiotic EcN has an impact on *JAM-A* expression and on the modulation of pro-inflammatory cytokines, enteropathogenic EPEC strain E2348/69 was employed as a reference to compare differences in host responses between probiotic and pathogenic bacteria. EPEC strain E2348/69, which in these experiments was employed as the representative EPEC strain, is well known to disrupt intestinal epithelial tight junction architecture causing chronic diarrhea. The mucin-producing HT29-MTX-E12 cells were infected with EPEC strain E2348/69 for 2 h and 4 h with a different MOI of 20, 50, and 100 to identify the best conditions for infection. These experiments were also performed in two different cell culture systems: the conventional 2D system, which contained 2 x 10^5 cells, and on transwells filters, which contained 1 x 10^5 cells (denoted as “2.5D” system). The 2D model allows cell-to-cell contact only on edges, and further differentiation of cells does not take place. The 2.5D model allows a cell culture environment that closely resembles the *in vivo* state. It allows apical-

basal polarity to contribute to cell morphology, directional vesicle transportation, ion and solute transport, and specific localization of proteins and lipids to different membrane domains (Tapia *et al*., 2017). Therefore, we compared *JAM-A* expression by quantitative real-time PCR (qRT-PCR) in cells growing in these two different cell culture systems. Infections carried out in the 2.5D cell culture system were done from the apical side.

JAM-A expression levels were increased in EPEC-infected cells growing in the 2.5D model (Figure 5.1). A statistically significant difference in *JAM-A* expression between both systems was seen after 2 h EPEC infection with an MOI 100 (Figure 5.1, **A,** 2D *vs*. 2.5D). EPEC E2348/69 had a higher impact on the downregulation of *JAM-A* expression at 2 h post-infection than at 4 h in the 2D system (0.3 *vs*. 0.1-fold decrease respectively, which means that *JAM-A* expression was 0.3 or 0.1 times smaller) (Figure 5.1, **A-B,** filled red columns). Similar results could be seen in the transwell inserts, except for the 2 h time point with an MOI 100, where *JAM-A* expression was elevated in comparison to the other samples (Figure 5.1, **A-B,** unfilled red columns). A statistically significant *JAM-A* downregulation between 2D untreated cells and 2D cells treated for 2 h at MOI 20 was seen (0.3-fold decrease) (Figure 5.1, **A**). Besides that, there were no significant changes in *JAM-A* expression between the different MOI in both systems. In the 2D model, the downregulation of the targeted gene was more evident than in the 2.5D model (Figure 5.1, **A-B**).

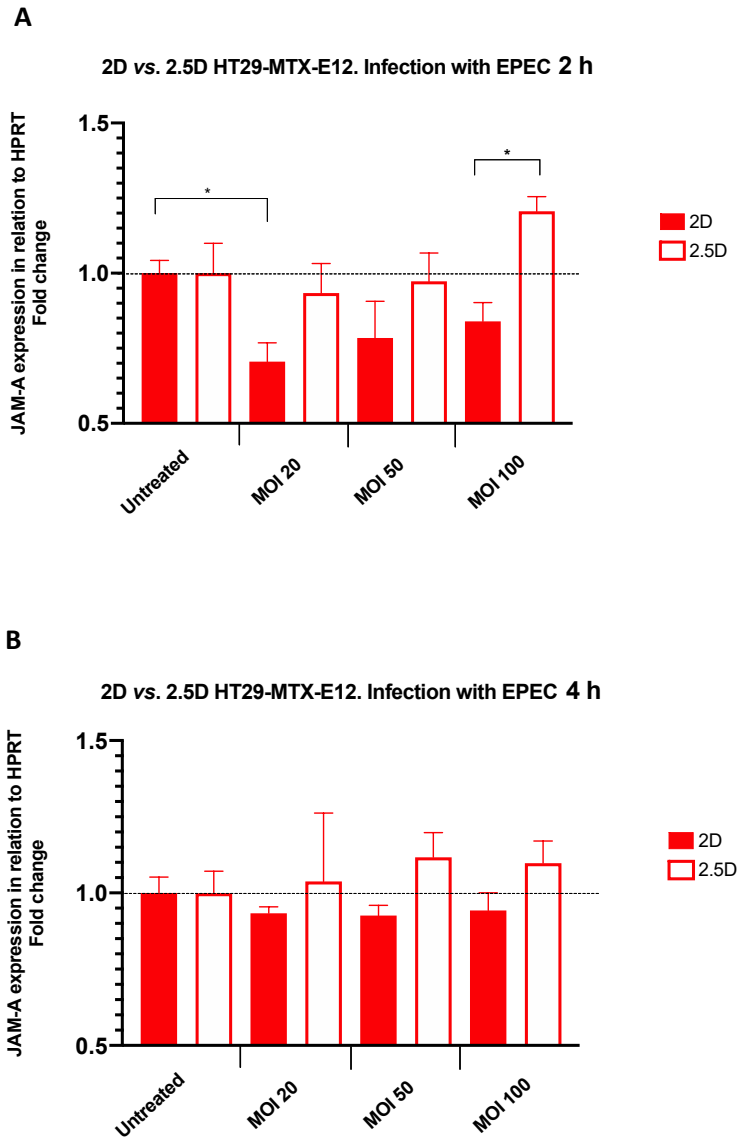

Figure 5.1. *JAM-A* expression in mucin-producing HT29-MTX-E12 cells grown in two different cell culture models in the conventional 2D system and in the 2.5D system (transwell filters). Cells were infected with the enteropathogenic strain *E. coli* EPEC strain E2348/69 for 2 h and 4 h with different MOIs: 20, 50, and 100**.** Control cells were left untreated. **A)** *JAM-A* expression at 2 h post-infection. **B)** *JAM-A* expression at 4 h post-infection. The analyses were performed by quantitative real-time PCR. The data were normalized using the housekeeping gene HPRT transcript levels. All results are presented as fold-changes relative to the untreated control. The data were obtained from at least three independent experiments performed in duplicates. The error bars show the standard error of the mean (SEM). *p<0.05.

These data show the importance of a cell culture model that allows a proper cellular differentiation and a complete tight junctional complex formation to study host-microbe interactions.

5.2 Kinetics of *JAM-A* expression in HT29-MTX-E12 cells after incubation with the probiotic *E. coli* strain Nissle 1917 variant 3595

To carry out incubation experiments with the EcN variants, we first wanted to optimize a proper time and MOI to establish suitable conditions for analysis. Therefore, just as described in 5.1 for EPEC incubation conditions, we first set up experiments with HT29-MTX-E12 cells incubated with the EcN variant 3595 (Chapter 3, Table 3.2). In the same way, the two different cell culture systems were employed, using the same number of cells as described before, to compare the expression of *JAM-A*. In Figure 5.2, it is shown that cells were incubated with EcN variant 3595 for different time intervals and with different MOIs. In general, *JAM-A* expression was higher in cells grown in the 2.5D system. After 2 h bacterial incubation, *JAM-A* expression decreased with increasing the MOI. The downregulation was significant at an MOI of 100 compared to control cells (0.3-fold decrease) (Figure 5.2, **A**. 2D system). In the 2.5D system, *JAM-A* expression was upregulated with increasing MOI (0.1 – 0.4-fold increase). *JAM-A* response was different between both systems; in one system (2D, filled black columns) the tendency was going down, while in the other (2.5D, filled blue columns) it was going up (Figure 5.2, **A**). Moreover, to evaluate different time points, an MOI of 20 was used to incubate cells with EcN variant 3595. At 6 h *JAM-A* expression reached its highest level in both systems. At 2 h there was no evident change of the expression in both models, and at 4 h *JAM-A* expression increased 0.3 fold, compared to the untreated cells, in the 2.5D system (blue columns), while in the 2D system *JAM-A* expression decreased 0.1 fold (black columns) (Figure 5.2, **B**). A time curve using an MOI of 50 was performed to analyze *JAM-A* expression in cells grown in the 2.5D culture system (transwell inserts). It can be seen that at 4 h *JAM-A* expression had a higher response with a 0.7-fold increase in comparison with the other time points (Figure 5.2, **C**).

A

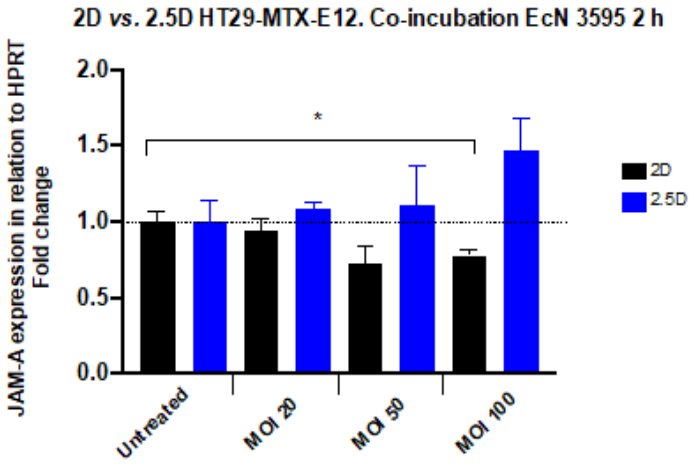

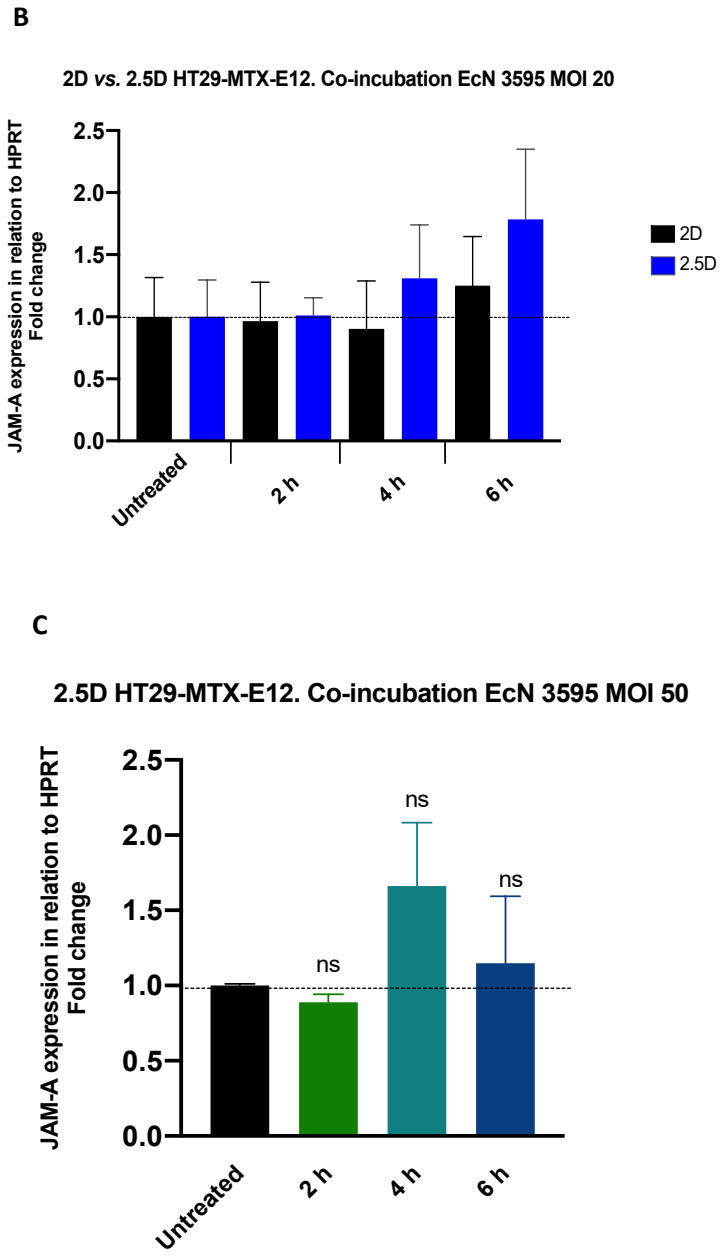

Figure 5.2. *JAM-A* expression in mucin-producing HT29-MTX-E12 cells grown in two different cell culture models in the conventional 2D system and in the 2.5D system (transwell filters). Cells were incubated with the variant 3595 of probiotic EcN for several hours and with different MOIs: 20, 50, and 100**.** Control cells were left untreated. **A)** *JAM-A* expression after 2 h incubation at different MOIs. **B)** *JAM-A* expression after 2 h, 4 h, and 6 h incubation at MOI 20. **C)** *JAM-A* expression after 2 h, 4 h, and 6 h incubation at MOI 50. The analyses were performed by quantitative real-time PCR. The data were normalized using the housekeeping gene HPRT transcript levels. All results are presented as fold-changes relative to the untreated control. The data were obtained from at least three independent experiments performed in duplicates. The error bars show the standard error of the mean (SEM). *p<0.05.

Levels of *JAM-A* transcript were different between the 2D and 2.D cell culture models. EcN variant 3595 also had a different effect on cells grown in one or another system. It was generally seen that this probiotic variant has a negative impact on *JAM-A* expression on cells cultured in 2D wells. Contrarily, a positive effect of this variant was seen for the *JAM-A* gene expression of cells cultured in the 2.5D wells.

5.3 Response of mucin-producing HT29-MTX-E12 cells to the EPEC strain E2348/69 and the different variants of the probiotic EcN

5.3.1 JAM-A response in HT29-MTX-E12 cells

To investigate the effect of the ten EcN variants and the EPEC strain E2348/69 used in this study, on intestinal epithelial mucin-producing cells, 1 x 10^5 human adherent HT29-MTX-E12 cells were grown on transwell filters until reaching confluency. The 3D cell culture model was also employed to compare JAM-A response in cells grown in two different culture systems.

Cells grown on beads (5 x 10^6 cells on 50 mg fibronectin-coated beads) showed a decrease in *JAM-A* expression levels (0.3-fold) after their incubation with different *E. coli* strains and EcN variants. However, a 0.4 and 0.1-fold increase of *JAM-A* expression was seen when cells were incubated with EcN variants 3598 and 3413, respectively (Chapter 3, Table 3.2) (Figure 5.3.1, **A**, green columns). Cells grown in the 2.5D system did not show a significant reduction of *JAM-A* expression in comparison with the non-incubated cells (Figure 5.3.1, **A**, grey columns). In general, *JAM-A* expression was higher in the 2.5D model than in the 3D model (Figure 5.3.1, **A**).

After 4 h incubation, there was an increase of *JAM-A* transcript levels of cells incubated with EPEC strain E2348/69, but a decrease after EcN WT, and EcN variant 3595 incubation (0.3-fold decrease). An increase of *JAM-A* expression was seen upon incubation with the other variants of EcN (Figure 5.3.1, **B**, 3D). In the 2.5D system, there was a decrease of 0.4-fold of *JAM-A* expression when cells were infected with EPEC strain E2348/69. HT29-MTX-E12 cells exhibited an increase of *JAM-A* transcript levels (0.10 - 0.15 fold) when incubated with the different variants of probiotic strain EcN, but a slight decrease of *JAM-A* was seen for the EcN variants 3426 and 3414 (Figure 5.3.1, **B**, 2.5D). These results demonstrate a higher bacterial effect on *JAM-A* expression levels when the epithelial cells are challenged with the different bacterial strains for 4 h.

A significant difference between the expression of *JAM-A* in the 2.5D and 3D systems was visible for those cells incubated with EcN WT and EcN variant 3595 for 4 h. *JAM-A* transcript levels were higher in the 2.5D system (Figure 5.3.1, **B**).

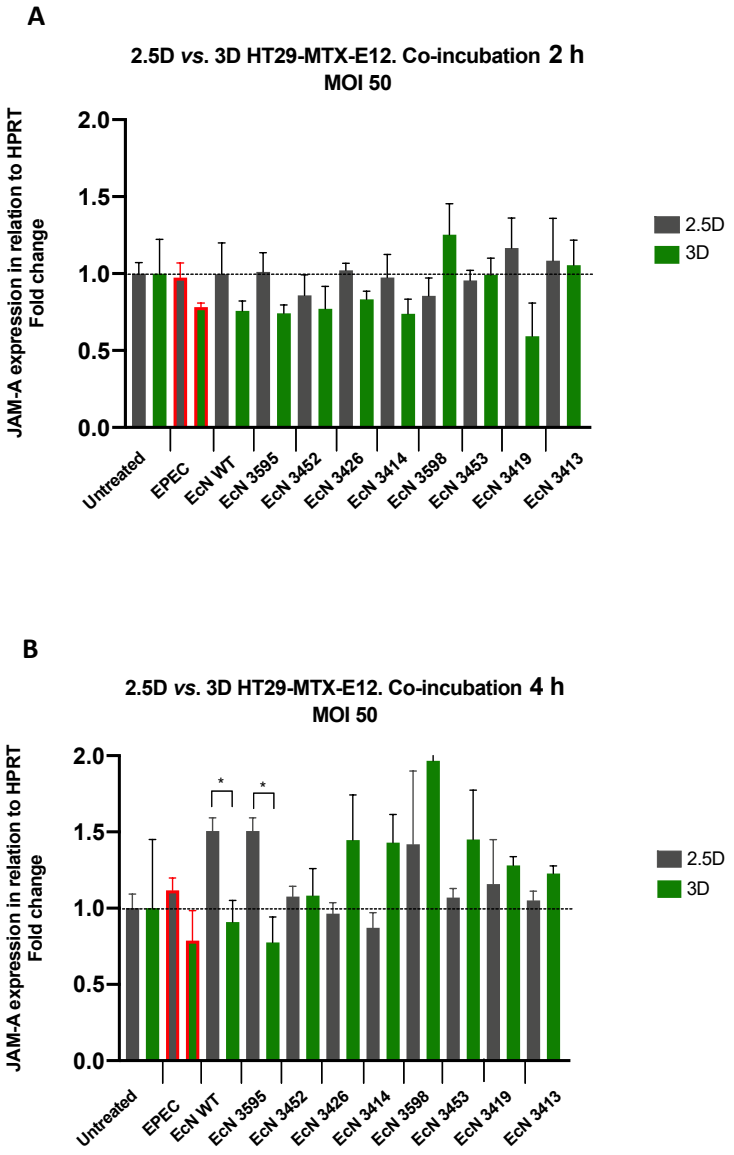

Figure 5.3.1. ***JAM-A*** **expression in mucin-producing HT29-MTX-E12 cells grown in two different cell culture models in the 2.5D system (transwell filters), and the Rotating Wall Vessel (RWV) bioreactor (3D system).** Cells were incubated with the EPEC strain E2348/69 strain and different variants of probiotic strain EcN for 2 h and 4 h with an MOI 50**.** Control cells were left untreated. **A)** *JAM-A* expression after 2 h incubation at MOI 50. **B)** *JAM-A* expression after 4 h incubation at MOI 50. Analyses were performed by quantitative real-time PCR. The data were normalized using the housekeeping gene HPRT transcript levels. All results are presented as fold-changes relative to the untreated control. The data were obtained from at least three independent experiments performed in duplicates. The error bars show the standard error of the mean (SEM). *p<0.05. The red outline represents cells infected with the EPEC strain E2348/69.

These data show that *JAM-A* expression levels were different between the 2.5D and 3D systems. In the same way, differences in *JAM-A* transcript levels could be seen between the two intervals of time. EPEC and EcN variants induced a different effect on the *JAM-A* expression of HT29-MTX-E12 cells; however, these differences were not significant.

5.3.2 Myeloid differentiation primary response (*MyD88*) expression in HT29-MTX-E12 cells

MyD88 is a central regulator during innate immune response and a primary adaptor protein of nearly all Toll-Like receptors signaling pathways. It triggers the activation of the NF-κB pathway for the induction of inflammatory cytokines genes conferring protection against several enteric bacterial pathogens (Kawasaki *et al*., 2014). To determine the response of the mucin-producing HT29-MTX-E12 epithelial cells to EPEC infection and different EcN variants incubations in terms of expression levels of the MyD88 adaptor factor, HT29-MTX-E12 cells grown in the 2.5D and 3D cell culture systems were treated with an MOI of 50 for 2 h and 4 h (Figure 5.3.2, A-B).

Cells grown in the 3D cell culture system showed a slight decrease in *MyD88* expression in comparison with the untreated samples. But in the case of those cells incubated with the EcN variants 3598, 3419, and 3413 *MyD88* expression levels increased between 0.1 and 0.5-fold, being also higher than the *MyD88* transcript levels in cells infected with the enteropathogenic *E. coli* strain (Figure 5.3.2, A, green columns). The relative expression of *MyD88* was higher in the cells cultured in the 2.5D system. However, for the EcN variants 3598 and 3453, the expression of the adaptor protein was higher in the 3D system than in the 2.5D system. After 2 h incubation, cells infected with the EPEC strain E2348/69 showed the highest value of *MyD88* expression in the 2.5D cell culture system (1-fold increase) (Figure 5.3.2, A, grey columns).

After 4 h of incubation, *MyD88* expression decreased in HT29-MTX-E12 cells cultured on the 3D model and incubated with the enteropathogenic and probiotic bacteria. However, the two EcN variants 3414 and 3598 induced an increase (0.3-fold) in the relative *MyD88* expression level (Figure 5.3.2, B, 3D, green columns). Similarly, a decrease of *MyD88* expression was seen in cells cultured in the 2.5D system except for EcN variant 3426 that induced a 0.3-fold increase in *MyD88* transcript levels (Figure 5.3.2, B, 2.5D, grey columns). EPEC strain E2348/69 had a stronger effect on the reduction of *MyD88* expression after 4 h than after 2 h in both cell culture systems (Figure 5.3.2, A-B).

There were no significant differences in the expression of *MyD88* between cells cultured in the 3D or 2.5D models.

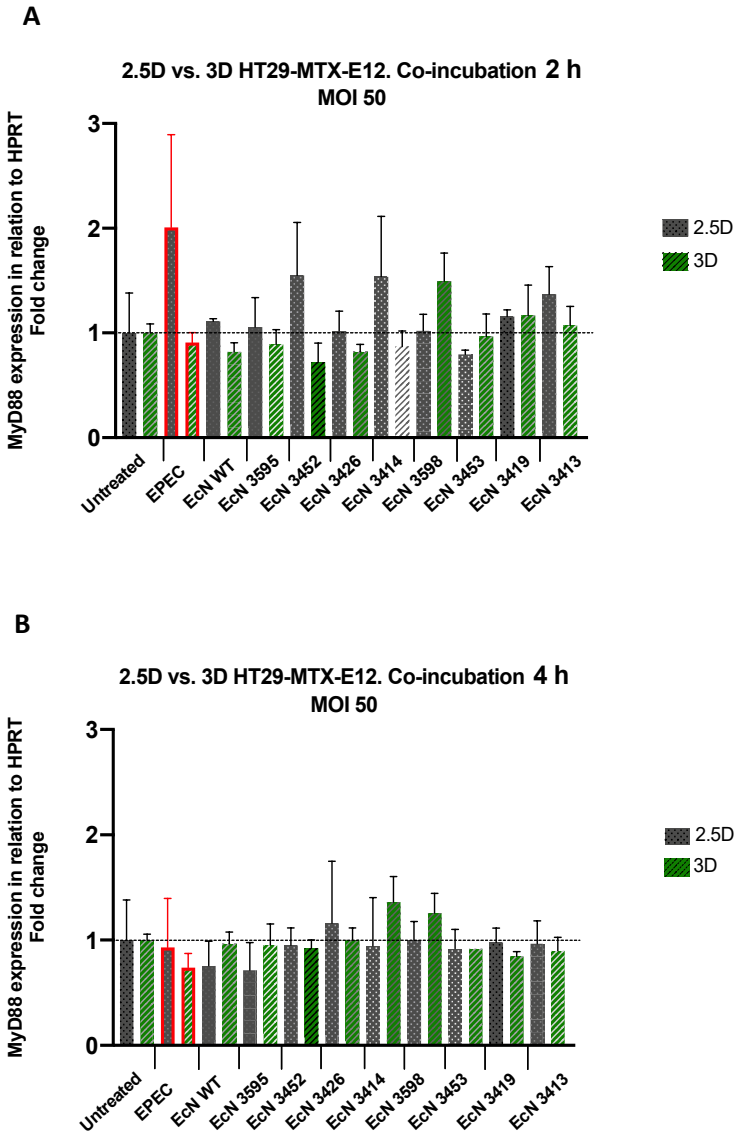

Figure 5.3.2. *MyD88* expression in mucin-producing HT29-MTX-E12 cells grown in two different cell culture models employing transwell filters (2.5D system) or the Rotating Wall Vessel (RWV) bioreactor (3D system). Cells were incubated with the EPEC strain E2348/69, and different probiotic variants of probiotic strain EcN for 2 h and 4 h with an MOI of 50. Control cells were left untreated. **A)** *MyD88* expression after 2 h incubation at MOI 50. **B)** *MyD88* expression after 4 h incubation at MOI 50. The analyses were performed by quantitative real-time PCR. The data were normalized using the housekeeping gene HPRT transcript levels. All results are presented as fold-changes relative to the untreated control. The data were obtained from at least three independent experiments performed in duplicates. The error bars show the standard error of the mean (SEM). The red outline represents cells infected with the EPEC strain E2348/69.

In summary, *MyD88* expression levels differed between the 2.5D and 3D systems. In general, after 4 h incubation, there was a higher decrease of *MyD88* than after 2 h incubation. A downregulation of *MyD88* transcript levels might be necessary for bacterial survival with respect to the hosts´ immune system.

5.3.3 Occludin response in HT29-MTX-E12 cells

Occludin is part of the tetraspanin family of integral proteins with a molecular mass of ~ 65 kDa. It has four membrane-spanning domains and two extracellular loops. Occludin is located at the tight junctions of epithelial and endothelial cells and plays a role in the barrier properties of tight junctions (Feldman *et al*., 2005). In Figure 5.3.3 the relative expression of *occludin* is shown as fold-change relative to the untreated control. At 2 h post-incubation (hpi) of HT29-MTX-E12 cells and different *E. coli* strains, there was an increase in the expression of the tight junction protein in cells incubated with all tested bacterial variants. There was a significant increase of 0.3-fold in occludin gene expression in cells incubated with the EcN variant 3595 (Figure 5.3.3, 2 hpi). At 4 h post-incubation, there was a reduction in the transcript levels of occludin. A significant decrease was seen in cells incubated with EPEC strain E2348/69, EcN WT, EcN variants 3595 and 3452 compared to untreated cells (Figure 5.3.3, 4 hpi).

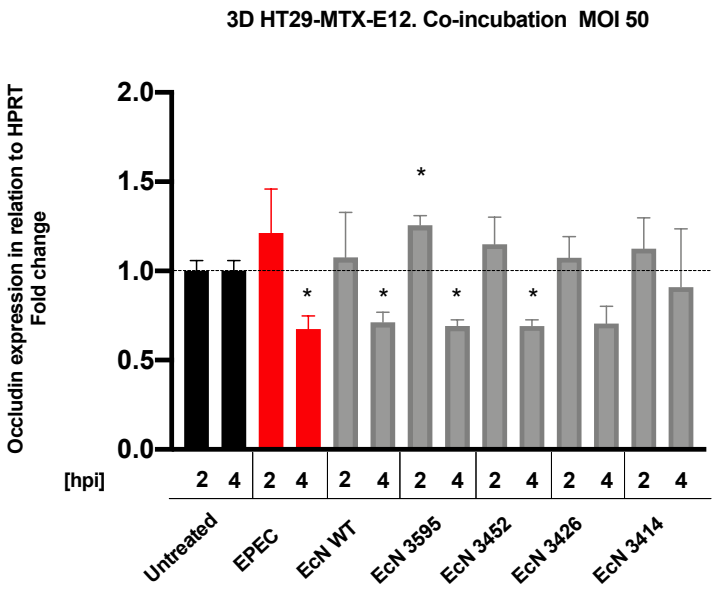

Figure 5.3.3. Occludin expression in mucin-producing HT29-MTX-E12 cells grown in the 3D system. Cells were incubated with the EPEC strain E2348/69 and different variants of probiotic strain EcN for 2 h and 4 h and at an MOI of 50. Control cells were left untreated. The analysis was performed by quantitative real-time PCR. The data were normalized using the housekeeping gene HPRT transcript levels. All results are presented as fold-changes relative to the untreated control. The data were obtained

from at least three independent experiments performed in duplicates. The error bars show the standard error of the mean (SEM). *p<0.05. [hpi] = hours post-incubation.

Occludin expression increased in HT29-MTX-E12 cells, cultured in the RWV bioreactor, after 2 h incubation with pathogenic and probiotic bacteria, while it decreased after 4 h incubation compared to control cells.

RNA expression levels of Toll-like receptor 5 (*TLR5*) and human β-defensin 2 (*hBD-2*) encoding genes in HT29-MTX-E12 cells incubated with pathogenic and probiotic strains, were also analyzed. hBD-2 is an antimicrobial peptide synthesized by the mucosal epithelium. It has a broad antibiotic spectrum against Gram-negative and Gram-positive bacteria, as well as against fungi and viruses. hBD-2 is induced by a bacterial infection and it might reinforce the mucosal barrier, thus limiting bacterial adherence and invasion (Schlee *et al*., 2007). Schlee *et al*. showed the induction of *hBD-2* by the probiotic EcN in Caco-2 cells (Schlee *et al*., 2007). However, the expression levels of *TLR5* and *hBD-2* genes were drastically downregulated in the experiments done in this study. We could not confirm the induction of *hBD-2* by the probiotic strain (data not shown).

5.4 Evaluation of the quality of the isolated RNA from HT29-MTX-E12 cells

Before analyzing gene expression, under different incubation conditions by qRT-PCR, we evaluated size, quality, and quantity of the RNA that was isolated using the RNeasy® Mini Kit (50) (Qiagen) according to standard methods and as described before (Chapter 4, Section 4.3.2). Total RNA isolation samples were prepared for capillary electrophoresis according to the protocol in the *QIAxcel RNA Handbook*. Figure 5.4 **A**, shows a screen gel of the total RNA purified from HT29-MTX-E12 cells incubated with pathogenic and probiotic *E. coli* strains. There were two distinct rRNA bands: 18S with a size of approximately 1950 nt, and 28S with a size of around 5000 nt. Figure 5.4 **B**, shows an example of an electropherogram of the total RNA purified from HT29-MTX-E12 cells infected with the EPEC strain E2348/69. The two distinct peaks correspond to the 18S and 28S RNA. The first peak with 15 nt corresponds to the marker sample, and a small peak with 87 nt might correspond to tRNA that has a size of about 80 nt in eukaryotic cells.

A

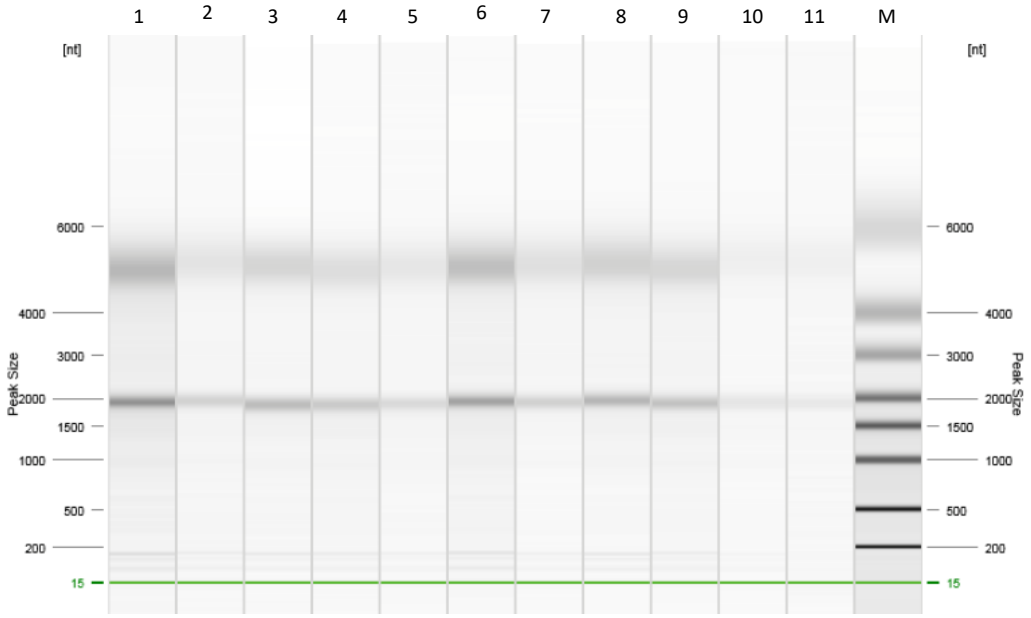

B

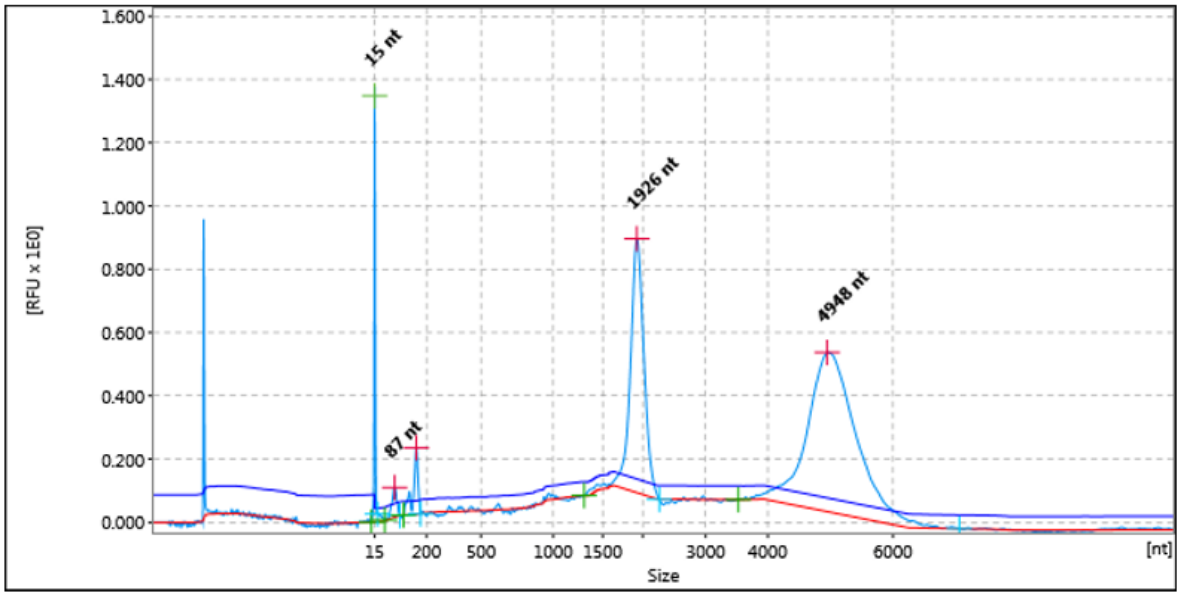

Figure 5.4. Streamlined RNA analysis using the QIAxcel system. Results presented **A)** as a gel view of 18S and 28S ribosomal subunits. **B)** an electropherogram view of the total RNA isolated from HT29-MTY-E12 cells infected with EPEC strain E2348/69. 1. EPEC, 2. EcN WT, 3. EcN variant 3595, 4. EcN variant 3452, 5. EcN variants 3426, 6. EcN variant 3414, 7. EcN variant 3598, 8. EcN variant 3453, 9. EcN variant 3419, 10. EcN variant 3413, 11. EcN variant 3452.

In Table 5.1, RNA integrity scores (RIS) values, and 28S/18S peak ratios are described for each RNA sample under a particular condition. On the one hand, RIS provides an objective quality measurement for eukaryotic RNA samples and allows the interpretation of sample integrity. The RIS is a value from 1 to 10, where a value of 10 indicates completely intact RNA. On the other hand, the 28S/18S ratio indicates the quality of the total RNA.

Table 5.1. Quality parameters of the isolated RNA samples from HT29-MTX-E12 cells

Sample	RIS	28S/18S ratio	Total concentration (ng/µl)
EPEC strain E2348/69	8.2	1.62	331.18
EcN WT	7.4	1.29	93.74
EcN variant 3595	7.0	1.38	147.72
EcN variant 3452	7.4	1.29	102.40
EcN variant 3426	7.4	1.34	46.98
EcN variant 3414	7.9	1.64	209.77
EcN variant 3598	7.7	1.5	73.82
EcN variant 3453	8.3	1.46	179.37
EcN variant 3419	8.0	1.49	125.84
EcN variant 3413	7.0	1.26	25.99

These data indicated that we were able to isolate RNA from HT29-MTX-E12 cells under different incubation conditions. The RIS and 28S/18S values indicated good integrity of the extracted RNA. Therefore, downstream processes could be done successfully.

5.5 Physical features of HT29-MTX-E12 cultured on Cytodex-3 dextran microcarrier beads and employing the Rotating Wall Vessel bioreactor

Physical characteristics of HT29-MTX-E12 cells were observed to confirm proper differentiation. Figure 5.5 **A** shows a light microscopy picture of empty Cytodex-3 dextran microcarrier beads used as scaffolds to grow cells in the RWV bioreactor. **B** shows microcarriers beads covered by cells after 15 days of co-culture. The beads were entirely covered by the cells, and they formed aggregates. **C** shows a TEM picture of the mucin-producing cells. The large filaments were microvilli (MV), and close to them, there

were small mucin (MUC) blebs secreted to the outside environment. Inside the cells, there were prominent inner mucin blebs that eventually were secreted to the outside. D and E TEM pictures show in a more extensive and closer look, respectively a tight cell-cell contact and a complete tight junctional complex formation with the presence of tight junctions (TJ), adherent junctions (AD) and desmosomes (DS). Identical features were found in cells grown in the 2.5D system. Images can be found in the appendix data (Section 8.1).

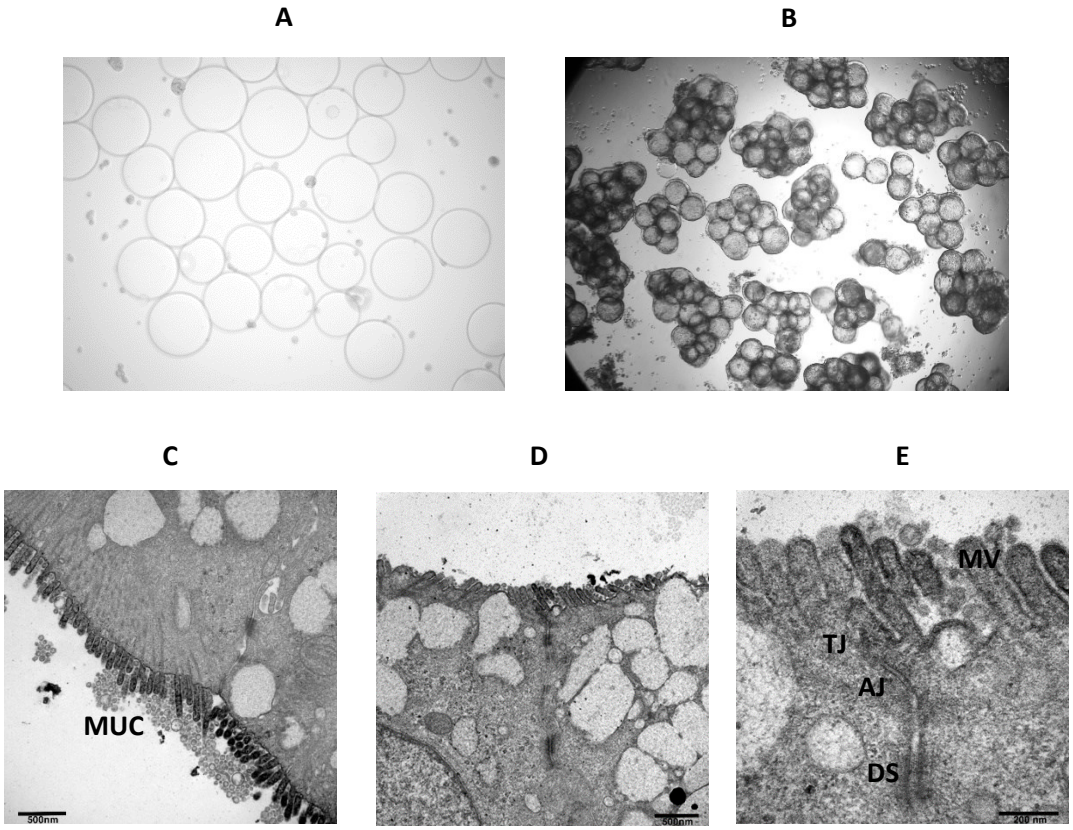

Figure 5.5. Physical features of HT29-MTX-E12 cells cultured on Cytodex-3 dextran microcarrier beads. A) Naked Cytodex-3 dextran microcarrier beads. **B)** Beads covered by HT29-MTX-E12 cells. **C, D, E)** TEM pictures of the cells. The cells were properly differentiated with microvilli formation, a complete tight junctional complex development, and the production of mucin. TJ: tight junctions, AD: adherent junctions, DS: desmosome, MV: microvilli, MUC: mucin. TEM pictures courtesy of Lilo Greune.

The Rotating Wall Vessel bioreactor allowed a closer *in vivo*-like differentiation of epithelial cells.

5.6 Localization of JAM-A protein in HT29-MTX-E12 cells incubated with pathogenic and probiotic bacteria

It is known that EPEC causes rearrangement of the actin cytoskeleton and enhances the perturbation of the tight junction barrier. In the same way, it has been shown that EcN redistributes the peripheral junctional protein zonula occludens-2 (ZO-2), increasing the barrier function (Zyrek *et al*., 2006). To analyze the effects of the pathogenic EPEC strain E2348/69 and the probiotic strain EcN on the distribution of the junctional complex protein JAM-A, HT29-MTX-E12 grown on transwell filters and on beads (2.5D and 3D systems) were incubated with the EPEC strain and the different variants of EcN. Immunofluorescence microscopy image analyses were performed to observe JAM-A distribution after incubation under static conditions. Figure 5.6.1-3 shows immunofluorescence images of JAM-A (green), the actin cytoskeleton (red), and Draq5. Figure 5.6.1, **A** shows a comparison between untreated cells grown in the three different cell culture systems (2D, 2.5D, and 3D). No clear differences in JAM-A distribution were observed between cells cultured in the different culture systems. JAM-A was interconnected to the actin cytoskeleton via zonula occludens proteins (ZO-1, ZO-2) (Monteiro *et al*., 2013). Colocalization of JAM-A and actin was quantified (yellow color) and the colocalization increased with increasing culture system complexity (Figure 5.6.1, **B**), suggesting greater formation of the tight junctions.

In Figure 5.6.2, images of HT29-MTX-E12 cells are shown upon growth in the 2.5D system and incubated for 4 h with an MOI 50 with EPEC strain E2348/69, EcN WT, and the EcN variant 3595. No striking differences between the different strains were found. Pedestal formation by the EPEC strain leading to a significant rearrangement of actin and a re-localization of JAM-A from the cell boundaries to the cytoplasm was not observed. Therefore, under these incubation conditions, EPEC was no longer able to disrupt the epithelial barrier via the T3SS. This might suggest that the presence of a mucin layer plays an essential role in protecting the epithelial cells. Cells treated with probiotic strains showed a similar phenotype to the untreated ones, indicating that the probiotic strain might not have a strong effect on the expression and distribution of JAM-A in a “healthy environment.” It means that a previous disruption of the barrier function should occur or incubation of both pathogenic and probiotic strain at the same time must be performed in order to induce a probiotic effect.

The same conditions used for the 2.5D system were employed for cells cultured on beads to analyze the distribution of JAM-A under static conditions. In Figure 5.6.3, immunofluorescence microscopy images are shown. Similar results were obtained: EPEC strain E2348/69 did not cause A/E lesion formation, thus having no adverse effect on the barrier function under these current conditions. No differences in JAM-A distribution between untreated and EcN-treated cells were found.

HT29-MTX-E12 cells in the 3D model were incubated with EPEC strain E2348/69 and EcN variants for 2 h and 4 h with an MOI of 50 and 100 to define an adequate infection condition. We visualized by immunofluorescence microscopy analyses that an MOI of 50 was the most suitable to incubate cells, grown in the 3D cell culture system, with bacteria under static conditions. A difference in JAM-A distribution between both strains, time, and multiplicity of infection was not detected. The percentage (%) of colocalization of JAM-A and actin cytoskeleton was quantified (Figure 5.6.4). In general, there was a constant percentage of colocalization between 2 h and 4 h. A decrease in colocalization did not suggest that less JAM-A was present at cell boundaries. As it can be seen in the immunofluorescence microscopy pictures, cells had clear and defined cell boundaries and a tight epithelial barrier could be observed. Differences in colocalization between strains might be due to the quality of the staining in the analyzed area. In this case, actin might not be involved in epithelial damage. The fact that some probiotics variants stimulated more than others JAM-A-actin colocalization could be related to JAM-A trafficking to the cell membrane. Some variants could induce the transport of JAM-A to the cell surface more than other variants.

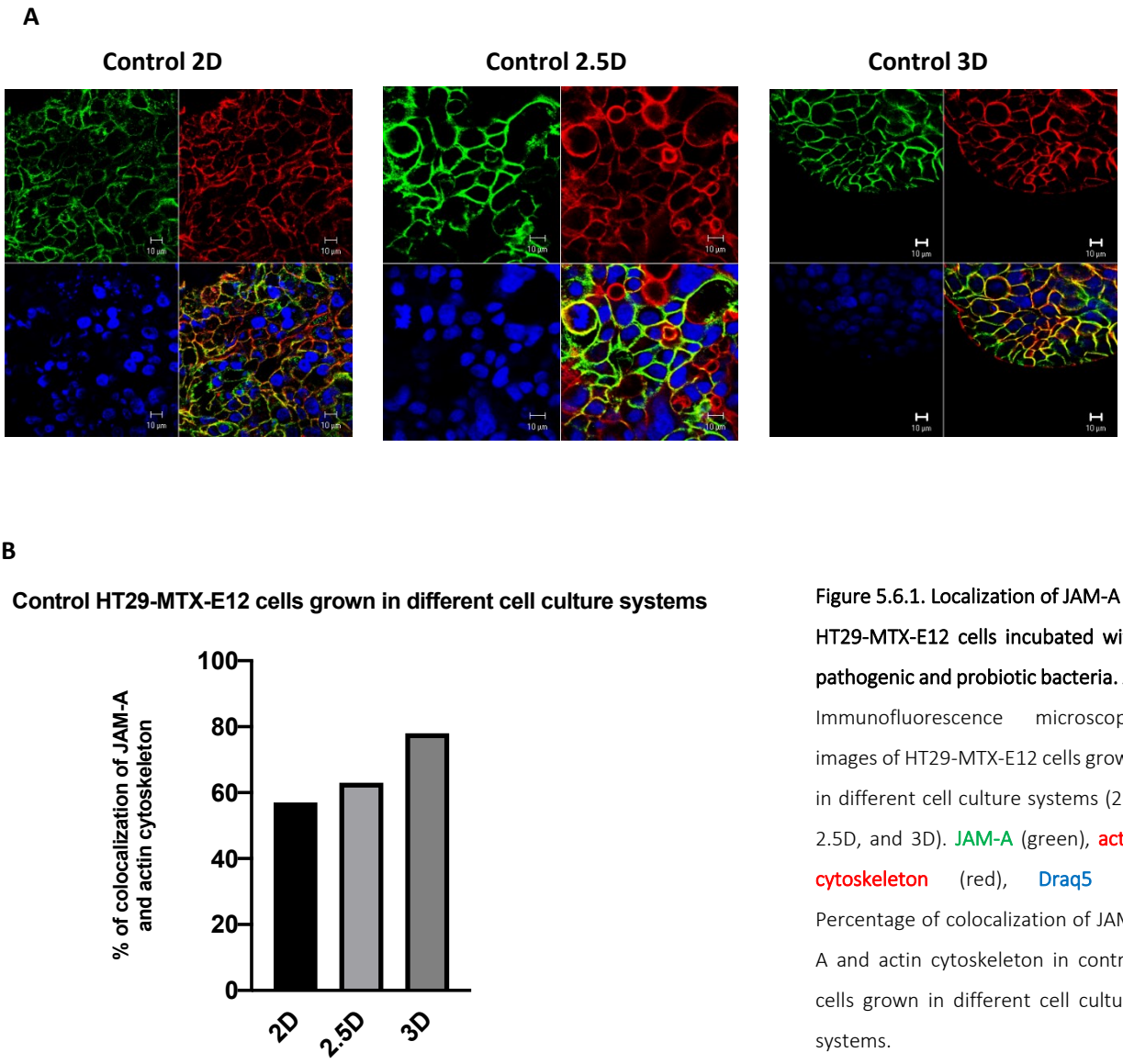

Figure 5.6.1. Localization of JAM-A in HT29-MTX-E12 cells incubated with pathogenic and probiotic bacteria. A) Immunofluorescence microscopic images of HT29-MTX-E12 cells grown in different cell culture systems (2D, 2.5D, and 3D). JAM-A (green), actin cytoskeleton (red), Draq5 **B)** Percentage of colocalization of JAM-A and actin cytoskeleton in control cells grown in different cell culture systems.

2.5D system

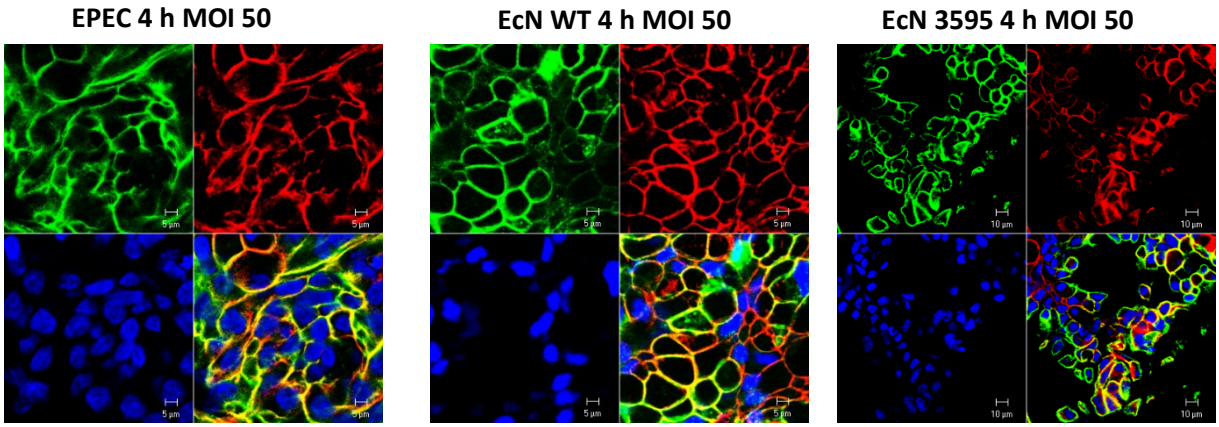

Figure 5.6.2. Localization of JAM-A in HT29-MTX-E12 cells incubated with pathogenic and probiotic bacteria. Immunofluorescence microscopic images of HT29-MTX-E12 cells grown in the 2.5D cell culture model and infected with EPEC strain E2348/69, EcN WT or EcN variant 3595. JAM-A (green), actin cytoskeleton (red), Draq5. Yellow: JAM-A and actin colocalization.

3D system

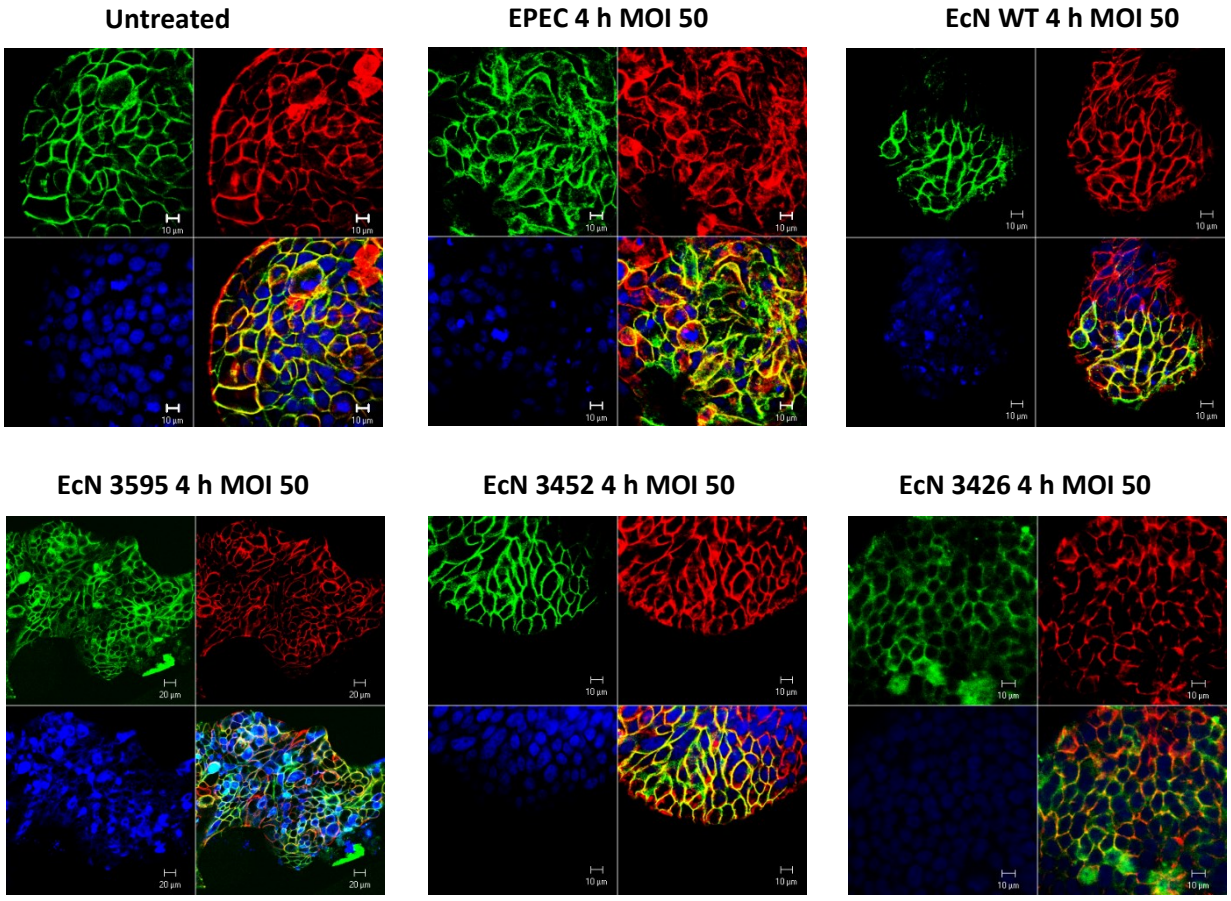

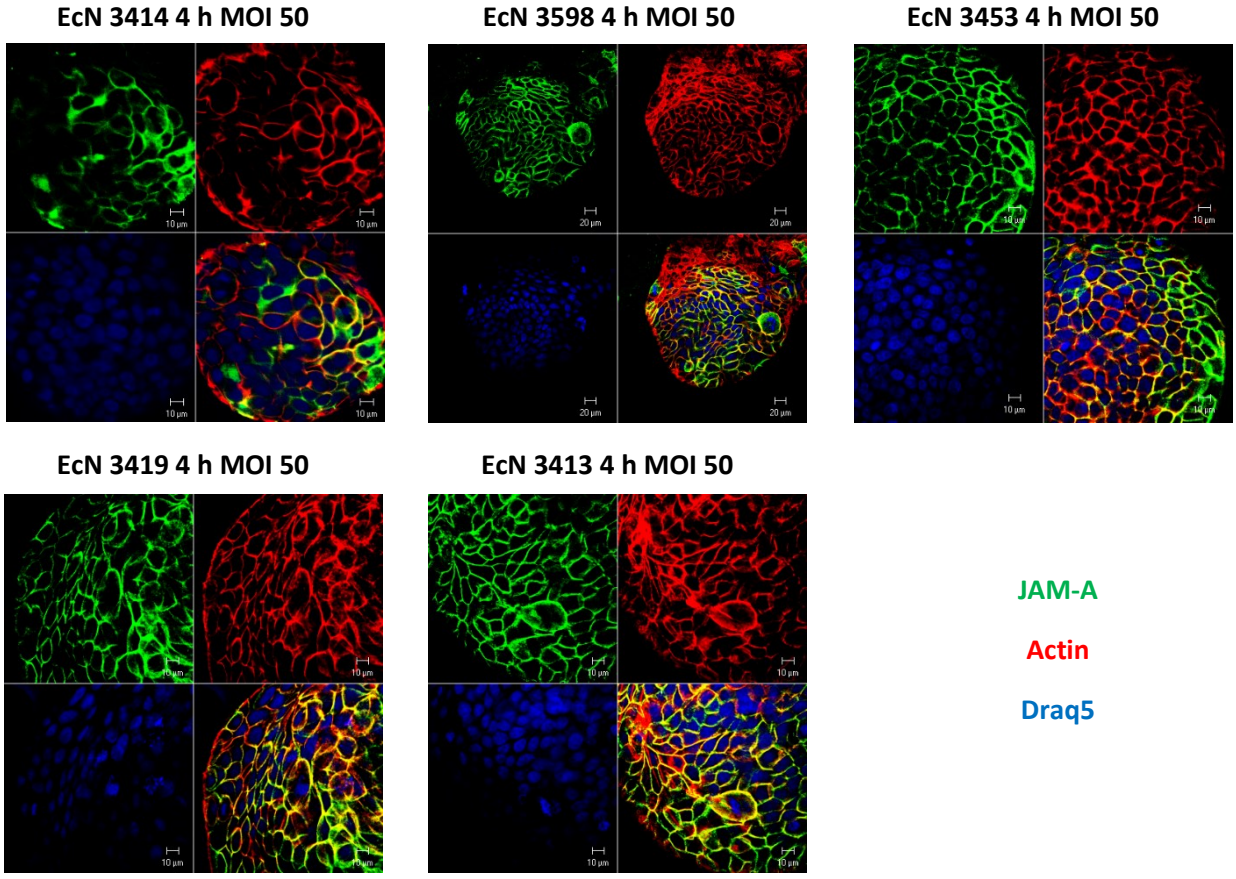

Figure 5.6.3. Localization of JAM-A in HT29-MTX-E12 cells incubated with pathogenic and probiotic bacteria. Immunofluorescence microscopic images of HT29-MTX-E12 cells grown in the 3D cell culture model and infected with EPEC strain E2348/69, EcN WT or different EcN variants. JAM-A (green), actin cytoskeleton (red), Draq5. Yellow: JAM-A and actin colocalization.

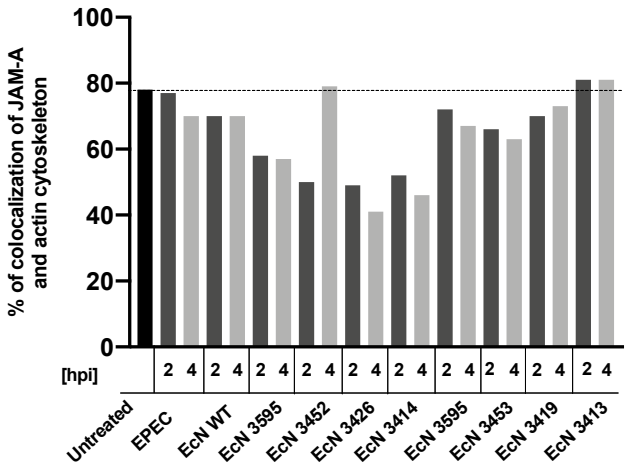

Figure 5.6.4. Percentage (%) of colocalization of JAM-A and actin cytoskeleton of HT29-MTX-E12 cells cultured in the 3D system and incubated with EPEC strain E2348/69 and EcN variants for 2 h and 4 h at MOI 50. The quantification was based on the immunofluorescence microscopy pictures shown before (Figure 5.6.3). BioImageXD was used to determine the colocalization percentage. [hpi] = hours post-incubation.

In summary, a more complex cell culture system promoted a complete cell differentiation closer to an *in-vivo* environment, which is fundamental to understand host-microbe interactions. The enteropathogenic *E. coli* strain did not cause A/E lesion formation under static conditions and also did not induce a re-localization of the tight junction proteins from the cell surface to the cytoplasm. An increase of JAM-A trafficking to the cell boundaries by probiotic bacteria could not be seen under current conditions.

5.7 Outer membrane vesicles isolation from the *E. coli* strains E2348/69, EcN WT and EcN variant 3595

Extracellular vesicles (EVs) are secreted by prokaryotic and eukaryotic cells and are involved in cell-to-cell communications (Lee, 2019). Outer membrane vesicles (OMVs) are constitutively produced by Gram-negative bacteria being relevant in bacteria-host interactions (Aguilera *et al*. 2014). To that extent, we asked ourselves whether the presence of a living microbe might be necessary to induce an effect on host cells. Therefore, OMVs from the EPEC strain E2348/69 and the probiotic strain EcN WT as well as its variant 3595 were isolated, as described in Chapter 4, Section 4.1.3, to perform incubation experiments of HT29-MTX-E12 cells with OMVs and investigate *JAM-A*, *MyD88*, and *TLR5* responses.

The isolated OMVs samples were resolved by SDS-PAGE, stained with Coomassie blue to visualize protein bands. A prominent band around 63 kDa was observed and identified as flagellin protein. Protein bands around 100 kDa are aldehyde-alcohol dehydrogenases. The information about the protein content within OMVs was taken from studies done by Dr. Doreen Baumann (Infectiology-ZMBE).

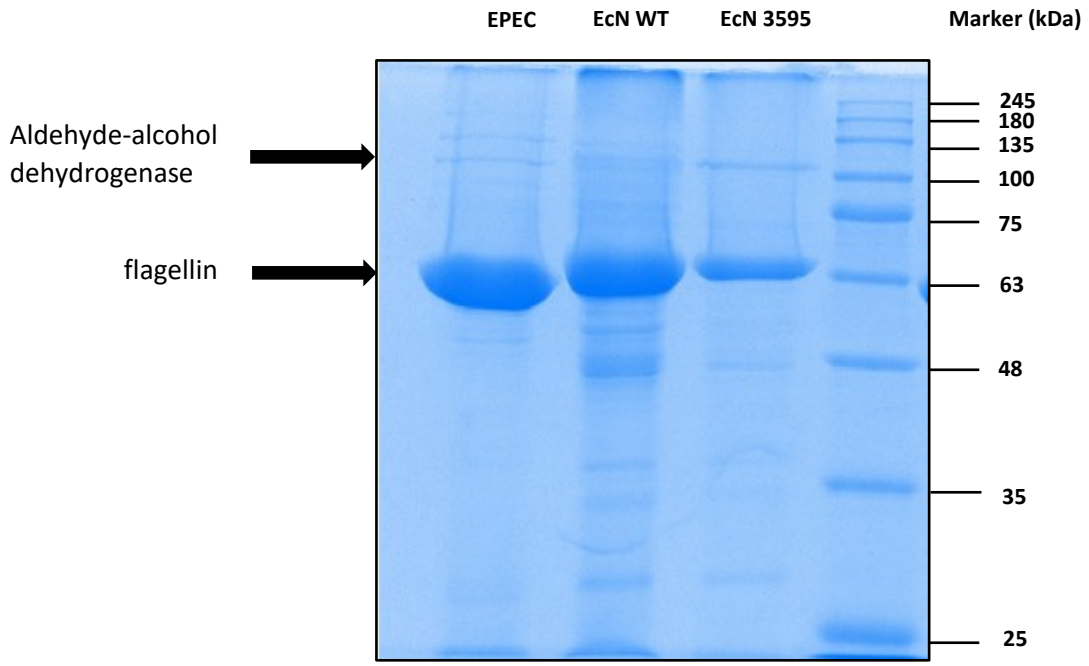

Figure 5.7.1. Protein content of OMVs isolated from EPEC strain E2348/69, EcN WT and EcN variant 3595. OMVs were isolated as described in Chapter 4, Section 4.1.3. 10 µg/ml of purified OMVs were loaded onto an SDS-PAGE gel. Information about the OMVs content was taken from a former Ph.D project.

5.7.1 *JAM-A* expression in HT29-MTX-E12 cells incubated with OMVs of EPEC strain E2348/69, EcN WT and EcN variant 3595

To investigate whether OMVs from different bacterial strains can induce a molecular response in epithelial cells, HT29-MTX-E12 cells were incubated in the 3D system for 4 h with varying concentrations of OMVs (20, 25, 30, 35 µg/ml). We found that OMVs from pathogenic and probiotic bacteria rose *JAM-A* expression at the transcriptional level compared to untreated cells (0.1 – 0.5-fold), except for 20 µg/ml EPEC E2348/69 OMVs where *JAM-A* transcriptional response was not affected (Figure 5.7.2). At 30 µg/ml OMVs isolated from EcN WT induced the highest response regarding *JAM-A* expression (0.5-fold), while OMVs of EcN variant 3595 had the strongest effect at a concentration of 20 µg/ml. EPEC OMVs slightly increased *JAM-A* transcript levels (Figure 5.7.2). Differences in *JAM-A* expression between untreated and treated cells did not differ significantly.

Given our previous results of *JAM-A* expression upon incubation with living bacteria (Figure 5.3.1, B), we could see that OMVs of probiotic strains had a stronger positive effect on *JAM-A* transcript levels. In the same way, OMVs of EPEC strain E2348/69 did not repress but induced the transcription of the *JAM-A* encoding gene. These results differed from those obtained from experiments where

HT29-MTX-E12 cells were infected with the whole EPEC microorganism, in which *JAM-A* expression was lower than in untreated cells (3D cell culture model).

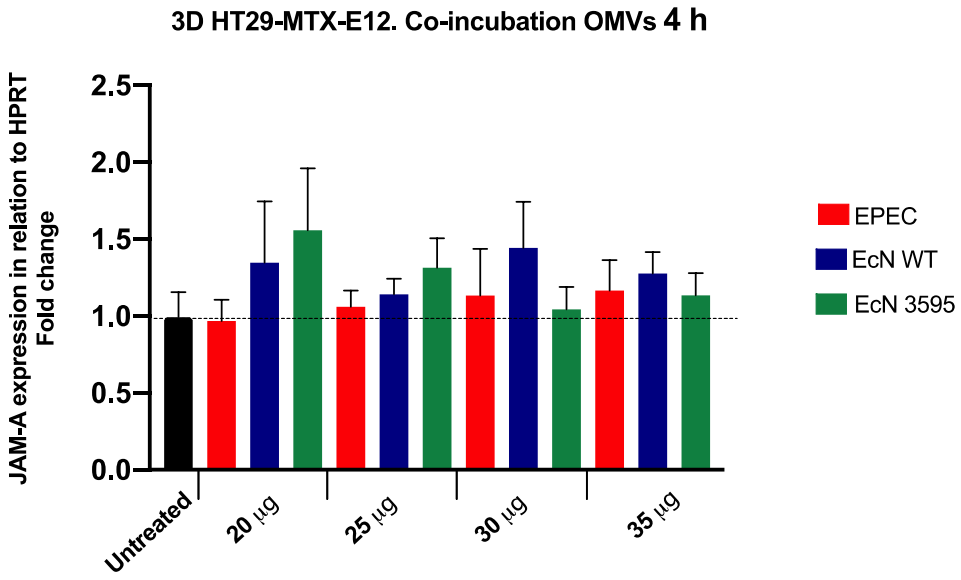

Figure 5.7.2. Impact of bacterial OMVs on *JAM-A* expression at the transcriptional level in mucin-producing HT29-MTX-E12 cells grown in the 3D system. Cells were incubated with variable OMVs concentrations of the EPEC strain E2348/69 and probiotic strains EcN WT and EcN variant 3595 for 4 h**.** Control cells were left untreated. The analysis was performed by quantitative real-time PCR. The data were normalized using the housekeeping gene HPRT transcript levels. All results are presented as fold-changes relative to the untreated control. The data were obtained from at least three independent experiments performed in duplicates. The error bars show the standard error of the mean (SEM).

5.7.2 *MyD88* expression in HT29-MTX-E12 cells incubated with OMVs of EPEC strain E2348/69, EcN WT and EcN variant 3595

The transcript levels of the *MyD88* encoding gene were also analyzed after incubation of HT29-MTX-E12 cells, grown on dextran beads, with isolated OMVs from pathogenic and probiotic bacteria. Figure 5.7.3 shows the relative expression of *MyD88* at the transcriptional level under different OMVs concentration conditions (20, 25, 30, 35 µg/ml). EPEC E2348/69E OMVs showed the strongest effect on *MyD88* expression. For the probiotic strain, isolated OMVs from both variants caused a decrease of *MyD88* mRNA levels in the cells. But at 20 µg/ml, OMVs from EcN variant 3595 induced a 0.3-fold increase of *MyD88* transcript levels. Differences in *MyD88* expression between untreated and treated cells were not significant.

MyD88 levels were downregulated when cells were incubated either with probiotic living bacteria or OMVs from probiotic bacteria (Figure 5.3.2, **B** and Figure 5.7.3). In contrast, OMVs from EPEC strain E2348/69 induced the upregulation of *MyD88* expression; however, a slight downregulation when HT29-MTX-E12 cells were incubated with EPEC strain itself. This evidence could suggest that the mucus layer interferes with bacterial behavior, perhaps suppressing the release of virulence factors or downregulating bacterial gene expression associated with pathogenicity. OMVs alone can be transferred across the mucus barrier due to their small size, targeting host cells efficiently.

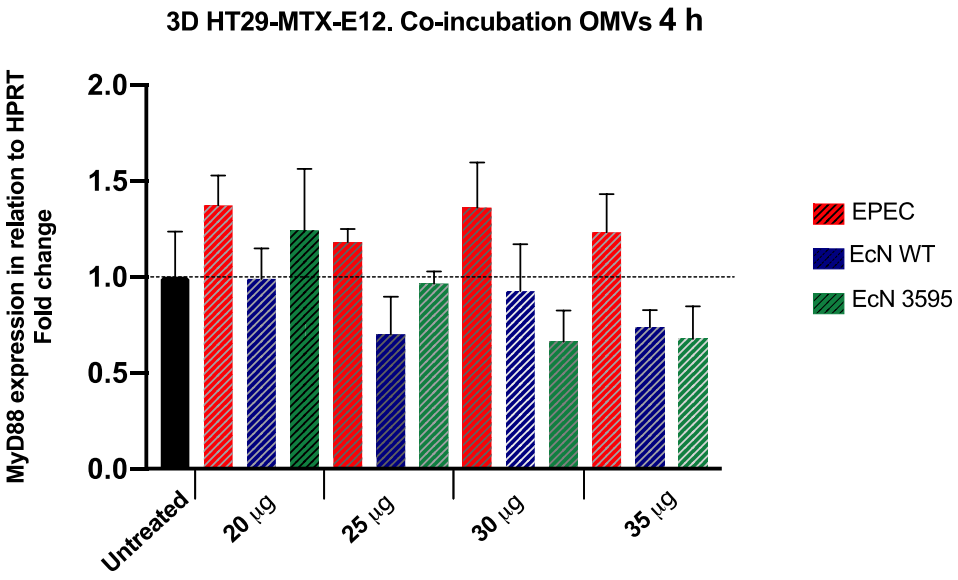

Figure 5.7.3. *MyD88* expression at the transcriptional level in mucin-producing HT29-MTX-E12 cells grown in the 3D system. Cells were incubated with variable OMVs concentrations of the EPEC strain E2348/69 and probiotic strain EcN WT and its variant 3595 for 4 h**.** Control cells were left untreated. The analysis was performed by quantitative real-time PCR. The data were normalized using the housekeeping gene HPRT transcript levels. All results are presented as fold-changes relative to the untreated control. The data were obtained from at least three independent experiments performed in duplicates. The error bars show the standard error of the mean (SEM).

5.8 Incubation of HT29-MTX-E12 cells with supernatants of the strains EPEC E2348/69, EcN WT and EcN variant PZ816

Supernatants from the pathogenic and probiotic bacteria were collected as described in Chapter 4, Section 4.1.4. We obtained supernatants from a different EcN variant, which is highly flagellated and named under the code number "EcN PZ816." In order to investigate whether the bacterial flagellum mediates bacterial pathogenicity and host immune responses regarding *JAM-A* and *MyD88* expression, incubation experiments of HT29-MTX-E12 epithelial cells and various concentrations (20, 25, 30, and

35 µg/ml) of bacterial supernatants were performed. Figure 5.8.1 shows the negative staining of supernatants from the different *E. coli* strains. **A)** The supernatant of the EPEC strain E2348/69. **B)** The supernatant of the probiotic EcN WT. **C)** The supernatant of the probiotic EcN variant PZ816. In general, it was observed that supernatants of EPEC strain E2348/69 and EcN WT contained low amounts of flagella (long filaments) compared to supernatants of hyperflagellated strain EcN variant PZ816.

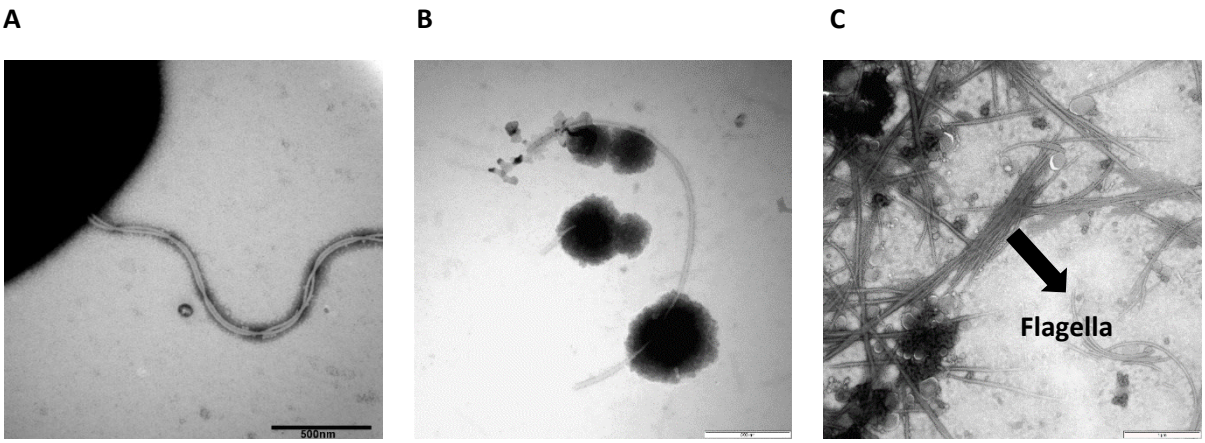

Figure 5.8.1. Detection of bacterial flagella in supernatants of EPEC strain E2348/69, EcN WT, and EcN variant PZ816. Supernatants were collected as described in Chapter 4, Section 4.1.4, and detected by negative staining and electron microscopy. **A)** EPEC strain E2348/69 supernatant. **B)** EcN WT supernatant. **C)** EcN variant PZ816 supernatant. Flagella were more abundant in the EcN variant PZ816 supernatant. Pictures are courtesy of Lilo Greune.

The supernatant proteins were also loaded onto an SDS-PAGE gel to visualize differences in their protein pattern. Different concentrations (2.2 and 4.4 µg/ml) of each supernatant were loaded. A prominent band around ~63 kDa was observed in supernatants of EcN variant PZ816. However, no detectable protein bands were visible in the EcN WT supernatants (Figure 5.8.2, **A**). Therefore, protein precipitation with TCA was done to precipitate proteins from the EcN supernatant. After the precipitation, a protein pattern of the EcN WT supernatant was detected. In the same way, a 63 kDa band was observed (Figure 5.8.2, **B**). These bands might correspond to the flagellin protein, which is the main protein component of the bacterial flagellum. These results indicated evident differences between both variants. The PZ816 variant expressed higher amounts of flagella on its surface than the wild type strain EcN.

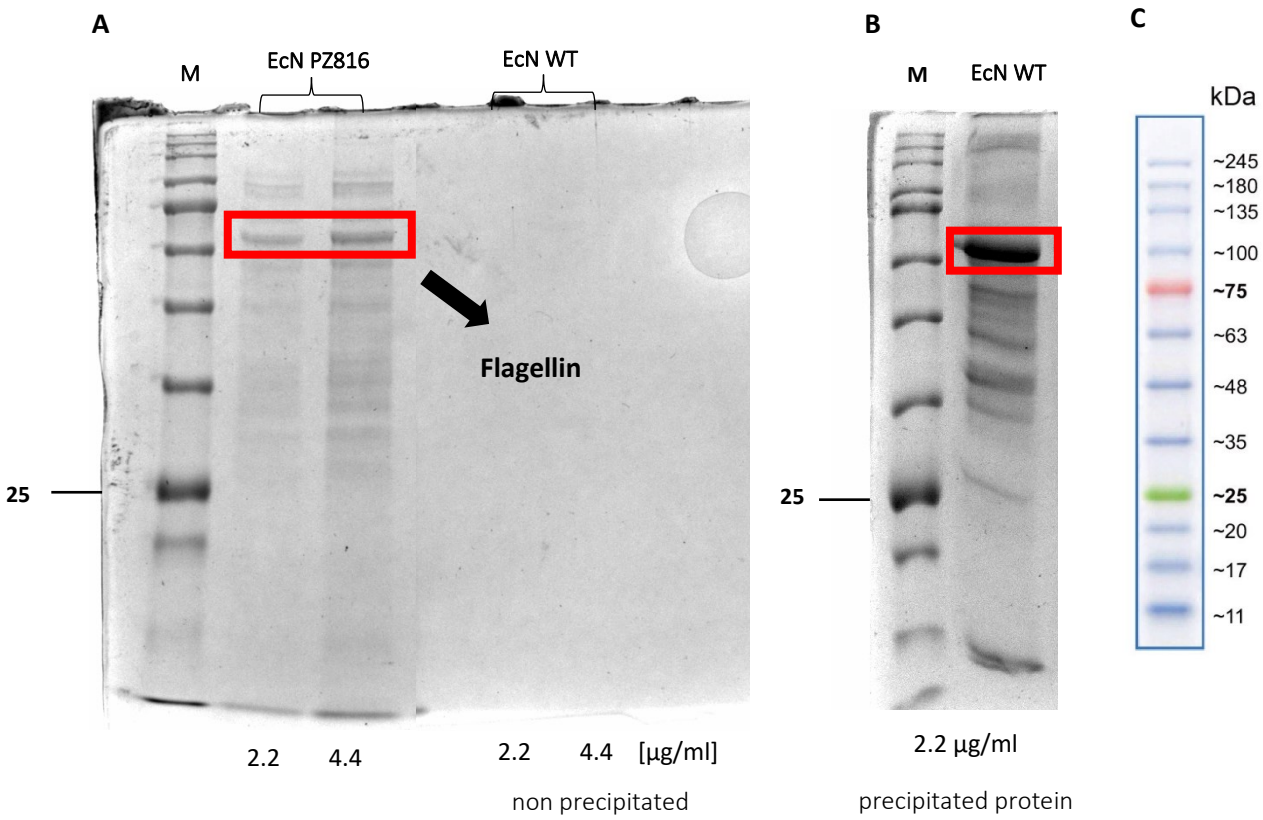

Figure 5.8.2. Protein content of EcN WT and EcN variant PZ816 supernatants. Supernatants were collected as described in Chapter 4. 2.2 µg/ml and 4.4 µg/ml of supernatants were loaded onto an SDS-PAGE gel. **A)** Non-treated supernatants of EcN variant PZ816 and EcN WT. **B)** Precipitated proteins of the EcN WT supernatant. **C)** Protein marker (245 kDa). A prominent protein band of approximately 63 kDa was detectable in the supernatant of EcN variant PZ816 and the precipitated protein content of EcN WT supernatant. This band might correspond to the flagellin protein, which has a molecular mass of ~63 kDa.

5.8.1 *JAM-A* expression in HT29-MTX-E12 cells incubated with supernatants of EPEC strain E2348/69, EcN WT and EcN variant PZ816

Flagella are essential structures enabling bacterial motility or even promoting bacterial adhesion. When host cells detect the presence of bacterial flagellin, immune responses are induced. To investigate whether flagellin has an impact on the epithelial barrier function, HT29-MTX-E12 cells were incubated with different concentrations of supernatants of pathogenic and probiotic bacteria. *JAM-A* mRNA levels increased with increasing supernatant concentrations of EPEC strain E2348/69, but at a concentration of 35 µg/ml , *JAM-A* transcript levels decreased. The EcN WT supernatant induced the strongest effect on *JAM-A* gene transcription at a concentration of 35 µg/ml. There were no striking differences in *JAM-A* transcript levels between both probiotic strains (Figure 5.8.3). This could suggest that a higher

amount of flagellin does not necessarily have a more positive impact on *JAM-A* gene expression. Differences in *JAM-A* response between *E. coli* supernatants were not significant.

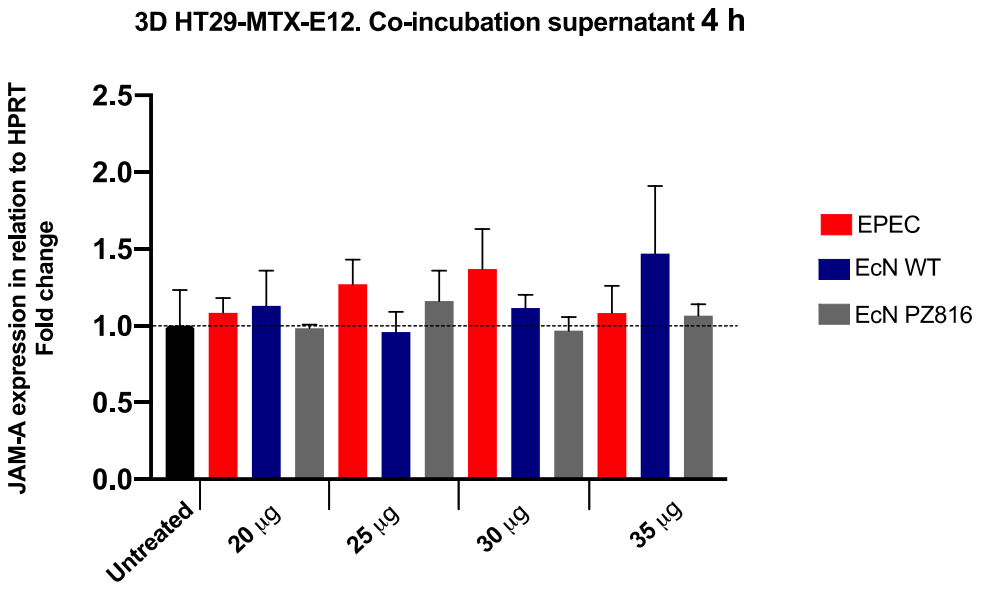

Figure 5.8.3. Impact of bacterial supernatants on *JAM-A* expression in mucin-producing HT29-MTX-E12 cells grown in the 3D system. Cells were incubated with variable supernatant concentrations of the EPEC strain E2348/69 or supernatants of probiotic EcN WT and EcN variant PZ816 for 4 h. Control cells were left untreated. The analysis was performed by quantitative real-time PCR. The data were normalized using the housekeeping gene HPRT transcript levels. All results are presented as fold-changes relative to the untreated control. The data were obtained from at least three independent experiments performed in duplicates. The error bars show the standard error of the mean (SEM).

5.8.2 *MyD88* expression in HT29-MTX-E12 cells incubated with supernatants of EPEC strain E2348/69, EcN WT and EcN variant PZ816

MyD88 expression of epithelial cells grown in the 3D cell culture system were also analyzed at the transcriptional level. In general, EPEC strain E2348/69 supernatant had the highest impact on *MyD88* expression except for the initial concentration (20 µg/ml) in which *MyD88* expression was lower than its expression in HT29-MTX-E12 cells incubated with probiotic supernatants. Supernatants of EcN WT and its variant PZ816 did not upregulate *MyD88* expression compared to untreated samples. The supernatant of EcN PZ816 showed the lowest impact on *MyD88* mRNA levels. Here, mRNA levels decreased with raising the supernatant concentration. The results could suggest that high flagellin amounts of the probiotic strain did not induce the activation of host immune responses via the MyD88

pathway. No significant differences between untreated and treated HT29-MTX-E12 regarding *MyD88* expression were obtained.

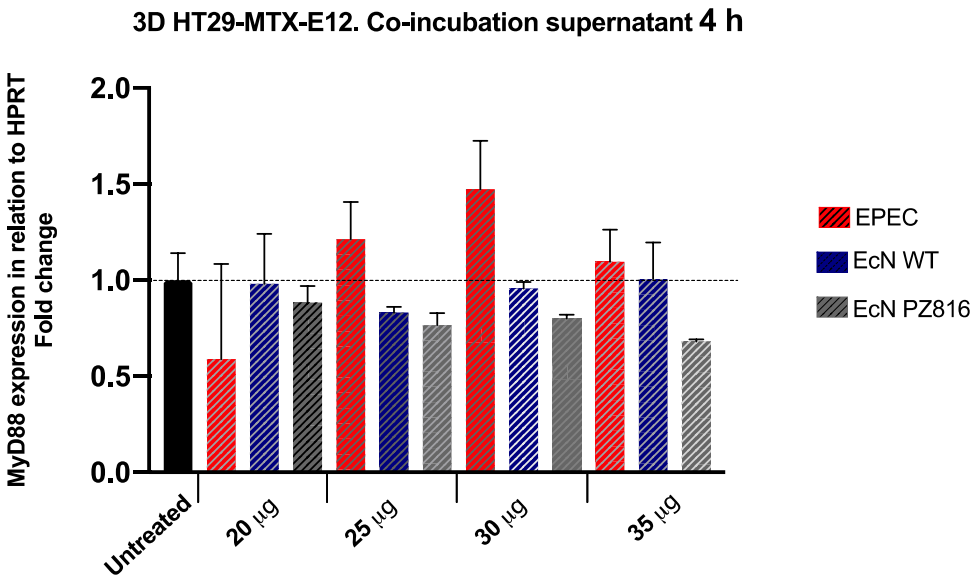

Figure 5.8.4. Impact of bacterial supernatant on *MyD88* expression in mucin-producing HT29-MTX-E12 cells grown in the 3D system. Cells were incubated with variable supernatant concentrations of the EPEC strain E2348/69 and supernatants of probiotic strain EcN WT and its variant EcN PZ816 for 4 h. Control cells were left untreated. The analysis was performed by quantitative real-time PCR. The data were normalized using the housekeeping gene HPRT transcript levels. All results are presented as fold-changes relative to the untreated control. The data were obtained from at least three independent experiments performed in duplicates. The error bars show the standard error of the mean (SEM).

TLR5 expression levels in epithelial cells after incubation with pathogenic and probiotic OMVs and supernatants were also quantified at the transcript levels. No *TLR5* cell response under the used incubation conditions was detectable by qRT-PCR.

Taking these results together, a cellular response concerning *JAM-A* and *MyD88* expression after HT29-MTX-E12 incubation with OMVs and supernatants from pathogenic and probiotic bacteria was observed. Thus, the presence of living microorganisms was not necessary to produce an activation of cellular pathways in host cells. High amounts of probiotic flagellin did not trigger MyD88-mediated inflammatory response in epithelial cells. Similarly, it was seen that exposure to higher flagellin concentrations did not increase *JAM-A* expression levels compared to untreated cells. With this, we can

conclude that probiotic flagellin might be involved in regulating junctional proteins at post-transcriptional levels to reinforce the integrity of the intestinal monolayer.

5.9 *JAM-A* expression in HT29-MTX-E12 cells pre-infected with EPEC strain E2348/69 and followed by incubation with EcN WT

Positive changes in *JAM-A* mRNA expression and protein distribution when cells were incubated with probiotic bacteria for 4 h at MOI 50, were not visible. Therefore, it can be assumed that a disruption of the epithelial layer might be necessary to obtain probiotic effects by EcN. HT29-MTX-E12 cells were previously infected with the EPEC strain E2348/69 for 2 h with an MOI 20. A PBS washing step was followed to clear the pathogenic bacteria away and then cells were incubated either with fresh cell culture medium or with EcN WT (MOI 20) in fresh medium for an additional period of 4 h. Experiments including only 1 h EPEC infection followed by 2 h EcN incubation were also performed (data not shown). Experiments were carried out in three different cell culture systems, which were described above. *JAM-A* expression was higher in cells cultured in the 3D system. In the 2D model, there was a downregulation of *JAM-A* gene expression detectable after 2 h of EPEC infection. After EPEC strain E2348/69 was washed away, a slight increase of *JAM-A* expression was seen. However, the expression levels were lower than *JAM-A* levels in untreated cells. In the same way, an upregulation (0.2 fold) of *JAM-A* is induced when EPEC strain E2348/69 was replaced by the wild type probiotic strain EcN. When cells were incubated with EcN WT for 4 h alone, a 0.5-fold downregulation of *JAM-A* expression was observed (Figure 5.9.1, black columns).

Cells cultured in the 2.5D system, did not show changes in *JAM-A* expression after 2 h infection with EPEC strain E2348/69. There was a slight decrease in *JAM-A* mRNA levels when the EPEC strain was washed away, and new medium was added onto the epithelial cells. *JAM-A* expression rose (0.2 – 0.3-fold) when EcN WT was applied to the HT29-MTX-E12 cells (Figure 5.9.1, blue columns).

Cells cultured in the 3D system show, in general, an upregulation between 0.1 – 0.5-fold when they are incubated with pathogenic and probiotic bacteria. After EPEC infection, an increase of 0.1-fold in *JAM-A* expression is seen. There is a higher increase (0.5-fold) when EPEC is cleared from the cell medium, and fresh medium is added. No differences in *JAM-A* expression were seen between cells incubated with EPEC alone for 2 h and cells previously incubated with EPEC for 2 h, and then with EcN WT for 4 h (Figure 5.9.1, green columns). Differences in *JAM-A* expression between different conditions are not significant.

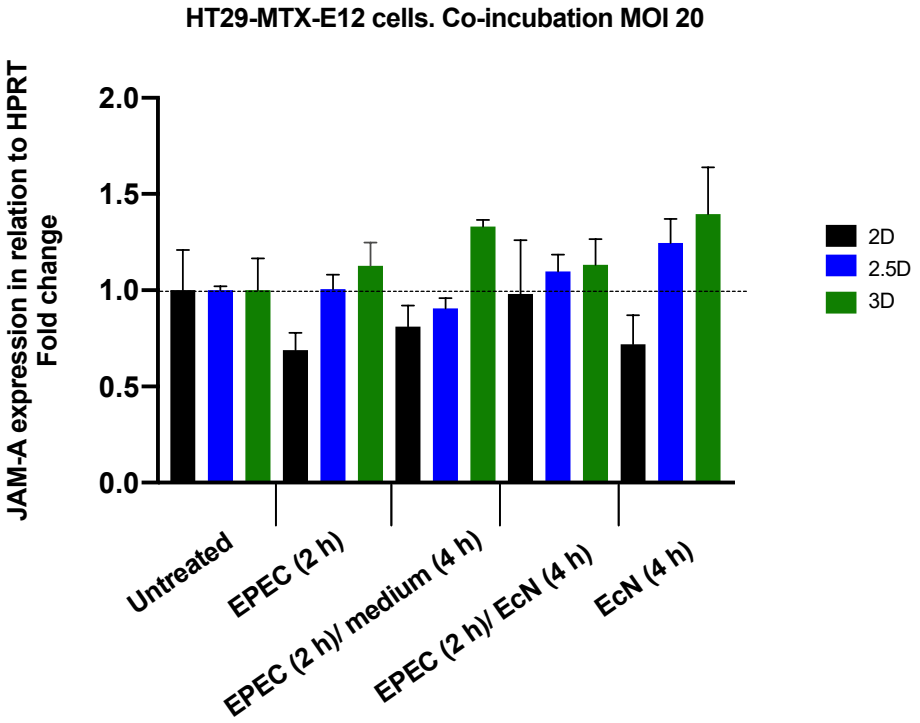

Figure 5.9.1. *JAM-A* expression in mucin-producing HT29-MTX-E12 cells grown in the three different cell culture systems. Cells were incubated under different conditions**.** Epithelial cells were previously infected with EPEC strain E2348/69 for 2 h, a PBS washing step was followed to remove the pathogenic bacteria, and finally, the cells were incubated with fresh medium for 4 h or with probiotic strain EcN WT for 4 h**.** A multiplicity of infection (MOI) of 20 was used. Control cells were left untreated. The analysis was performed by quantitative real-time PCR. The data were normalized using the housekeeping gene HPRT transcript levels. All results are presented as fold-changes relative to the untreated control. The data were obtained from at least three independent experiments performed in duplicates. The error bars show the standard error of the mean (SEM).

5.10 Localization of JAM-A protein in HT29-MTX-E12 cells pre-incubated with the EPEC strain E2348/69

Immunostaining analyses of JAM-A distribution inside HT29-MTX-E12 cells grown in the 3D cell culture system were also performed. The same conditions, as explained before (Results 5.9) were used to carry out the incubation experiments. JAM-A was relocalized from the cell membrane to the cytoplasm when cells were pre-incubated with EPEC strain E2348/69 for 2 h prior to bacterial removal. We could see that upon this treatment the HT29-MTX-E12 cell boundaries were blurrier. In contrast, for the other conditions used, we did not observe a re-localization of the tight junction protein JAM-A from the cell borders to the cytoplasm. Close cell-to-cell contact with clear boundaries was present (Figure 5.10.1).

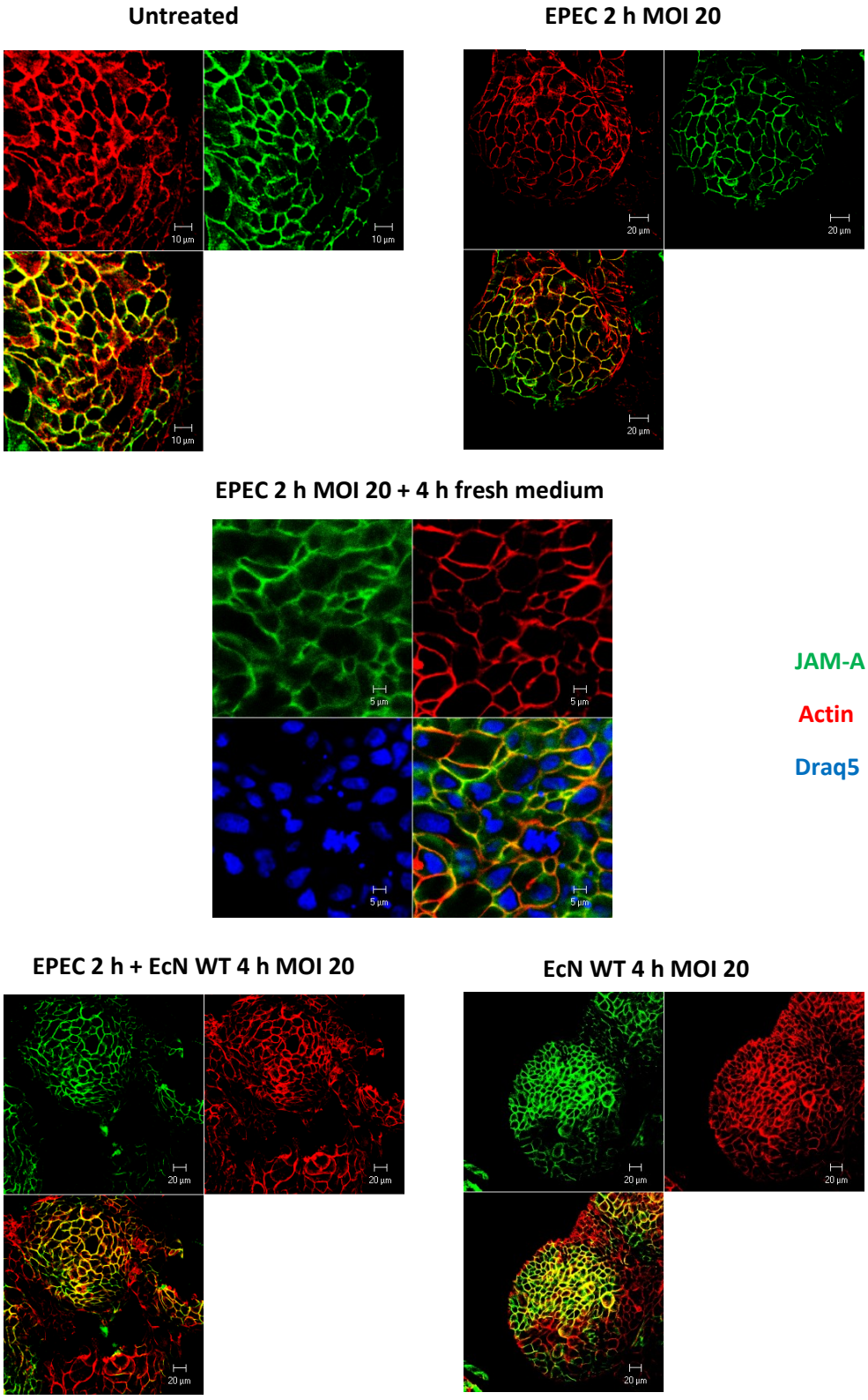

Figure 5.10.1. Localization of JAM-A in HT29-MTX-E12 cells grown in the 3D model and incubated with pathogenic and probiotic bacteria. Immunofluorescence microscopic images of HT29-MTX-E12 cells grown in the 3D cell culture model. JAM-A (green), actin cytoskeleton (red), Draq5. Yellow: JAM-A and actin colocalization.

Figure 5.10.2 shows the percentage of colocalization of JAM-A and the actin cytoskeleton in HT29-MTX-E12 cells. Cells pre-incubated with the EPEC strain for 2 h showed less colocalization of JAM-A and actin compared to untreated and EcN-treated cells. However, it was possible to see that JAM-A was mainly localized at the cell borders. As explained before, less colocalization between JAM-A and the cytoskeleton does not necessarily mean a disruption of the barrier function under these conditions.

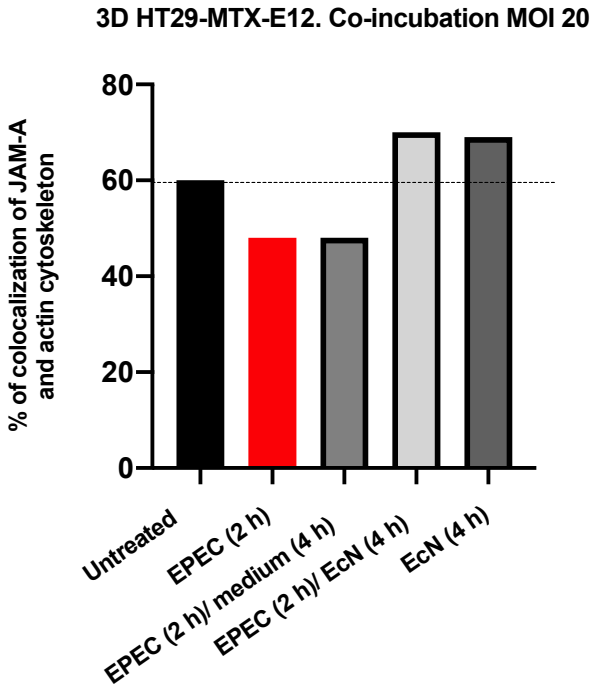

Figure 5.10.2. Percentage (%) of colocalization of JAM-A and actin cytoskeleton in HT29-MTX-E12 cells cultured in the 3D system. Cells were pre-incubated with EPEC strain E2348/69 followed by 4 h incubation with EcN WT with an MOI 20. Quantification was based on the immunofluorescence microscopic pictures shown before (Figure 5.10.1). BioImageXD was used to determine the colocalization percentage. Values were obtained from single images.

A disruption of the epithelial barrier function might be required to induce a positive cell response by probiotic bacteria. Hence, we conclude that a pre-incubation of cells with a pathogen to damage the epithelial layer partially could increase the positive effect of EcN regarding the expression and distribution of the tight junction protein JAM-A. The pre-incubation time and MOI had to be changed to figure out which conditions were the best not to induce total but moderate cell layer damage.

5.11 EPEC strain E2348/69 time kinetics and JAM-A distribution in HT29-MTX-E12 cells

To visualize at which time point EPEC strain E2348/69 could start to induce a disruption of the cell-to-cell contact, a time kinetics infection was done using an MOI of 50. Since we could not identify epithelial damage until 4 h of EPEC infection, we decided to set 4:30 h as the initial point of the incubation and 6 h as the last time point. Once the incubation time was completed, cells were stained by immunofluorescence to visualize the JAM-A protein, the actin cytoskeleton, and the nuclei. We observed a minimum disruption of the cell-cell contact after 4:30 h infection. From then on, an increase in the epithelial damage occurred: cell edges were cut and blurry compared to untreated cells, re-localization of JAM-A to the cytoplasm, and there was a dysfunction of the actin cytoskeleton that contributed to the disruption of the cell membrane. These findings suggested that JAM-A did not connect the intercellular space between neighboring cells, causing a loose cell-cell contact (Figure 5.11.1). For further EPEC pre-incubation experiments, 4:30 h was chosen as the time point at which a moderate epithelial disruption can be observed.

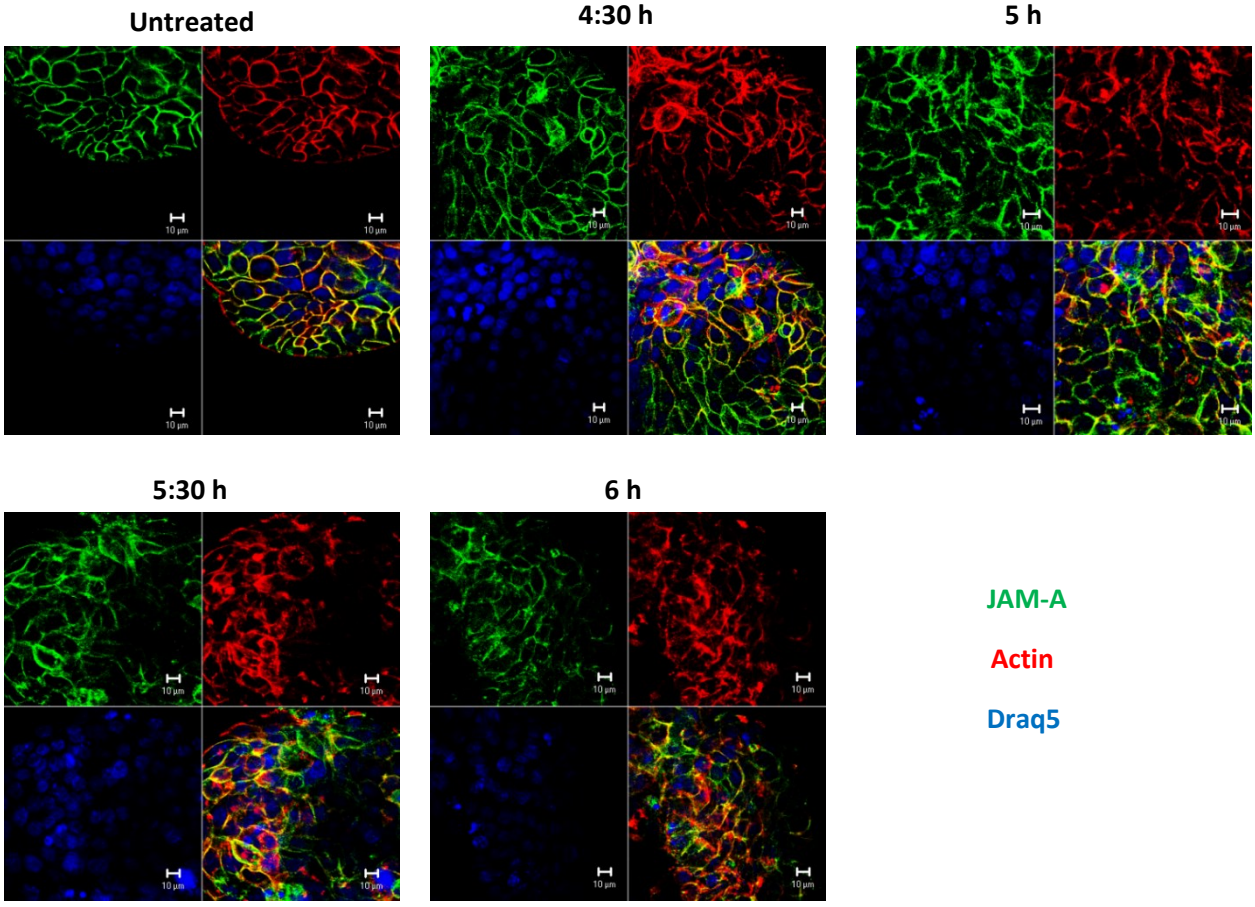

Figure 5.11.1. Time kinetics and JAM-A distribution in HT29-MTX-E12 cells grown in the 3D system upon infection with EPEC strain E2348/69. Immunofluorescence microscopic images of HT29-MTX-E12 cells grown on the 3D cell culture model. Control cells were left untreated JAM-A (green), actin cytoskeleton (red), Draq5 (blue). Yellow: JAM-A and actin colocalization.

5.12 Effect of EcN on JAM-A distribution after infection of HT29-MTX-E12 cells with the EPEC strain E2348/69

To evaluate a positive impact of EcN on JAM-A localization in epithelial cells, HT29-MTX-E12 cells grown on dextran beads were pre-infected for 4:30 h with the EPEC strain E2348/69 (MOI 50). After this time, the cells were washed with PBS to remove EPEC, and fresh cell culture medium was added. Later, the cells were incubated for 1 h , 2 h, and 3 h with EcN WT (MOI 50), and some were incubated for 2 h with fresh medium only (Figure 5.12.1). Upon incubation with EcN WT, there was a recovery of the cells from the damage caused by the EPEC infection. JAM-A (green) was re-distributed to the cell membrane. There was a more significant recovery of the cells after 2 h and 3 h incubation with EcN. The incubation of HT29-MTX-E12 cells with fresh culture medium, after the EPEC pre-infection, could help to restore the epithelial condition prior to infection (EPEC 4:30 h + medium 2 h). However, incubation with the probiotic strain EcN accelerated the healing process of the epithelial barrier (Figure 5.12.1).

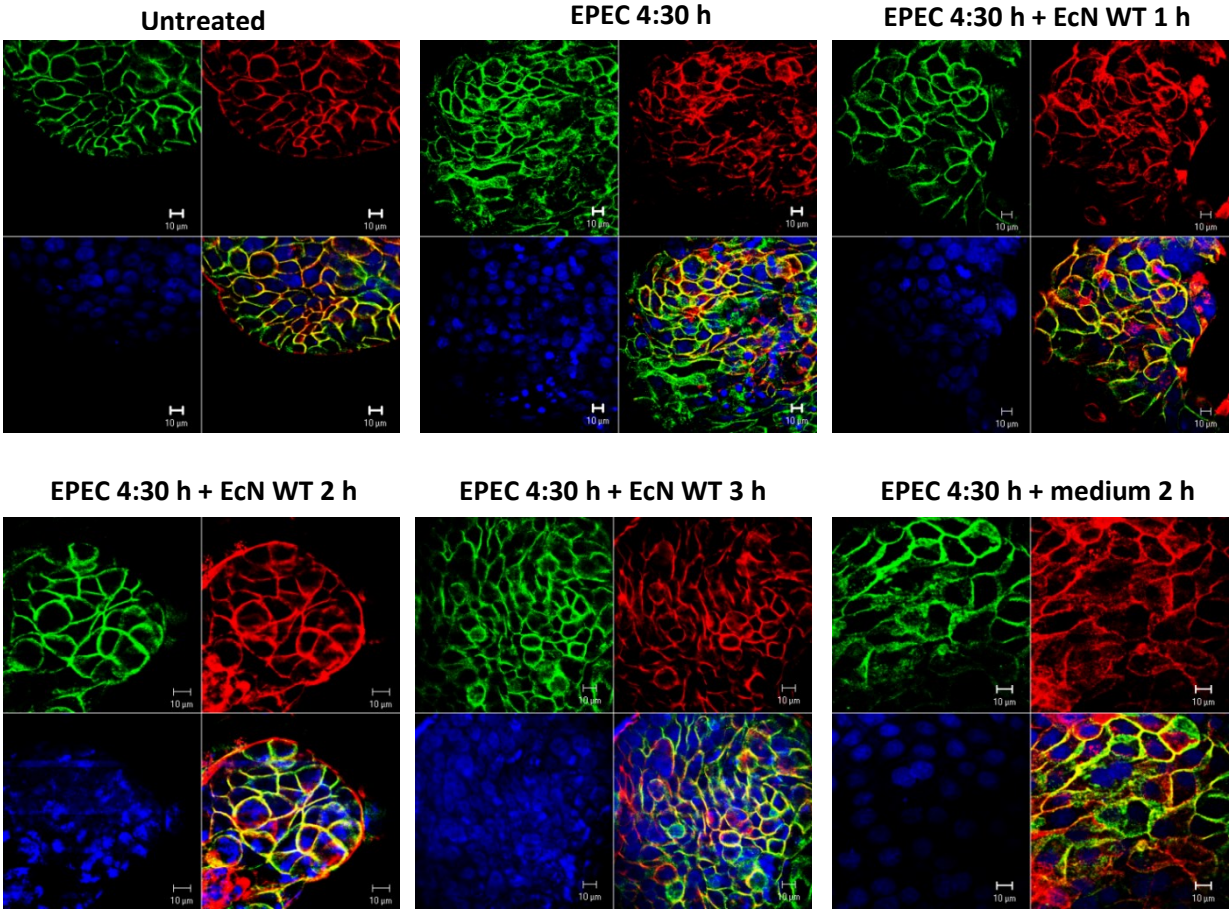

Figure 5.12.1. Effect of EcN on JAM-A distribution after infection of HT29-MTX-E12 cells grown in the 3D system with the EPEC strain E2348/69. After 4:30 h of EPEC infection, cells were incubated with EcN WT at an MOI 50 for 1 h, 2 h, and 3 h. Some cell samples were incubated with fresh cell culture medium only, after EPEC has been removed. Immunofluorescence microscopic images of HT29-MTX-E12 cells grown in the 3D cell culture model are shown. Control cells were left untreated. JAM-A (green), actin cytoskeleton (red), Draq5. Yellow: JAM-A and actin colocalization.

A disturbance of the epithelial monolayer was needed to obtain a positive effect by EcN WT on the trafficking of JAM-A from the cytoplasm into the cell membrane. The less JAM-A is in the intercellular space, the more permeable is the epithelial barrier.

5.13 Effect of two EcN variants on JAM-A distribution after infection of HT29-MTX-E12 cells with the EPEC strain E2348/69

Two EcN variants 3595 (*fliM*), and 3413 (*flgB*), were selected to evaluate their impact on JAM-A distribution in epithelial cells after an EPEC strain E2348/69 (MOI 50) pre-infection step for 4:30 h. In Table 3.2 (Chapter 3, Section 3.1), features about the different EcN variants are described. EcN variant 3595 possesses a missense mutation in the *fliM* gene. The FliM protein is associated with the flagellar motor´s switch complex and determines the direction of the flagellar rotation. EcN variant 3413 carries a disruptive inframe deletion in *flgB*. The FlgB gene product is a flagellar basal body rod protein involved in bacterial motility. This mutation interferes with bacterial movement. Therefore, we were interested in visualizing whether the effect of these two variants with mutated flagella basal body could be improved as the EcN WT strain.

Similar as described before, HT29-MTX-E12 cells were infected for 4:30 h with EPEC strain E2348/69 (MOI 50). Then, the cells were washed with PBS and incubated with gentamicin (250 µg/ml) for 1 h at 37 °C to ensure that the majority of the EPEC bacteria were killed and removed. In previous experiments, the gentamicin step was not performed. Hence, a few EPEC bacteria could remain on the cells increasing the epithelial damage for a longer time than the one already defined as infection time. Next, gentamicin-containing cell culture medium was removed, and the cells were intensively and carefully washed to eliminate any rest of the antibiotic. Fresh cell culture medium was added onto the cells. Based on previous immunostaining experiments (5.12), we conclude that a 2 h incubation with EcN WT (MOI 50) could be the shortest time point to start observing a recovery of the epithelial barrier function. Hence, some HT29-MTX-E12 cells grown in the 3D system were incubated with EcN WT for 2 h. An incubation with EcN variants 3595 and 3413 at an MOI 50 for 1 h, 2 h, and 3 h was also performed.

EcN variant 3595 had a positive effect on the epithelial barrier. This effect progressed until 3 h incubation. At this time, the cells showed sharper borders even though some JAM-A protein was still localized in the cytoplasm (Figure 5.13.1, EPEC 4:30 h + EcN 3595). Different results were observed for cells incubated with EcN variant 3413. The fluorescence of JAM-A (green color) was weak, suggesting that cell-to-cell contact was disturbed. Cell damage could not be reverted with an increasing incubation time of EcN variant 3413. The lack of a functional flagellar structure might be responsible for the lack

of a positive effect of EcN variant 3414 on JAM-A distribution. These data might indicate that the flagella might have an indirect impact on JAM-A phosphorylation and its cellular distribution (Figure 5.13.1, EPEC 4:30 h + EcN 3413 1 h, 2 h, and 3 h).

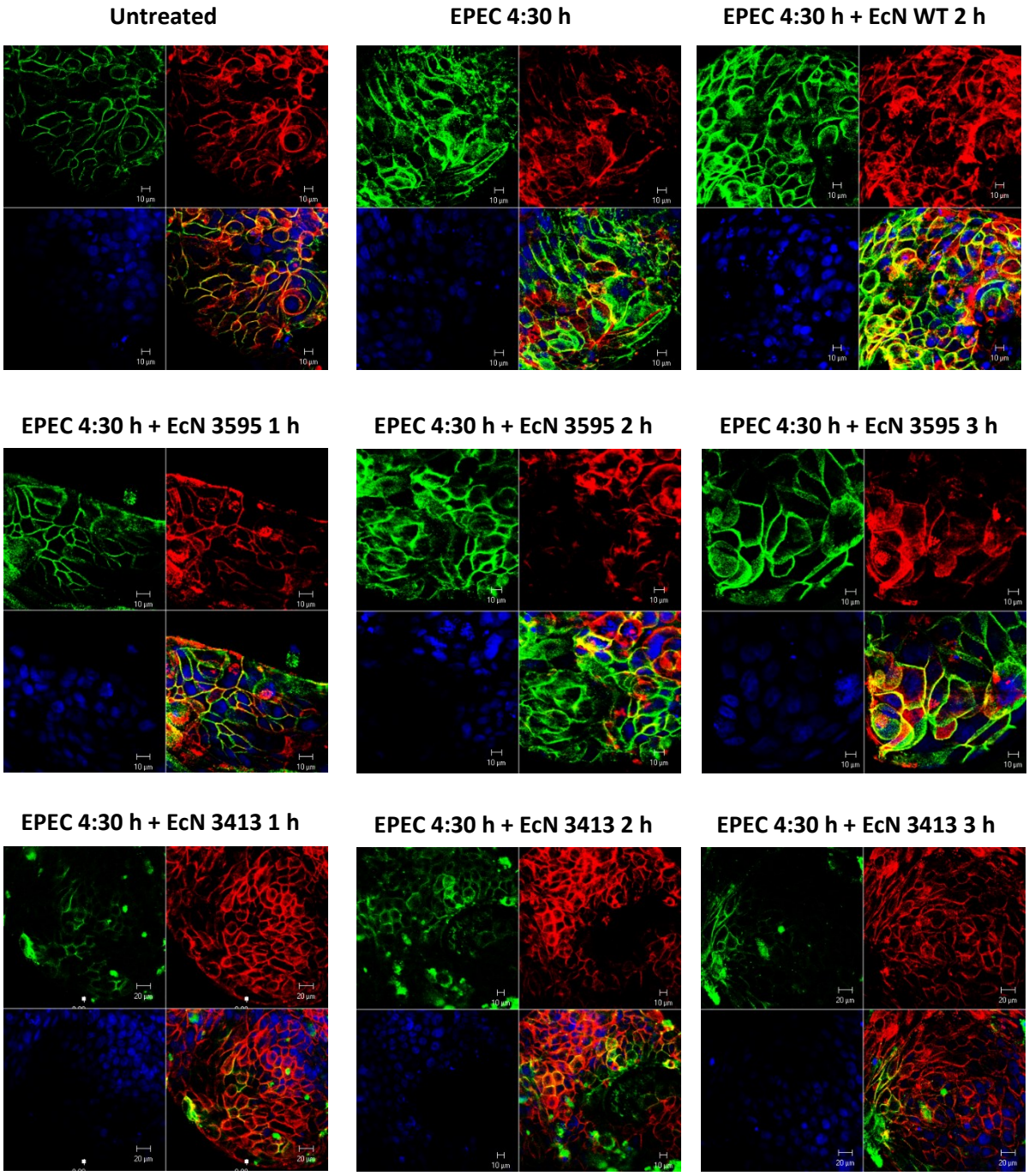

Figure 5.13.1. Effect of two EcN variants on JAM-A distribution after infection of HT29-MTX-E12 cells grown in the 3D system with the EPEC strain E2348/69. Epithelial cells were grown in the 3D cell culture system. They were infected with EPEC strain E2348/69 (MOI 50) for 4:30 h. A gentamicin (250 µg/ml) step was followed to remove the EPEC bacteria, and finally, cells were incubated with EcN variants 3595 and 3413 at an MOI 50 for 1 h, 2 h, and 3 h. Immunofluorescence microscopic images of HT29-MTX-E12 cells are shown. Control cells were left untreated. JAM-A (green), actin cytoskeleton (red), Draq5. Yellow: JAM-A and actin colocalization.

In summary, EcN variant 3595 stimulated a reinforcement of the epithelial barrier. This reinforcement could be achieved by phosphorylation of JAM-A and its subsequent trafficking to the cell membrane, thus increasing the formation of the tight junction complex. Conversely, possible genetic modification of the EcN variant 3413, leading to a non-functional flagellar structure, might not contribute to the phosphorylation of JAM-A, thus preventing its activation and further distribution to the intercellular contacts.

5.14 Effect of OMVs and the supernatant of EcN WT on JAM-A expression and distribution after infection of HT29-MTX-E12 cells with the EPEC strain E2348/69

Incubation experiments using isolated OMVs and supernatant from the probiotic EcN WT after a pre-infection with the EPEC strain E2348/69 were also done. Similar to the described procedure before, HT29-MTX-E12 cells were infected for 4:30 h with EPEC strain E2348/69 (MOI 50). After this time, the cells were washed with PBS and incubated with gentamicin (250 µg/ml) for 1 h at 37 °C. Next, gentamicin was removed, and the cells were intensively and carefully washed to eliminate any rest of the antibiotic. Some samples were incubated with OMVs of EcN WT (30 µg/ml). Others were incubated with the supernatant (20 µg/ml) of this strain for 1 h, 2 h, 3 h, and 4 h. Figure 5.14.1 shows the relative expression of *JAM-A* at the transcriptional level in HT29-MTX-E12 cells grown on beads. We obtained higher *JAM-A* transcript levels when the cells were incubated with the isolated bacterial OMVs, except for the 2 h time point, where the *JAM-A* transcript levels were slightly lower than in cells incubated with the supernatant. After 4 h, EcN WT OMVs induced the highest *JAM-A* response in the epithelial cells (0.6 fold). The increase of *JAM-A* mRNA levels, when cells are incubated with the EcN WT supernatant, varied between 0.1 – 0.3-fold. The lowest response of *JAM-A* was seen after 3 h incubation with the supernatant (Figure 5.14.1).

Immunofluorescence confocal microscopic images are shown in Figure 5.15.1. We analyzed the distribution of JAM-A after 4:30 h pre-infection with EPEC strain E2348/69, followed by an incubation time curve up to 4 h of incubation time with OMVs and the supernatant of wild type EcN. As also seen in previous results, we could observe a re-distribution of JAM-A from the cell membrane to the cytoplasm after 4:30 h EPEC infection. In general, we observed that after a cell-cell contact disturbance, the EcN WT supernatant had a greater impact on the re-localization of JAM-A to the cell membrane than the EcN OMVs. There was a reinforcement of the barrier function after 1 h incubation with the supernatant. Cell boundaries became more evident, and the actin cytoskeleton is less polymerized. Cells incubated with the isolated OMVs, showed recovery after 3 h incubation (Figure 5.14.2).

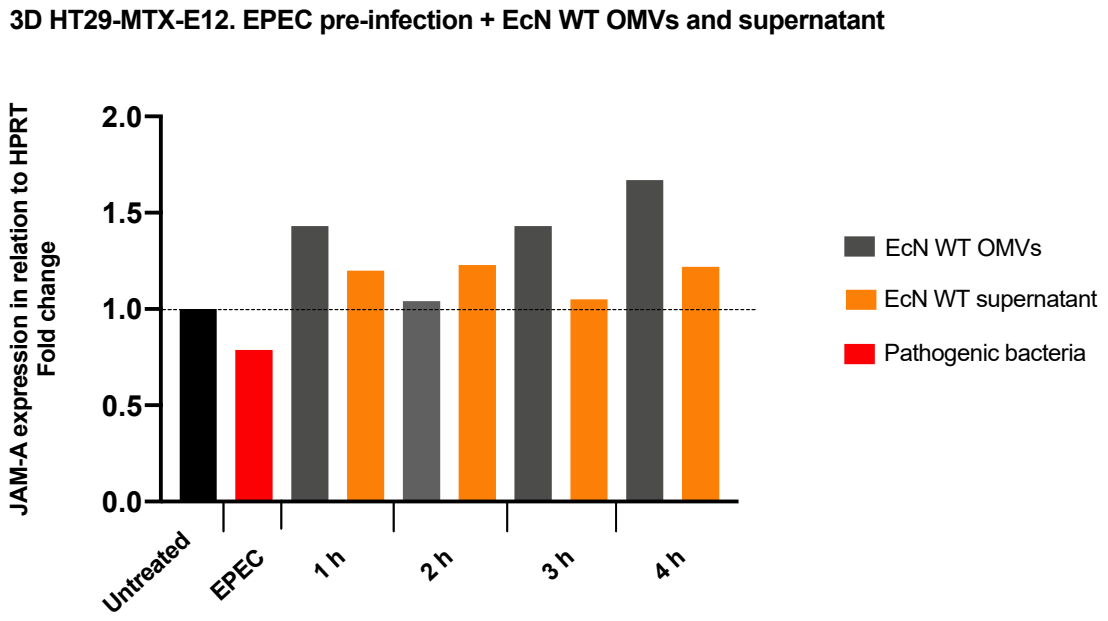

Figure 5.14.1. Effect of OMVs and supernatant of EcN WT on *JAM-A* expression after infection of HT29-MTX-E12 cells with the EPEC strain E2348/69. Epithelial cells were grown in the 3D cell culture system. They were infected with EPEC strain E2348/69 (MOI 50) for 4:30 h. A gentamicin (250 µg/ml) treatment step was followed to eradicate the EPEC bacteria. Finally, the cells were incubated with 30 µg/ml EcN WT OMVs or 20 µg/ml EcN WT supernatant. Control cells were left untreated. The analysis was performed by quantitative real-time PCR. The data were normalized using the housekeeping gene HPRT transcript levels. Results are presented as fold-changes relative to the untreated control. The data were obtained from one single experiment.

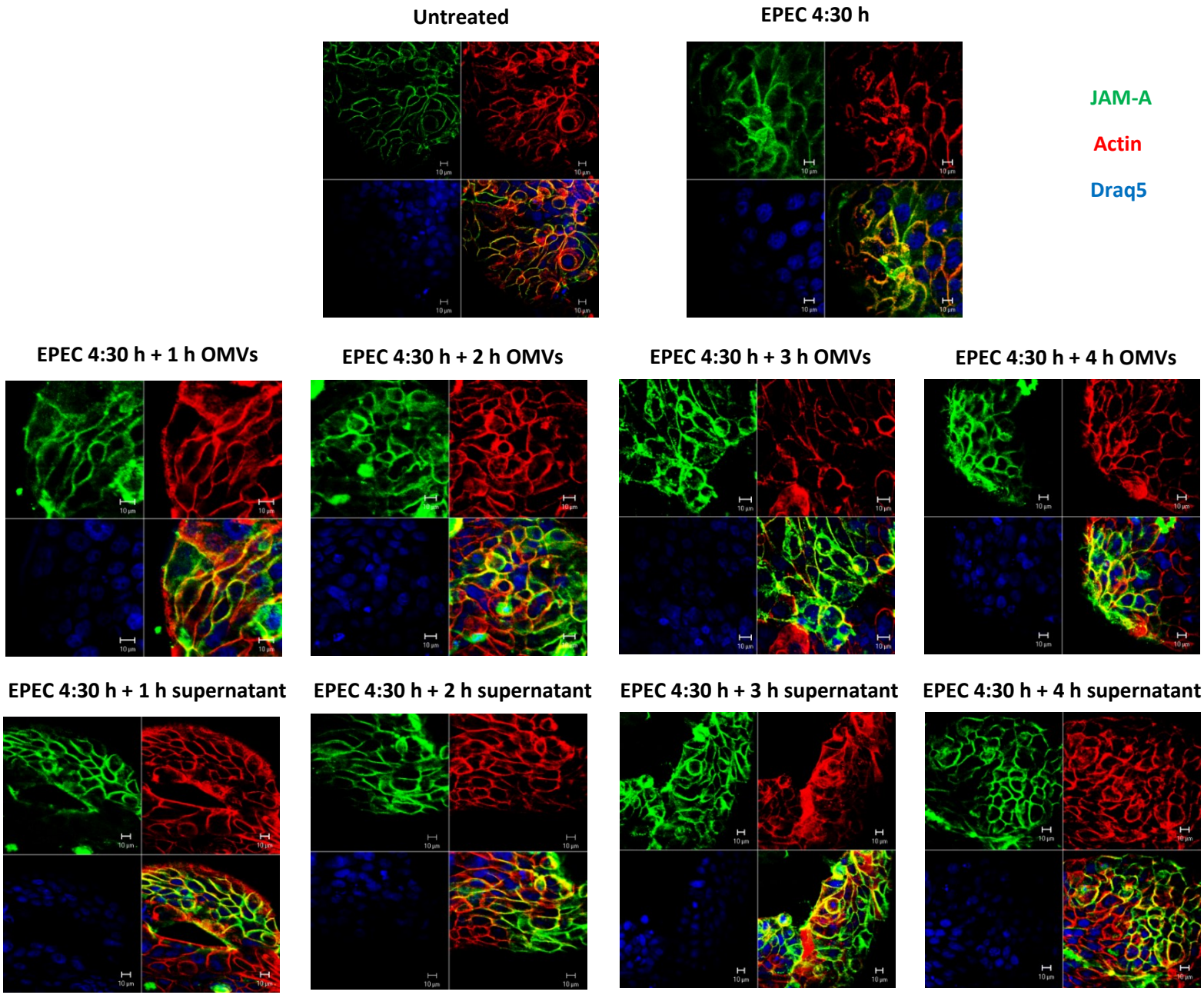

Figure 5.14.2. Effect of OMVs and the supernatant of EcN WT on JAM-A distribution after infection of HT29-MTX-E12 cells with the EPEC strain E2348/69. Epithelial cells were grown in the 3D cell culture system. They were infected with EPEC strain E2348/69 (MOI 50) for 4:30 h. A gentamicin (250 µg/ml) step was followed to kill the EPEC bacteria. Finally cells were incubated with 30 µg/ml EcN WT OMVs or 20 µg/ml EcN WT supernatant. Control cells were left untreated. **JAM-A** (green), **actin cytoskeleton** (red), **Draq5**. Yellow: JAM-A and actin colocalization.

5.15 Effect of OMVs and the supernatant of EcN WT on *MyD88* expression after infection of HT29-MTX-E12 cells with the EPEC strain E2348/69

The expression of *MyD88* levels in cells incubated under the conditions mentioned previously was also analyzed. EPEC strain E2348/69 induced a 0.3-fold reduction of *MyD88* mRNA transcription. EcN WT supernatant induced a slight increase in *MyD88* expression at the transcript level after 1 h and 3 h incubation (0.2-fold), while at 2 h and 4 h, *MyD88* gene transcription was downregulated. EcN WT OMVs had a minor and smaller effect on *MyD88* transcript levels than the supernatant. But, after 3 h and 4 h incubation, there was an upregulation of *MyD88* about 0.1 and 0.2-fold, respectively, in cells incubated with OMVs (Figure 5.15.1).

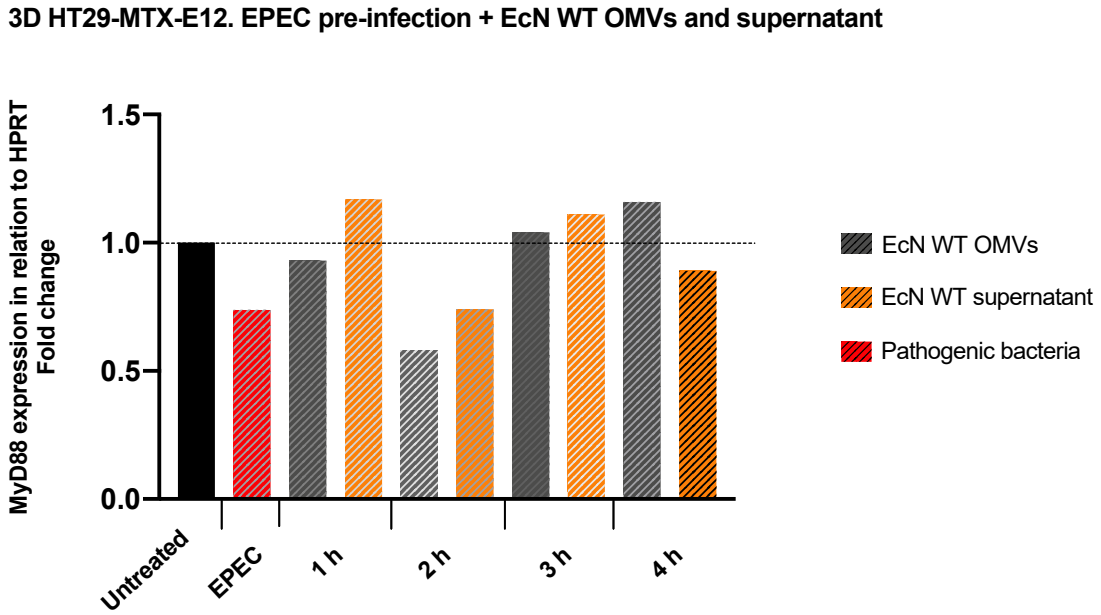

Figure 5.15.1. Effect of OMVs and the supernatant of EcN WT on *MyD88* expression after infection of HT29-MTX-E12 cells with the EPEC strain E2348/69. Epithelial cells were grown in the 3D cell culture system. They were infected with EPEC strain E2348/69 (MOI 50) for 4:30 h. A gentamicin (250 µg/ml) step was followed to remove the EPEC bacteria. Finally, cells were incubated either with 30 µg/ml EcN WT OMVs or 20 µg/ml EcN WT supernatant. Control cells were left untreated. The analysis was performed by quantitative real-time PCR. The data were normalized using the housekeeping gene HPRT transcript levels. Results are presented as fold-changes relative to the untreated control. The data were obtained from one single experiment.

OMVs and the supernatant from EcN WT induced the upregulation of *JAM-A* mRNA levels after an epithelial disruption. Even though the OMVs had a greater effect on *JAM-A* expression, it seemed that the supernatant had a stronger impact on JAM-A distribution to the cell boundaries. *MyD88* showed a slight upregulation after incubation with the EcN OMVs and supernatant. No *TLR5* expression was

detected under these conditions. These data are from single experiments. Therefore, more repetitions should be done to confirm what we already obtained.

5.16 Static *vs*. rotating infection

5.16.1 JAM-A expression and distribution after incubation of HT29-MTX-E12 cells with EPEC strain E2348/69, EcN WT and EcN 3595

To get even closer to an *in vivo* situation, we also performed host-bacteria incubations under rotating conditions. The previous results were based on static conditions. This means that cells on beads, incubated for some time in the RWV bioreactor, were taken out from the chamber and placed in a 24-well plate. The corresponding bacteria strain was inoculated into the well, and the plate was incubated at 37 °C for a specific time (Figure 5.16.1). Under rotating conditions, the beads were not taken out from the RWV bioreactor, but instead, bacteria were added into a disposable bioreactor that was in constant movement (15 rpm). During the infection time, fluid shear was not absent, and this movement could represent the peristaltic contractions of the gut.

Figure 5.16.2 shows the expression of *JAM-A* under both conditions. Cells were incubated with EPEC strain E2348/69, EcN WT, and EcN variant 3595 for 4 h at an MOI 50. *JAM-A* levels rose when HT29-MTX-E12 cells and bacteria were under constant movement (green columns), but they decreased when the fluid shear was removed (black columns). However, there were no significant differences in *JAM-A* expression between the two conditions and between incubations with the different bacterial types.

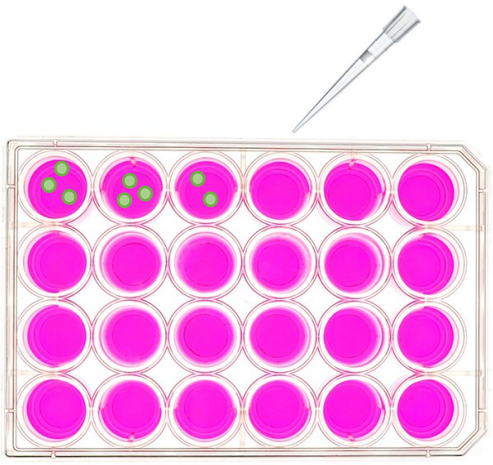

Figure 5.16.1. Schematic representation of HT29-MTX-E12 cells grown on beads and incubated under static conditions.

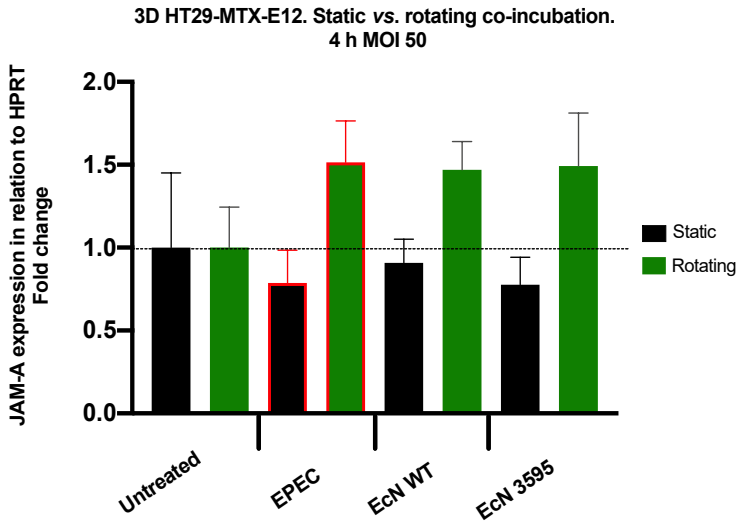

Figure 5.16.2. *JAM-A* expression after incubation of HT29-MTX-E12 cells with the EPEC strain E2348/69 and the probiotic strain EcN WT as well as its variant EcN 3595, for 4 h at an MOI 50 under static and rotating conditions.

Time kinetics of the effect of EPEC strain E2348/69 on JAM-A distribution under rotating conditions were done to determine a suitable EPEC pre-incubation time period before incubating the cells with the probiotic strain. Figure 5.16.3 shows an immunofluorescence staining of HT29-MTX-E12 cells infected with EPEC strain E2348/69 (MOI 50) for 4 h, 5 h, and 6 h under rotating and static conditions. We also wanted to compare JAM-A distribution between the two types of infection mode. EPEC induced a more substantial negative effect under static conditions. At 5 h infection, the epithelial damage was more visible, and after 6 h infection an impairment of the actin cytoskeleton and JAM-A was evident (Figure 5.16.3, **B**). Cells infected under rotating conditions seemed to be more protected against EPEC infection. After 5 h of infection, there was a re-localization of JAM-A to the cytoplasm. However, the re-localization was more prominent under static conditions (Figure 5.16.3, **A**). We assumed that the presence of fluid shear made it more difficult for the bacteria to get into contact with the HT29-MTX-E12 cells.

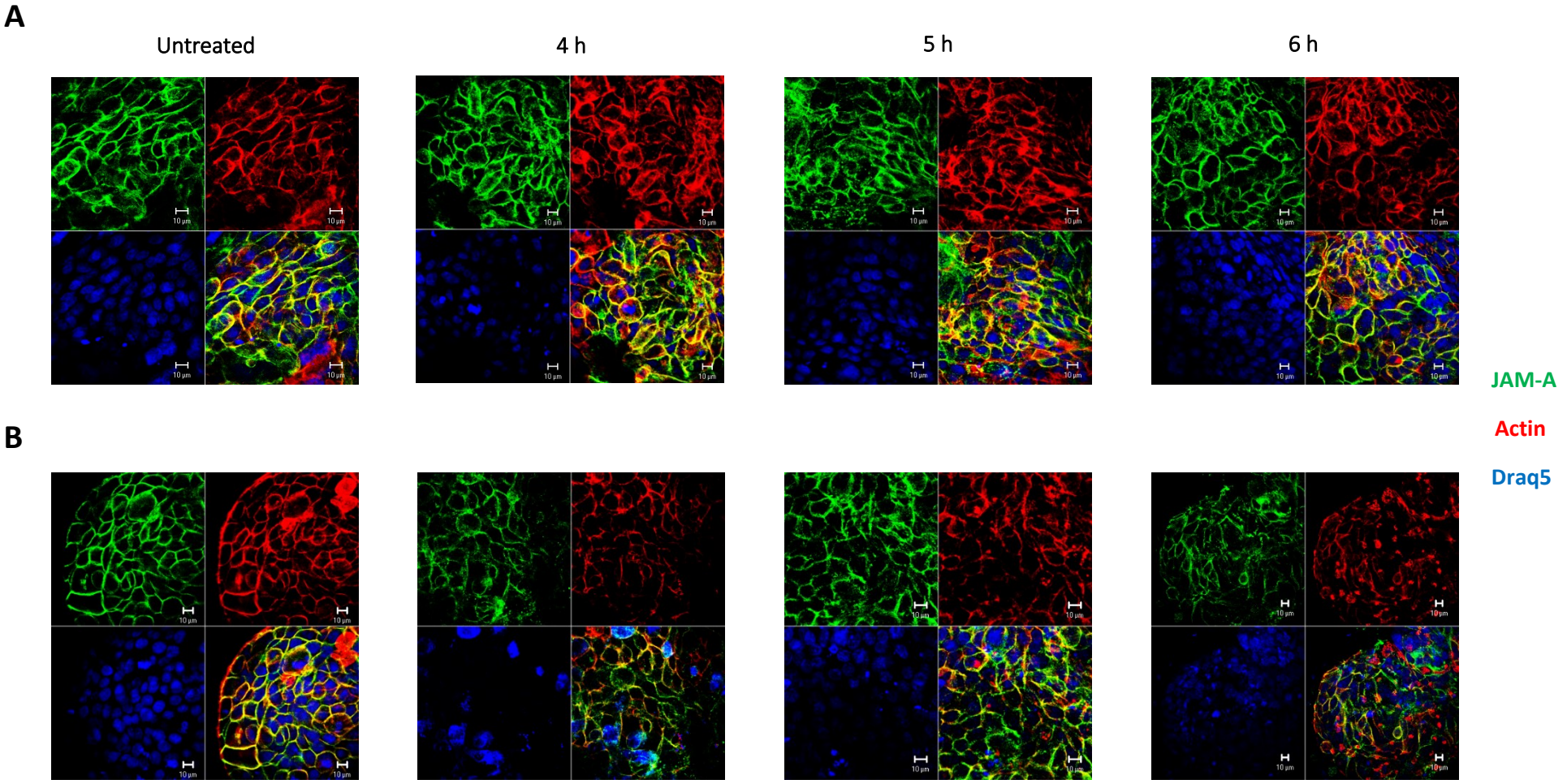

Figure 5.16.3. Kinetics of JAM-A distribution in HT29-MTX-E12 cells grown in the 3D cell culture system upon infection with EPEC strain E2348/69. Immunofluorescence confocal microscopic images. **A)** Rotating infection. **B)** Static infection. MOI 50. Control cells were left untreated. **JAM-A** (green), **actin cytoskeleton** (red), **Draq5**. Yellow: JAM-A and actin colocalization.

5.16.2 *MyD88* expression after incubation of HT29-MTX-E12 cells with EPEC strain E2348/69, EcN WT and EcN 3595

The expression of *MyD88* was also evaluated with the same incubation conditions of the epithelial cells. Under the static conditions, transcript levels of *MyD88* encoding gene were downregulated compared to untreated cells. Under rotating conditions, there was an increase of 0.2-fold in *MyD88* mRNA levels. However, there were no significant differences in *MyD88* expression between the two different conditions, and between incubation with the different bacterial types (Figure 5.16.4). These observations made us think that perhaps there was a different cellular response to bacterial infection when the interacting bacteria and epithelial cells are subjected to fluid shear stress.

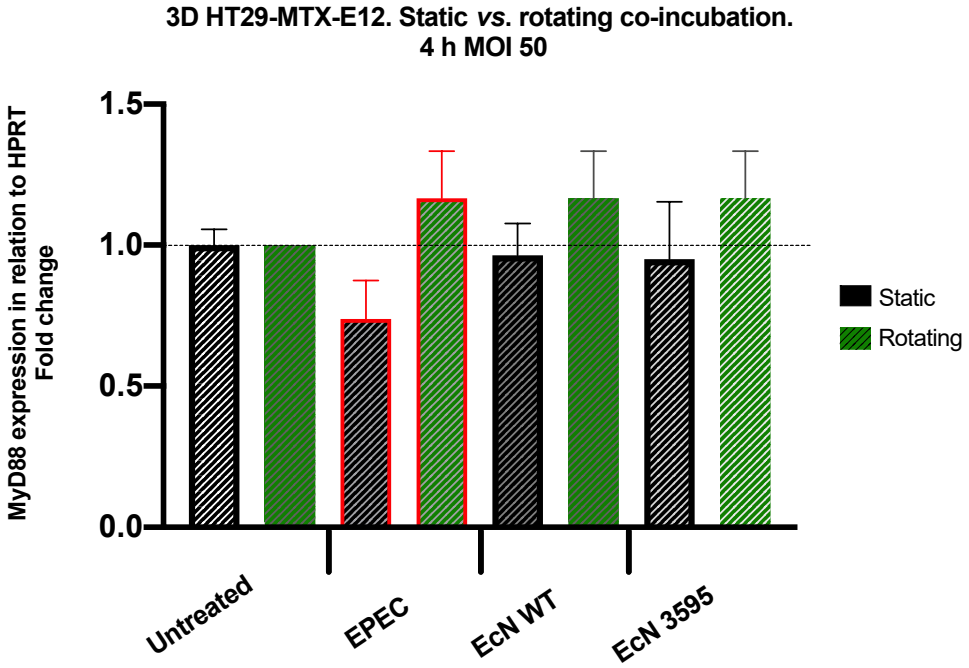

Figure 5.16.4. Impact of static or rotating incubation on *MyD88* expression in HT29-MTX-E12 cells, grown in the 3D cell culture system upon infection with the EPEC strain E2348/69, probiotic strain EcN WT and its variant 3595. The epithelial cells were infected for 4 h at an MOI 50, under static or rotating conditions.

The presence of low-fluid shear stress during cells and bacteria incubation triggered a different cellular response. In the same way, a constant movement might protect the cells from being rapidly targeted by microorganisms in the gut.

5.17 RT^2 profiler arrays to analyze bacteria – host interactions at the transcriptional level

To allow a more reliable gene expression analysis, we used RT^2 Profiler PCR arrays (Qiagen, Hilden) to quantify relative expression changes of 84 related genes involved in the host immune response to bacterial infection. Figure 5.17.1 shows a comparison of the differential cellular immune response of HT29-MTX-E12 cells under different culture and incubation conditions. In all cases, the cells were incubated with bacteria for 4 h with an MOI of 50. Epithelial cells grown in the conventional cell culture system (2D) responded differently compared to those that were cultivated in the 3D cell culture system (Figure 5.17.1, **A, B**). Six distinct genes were highlighted inside red boxes: MyD88, a central regulator during the innate immune response; TLR5 that recognizes bacterial flagellin; TLR4, that recognizes lipopolysaccharides (LPS); TNF, a cytokine involved in systemic inflammation and regulates immune cells, and CXCL1 and CXCL2, which are chemokines with neutrophil recruitment activity. The expression of these genes changed between incubation with pathogenic or probiotic bacteria, and it also depended on the cell culture system that was employed to grow the cells. For example, on the 2D cell culture system, *MyD88* expression was high in untreated and EcN-treated cells, but low in cells infected with EPEC strain E2348/69. Contrarily, on the 3D cell culture system, the response of *MyD88* towards EPEC infection was downregulated but upregulated when cells were incubated with EcN WT. In untreated cells, *MyD88* expression was also low (Figure 5.17.1, **A, B**).

Figure 5.17.1, **C, D** shows cellular immune responses of HT29-MTX-E12 cells cultured in the 3D system and incubated under static and rotating conditions. In this case, the cells were also incubated with the EcN variant 3595. Differences in gene expression between both incubation conditions were also obtained. Under rotating incubation, *MyD88* expression was high in untreated cells, a little bit less in EcN WT and EcN variant 3595-treated cells and low in EPEC-infected cells. Another example was *TNF*, which was expressed at a low level in untreated cells, but higher in cells treated with the different bacteria. Cells infected with EPEC strain E2348/69 showed less *TNF* expression than those incubated with the probiotic strain EcN (Figure 5.17.1, **D**). When cells were incubated statically, *MyD88* expression was low in untreated and EPEC-treated cells but elevated in cells incubated with probiotic wild type strain EcN. EcN variant 3595 induced a lower *MyD88* response than EcN WT. *TNF* expression was low in untreated cells and cells treated with EcN variant 3595 and EPEC strain E2348/69 but higher in cells incubated with EcN WT (Figure 5.17.1, **C**).

The most expressed genes obtained from RT^2 Profiler PCR arrays are summarized in Table 5.2. This Table displays the fold-change values of 9 out of 84 genes involved in host immune response to a bacterial infection. Additionally, Table 5.2 shows the expression levels of these genes in HT29-MTX-E12 cells cultured in the 3D system and incubated with supernatants (8 µg/ml) from pathogenic and

probiotic bacteria for 4 h, and under static conditions (the complete set of array data is not shown). Bacterial supernatant has been added to the HT29-MTX-E12 cells at the following concentrations: 2 µg/ml, 4 µg/ml, 6 µg/ml, and 8 µg/ml (data not shown). Cells incubated with 8 µg/ml of supernatant showed the highest expression of *JAM-A*. Therefore, this amount was used to perform the PCR array analysis. The cellular expression profile was different between cells incubated with bacteria or with bacterial supernatants. Some genes were more expressed upon bacterial infection but less expressed when supernatants were added (under static conditions as well). One example is *CXCL1*, which expression was much higher in the presence of live bacteria but lower when cells were incubated with the bacterial supernatants. *TLR5* was more expressed upon the addition of supernatant than upon bacterial infection (Table 5.2, 3D system static infection *vs.* 3D system, supernatant infection). It is important to remember that the supernatant of EcN variant 3595 was not used but instead the supernatant of the highly flagellated EcN variant PZ816.

In Table 5.2, the green color represents the lowest value, and it gets closer to red when the fold change value increases.

RT^2 profiler arrays (bacteria-host interactions)

A

2D cell culture: HT29-MTX-E12 static infection

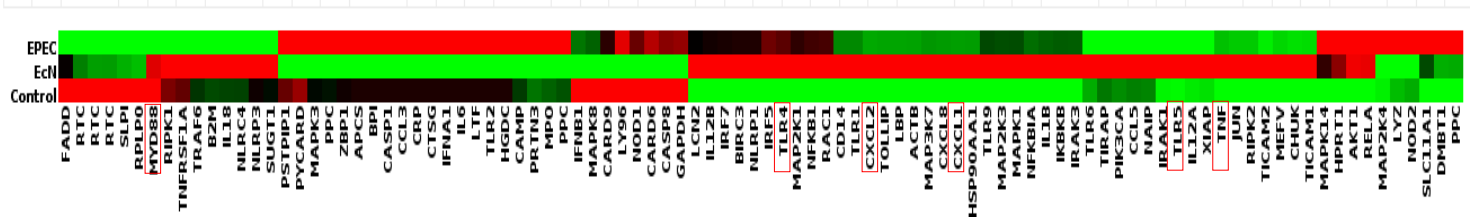

B

3D cell culture: HT29-MTX-E12 static infection

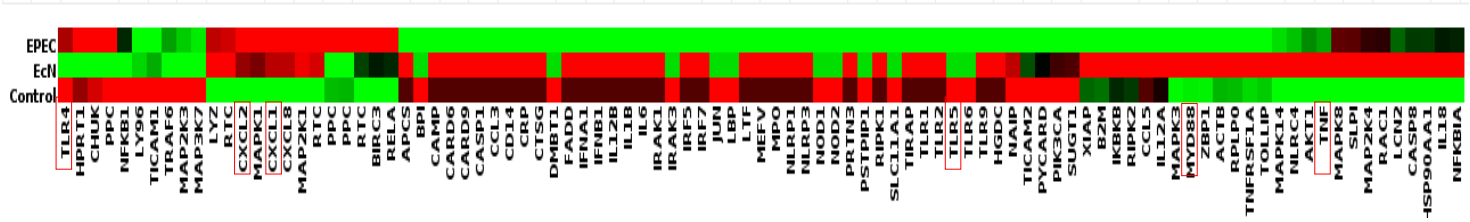

C

3D cell culture: HT29-MTX-E12 static infection

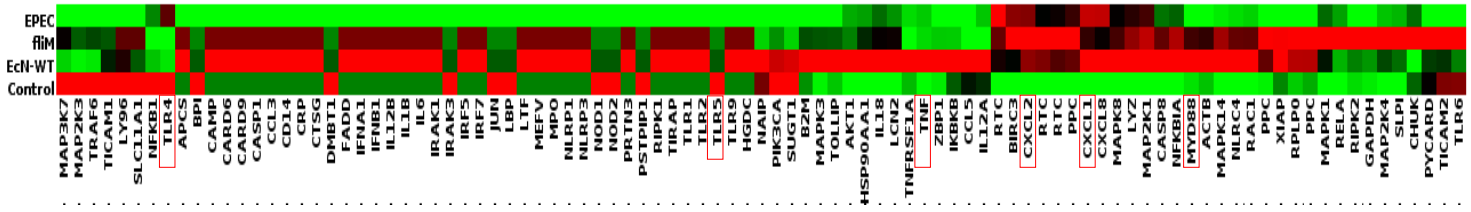

D

3D cell culture: HT29-MTX-E12 rotating infection

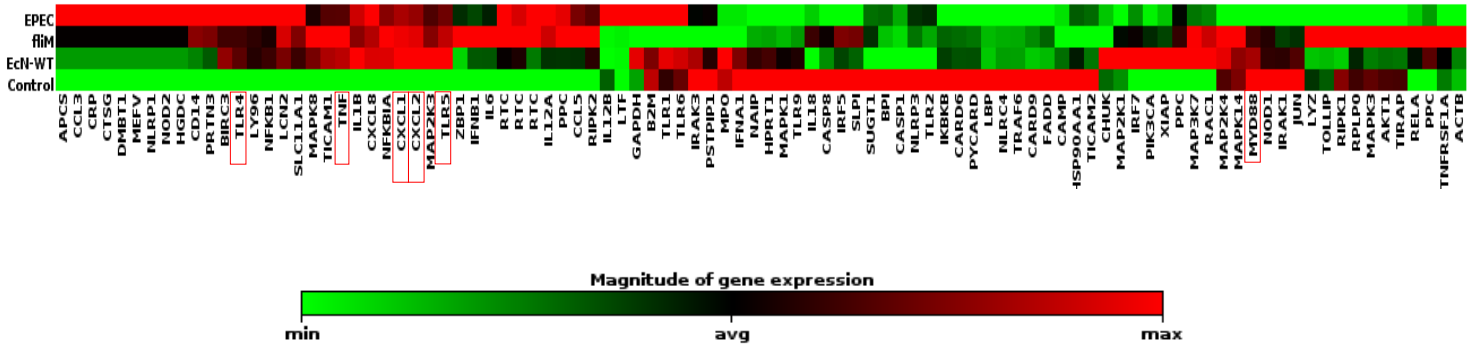

Figure 5.17.1. Analysis of the cellular immune response of HT29-MTX-E12 cells to bacterial infection using RT² Profiler arrays. **A)** Cells were grown in the conventional 2D cell culture system and incubated with EPEC strain E2348/69 and strain EcN WT. **B)** Cells were grown in the 3D cell culture system and incubated with EPEC strain E2348/69 and EcN strain WT. **C)** Cells were grown in the 3D cell culture system and incubated with the EPEC strain E2348/69, the probiotic EcN WT and its variant 3595 under static conditions. **D)** Cells were grown in the 3D cell culture system and incubated with the EPEC strain E2348/69, the probiotic EcN WT and its variant 3595 under rotating conditions.

Table 5.2. Fold-change values, compared to control samples, of HT29-MTX-E12 cell gene expression related to the host immune response to bacterial infection

Genes	2D system		3D system. Static infection			3D system. Rotating infection			3D system. Supernatants infection		
	EcN WT	EPEC	EcN WT	EcN 3595	EPEC	EcN WT	EcN 3595	EPEC	EcN WT	EcN PZ816	EPEC
CXCL1	180.3	34.7	182.3	109.1	162.0	57.5	55.9	48.0	25.6	71.0	55.7
CXCL2	238.0	40.7	221.3	282.1	213.8	84.2	79.6	67.0	27.1	68.1	60.1
IL1B	92.1	29.2	1.3	1.2	0.9	25.9	20.2	23.5	15.8	77.7	72.0
NFKB1	4.1	3.0	0.6	0.6	0.7	1.5	1.4	1.8	1.9	4.7	3.9
NFKBIA	21.9	6.9	6.0	5.2	2.5	16.5	17.6	13.7	5.0	7.6	6.8
TNF	503.1	60.4	3.6	1.2	1.3	558.3	641.2	429.1	117.8	238.9	213.8
MyD88	1.0	0.8	2.3	1.8	0.9	1.0	0.9	0.7	1.8	2.1	1.8
TLR4	1.4	1.3	0.6	0.6	0.9	1.2	1.2	1.4	1.8	2.3	3.2
TLR5	1.8	1.0	0.6	0.6	0.5	1.4	1.3	1.3	2.4	4.7	4.7

Briefly, RT^2 Profiler arrays indicated distinct cellular immune responses to different bacterial infections and incubation conditions. The probiotic and pathogenic effect varied depending on the degree of cellular development, confluency, and an essential factor, the presence or absence of fluid shear stress that influences cell growth, gene expression pattern, and host-microbe interactions.

5.18 Cellular gene expression profiles in the presence or absence of mucin

To evaluate the protective role of the mucin present on top of the intestinal epithelial cells, we performed incubation experiments using an additional cell line, i.e., HT29 cells, which do not secrete mucin blebs. HT29-MTX-E12 cells were used as well to have a comparison of cellular gene expression profiles resulting from the presence or absence of mucin production. For that, 1 x 10^5 cells from both cell lines were seeded in the 2.5D system (transwell filters) until they reached confluency. Each cell line was pre-infected with EPEC strain E2348/69 (MOI 50) for 4:30 h under static conditions. Afterward, the EPEC strain was removed and cells were incubated for 1 h with 30 µg/ml gentamicin (less toxic for the cells than 250 µg/ml) to kill most of the remaining EPEC bacteria. Then, cells were washed carefully and intensively to ensure the antibiotic was removed well. Next, either fresh cell culture medium or EcN WT (MOI 50) was added to the cells for 2 h to further analyze the cellular response to the probiotic strain after an epithelial disruption. Incubations for 4:30 h with EPEC strain E2348/69 and 2 h with EcN WT alone were done as controls.

Similar to the previous experiments, RT^2 Profiler PCR array analyses of each sample were done to investigate the cellular immune response at the transcriptional level. Table 5.3 lists the most expressed genes under the tested conditions. Figure 5.18.1 shows the heat maps of the 84 genes whose expression was evaluated in HT29 and HT29-MTX-E12 cells. In general, “naked” HT29 cells showed a higher upregulation of some of the genes listed in Table 5.3. Two examples are *CXCL1* and *CXCL2*, whose expression was stronger in HT29 cells than in HT29-MTX-E12 cells after EPEC and EcN incubation. Mainly, the EcN WT strain induced the strongest upregulation of these genes in HT29 cells. These results confirm that the presence of mucin in cell culture models confers protection to the cells.

Table 5.3. Comparison of cellular transcriptional responses between non-mucin and mucin-producing cell lines to bacterial infection under static conditions

Genes	EPEC		EPEC + EcN WT		EPEC + medium		EcN WT	
	HT29	HT29-MTX-E12	HT29	HT29-MTX-E12	HT29	HT29-MTX-E12	HT29	HT29-MTX-E12
CXCL1	37.6	7.9	8.4	6.0	10.3	4.7	429.4	39.6
CXCL2	33.4	7.8	6.5	3.8	9.4	3.7	463.4	39.3
IL1B	3.4	8.5	2.0	4.6	3.7	4.6	10.3	4.7
NFKB1	2.1	1.8	1.4	2.1	1.6	1.8	1.5	1.5
NFKBIA	5.7	4.2	1.5	2.3	1.6	1.7	21.8	15.9
TNF	60.2	18.6	6.4	7.2	7.1	2.1	297.4	82.0
MyD88	0.7	1.3	0.6	1.6	0.7	1.1	0.7	1.2
TLR4	1.6	1.7	1.3	1.3	1.4	1.5	0.7	1.0
TLR5	1.4	3.6	0.8	4.1	1.0	3.2	1.6	2.0

Fold-change values, compared to control samples of genes related to the host immune response to bacterial infection are included in Table 5.3.

A

2.5D cell culture: HT29

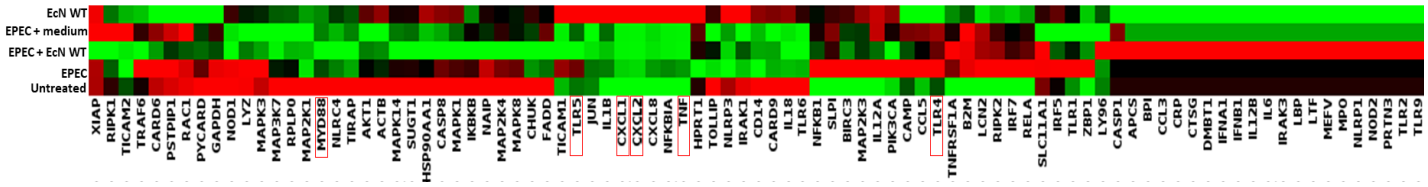

B

2.5D cell culture: HT29-MTX-E12

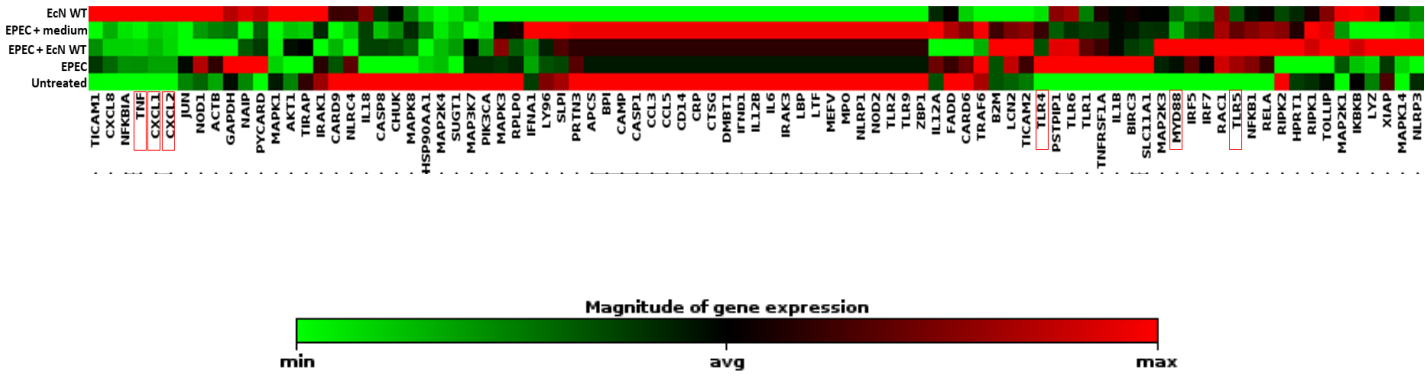

Figure 5.18.1. Comparison of the cellular immune response of HT29 and HT29-MTX-E12 cells to bacterial infection using RT² Profiler arrays. One set of cells was incubated with EPEC strain E2348/69 and EcN WT strain alone. Others were pre-infected with EPEC strain E2348/69, followed by an incubation either with fresh medium or with EcN WT. An MOI of 50 was used. **A)** non-mucin-producing HT29 cells grown in the 2.5D system and incubated under static conditions. **B)** mucin-producing HT29-MTX-E12 cells grown in the 2.5D system and incubated under static conditions.

The presence of a mucin layer resulted in a differential response of the cells to react differently, in terms of gene expression, to bacterial infection. This is why it is necessary to mimic closer *in vivo* conditions of the human gut to understand host-microbe crosstalk better.

Additionally, Figure 5.18.2 shows TEM pictures of non-mucin and mucin-secreting cells infected with EPEC strain E2348/69. HT29 cells, which do not produce mucin blebs on the inside, were infected with the EPEC strain for 3 h with an MOI 20. After this time, we visualized actin pedestals formation, which promotes bacterial attachment on the surface of the epithelial cells (Figure 5.18.2, **A, B**). In contrast, HT29-MTX-E12 cells, which produce and secrete a high amount of mucin (Figure 5.18.2, **C**, MUC), did not present actin pedestal formation after 4 h of infection with EPEC strain E2348/69 with an MOI 50 (Figure 5.18.2, **D**). These results were also confirmed by light confocal microscopy images. An MOI of 50 was used to infect both cell lines (Figure 5.18.3). Actin cytoskeleton protrusions were visualized on HT29 cells after 3 h of EPEC infection (Figure 5.18.3, **A**, white arrows). Figure 5.18.3, **B** shows the last time point (6 h) of HT29-MTX-E12 and EPEC co-incubation. Similar to TEM pictures, no pedestal formation was seen.

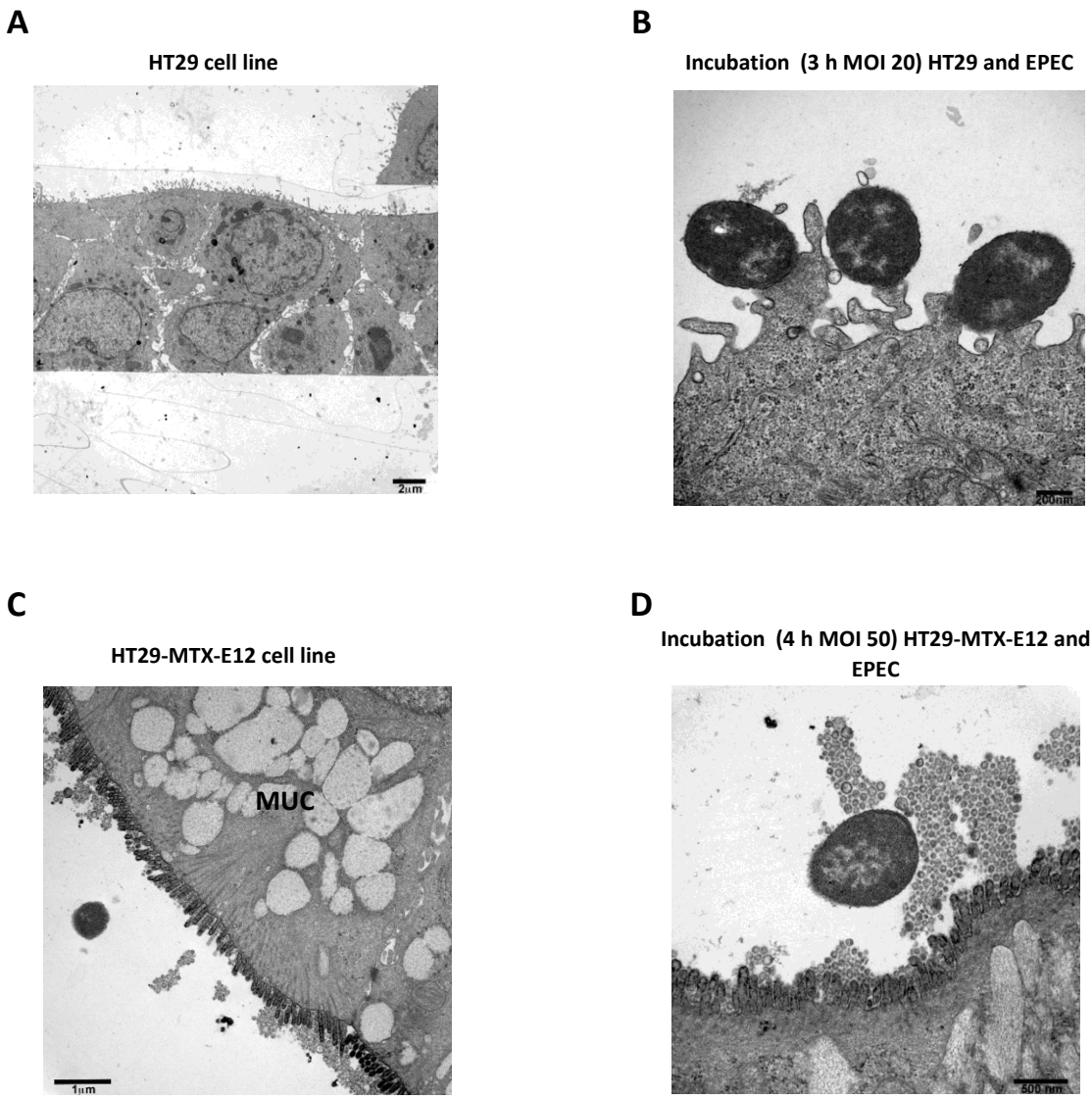

Figure 5.18.2. Incubation of EPEC strain E2348/69 and mucin or non-mucin secreting epithelial cells. A) Physical features of HT29 cells. There was a lack of mucin blebs inside the cells. **B)** Pedestal formation after infection of HT29 cells with EPEC strain E2348/69 for 3 h at MOI 20. **C)** Physical features of HT29-MTX-E12 cells. There was a high amount of mucin blebs inside the cells that can eventually be secreted to the outside. **D)** No pedestal formation was visible after infection of HT29-MTX-E12 cells with EPEC strain E2348/69 for 4 h at MOI 50. Pictures are courtesy of Lilo Greune.

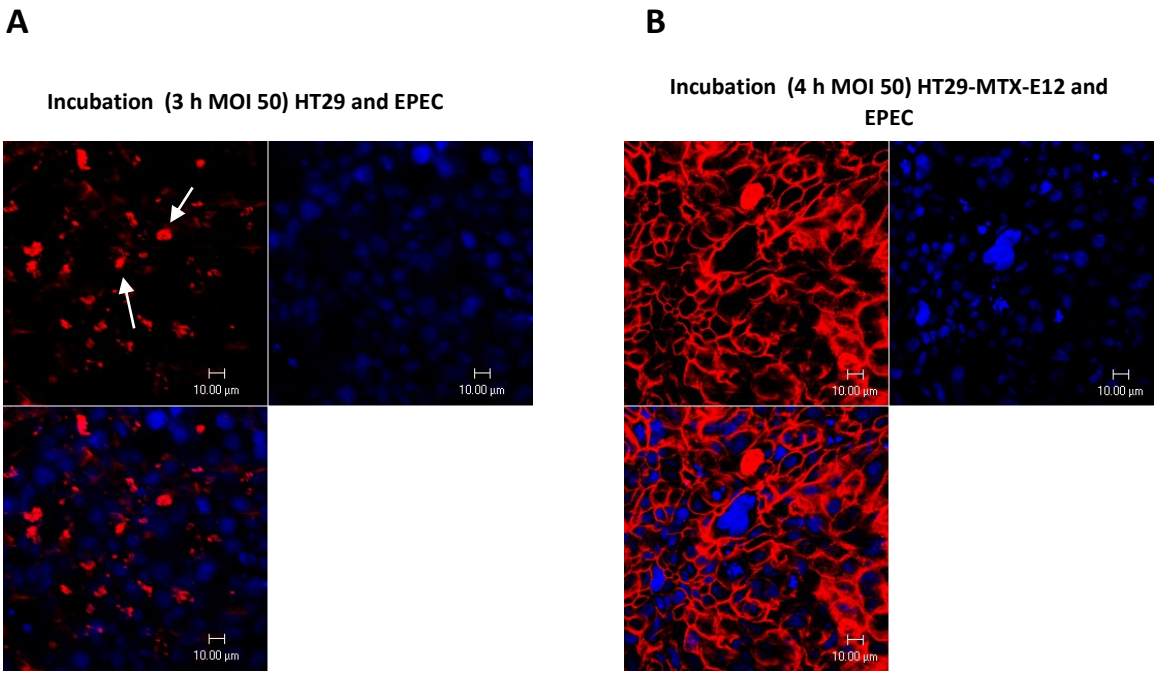

Figure 5.18.3. Analysis of EPEC strain E2348/69 infection of mucin or non-mucin secreting epithelial cells by light scanning confocal pictures. A) White arrows indicate pedestal formation after infection of HT29 cells with EPEC strain E2348/69 for 4 h at MOI 50. **B)** No pedestal formation was visible after infection of HT29-MTX-E12 cells with EPEC strain E2348/69 for 6 h at MOI 50.

5.19 JAM-A detection in HT29-MTX-E12 cells by Western blot

The quantification of JAM-A protein levels was done using the Western blot technique. HT29-MTX-E12 cells grown in the 2.5D or 3D cell culture systems were incubated with EPEC strain E2348/69 and the different variants of EcN, for 4 h with an MOI of 50. Afterward, the epithelial cells were harvested to detect the amount of JAM-A levels. We used a JAM-A antibody to identify the presence of the total protein and the JAM-A PY280 to detect JAM-A phosphorylated at the tyrosine 280. It is known that JAM-A has a molecular mass of approximately 37 kDa. However, it has also been published that JAM-A can be found as monomers and dimers (Monteiro *et al*., 2014). Figure 5.19.1 shows Western blot results, from HT29-MTX-E12 cells grown in the 3D cell culture system, with bands corresponding to JAM-A monomers with a molecular weight of ~ 20 kDa, and JAM-A dimers with a molecular weight of ~ 50 kDa. Weak bands at 37 kDa also correspond to the JAM-A protein. The anti-JAM-A PY280 antibody recognized JAM-A monomers that should be phosphorylated at the tyrosine 280 residue, while anti-JAM-A recognized dimers of JAM-A present in the epithelial cells. Alpha- tubulin (about 55 kDa) was used as a housekeeping protein to normalize JAM-A protein levels.

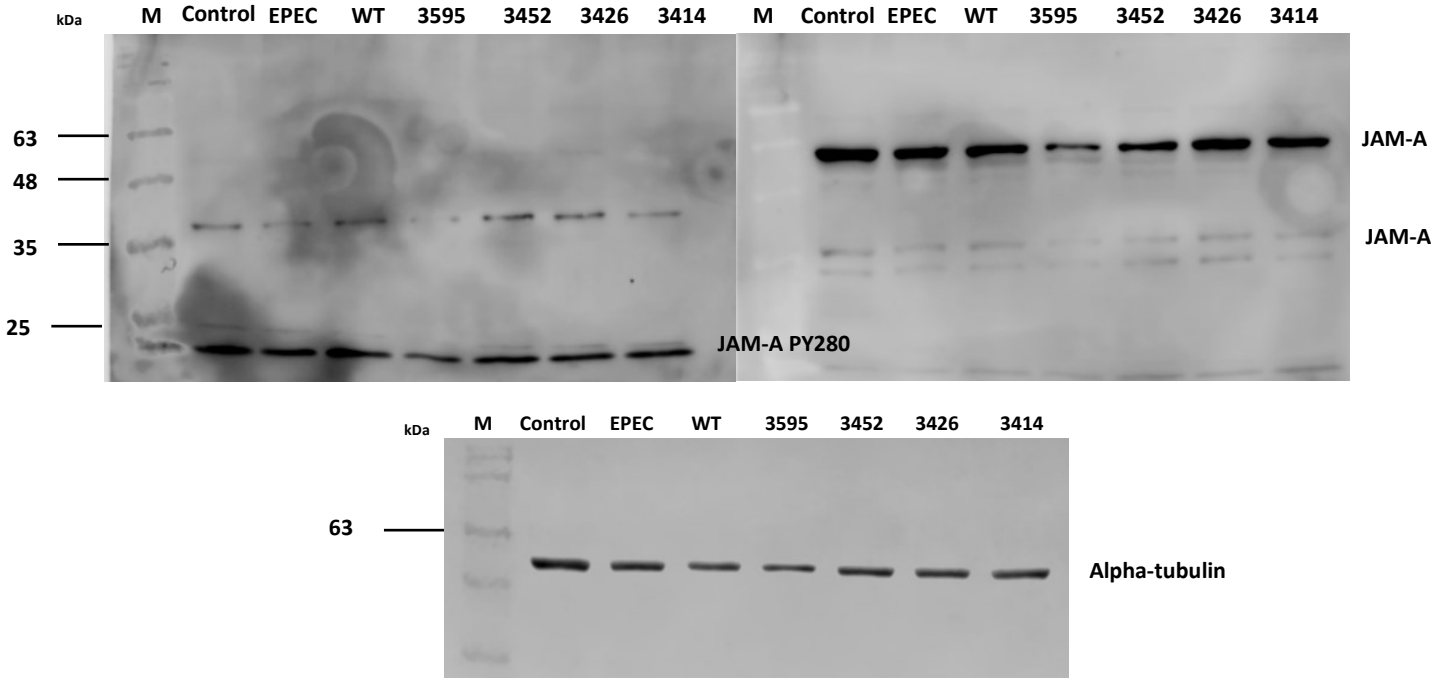

Figure 5.19.1. Quantification of JAM-A protein levels in HT29-MTX-E12 cells cultured in the 3D system and incubated with the pathogenic EPEC strain E2348/69 and the different variants of the probiotic strain EcN for 4 h with an MOI of 50. The Western blot technique was used to transfer denaturated proteins onto a PVDF membrane. JAM-A monomers have a molecular weight of ~ 25 kDa, and JAM-A dimers a molecular weight of ~ 50 kDa. Bands at 37 kDa also correspond to JAM-A protein. Alpha-tubulin was used as a housekeeping protein to normalize JAM-A protein levels. M: molecular size marker.

Figure 5.19.2 shows JAM-A and JAM-A PY280 protein levels in cells cultured in the 2.5D and 3D systems and incubated with pathogenic and probiotic bacteria. In general, total and phosphorylated protein levels were different depending on the infecting strains and cell culture systems. Cells in the 2.5D model showed about 0.1 and 5-fold increase of JAM-A and JAM-A PY280 levels compared to untreated cells. EcN WT led to higher levels of phosphorylation of JAM-A at the tyrosine 280 (6-fold), resulting in significant differences compared to control cells. Similarly, the infection with EcN variants 3452 and 3426 also increased levels of JAM-A phosphorylation significantly (0.3-fold) (Figure 5.19.2, **A**). The percentage of JAM-A PY280 was calculated. Even though EcN WT induced an elevated JAM-A phosphorylation, the portion of the phosphorylated protein corresponded to approximately 1% of the total amount of JAM-A. Cells incubated with the EcN variant 3598, had a higher proportion of JAM-A PY280-positive signal (12%). Differences in the percentage of JAM-A PY280 were not significant between untreated and treated cells (Figure 5.19.2, **B**).

JAM-A and JAM-A PY280 protein levels increased about 0.1 and 1.5-fold in epithelial cells cultured in the 3D model. No significant differences between treated and untreated cells and between the total amount of JAM-A and JAM-A PY280 were obtained (Figure 5.19.2 **C**). EPEC strain E2348/69 and the EcN variant 3595 induced the highest proportion of JAM-A PY280 (13%). In the same way, the degree of phosphorylation of JAM-A in epithelial cells differed between the cell culture systems (Figure 5.19.2, **B**, **D**).

The quantification of the total JAM-A and JAM-A PY280 protein levels were also analyzed under rotating conditions. HT29-MTX-E12 cells were incubated for 4 h with an MOI 50 with the EPEC strain E2348/69, the probiotic strain EcN WT and its variant 3595. The levels of JAM-A and JAM-A PY280 were similar in cells incubated with the EPEC isolate (Figure 5.19.2, **E**). These levels were higher under rotating conditions than under static conditions (0.5 *vs.* 0.1-fold, respectively). Levels of total and phosphorylated JAM-A were similar in epithelial cells incubated with EcN WT under rotating and static conditions. A downregulation of JAM-A and JAM-A PY280 protein levels were detectable when cells were incubated with the EcN variant 3595 under rotating conditions. Contrarily, EcN variant 3595 induced an upregulation of the protein levels under static conditions (Figure 5.19.2, **C** and **E**). EPEC strain E2348/69 stimulated higher phosphorylation of JAM-A at tyrosine 280 residue compared to cells treated with probiotic bacteria under rotating conditions (Figure 5.19.2, **F**).

A

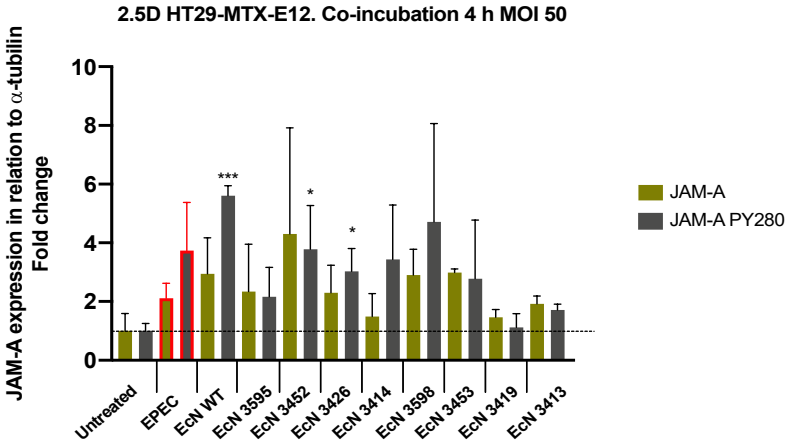
2.5D HT29-MTX-E12. Co-incubation 4 h MOI 50
JAM-A expression in relation to α-tubilin
Fold change
10
8
6
4
2
0
***
*
*
Untreated
EPEC
EcN WT
EcN 3595
EcN 3452
EcN 3426
EcN 3414
EcN 3598
EcN 3453
EcN 3419
EcN 3413
JAM-A
JAM-A PY280

B

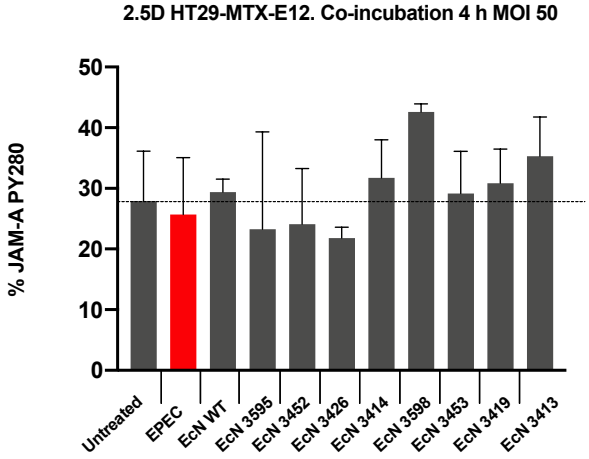
2.5D HT29-MTX-E12. Co-incubation 4 h MOI 50
% JAM-A PY280
50
40
30
20
10
0
Untreated
EPEC
EcN WT
EcN 3595
EcN 3452
EcN 3426
EcN 3414
EcN 3598
EcN 3453
EcN 3419
EcN 3413

C

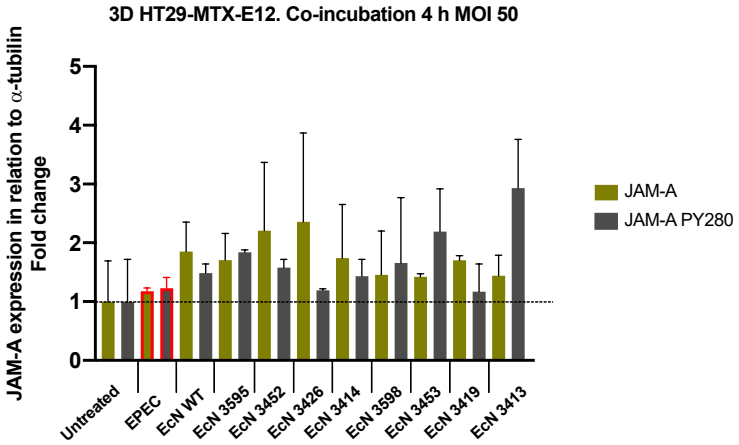
3D HT29-MTX-E12. Co-incubation 4 h MOI 50
JAM-A expression in relation to α-tubilin
Fold change
5
4
3
2
1
0
Untreated
EPEC
EcN WT
EcN 3595
EcN 3452
EcN 3426
EcN 3414
EcN 3598
EcN 3453
EcN 3419
EcN 3413
JAM-A
JAM-A PY280

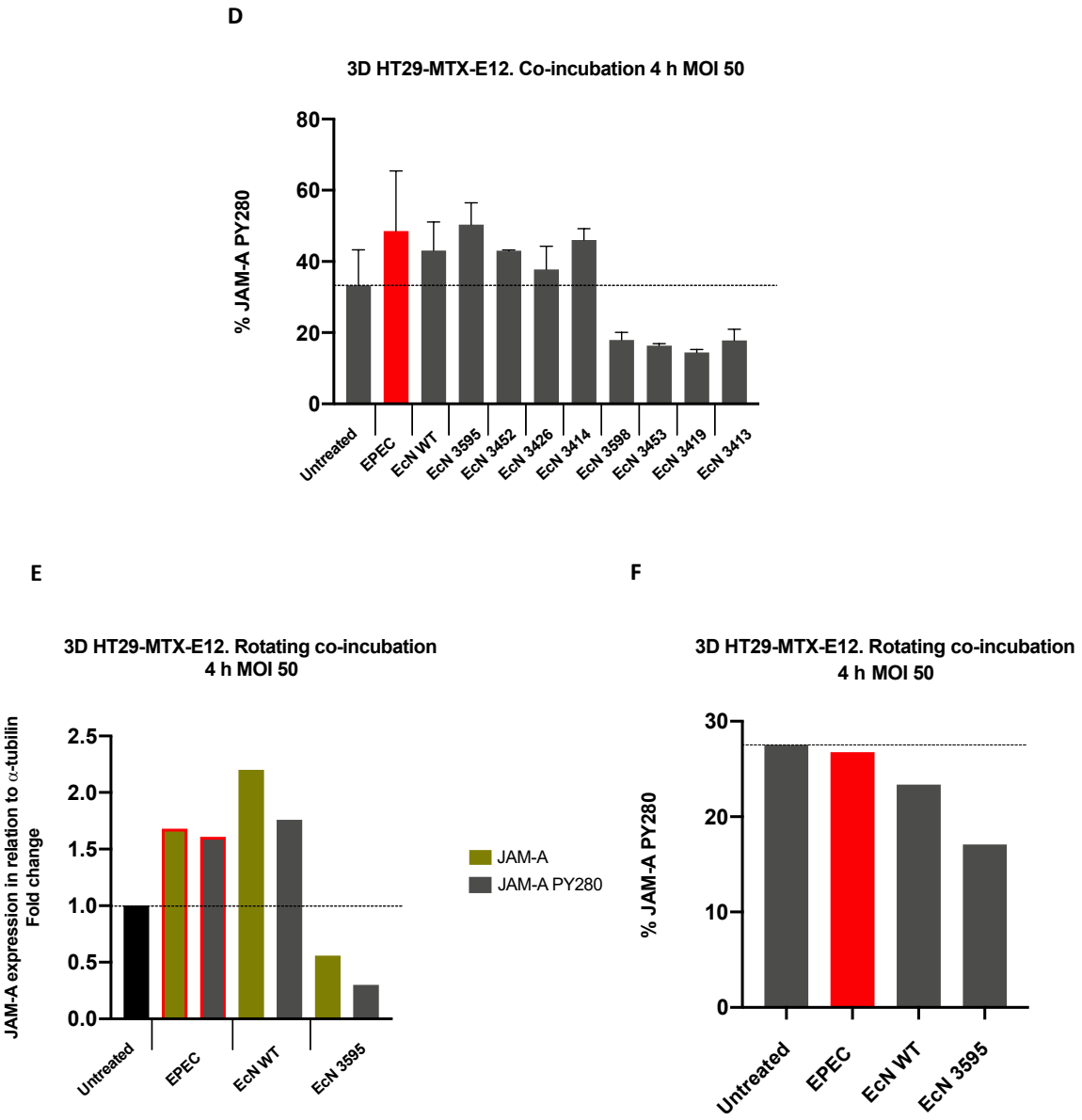

Figure 5.19.2. Quantification of JAM-A protein levels in HT29-MTX-E12 cells cultured in the 2.5D and 3D system after incubation with the EPEC strain E2348/69 and different variants of the probiotic strain EcN for 4 h with an MOI 50. A) JAM-A and JAM-A PY280 protein levels in cells cultured in the 2.5D model. **B)** JAM-A and JAM-A PY280 protein levels in cells cultured in the 3D model. **C)** Percentage of JAM-A PY280, based on the total amount of the JAM-A protein, in cells cultured in the 2.5D model. **D)** Percentage of JAM-A PY280 in cells cultured in the 3D model. **E)** JAM-A and JAM-A PY280 protein levels in cells cultured in the 3D model and incubated under rotating conditions. **F)** Percentage of JAM-A PY280, based on the total amount of the JAM-A protein, in cells cultured in the 3D model and incubated under rotating conditions. Alpha-tubulin was used as a housekeeping protein to normalize JAM-A protein levels. The data were obtained from at least two independent experiments performed in duplicates. A single experiment under rotating conditions was performed. The error bars show the standard error of the mean (SEM). *p<0.05, ***p<0.001. The red outline represents cells infected with the EPEC strain E2348/69.

Pre-infection experiments, as described before (Results 5.9), to analyze JAM-A protein levels in response to epithelial disruption and "probiotic treatment" were also performed. Figure 5.19.3 shows JAM-A protein levels in epithelial cells grown in the 2D and 2.5D cell culture systems. JAM-A protein levels were slightly higher in cells grown in the 2.5D model. In both systems, JAM-A protein levels decreased when cells were pre-incubated with EPEC strain E2348/69. There were no changes in JAM-A protein levels once EPEC was removed, and cells were incubated with fresh medium or with the probiotic bacterium (Figure 5.19.3, 2D system, black columns). Similar results were obtained in cells grown in the 2.5D system. There was a slight decrease in JAM-A when the EPEC strain was removed, and fresh cell culture medium was added onto the cells (Figure 5.19.3, 2.5D, blue columns). However, differences between treated and untreated cells were not significant.

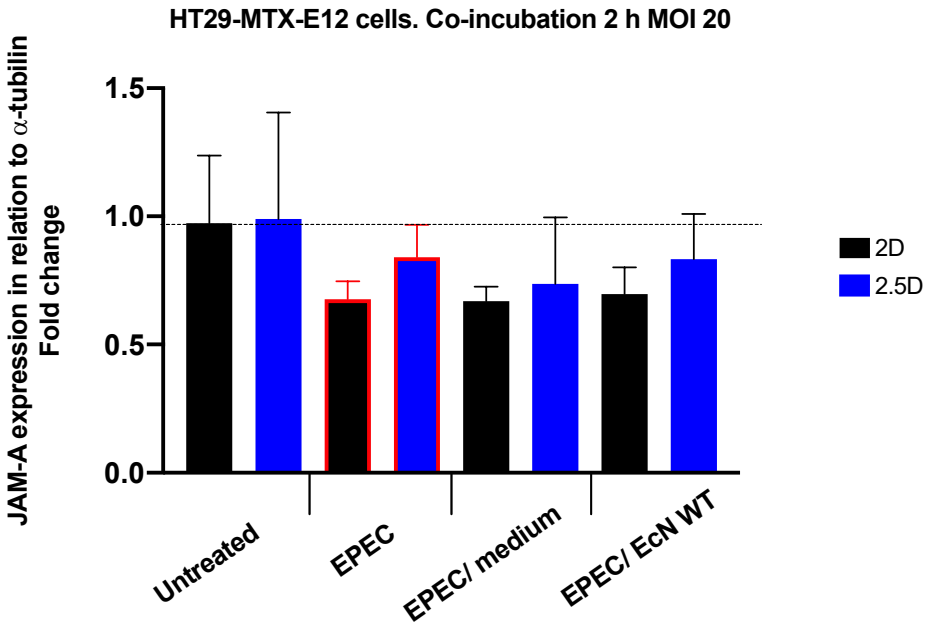

Figure 5.19.3. Quantification of JAM-A protein levels in HT29-MTX-E12 cells cultured in the 2D and 2.5D system and pre-infected with the EPEC strain E2348/69 followed by incubation with fresh medium or EcN WT. Epithelial cells were infected with EPEC strain E2348/69 for 2 h. A washing step with PBS was followed to remove the pathogenic bacteria. Finally, cells were incubated either with clean fresh medium for 4 h or with EcN WT for 4 h. A multiplicity of infection (MOI) of 20 was used. Control cells were left untreated. Alpha-tubulin was used as a housekeeping protein to normalized JAM-A protein levels. The data were obtained from at least two independent experiments performed in duplicates. The error bars show the standard error of the mean (SEM). The red outline represents cells infected with the EPEC strain E2348/69.

In general, there was a positive impact on JAM-A expression when cells were incubated with pathogenic and probiotic bacteria under static conditions. The percentage of phosphorylated JAM-A differed from strain to strain. Under rotating conditions, JAM-A was downregulated after 4 h incubation with EcN variant 3595. In the same way, JAM-A was less phosphorylated when a constant movement was present. Comparing the 2D and 2.5D cell culture systems, the amount of JAM-A was higher in cells grown in the 2.5D model. After infection with the EPEC strain, the amount of JAM-A decreased compared to untreated cells. A small increase in the amount of JAM-A was seen after EcN was added onto the cells.

5.20 Response of mucin-producing LS174T cells to the EPEC strain E2348/69 and the different variants of the probiotic strain EcN

To figure out whether our results were cell line dependent, we employed another epithelial cell line to analyze and compare cellular responses to bacterial infection. The cell line LS174T consists of adherent epithelial cells taken from the human colon. It expresses abundant microvilli and intracytoplasmatic mucin vacuoles (Tom *et al*., 1976). As in HT29-MTX-E12 cells, mucin production is important in this study to investigate host-microbe interactions. Figure 5.20.1 shows the expression of *JAM-A*, *MyD88*, and *TLR5* after 2 h and 4 h incubation with pathogenic and probiotic bacteria (MOI 50). Host response at the gene expression level was different between both cell lines. *JAM-A* expression was upregulated upon bacterial infection. After 4 h incubation, *JAM-A* mRNA levels were more elevated in cells treated with the different variants of probiotic strain EcN (Figure 5.20.1, A). Under these conditions, *JAM-A* relative expression in HT29-MTX-E12 cells grown in the 2.5D showed basal levels at 2 h and 4 h post-incubation. Only cells incubated with EcN WT and EcN variant 3595 showed a 0.5-fold increase after 4 h (Figure 5.3.1, 2.5D).

Different results were also obtained for the expression of *MyD88* in LS174T cells. *MyD88* expression was downregulated at 2 h and 4 h post-incubation with the different *E. coli* strains. EcN variant 3414 induced a slight increase in *MyD88* transcript levels after 4 h incubation (Figure 5.20.1, B). In HT29-MTX-E12 cells, *MyD88* expression was upregulated in response to specific bacterial strains (Figure 5.3.2, 2.5D). Contrary to HT29-MTX-E12 cells, the LS174T cells displayed a *TLR5* response to pathogenic and probiotic bacteria (Figure 5.20.1, C).

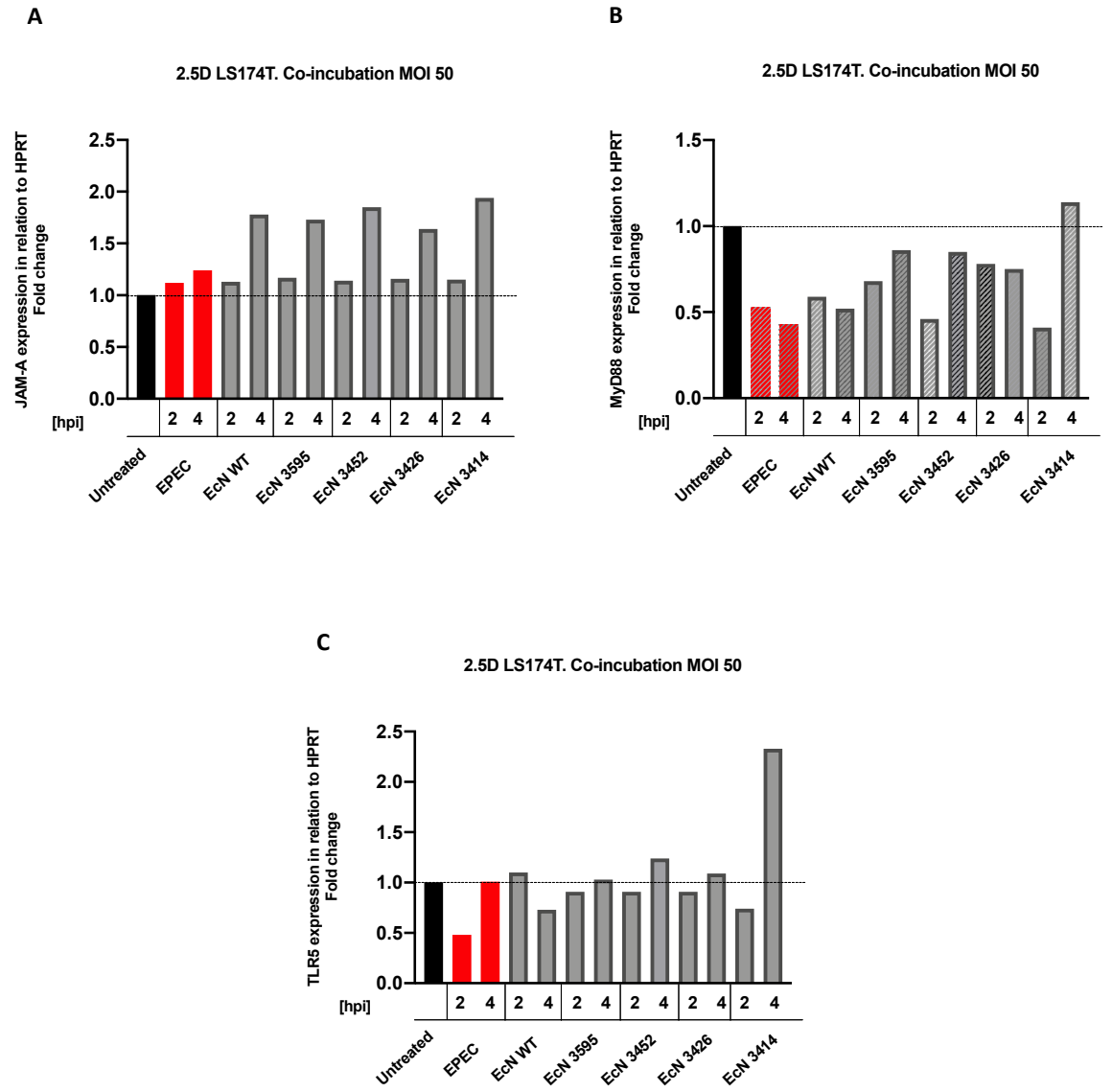

Figure 5.20.1. Incubation of LS174T cells, grown in the 2.5D cell culture system, with the EPEC strain E2348/69 and different variants of the probiotic strain EcN for 2 h and 4 h with an MOI of 50. A) *JAM-A* expression. **B)** *MyD88* expression. **C)** *TLR5* expression. Control cells were left untreated. The analysis was performed by quantitative real-time PCR. The data were normalized using the housekeeping gene HPRT transcript levels. All results are presented as fold-changes relative to the untreated control. The data were obtained from a single experiment. [hpi] = hours post-incubation.

We evaluated the effect of pathogenic and probiotic bacteria as well on *JAM-A* and *MyD88* expression in LS174T cells grown in the 3D cell culture system. Like HT29-MTX-E12 cells, LS174T cells were incubated for 4 h with the different strains (MOI 50) under static conditions. After 4 h incubation, *JAM-A* expression was 1.5 fold higher in LS174T cells cultured in the Rotating Wall Vessel bioreactor than in LS174T cells cultured in the 2.5D system. Moreover, 3D LS174T cells incubated with EcN variants 3598, 3419, and 3413 did not show an elevated *JAM-A* expression like the other variants (Figure 5.20.2, **A**). In general, the expression of *JAM-A* was much higher and significant in LS174T cells than in HT29-MTX-E12 cells after incubation under static conditions (Figure 5.20.2, **A** and Figure 5.3.1 **A, B**). Similar results were obtained for *MyD88*, which expression was higher in LS174T cells incubated with EcN variants 3598, 3453, 3419, and 3413 but lower in HT29-MTX-E12 cells (Figure 5.20.2, **B**, and Figure 5.3.2 **A, B**).

Furthermore, LS174T cells were incubated with pathogenic and probiotic bacteria under rotating conditions. Figure 5.20.2, **C** and **D** show *JAM-A* and *MyD88* expression levels after incubation with EPEC strain E2348/69, EcN WT, and EcN variant 3595 for 4 h with an MOI of 50 with and without rotating movements. There were substantial differences in *JAM-A* transcript levels between untreated and treated cells under static conditions, while under rotating conditions, these differences were not significant. Contrarily, in HT29-MTX-E12 cells, *JAM-A* expression was more pronounced under rotating incubation conditions (Figure 5.20.2, **C**, and Figure 5.16.2). The expression of *MyD88* differed as well between both cell lines (Figure 5.20.2, **D**, and Figure 5.16.4).

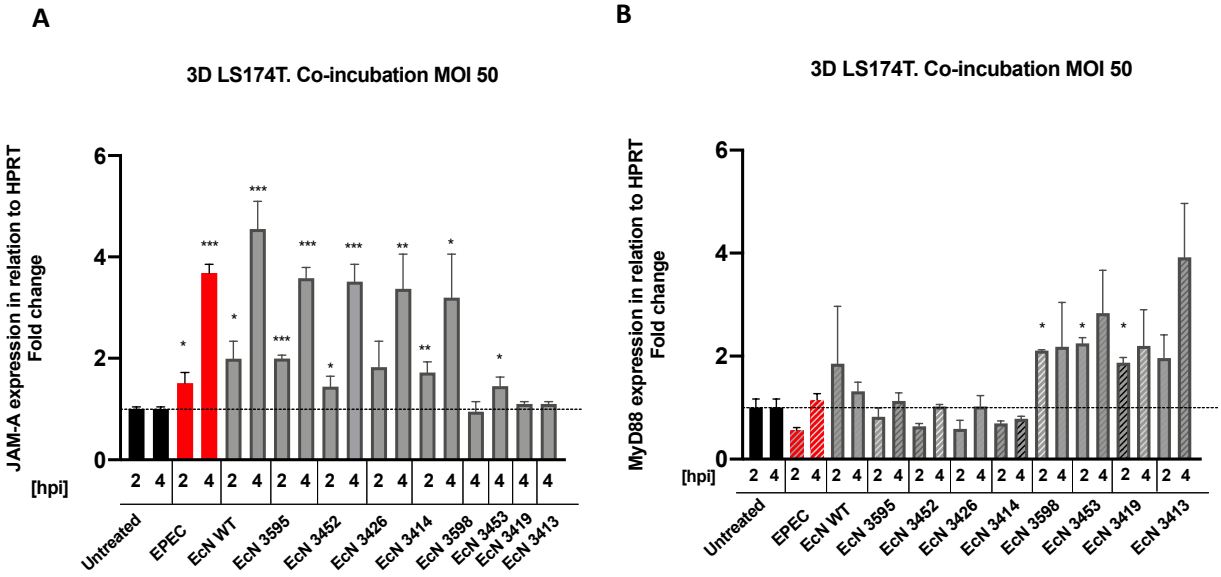

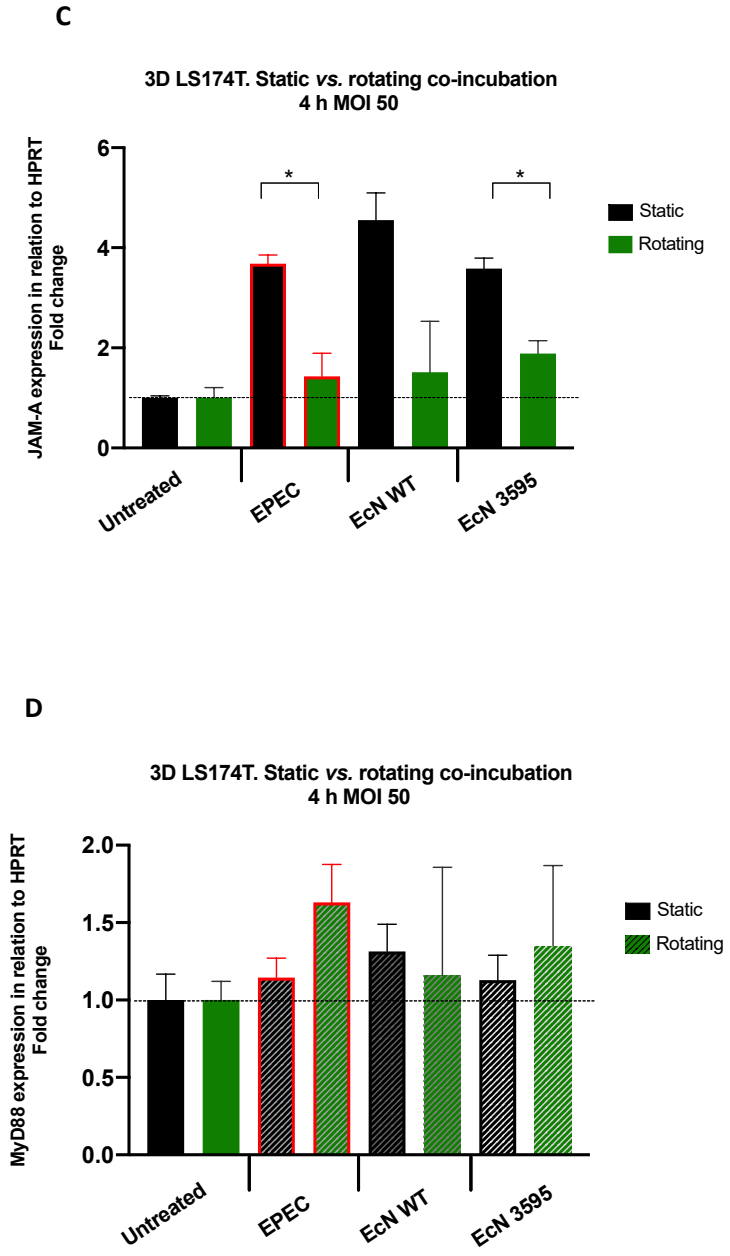

Figure 5.20.2. Incubation of LS174T cells, grown in the 3D cell culture system, with the EPEC strain E2348/69 and different variants of the probiotic strain EcN for 4 h with an MOI of 50 under static and rotating conditions. **A)** *JAM-A* expression. **B)** *MyD88* expression. **C)** *JAM-A* expression under static and rotating conditions. **D)** *MyD88* expression under static and rotating conditions. Control cells were left untreated. The analysis was performed by quantitative real-time PCR. The data were normalized using the housekeeping gene HPRT transcript levels. All results are presented as fold-changes relative to the untreated control. The data were obtained from three independent experiments. [hpi] = hours post-incubation. The red outline represents cells infected with the EPEC strain E2348/69.

In summary, under static conditions, the expression of *JAM-A* was much higher in cells cultured in the 3D system than those cultured in the 2.5D system. In general, the pathogenic and probiotic strains induced an upregulation of *JAM-A* expression in LS174T cells after 2 h and 4 h incubation. The expression of *MyD88* varied between cell culture systems and it depended on the strain (pathogenic or probiotic), which was incubated with the cells. A weak expression of *TLR5* in the epithelial LS174T cells was obtained. *TLR5* expression varied between bacterial strains. Some of them promoted upregulation of *TLR5*, but others a downregulation. Under rotating conditions, *JAM-A* expression was lower than under static conditions. LS174T and HT29-MTX-E12 cell lines showed different behavior regarding gene responses.

5.21 *JAM-A* and *MyD88* expression in LS174T cells incubated with OMVs of EPEC strain E2348/69, EcN WT and EcN variant 3595

LS174T cells cultured in the 3D model were incubated with 20 µg/ml, 25 µg/ml, 30 µg/ml, and 35 µg/ml of OMVs from EPEC strain E2348/69, EcN WT, and the EcN variant 3595 for 4 h under static conditions. The expression levels of *JAM-A* and *MyD88* in untreated and treated cells were quantified. EcN WT OMVs induced the highest expression of both genes compared to the OMVs from the other strains. *JAM-A* and *MyD88* expression decreased as the OMVs concentration increased (Figure 5.21.1, **A, B**, blue columns). EcN variant 3595 OMVs induced a slight increase of *JAM-A* and *MyD88* when cells were incubated with 20 µg/ml, 25 µg/ml, and 30 µg/ml (Figure 5.21.1, **A, B**, green columns). There was a 0.3-fold increase of *JAM-A* and *MyD88* after incubation of LS174T cells with 20 µg/ml and 35 µg/ml OMVs of EPEC strain E2348/69 but a downregulation when the cells were incubated with 25 µg/ml and 30 µg/ml (Figure 5.21.1, **A, B**, red columns). The positive effect of EcN WT OMVs on *JAM-A* expression in LS174T cells was more elevated than in HT29-MTX-E12 cells. Similarly, *MyD88* mRNA levels were upregulated in LS174T cells after incubation with EcN WT OMVs but downregulated in HT29-MTX-E12 cells (Figure 5.21.1, **A, B**, and Figure 5.7.1-2). Both epithelial cell lines displayed different behavior when they were incubated with OMVs from different *E. coli* strains.

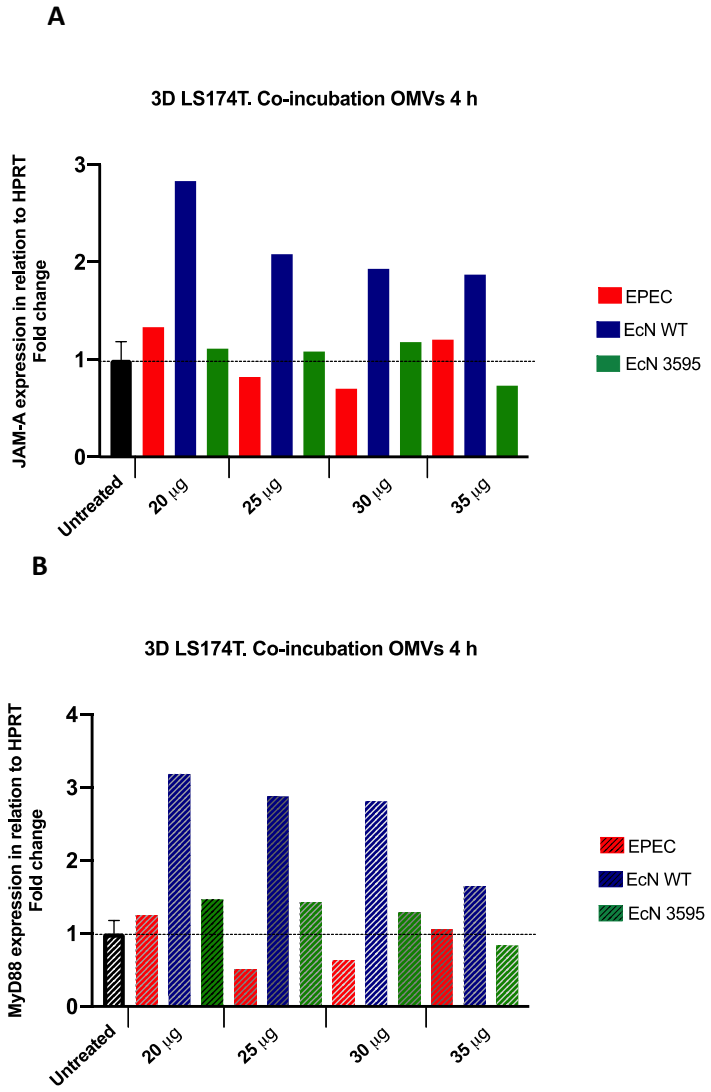

Figure 5.21.1. Incubation of mucin-producing LS174T cells grown in the 3D system with variable concentrations of OMVs of the EPEC strain E2348/69, probiotic EcN WT and EcN variant 3595 for 4 h. A) *JAM-A* relative expression. **B)** *MyD88* relative expression. Control cells were left untreated. The analysis was performed by quantitative real-time PCR. The data were normalized using the housekeeping gene HPRT transcript levels. All results are presented as fold-change relative to the untreated control. The data were obtained from one single experiment.

5.22 *JAM-A* and *MyD88* expression in LS174T cells incubated with supernatants of EPEC strain E2348/69, EcN WT and EcN variant PZ816

Incubation experiments of LS174T cells and supernatants from the different strains were performed. There was an upregulation of about 0.3-fold, 0.4-fold, and 0.1-fold in *JAM-A* expression after infection of the cells with 20 µg/ml, 25 µg/ml, and 35 µg/ml of protein in the supernatant of EPEC strain

E2348/69, respectively (Figure 5.22.1, **A**, red columns). With 25 µg/ml of protein in supernatant of the EcN WT, there was an increase in *JAM-A* expression levels (0.4-fold). At 20 µg/ml, 30 µg/ml, and 35 µg/ml, there was a downregulation in *JAM-A* transcript levels (Figure 5.22.1, **A**, blue columns). The supernatant from the highly flagellated EcN variant PZ816 induced an about 0.1-fold increase of *JAM-A* expression at 30 µg/ml only (Figure 5.22.1, **A**, grey columns).

Regarding *MyD88* expression in LS174T cells, at 25 µg/ml protein of EPEC and EcN WT supernatants induced an increase of about 0.6-fold and 0.2-fold, respectively. At 30 µg/ml, only the supernatant of EcN variant PZ816 induced the upregulation of *MyD88* transcription (0.3-fold). There was a slight increase of 0.1-fold in *MyD88* transcript levels after incubation of LS174T cells with 35 µg/ml supernatant of the EPEC strain (Figure 5.22.1, **B**). These results showed a similar trend in *MyD88* expression compared to the results obtained from HT29-MTX-E12 epithelial cells incubated with the different bacterial supernatants (Figure 5.8.4). However, it should be considered that the present data (Figure 5.22.1) resulted from a single experiment.

A

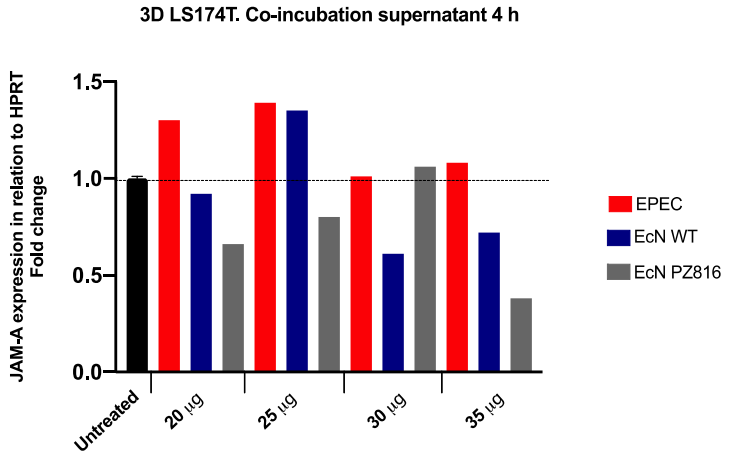

B

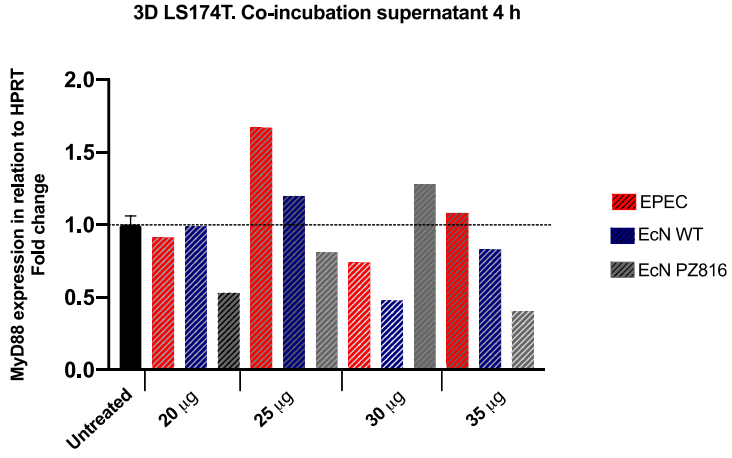

Figure 5.22.1. Incubation of mucin-producing LS174T cells, grown in the 3D system, with variable supernatant concentrations of the EPEC strain E2348/69, the probiotic EcN WT, and EcN variant PZ816 for 4 h under static conditions. A) *JAM-A* relative expression. **B)** *MyD88* relative expression. Control cells were left untreated. The analysis was performed by quantitative real-time PCR. The data were normalized using the housekeeping gene HPRT transcript levels. All results are presented as fold-change relative to the untreated control. The data were obtained from one single experiment.

Addition of OMVs and supernatants from the different strains induced distinct regulation in the expression of *JAM-A* and *MyD88* in LS174T cells.

5.23 JAM-A detection in LS174T cells by Western blot

The quantification of JAM-A protein levels, using the Western blot technique, was performed as well. Similar to the HT29-MTX-E12 cells, LS174T cells grown in the 2.5D and 3D cell culture systems were incubated with EPEC strain E2348/69 and the different variants of EcN for 4 h with an MOI of 50 under static conditions. Rotating incubations were also done. Figure 5.23.1 shows the protein bands detected corresponding to JAM-A monomers, with a molecular weight of ~ 25 kDa, and JAM-A dimers, with a molecular weight of ~ 50 kDa. A 37 kDa bands, corresponding to JAM-A protein, were not seen on the PVDF membrane with the different samples of LS174T cells (Figure 5.23.1).

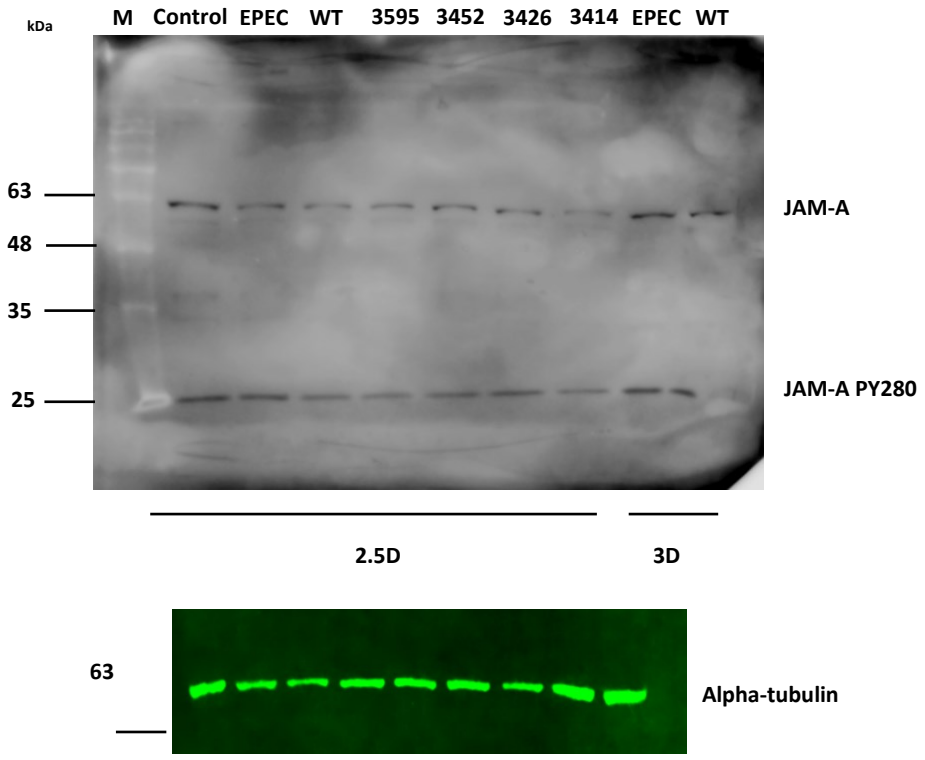

Figure 5.23.1. Quantification of JAM-A protein levels in LS174T cells cultured in the 2.5D and 3D systems and incubated with the EPEC strain E2348/69 and the different variants of probiotic strain EcN for 4 h with an MOI of 50. The Western blot technique was used to transfer denaturated proteins onto a PVDF membrane. JAM-A monomers have a molecular weight of ~ 25 kDa, and JAM-A dimers a molecular weight of ~ 50 kDa. Alpha-tubulin was used as a housekeeping protein to normalize JAM-A protein levels. M: molecular size marker.

There was a slight increase in the amount of JAM-A after infection of LS174T cells upon infection with the EPEC strain (MOI 50) for 2 h (0.1-fold). Similarly, a slight increase in the amount JAM-A was seen after incubation with the EcN variant 3452 for 4 h (0.3-fold). EcN WT induced the highest upregulation of JAM-A only after 2 h incubation. However, there were no significant differences in the amount of JAM-A in LS174T cells after different incubation conditions (Figure 5.23.2). Compared to the HT29-MTX-E12 cells grown in the 2.5D system, Western blot analyses showed that the amount of JAM-A protein increased after incubation with the pathogenic and different probiotic strains (Figure 5.19.2, **A**).

Under rotating incubation conditions, EPEC strain E2348/69 promoted an extreme increase in the amount of JAM-A (14-fold) after 4 h infection. EcN WT and EcN variant 3595 induced an approximately 2-fold increase in JAM-A amount. The phosphorylation of JAM-A at the tyrosine 280 (JAM-A PY280) was much lower than the non-phosphorylated JAM-A. EPEC strain E2348/69 also induced the highest phosphorylation of JAM-A in LS174T cells (Figure 5.23.2, **B**). The percentage of the JAM-A PY280 signal, based on the total amount of the JAM-A protein, was lower in cells infected with the EPEC strain than in cells incubated with the probiotic EcN. However, the percentage of phosphorylated JAM-A was lower in cells treated with EcN than in the untreated ones (Figure 5.23.2, **C**). In HT29-MTX-E12 cells, the rate of JAM-A PY280 was higher in cells infected with the EPEC strain. Moreover, EcN WT promoted the most elevated increase in the amount of JAM-A after 4 h incubation under rotating conditions (Figure 5.19.2, **E,** and **F**).

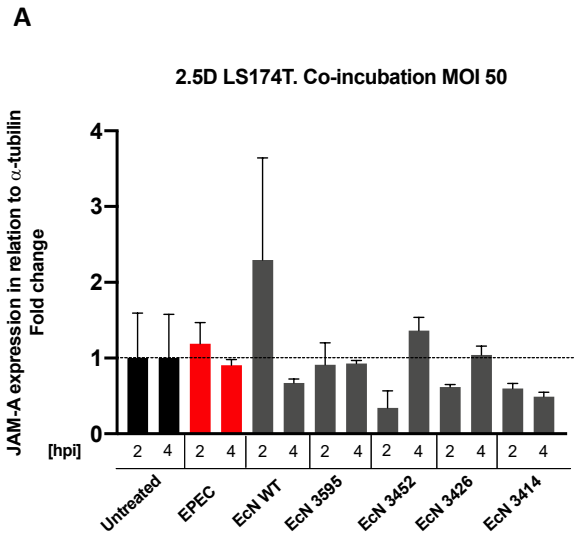

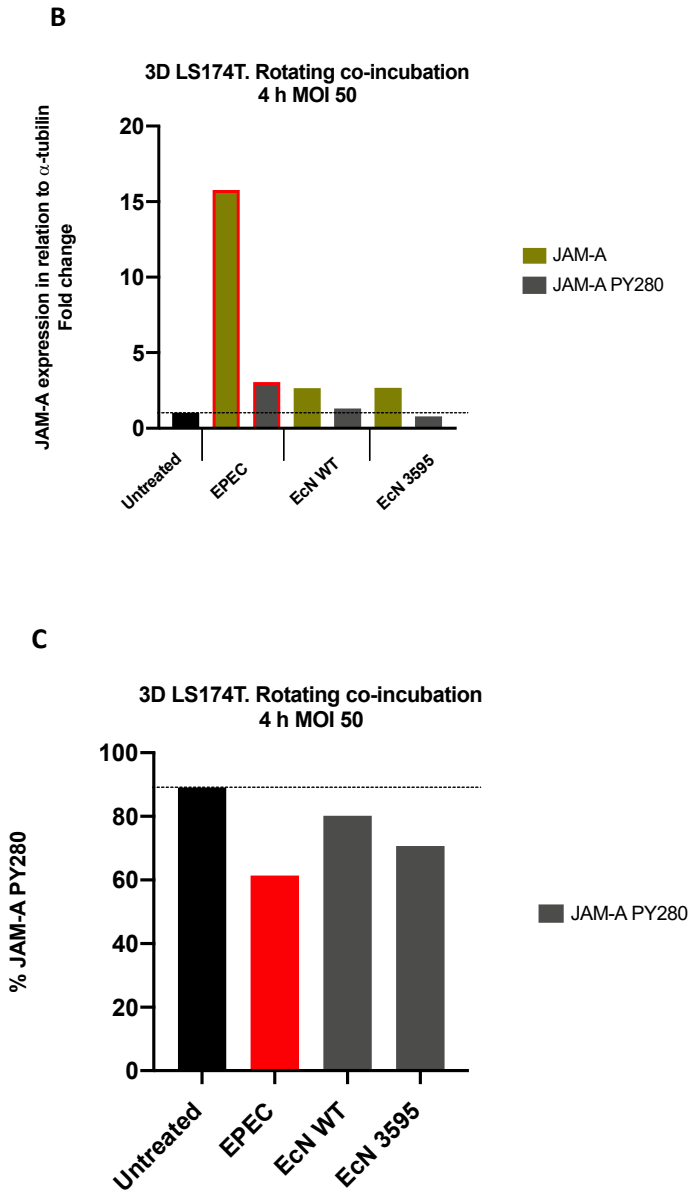

Figure 5.23.2. Quantification of JAM-A protein levels in LS174T cells, cultured in the 2.5D and 3D system, after incubation with the EPEC strain E2348/69 and the different variants of probiotic strain EcN for 2 h and 4 h with an MOI 50. A) JAM-A protein levels in cells cultured in the 2.5D model. **B)** JAM-A and JAM-A PY280 protein levels in cells cultured in the 3D model and incubated under rotating conditions. **C)** Percentage of JAM-A PY280, based on the total amount of the JAM-A protein, in cells cultured in the 3D model and incubated under rotating conditions. Alpha-tubulin was used as a housekeeping protein to normalized JAM-A protein levels. The data were obtained from at least two independent experiments performed in duplicates. A single experiment under rotating conditions was performed. The error bars show the standard error of the mean (SEM). The red outline represents cells infected with the EPEC strain E2348/69.

In LS174T cells, EPEC strain E2348/69 had a more substantial effect on the increase of the total JAM-A levels than on its phosphorylation.

CHAPTER 6

DISCUSSION

The intestinal epithelium plays a central role in defining the barrier between the host and the external environment. This barrier protects the body permanently against invasion and systemic dissemination of pathogenic and commensal microorganisms (Sansonetti, 2004). Lesions of the intestinal epithelium must be rapidly repaired to avoid penetration of commensal or pathogenic bacteria into the Lamina Propria (Sansonetti, 2004). Probiotics can contribute to human health in many ways. For example, they may promote the competitive exclusion of pathogenic bacteria, specific probiotics may enhance epithelial barrier function, and they may also modulate the immune system of the host (Bron *et al*., 2012).

In this study, we investigated the impact of the probiotic strain EcN on the human intestinal barrier function and immune response in an experimental setup that is closely related to *in vivo* conditions. Understanding host-microbe interactions in a detailed and precise way will facilitate and improve the development of potential probiotic therapies to treat immunocompromised or health-challenged patients. Employing the mucin-producing HT29-MTX-E12 and LS174T cell lines, co-incubation experiments were done challenging cells with different E. *coli* strains, including the enteropathogenic *E. coli* (EPEC strain E2348/69), the probiotic strain EcN and various variants of this particular probiotic strain. Subsequently, the expression and distribution of the Junctional Adhesion Molecule A (JAM-A) were monitored. In the same way, the expression of myeloid differentiation primary response (*MyD88*) and other immune response associated genes were analyzed.

6.1 Gene expression and protein distribution in eukaryotic cells growing in different cell culture systems

2D cultures have advantages associated with low-cost and simple maintenance of cell cultures. However, cells cultured in the 2D tissue culture system do not mimic the natural structures of tissues or tumors. In this model, cell-cell interactions are not represented as they would be in the *in vivo* situation (Kapalczńska *et al*., 2018). These interactions, however, are responsible for cell differentiation, proliferation, expression of genes, drug metabolism, among other functions. 2D culturing results in a change of cell morphology that can affect their function, the organization of the structures inside the

cell, secretion, and cell signaling (Kapalczńska *et al*., 2018). Disturbances in cell-cell interactions cause a loss in cell polarity, which changes the response of these cells to various stimuli (Kapalczńska *et al*., 2018).

Epithelial cells cultured on a permeable membrane filter, as in our case the "2.5D" cell culture system, exhibit a fully polarized architecture, including the presence of functional tight junctions. The same features are seen in cells cultured on porous fibronectin-coated microcarrier beads (3D cell culture system) (Figure 5.5). 3D cultures even more closely represent the *in vivo* situation of tissues and organs. There is a proper interaction between cell-cell and cell-extracellular environments. The cellular morphology is also preserved, and biological mechanisms such as proliferation, differentiation, response to stimuli, gene expression and protein synthesis are similar to *in vivo* (Kapalczńska *et al*., 2018). However, there are a few disadvantages: the cultivation time is longer than in 2D cultures, due to the larger size of 3D cell cultures some types of measurement and microscopic analyses can be difficult, and for larger cultures, the right supply with oxygen and other essential nutrients can be a challenge (Kapalczńska *et al*., 2018).

When evaluating the gene expression levels of *JAM-A*, we found that they were lower in HT29-MTX-E12 cells grown in the 2D system than in the 2.5D system (Figure 5.1 and Figure 5.2). As mentioned before, the morphology of the cells and the mode of cell division were altered in 2D cultures. This phenomenon might explain the higher reduction of *JAM-A* mRNA levels in cells grown in the 2D cell culture system than in the 2.5D system. Confluent monolayers, grown in the 2.5D and 3D models, were polarized, developed apically located cell junctions, microvilli, and showed mucin production. Although physical features were similar, the relative expression levels of *JAM-A* and *MyD88* in HT29-MTX-E12 cells also differed (Figure 5.3.1 and Figure 5.3.2). However, in most cases these differences were not significant. The presence of a low-fluid shear during cell growth on beads might modulate the level of gene expression. Shear stress is defined as force per unit area. Pressure, frictional shear at the cell surface, and tensile or compensatory forces might be considered as shear stress (Braddock *et al*., 1998). The stimulus derived from fluid shear stress is transduced to the nucleus to regulate gene expression via a distinct set of mitogen-activated protein (MAP) kinase signal transduction cascades (Kunnen *et al*., 2018).

RT^2 Profiler array analysis with RNA of HT29-MTX-E12 cells, grown in the 2D and 3D cell culture models, showed remarkable differences in gene expression (Table 5.2, Figure 5.17.1, A-B). These results showed that the changed morphology of the cells grown in 2D cultures can affect cell signaling. These changes in cells´ morphology were also reflected in the amount of JAM-A protein localized at the cell boundaries. Immunofluorescence images showed that cells cultured in the 2D model had more diffuse

cell-cell contacts compared to 2.5D and 3D cultures (Figure 5.6.1, A). Rocha *et al*. performed RNA and proteomic profile analyses of extracellular vesicles (EVs) secreted by 2D *vs.* 3D cultures of gastric cancer cells. Cells cultured in 3D conditions were highly efficient in producing EVs. The average number of EVs per cell was significantly higher in 3D in comparison to 2D systems (Rocha *et al*., 2019). In the same way, they reported an upregulation of microRNAs in cells and EVs together with a downregulation of proteins in EVs of cells cultured in the 3D system. These findings suggest that the 3D cellular architecture modifies production levels and content of EVs, which may affect their potential impact and consequently uptake, inducing a different functional behavior on recipient cells (Rocha *et al*., 2019).

Further studies, where the proteome of cancer-associated fibroblasts grown in 3D cell culture was analyzed, showed that 3D culture conditions significantly altered the protein composition of cells and led to an upregulation of cellular proteins critical for the establishment and maintenance of ECM-cell contacts. The authors also suggest that 3D culture conditions might reveal differentially regulated proteins important in disease, which are not detectable or regulated under 2D cell cultures (Tölle *et al*., 2018). These discoveries led us to hypothesize that JAM-A trafficking to the boundaries of the cells might be modified in cells grown in the 2D cell culture system.

6.2 Importance of mucin production to study host-microbe interactions in the gut

6.2.1 Infection of eukaryotic cells with EPEC strain E2348/69

It has been described that EPEC attaches to intestinal cells and secretes several effector proteins into host intestinal epithelial cells (IECs) through the Type Three Secretion System (T3SS) (Celli *et al*., 2001). These effector molecules mediate several physiopathological changes in IECs, causing the recruitment and rearrangement of actin and other cytoskeletal proteins to form attaching and effacing (A/E) lesions. These lesions trigger loss of the epithelial tight junctions (TJs) barrier and inflammation (Tomson *et al*., 2005). In this study, A/E lesions were not visualized when HT29-MTX-E12 cells were challenged with EPEC strain E2348/69 for up to 6 h (Figure 5.11.1 and Figure 5.18.2, D). Contrarily, we did visualize A/E lesions in HT29 cells, which do not secrete mucins, after 3 h infection with this EPEC strain (Figure 5.18.2, B and Figure 5.18.3, A). These differences might be due to the presence or absence of a secreted mucin layer on top of the epithelial cells. Mucus forms the first line of defense while harboring trillions of microorganisms constituting the microbiota. In a healthy environment, these microorganisms rarely cause epithelial damage and subsequent infection (Schroeder, 2019). This suggests that the mucus layer activates mechanisms that regulate virulence, and this regulatory function is likely to be dependent on glycan complexity (Wheeler *et al*., 2019). The complex macromolecular network within

the mucus layer is capable of regulating microbial interactions and this regulation is lost when glycan structures are disrupted into monosaccharides (Wagner *et al*., 2018).

On the one hand, in 2010, Vieira *et al*. showed inhibition of adhesion by mucin for the human EPEC strain E2348/69. These results are in accord with ours. We determined low numbers of cell-associated EPEC bacteria with mucin-secreting HT29-MTX-E12 cells (4.7 log CFU/ml, data not shown). On the other hand, Wheeler *et al*. confirmed that mucin glycans attenuate the virulence of *Pseudomonas aeruginosa* during infection. These results demonstrated that **1)** mucin glycans are potents host signals that "tame" microorganisms, rendering them less harmful to the host, **2)** mucin triggers an active motility-driven escape of bacterial biofilms, rather than mechanical disruption, **3)** mucus contains factors that modulate bacterial behaviors at the level of gene expression and phenotype, suppressing virulence gene expression, and **4)** mucin suppresses aggregation and bacterial attachment to surfaces (Wheeler *et al*., 2019). With these findings, we could corroborate our observations regarding the formation of pedestals in non-secreting HT29 cells and the deficiency of EPEC strain E2348/69 to form these protruding structures in HT29-MTX-E12 mucin-secreting cells. Infection studies with other pathogenic strains should be performed in order to corroborate the microbe-disarming activity of mucin secretion in HT29-MTX-E12 cells.

2D and 2.5D cell cultures lack mechanophysical stresses, including low fluid shear stress. Davidovich *et al*. investigated the role of mechanophysical stimulations in mucin secretion in cultures of nasal epithelial cells. They found that mucin secretion significantly increased in response to wall shear stress in a magnitude-dependent manner with respect to static cultures. Moreover, under wall shear stress, the polymerization of actin microfilaments was shown to increase mucin secretion, indicating that mucin secretion is sensitive to oscillatory shear stress (Davidovich *et al*., 2011). Tarran *et al*. demonstrated that wall shear stress induces the release of ATP from the cells, increasing the ATP concentration in the airway surface liquid. This increase induces chloride ion secretion via P2Y2 receptor-mediated ion channel activation. The activation of P2Y2 receptors by ATP also results in an elevation on intracellular Ca^{2+} concentrations, which modulates mucin secretion (Tarran *et al*., 2005).

In Figure 5.1, **A,** we observed in both cell culture systems that at 2 h infection with the EPEC strain the relative expression of *JAM-A* increased depending on the multiplicity of infection (MOI). After 4 h, *JAM-A* expression was still increasing and then declined again to a plateau in the 2D cell culture system (Figure 5.1, **B**). Based on other scientific investigations concerning a direct effect of shear stress on mucin secretion, we hypothesize that **1)** the level of mucin secretion directly correlated with mucin-dependent modulation of bacterial gene expression and phenotypes, **2)** EPEC pathogenicity-associated genes are more expressed in HT29-MTX-E12 cells grown in the 2D system than in the 2.5D or 3D

systems, resulting in a higher impairment of the cells, and **3)** epithelial cells activate a cell defense response, and that this response rose with increased bacterial infection. A mechanism related to a protective cell response under inflammatory stimuli might be associated with *de novo* JAM-A synthesis and subsequent trafficking to the apical surface of the cells. At the apical surface, JAM-A plays a role as a leukocyte adhesion molecule participating in transendothelial cell migration of neutrophils and monocytes (Stamatovic *et al*., 2012). Quantification of mucin expression and secretion should be performed to support and confirm our hypotheses under these conditions. In the same way, the trafficking of JAM-A to the apical cell surface should be investigated after EPEC infection. Furthermore, it would be useful to employ a non-mucin secreting cell line, like HT29 cells, to quantify *JAM-A* transcript levels after infection with EPEC strain E2348/69 to evaluate whether *JAM-A* expression is much higher in cells without a mucin layer on top.

Epithelial cells in the 3D culture system showed a decrease in *JAM-A* expression after 2 h and 4 h of EPEC infection (Figure 5.3.1, **A-B**, green columns). These results could be related to **1)** the presence of low-fluid shear stress in the Rotating Wall Vessel (RWV) bioreactor culture influencing the expression of *JAM-A*, **2)** higher amounts of secreted mucin to the luminal space modifying the gene expression and phenotype of EPEC strain E2348/69 making it less pathogenic, and **3)** more differentiated cells with a complete junctional complex formation. EPEC, like model isolate E2348/69, is supposed to induce disruption of the PAR complex, a crucial regulator of apical-basal polarity, prior to disrupting tight junctions. Additionally, EPEC does not alter the localization of total JAM-A from the cell-cell contacts but internalizes JAM-A S285 at 30 min of infection (Tapia *et al*., 2020). The phosphorylation of JAM-A at serine 285 is required for the development of a functional epithelial barrier (Iden *et al*., 2012). With this, we can assume that as EPEC is less pathogenic when incubated with fully differentiated HT29-MTX-E12 cells, thus the epithelial cells sense less threat. Since EPEC strain E2348/69 did not affect the total JAM-A level at the cell boundaries after 4 h of infection (Figure 5.6.2, and Figure 5.6.3, EPEC infection), downregulation of *de novo* protein synthesis might occur, while a replacement of JAM-A from an intercellular pool to the apical cell surface takes place. In this sense, cells invest energy in the active transport of JAM-A to the apical surface to activate leukocyte recruitment and modulate the immune response. To further elucidate this hypothesis, JAM-A re-distribution to the apical side has to be analyzed. Bacterial RNA sequencing might be done to analyze bacterial gene expression in the presence of high amounts of mucin.

MyD88 expression differed in 2.5D and in 3D cultures; however, not significantly (Figure 5.3.2). In cells grown in the 2.5D system, the expression of *MyD88* increased after 2 h of infection and decreased again after 4 h of infection (Figure 5.3.2, **A-B**, grey columns). The increasing *MyD88* transcript level after 2 h of EPEC strain E2348/69 infection might be a transient cell response to bacterial infection.

MyD88 expression decreased in cells grown in the 3D cell culture system (Figure 5.3.2, **A-B**, green columns). Similarly, qRT-PCR and RT^2 Profiler array data showed a low expression of *TLR4*, *TLR5*, and *MyD88* after 4 h of EPEC strain E2348/69 infection of epithelial cells in the 3D cell culture system compared to untreated cells (Table 5.2, 3D system, static infection). Litvak *et al.* showed that NF-κB activation was independent of the MyD88 signaling pathway in HeLa cells after infection with EPEC. The T3SS effectors inhibited the activation of MyD88 by TLR signaling (Litvak *et al.,* 2017). We did not detect an intimate host-pathogen interaction, as represented by actin pedestals, arguing against a high T3SS in the cell culture conditions that we have used. Even so, we did not obtain *TLR5* expression, and *MyD88* expression decreased after 4 h infection with EPEC strain E2348/69 in cells grown in the 2.5D and 3D cultures. These results might indicate that the EPEC strain translocates the effector proteins in a T3SS-independent manner subverting the host immune response via MyD88-mediated pathways.

After 4 h of infection with EPEC strain E2348/69, HT29-MTX-E12 cells grown in the RWV bioreactor showed a high increase in the expression of the inflammatory cytokines CXCL1 and CXCL2. CXCL1 is a potent neutrophil chemoattractant. Shea-Donohue *et al*. showed that the neutrophil infiltration induced by CXCL1 is important for the innate immunity and reinforcement of barrier integrity in mice, which suffer from dextran sodium sulfate (DSS) colitis (Shea-Donohue *et al*., 2008). CXCL2 mediates neutrophil trafficking, as well as the induction of inflammation (De Filippo *et al*., 2013). Additionally, the expression of the main NF-κB inhibitor, NFKBIA, was almost 3 times higher (Table 5.2, 3D System, static infection), suggesting that the production of CXCL1 and CXCL2 cytokines might be, in part, independent of NF-κB activation. Alternative pathways-induced cytokines such as p38, Erk, and Jnk signaling might be activated to stimulate pro-inflammatory gene expression. Quantification of the levels and activity of p38, Erk, and Jnk should be done to validate this assumption. In 2D cultures, the activation of *CXCL1* and *CXCL2* after EPEC infection was much lower compared to 3D cultures. The expression of *NFKBIA* was 7 times higher compared to untreated cells, indicating that the downregulation of neutrophil and leukocytes recruitment can be mediated via the inhibition of the NF-κB signaling pathway. Moreover, the expression of the pro-inflammatory cytokine Tumor Necrosis Factor (TNF) was also much higher in 2D cultures after EPEC infection (Table 5.2, 2D system). These results indicated differences in the activation of signaling pathways in cells grown in the 2D or 3D cell culture systems to bacterial infection. The secretion of high amounts of mucin and the presence of low-fluid shear stress in the 3D cell culture system play an essential role in host-microbe interactions.

Gene expression profiles differed between non-mucin and mucin-secreting cells after 4 h of infection with EPEC strain E2348/69. Cytokine expression was more downregulated in HT29-MTX-E12 than in HT29 cells grown in the 2.5D cell culture system after EPEC infection except for the cytokine Interleukin 1 beta (IL-1β), which is an essential mediator of the inflammatory response (Table 5.3). The

secretion of mucin contributes to a switch in bacterial phenotype and virulence neutralization, taming pathogenic microorganisms (Wheeler *et al*., 2019). Muc2-deficient mice exhibited rapid weight loss, ulceration in the colon, a significantly worsened intestinal barrier disruption, and suffered up to 90% mortality after *Citrobacter rodentium* infection, a murine A/E pathogen related to diarrheagenic A/E *E. coli.* Additionally, *C. rodentium* microcolonies contained numerous commensal microbes, which was not observed in WT mice, suggesting that Muc2 also impacted host-commensal interactions during infection (Bergstrom *et al*., 2010). Further studies showed that fragility in proper mucus exocytosis mechanisms increases an encounter with microbial antigens. Altered mucus exocytosis shifts the microbial diversity to a detrimental microbiota, increasing the abundance of pathogenic and mucolytic bacteria (Cornick *et al*., 2019).

6.2.2 Cellular response of HT29-MTX-E12 cells to EPEC strain E2348/69 outer membrane vesicles and supernatant

The small size of OMVs (20 to 250 nm) and secreted proteins or substances facilitate propagation across the epithelial mucus layer and direct contact to host cells (Maerz *et al*., 2018). The expression of J*AM-A* and *MyD88* mRNA levels increased upon infection of epithelial cells with OMVs and supernatant of EPEC strain E2348/69. After incubation with OMVs, *JAM-A* expression increased in a dose-dependent manner (Figure 5.7.1, red columns). Concerning the infection of HT29-MTX-E12 cells with EPEC supernatant, *JAM-A* expression increased in a dose-dependent way as well, but when a higher concentration of the supernatant was used (35 µg/ml of protein delivered by supernatant), its expression was reduced (Figure 5.8.3, red columns). Similarly, the expression of *MyD88* rose upon the addition of OMVs (Figure 5.7.2, red columns) or supernatant except for the lowest supernatant concentration (Figure 3.9.3, red columns) of EPEC strain E2348/69. OMVs and secreted proteins are generally internalized by epithelial cells through clathrin-mediated endocytosis and mediate immune signaling responses (Fábrega *et al*., 2017). Upregulation of *JAM-A* expression could be a cell defense response to reinforce the epithelial barrier function and activate leukocyte migration. In the same way, the activation of the immune response is boosted by the upregulation of the *MyD88* transcript levels. Modulation of MyD88 signaling pathways by EPEC is probably dependent on bacterial-associated factors.

These results differ from those obtained from experiments where cells were infected with the living EPEC E2348/69 cells, where *JAM-A* and *MyD88* expression was lower than in untreated cells (Figure 5.3.1, **B,** and Figure 5.3.2, **B**. 3D cell culture model). As explained before, in healthy conditions the presence of mucin glycans modulates the bacterial phenotype and gene expression suppressing the

upregulation of virulence genes. Therefore, OMV production and virulence factor secretion might be attenuated during bacterial infection in the presence of mucin, thus decreasing bacterial pathogenicity. It might be that the amount of isolated OMVs and supernatant used in this study were much higher than the amount produced by the EPEC bacteria when incubated with epithelial cells. Bielaszewska *et al*. showed that OMVs and nanoparticles released by enterohemorrhagic *E. coli* (EHEC) induce cytokine production in human intestinal epithelial cells (Caco-2, HCT-8, and HT29) by signaling via Toll-like receptors (TLRs) TLR4 and TLR5 (Bielaszewska *et al*., 2018). However, qRT-PCR results showed no detectable *TLR5* upregulation under the conditions we used in this study.

In Table 5.2, evaluation by RT^2 Profiler arrays showed that cells grown in the 3D culture responded differently when incubated with living EPEC bacteria or EPEC supernatant after 4 h under static conditions. The *CXCL1* and *CXCL2* transcript levels were more upregulated in the presence of the living microbes than under supernatant infection conditions. On the contrary, *TNF* and *IL-1β* were highly upregulated after infection with the supernatants of EPEC strain E2348/69. The release of the chemoattractants CXCL1 and CXCL2 initiate an early phase of neutrophil recruitment during tissue inflammation. The early stage of neutrophil recruitment is also mediated by mast cells, optimally positioned close to the vasculature (De Filipo *et al*., 2013). Results obtained from infection of HT29-MTX-E12 cells with the living EPEC microbes could suggest that epithelial cells, as sensors for microbial infection, activate CXCL1 and CXCL2 as an early defense response. The early stage of cytokine activation, together with mucin-mediated changes, could be sufficient to neutralize antagonistic interactions with EPEC.

Conversely, secreted proteins in the supernatant can disseminate into tissues provoking an early but less pronounced response. Once these soluble factors reach the endothelial cells and are subsequently internalized, a late defense response is activated. The delayed response includes the activation of *TNF* and *IL-1β*. In our models, the expression of *TLR4*, which encodes for the lipopolysaccharide (LPS) receptor, and *TLR5*, which encodes for the flagellin receptor, were higher after infection with EPEC supernatants than after infections with the EPEC strain itself. These results indicate that the expression of *TLR4* and *TLR5* was largely enhanced when bacteria or their secreted products were able to translocate from the luminal side and access the basolateral membrane domain. This is attributed to the compartmentalization of intestinal epithelial cell TLRs (Yu *et al*., 2015). It has been demonstrated that TLR4 protein is localized to the basolateral side of fetal ileal crypts and adult colon. However, TLR4 has also been found at the apical side of epithelial cells from patients who had ulcerative colitis and Crohn´s disease, and also at the apical side of polarized human colon cancer T84 cells. In contrast to TLR4, TLR5 has been consistently and predominantly detected at the basolateral cell surface and cytoplasm in colonic cells (Yu *et al*., 2015). This unique distribution pattern of TLR5 follows the

hypothesis that the epithelium tolerates the presence of luminal associated molecular patterns (PAMPs) and mounts only a restricted immune response thus, avoiding unnecessary immune responses in steady-state conditions. Gewirtz *et al*. have shown that apically presented flagellin does not affect pro-inflammatory gene expression. However, the detection of flagellin by basolateral TLR5 mediates epithelial-driven inflammatory responses to *Salmonella* (Gewirtz *et al*., 2001). In addition, the compartmentalization of TLRs also allows epithelial cells to differentiate between commensal bacteria, restricted to the gut lumen, and pathogens, which might often compromise the epithelial barrier and get access to the basolateral side (Gewirtz *et al*., 2001).

In conclusion, our results concerning RT^2 Profiler array analysis of gene expression of epithelial cells infected with living EPEC strain E2348/69 could indicate that **1)** epithelial cells sense pathogenic microbes inducing a global transcriptional response that downregulates bacterial virulence gene expression and secretion of effector proteins, and **2)** an early pro-inflammatory response related to *CXCL1* and *CXL2* upregulation is followed to fight agonistic interactions. Our results concerning epithelial cells infected with EPEC-free supernatants could indicate that **1)** soluble factors or secreted proteins in the supernatant do not trigger a primary immune response as enhanced as living EPEC bacteria, **2)** these nanoparticles get access to the epithelial cells triggering a delayed inflammatory response, and **3)** MyD88-dependent signaling pathways are activated via regulation of TLR4 and TLR5.

Differences in qRT-PCR and RT^2 Profiler array results concerning *TLR5* expression might be due to threshold setup. This could be explained by the different criteria used and may point to the fact that the qRT-PCR platform is too strict in the required threefold difference in the C_t value compared to the genomic control (Gaj *et al*., 2008). A difference in the interrogative regions might be another explanation for this discordance. Some platforms interrogate a region closer to the 3´ end of some genes, while other platforms interrogate a region that is closer to the 5´ end of the gene. Low detection signals for some genes may cause disagreements between different platforms (Arikawa *et al*., 2008).

6.3 Incubation of eukaryotic cells with variants of the probiotic strain EcN

Intriguingly, EcN is phylogenetically closely-related to clinically pathogenic strains, such as uropathogenic *E. coli*, other invasive *E. coli* strains, and some enteric pathogens such as EPEC strain E2348/69. Despite sharing many virulence factors with these related strains, EcN is distinct in its interactions with host tissues (van der Hooft *et al*., 2019). The probiotic capacity of EcN is multifaceted and involves competition with pathogens, promotion of mucosal integrity, modulation of the innate intestinal defense, among others (van der Hooft *et al*., 2019; Zyrek *et al*., 2006). Although EcN has

proven to be beneficial in various gastrointestinal disorders, the mechanisms by which it antagonizes pathogenic gastrointestinal microorganisms or exerts beneficial effects on the host *in vivo* is not entirely understood. Cordes *et al*. demonstrated that T84 cells treated with EcN show elevated levels of miR-320a, resulting in an increased expression of the tight junction protein JAM-A, which might be a potential regulatory mechanism (Cordes *et al*., 2016).

In this study, the expression of *JAM-A* transcript levels in HT29-MTX-E12 cells tended to be different between the 2.5D and 3D cultures after incubation with different EcN variants. But in general, these differences were not significant (Figure 5.3.1, **A-B**). In cells grown in the 3D cell culture system, the decrease of *JAM-A* gene expression after 2 h incubation with the probiotic strain might be due to the downregulation of mRNA synthesis. Spontaneous mutations in specific proteins of EcN variants 3598 and 3413 (Chapter 3, Section 3.1, Table 3.2) may confer to the bacteria another particular phenotype, such as interference with secretory pathways, localization, and the secretion of bacterial proteins. These distinct phenotypes have a different effect on *JAM-A* expression after 2 h incubation in comparison with EcN WT (Figure 5.3.1, **A**, green columns). After 4 h incubation, *JAM-A* mRNA levels were upregulated by most of the EcN variants. This indicates a later effect of these probiotic variants on *JAM-A* expression. EcN WT and the EcN variant 3595 did not induce an upregulation of *JAM-A* transcript levels after 4 h (Figure 5.3.1, **B**, green columns). These results could suggest that these two variants partly inhibit JAM-A *de novo* synthesis. As mentioned before, spontaneous mutations displayed by EcN variants (except for EcN WT and EcN variant 3595) may have a higher impact on *JAM-A* expression at a later stage. In the same way, EcN variants under healthy conditions do not have any effect in JAM-A re-distribution in cells grown in the 2.5D and 3D cell culture systems (Figure 5.6.2, and 5.6.3). Looking at the modulation of the bacterial transcriptional response of the different variants when incubated with host cells will facilitate a comprehensive detection and characterization of bacterial secretion systems.

Some reports have suggested that because JAM-A protein levels are expressed at an early stage in tight junction formation, it may be involved in the recruitment of other tight junction proteins to facilitate junction assembly (Bazzoni *et al*., 2000). Interestingly, Naik *et al*. showed that the reduction of JAM-A levels did not affect the localization of other tight junctional components. However, *JAM-A* depletion by small interfering RNA increased barrier paracellular permeability of macromolecules (Naik *et al*., 2006). Ebnet *et al*. showed a dual function for the JAM family. In essence, they appear to regulate leukocyte/platelet/endothelial cell interactions in the immune system and tight junction formation in epithelial and endothelial cells during the acquisition of cell polarity (Ebnet *et al*., 2004). In this study, we found that both bacterial types, EPEC and also some EcN variants, including EcN wily type, phosphorylated between 2% and 13% of JAM-A at tyrosine 280 (PY280) in cells grown in 3D cultures

(Figure 5.19.2, **D**). The JAM-A PY280 profile in cells grown in the 2.5D system differed from that of those cells grown in the 3D system (Figure 5.19.2, **C-D**). JAM-A PY280 is associated with increased barrier permeability (Fan *et al*., 2019). Therefore, our findings could indicate that both pathogenic and some probiotic variants stimulated partial phosphorylation at tyrosine 280 to redistribute JAM-A from intercellular junctions to the apical surface. This re-distribution could increase the transendothelial migration of leukocytes at the site of infection to clear away the pathogenic bacteria in the case of EPEC infection. In the case of probiotic bacteria, activation of leukocyte migration, together with a primary inflammatory cytokine response, such as mediated by CXCL1 and CXCL2 (Table 5.2, 3D system, static infection, EcN WT and EcN variant 3595), might be in response to vascular injury.

JAM-A is required for the activation of extracellular signal-related kinase (ERK) and basic fibroblast growth factor (bFGF) signaling pathways in endothelial cells. These pathways are fundamental to endothelial cell migration to seal an injured vasculature (Naik *et al*., 2006). Possibly, wound healing is an intrinsic effect of EcN, besides increasing the expression of other junctional proteins to restore and strengthens the barrier function. Sumagin *et al*. demonstrated that the intercellular adhesion molecule-1 (ICAM-1), which binds leukocytes firmly to the endothelium initiating leukocyte extravasation, has an important role in mucosal wound healing (Sumagin *et al*., 2016). Thus, the wound healing process in conjunction with EcN could be mediated by the upregulation of pro-inflammatory cytokines and a low degree of JAM-A distribution from the intercellular junctions. Additionally, it was observed that after limited damage of the epithelial cell-to-cell contact, EcN WT, and EcN variant 3595 could reheal cell boundaries (Figure 5.12.1 and Figure 5.13.1, EcN 3595). In the same way, EcN WT induced an upregulation of the expression of *JAM-A* mRNA levels when epithelial cells were perturbed. Curiously, when the infecting EPEC strain was washed away from the cells and fresh medium was added onto the cells, the expression of *JAM-A* was higher than when EcN was added after EPEC removal (Figure 5.9.1). In this experiment, gentamicin was not applied to the cells to kill most of the bacteria (Results 5.9). This might be explained by the notion that PBS washing steps could not be sufficient to remove all the pathogenic bacteria, and some of them might be left within the mucin layer, which continues to damage the epithelial barrier. Thus, a higher transcription of *JAM-A* mRNA levels could be a defense response from the cells. When cells were incubated with the probiotic EcN WT, the epithelial damage was attenuated and synthesis of *de novo* of JAM-A might not be urgent. EcN can prevent the impact of pathogens in the gut either directly by growth competition or indirectly via the production of inhibitory substances such as bacteriocins (Jiang *et al*., 2014).

In fully polarized cells, JAM-A phosphorylation at serine 285 (JAM-A S285) is localized exclusively at the tight junctions. JAM-A S285 promotes the maturation of immature cell-cell contacts, and it is required for the development of a functional epithelial barrier (Iden *et al*., 2012). EcN may likely

promote S285 phosphorylation of JAM-A to redistribute this protein from the cytoplasm to the intercellular junctions. Future studies will help to understand a possible link between EcN and the sublocalization of JAM-A.

The EcN variant 3413 has an inframe deletion in the *flgB* gene (Dobrindt *et al*., personal communication). FlgB is a subunit protein of the bacterial rod (Lee *et al*., 2006). The bacterial flagellum is a motile organelle driven by a rotary motor and its axial portions that serve as a drive shaft (rod), a universal joint (hook), and a helical propeller (filament) (Fuji *et al*., 2017). On the one hand, Lee *et al*. showed that *Salmonella enterica flgB* mutants are defective in rod assembly (Lee *et al*., 2006). On the other hand, Hirano *et al*. demonstrated that the overproduction of FlgB impaired the motility of wild-type *Salmonella* bacteria. The impairment of the motility was a consequence of failure to export flagellar protein causing an inability to swarm (Hirano *et al*., 2003). We did not perform an extensive study of this EcN variant, so we are not aware whether this inframe deletion caused an overproduction of the FlgB protein. EcN variant 3413 upregulated the expression of *JAM-A* in HT29-MTX-E12 cells (Figure 5.3.1). However, we detected that after disruption of the paracellular epithelial barrier function by EPEC strain E2348/69, the EcN variant 3413 did not restore the epithelial barrier integrity in terms of JAM-A re-distribution (Figure 5.13, EcN 3413). The flagellum may contribute to colonization at sites where the intestinal barrier is disrupted. In the case that this mutation causes a decrease in bacterial motility, proper migration at sites of injury could not happen. It has also been found that flagellin stimulates cell migration through the p38 MAP kinase pathway in cultured intestinal epithelial cells (Kondo *et al*., 2016). It would be interesting to know if this mutation affects the secretion of flagellar proteins, such as flagellin, that could somehow modulate JAM-A re-distribution and, therefore, cell migration.

Downregulation of *MyD88* expression by most of the EcN variants may confirm previous results where EcN upregulates miR-200c, a negative regulator of *MyD88* mRNA, in T84 cells (data not shown). Some EcN variants induced the upregulation of *MyD88* mRNA levels in HT29-MTX-E12 cells grown in the 3D culture after 2 h and 4 h of incubation. However, changes between untreated and treated cells were not significant (Figure 5.3.2, **A-B**, green columns). Hafez *et al*. showed that infection of Caco-2 cells with EcN increased the levels of the adaptor molecules MyD88 and TRIF, which was K5 capsule-dependent (Hafez *et al*., 2010). Even though we observed a downregulation of *MyD88* expression, its expression was not abolished. Thus, a pro-inflammatory response occurs. EcN WT and EcN variant 3595 slightly increased the expression of *TLR4* and *TLR5* when incubated with HT29-MTX-E12 cells grown in the 3D cell culture system under static conditions (Table 5.2. 3D system, static infection). This slight expression was sufficient to enhance MyD88-dependent and independent pathways activating pro-

inflammatory cytokines. As we can observe in Table 5.2, EcN WT and EcN variant 3595 highly upregulated the expression of the pro-inflammatory cytokines CXCL1 and CXCL2.

When EcN WT was added to the epithelial cells after a pre-infection with the EPEC strain, the pro-inflammatory response was slightly higher compared to cells with only fresh medium upon EPEC removal (Table 5.3, EPEC+ EcN WT, EPEC + medium). This might reveal that EcN induced a mild pro-inflammatory response after epithelial damage by a pathogen to increase cell repair. The question of why EcN alone induced a higher activation of inflammatory cytokines in the cells than when it was added after the EPEC infection remains to be elucidated.

It has been demonstrated that in response to commensal bacteria, CXCL1 production via TLR2, TLR4, and MyD88-mediated signaling recruit neutrophils and thereby renders a protective effect in the DSS-colitis model (Fukata *et al*., 2005; Shea-Donohue *et al*., 2008). Although the upregulation of inflammatory cytokines by a probiotic might appear unusual, this could suggest a mechanism by which EcN could confer a protective effect on the host and promote bacterial clearance. Hafez *et al*. were able to show that EcN increases the expression of a broad array of pro-inflammatory chemokines such as IL-1, IL-8, MCP-1, IP-10, among others, in Caco-2 cells (Hafez *et al*., 2009). Most Likely, EcN prevents intracellular pathogen invasion into the host cells via pro-inflammatory cytokines signaling. Modulation of both pro- and anti-inflammatory host cytokines by EcN is still controversial. Published results depend on the cell type and infection conditions.

6.3.1 Cellular response of HT29-MTX-E12 cells to EcN outer membrane vesicles and supernatant

Isolated OMVs from EcN WT and EcN variant 3595 increased the expression of *JAM-A* mRNA levels after 4 h incubation in HT29-MTX-E12 cells grown in the 3D cell culture system (Figure 5.7.1). Conversely to the incubation with living probiotic bacteria (Figure 5.3.1, **B**, green columns), the *de novo* synthesis of JAM-A protein was higher when the epithelial cells were incubated with purified “probiotic” OMVs. A similar pattern was seen with the “pathogenic” OMVs derived from EPEC strain E2348/69. As previously explained, the amount of purified OMVs used for infection of the epithelial cells might be much higher than the total amount of OMVs produced by living bacteria when incubated with the epithelial cells. These OMV concentrations that were used had a higher and faster effect on *JAM-A* gene expression than the whole microbe. In general, the *JAM-A* transcript levels were also upregulated by the EcN supernatants. Interestingly, the high amount of flagella in the supernatant of EcN variant PZ816 did not

significantly upregulate *JAM-A* mRNA levels (Figure 5.8.4). This makes it unlikely that the regulation of *JAM-A* expression is flagellin-dependent.

Overall, the expression of *MyD88* is downregulated after 4 h of incubation with OMVs and supernatants of the probiotic strain EcN. *MyD88* expression levels were lower upon infection with the probiotic strain than with the enteropathogenic isolate (Figure 5.7.2 and Figure 5.8.4). Under static conditions, the supernatant of the highly flagellated EcN variant PZ816 induced a strong increase in the expression levels of the pro-inflammatory cytokine genes *IL-1β*, *CXCL1*, *CXCL2*, and *TNF*. These expression levels were higher than those after infection with the supernatant of EPEC strain E2348/69 (Table 5.2, 3D system, supernatant infection). An excess of flagellin could be detrimental for the cells inducing to a higher degree the activation of the immuno-modulatory response.

Similarly to infection with the supernatant of the EPEC strain, *TNF* levels were more than 10 times elevated after incubation with supernatants of EcN WT and EcN variant PZ816 than after incubation with the probiotic bacteria themselves (Table 5.2). The presence of a mucin layer could influence the shed flagellin subunits and other bioactive compounds from the bacteria by modulation of the bacterial transcriptional response to avoid an extreme pro-inflammatory response. However, spent culture supernatants could have higher concentrations of signal molecules, like TcpC, which will be further explained, and flagellin, that can cross the mucosal barrier to encounter epithelial cells. The modulation of *TNF* might be one of the pivotal defense responses exerted by supernatants of EcN and the EPEC strain E2348/69. Previous studies have shown more intensive pro-inflammatory properties of EcN supernatants compared to supernatants of the probiotic *Lactobacillus rhamnosus* GG (Wan *et al*., 2018). Moreover, like for incubation with supernatants of the EPEC strain, increased *TLR4* and *TLR5* expression levels were detectable after incubation with supernatants of the probiotic strain as well, which may indicate an alertness status caused by EcN culture supernatants in HT29-MTX-E12 cells.

Intriguingly, Reuter *et al*. proved that the secretion of mucin and the formation of an adherent mucus layer on epithelial cells attenuate the genotoxic activity of colibactin of EcN, by preventing the induction of DNA double-strand breaks (Reuter *et al*., 2017). In agreement with this finding, we found an extreme pro-inflammatory response in non-mucin secreting HT29 cells after 2 h of EcN incubation compared to mucin-secreting HT29-MTX-E12 cells (Table 5.3). These results confirm that mucins can alter bacterial phenotypes. Measuring the concentration of flagellin or of other components released in the supernatant after infection with living bacteria would be necessary to compare to their concentrations in spent culture supernatants.

OMVs and culture supernatant from EcN WT enhanced the expression of *JAM-A* after pre-incubation with the EPEC strain E2348/69. In general, EcN OMVs had a higher impact on *JAM-A*

expression than the supernatants (Figure 5.14.1). However, the distribution of JAM-A to the cell borders was improved more efficiently upon the addition of culture supernatants of EcN than of OMVs (Figure 5.15.1). These observations could be due to the presence of other bacterial factors that are released in the supernatant and are not associated with OMVs. For example, the TcpC protein, a bacterial factor secreted by EcN, which is highly prevalent in many Gram-negative pathogens. Despite the fact that TcpC has been described as a pathogenicity factor in uropathogenic *E. coli*, it has been reported that TcpC from EcN plays a role in protecting mice from DSS-induced colitis (Hering *et al*., 2014). Alvarez *et al*. showed that TcpC is not exported through OMVs but is present in the EcN supernatant. Furthermore, they showed that EcN supernatant induced an upregulation of ZO-1 and claudin-14 barrier-forming tight junction proteins, and that this effect mainly relies on TcpC (Alvarez *et al*., 2016). Similarly, Hering *et al*. demonstrated that the TcpC protein of EcN induces phosphorylation of the protein kinase C-ζ (PKCζ) and of the extracellular signal-regulated kinases 1/2 (ERK1/2), which in turn results in upregulation of claudin-14 (Hering *et al*., 2014). Secreted soluble active factors from EcN, other than TcpC, could have a significant impact on the epithelial barrier.

6.4 Occludin expression in HT29-MTX-E12 cells after incubation with EPEC strain E2348/69 and probiotic strain EcN

The physiological function of occludin is still not completely clear. Some reports propose different roles, such as maintenance of the tight junction barrier, signaling, and junction remodeling (Van Itallie *et al*., 2010). Several studies have shown a downregulation of the expression of occludin as well as its cellular distribution by pathogens. In this study, a similar expression pattern of occludin was observed after incubation of HT29-MTX-E12 epithelial cells with pathogenic and probiotic *E. coli* strains. Occludin transcript levels were upregulated at 2 h incubation with the *E. coli* strains, but these levels decreased significantly after 4 h incubation, except for the EcN variants 3426 and 3414 (Figure 5.3.3). Murata *et al*. investigated the role of occludin in tight junction expression and apoptosis regulated by survival signal-transduction pathways, such as MAPK and Akt. Hepatocytes from occludin-deficient mice showed downregulation of MAPK and Akt levels, which results in apoptosis and disruption of the epithelial barrier function (Murata *et al*., 2005). Although we found lower mRNA levels of occludin in cells treated with probiotic and pathogenic *E. coli* strains, these levels might still be high enough to activate signaling pathways. At first sight, the downregulation of occludin by a probiotic might appear peculiar. However, Kuo *et al*. found that occludin increased the expression of caspase-3, which induced apoptosis. Biopsies of patients with Inflammatory Bowel Disease (IBD) showed reduced expression of occludin. A reduction in transcript levels of occludin led to caspase-3 downregulation that limited

epithelial apoptosis and attenuated colitis. Therefore, based on these findings, the authors suggested that inflammatory stimuli induced occludin downregulation, which may be a mechanism of epithelial preservation that promotes mucosal homeostasis (Kuo *et al*., 2019).

According to our results, EcN promotes a high pro-inflammatory response. Hence, a decrease in occludin expression after 4 h of EPEC strain E2348/69 and EcN incubation might be an adaptive mechanism of cells to prevent apoptosis and subsequent epithelial damage in response to extrinsic pathway stimuli.

6.5 Cellular response of HT29-MTX-E12 cells after incubation under rotating conditions with EPEC strain E2348/69 and probiotic EcN

Under rotating or dynamic conditions, the *JAM-A* gene expression was higher than under static conditions after epithelial cells were challenged with probiotic or pathogenic *E. coli* (Figure 5.16.2). This might be due to different amounts of OMVs secreted, as several studies have indicated that the production of OMVs changes with different growth or incubation conditions. For example, *P. aeruginosa* and *N. meningitidis* increase vesiculation under oxygen stress (Sabra *et al*., 2003; van de Waterbeemd *et al*., 2013). In the same way, via the SOS response, *P. aeruginosa* increased OMVs production after DNA-damaging antibiotics (Maredia *et al*., 2012). Therefore, physical stresses, such as fluid shear stress, osmotic pressure, and heat shock caused bacteria to increase the production and delivery of OMVs (Yu *et al*., 2018). Also, under physical stress, bacteria enhance the expression of a series of molecules to establish a firm attachment to the epithelial surface. These molecules are related to fibrillar protrusions (pili) and surface-anchored proteins that bind to human matrix proteins (Otto, 2014). Furthermore, under given shear stress, many bacteria produce multi-layered agglomerations with a sticky extracellular matrix, called biofilms, that protect the embedded cells from insults from fluid shear stress. The shear flow led to morphological changes in the cellular architecture of microcolonies, so early biofilm formation under dynamic conditions is not linked with the population size but with the 3D architecture of the microcolonies (Wang *et al*., 2018). Some studies have suggested that under dynamic conditions, biofilms are composed of low amounts of adhering bacteria.

Even though bacterial adhesion is perturbed under rotating conditions, an irreversible adhesion might be required to initiate proper colonization. Those attached bacteria stimulate the production of higher amounts of OMVs and soluble factors as an adaptive/protective response to rapid changes in environmental conditions. An increase in *JAM-A* gene expression after 4 h infection with EPEC strain E2348/69, under low-fluid shear stress (1,25 dyn/cm^2), might be a cellular defense response to

counteract epithelial damage due to EPEC effector proteins. It has been proposed that pathogenic bacteria release more OMVs than the non-pathogenic ones as a mechanism of adaptation to enhance their virulence (Yu *et al*., 2018). Similarly, EcN stimulated the expression of *JAM-A* in HT29-MTX-E12 cells more under rotating than under static conditions. Huang *et al*. showed that under shear stress, JAM-A enhanced cell migration (Huang *et al*.,2006). Hence, low-fluid shear stress could augment the probiotic properties of EcN through stimulating cell migration and increasing the epithelial barrier function by an upregulation of *JAM-A* expression.

Under static conditions, there was a higher re-distribution of JAM-A from the cellular borders to the cytoplasm detectable than under rotating movements after infection wit the EPEC strain (Figure 5.16.3). It is already mentioned that phosphorylation of JAM-A at residue S285 is required to localize this protein at the junctional complex. Exposure of epithelial cells to fluid shear stress or other mechanical forces rapidly increases JAM-A S285 phosphorylation, which is necessary for RhoA activation in response to tension. Activated RhoA promotes actomyosin-based contractility and subsequent regulation of the cytoskeletal organization (Scott *et al*., 2016). In this study, we found that phosphorylation of JAM-A at residue Y280, which is related to barrier disruption, was lower under low-fluid shear stress compared to static conditions. Additionally, HT29-MTX-E12 cells incubated with EcN showed a lower percentage of phosphorylated JAM-A than those infected with EPEC strain E2348/69 (Figure 5.19.2, F). Stimulation of *de novo* JAM-A synthesis that could be phosphorylated at S285 and a decrease in JAM-A PY280 phosphorylation after EPEC infection under rotating conditions could explain why the epithelial barrier was much less disrupted after 6 h under rotating conditions. A detailed analysis of JAM-A phosphorylation at position S285 and more biological replicates are necessary to confirm our assumptions and to obtain statistically significant data.

The expression of *MyD88* was also upregulated under rotating conditions (Figure 5.16.4). In the same way, the expression of the central inflammatory mediator *TNF* was highly upregulated after incubation with EPEC strain E2348/69 and EcN (Table 5.2. 3D system, rotating infection). Several studies have shown that low-fluid shear stress increases the expression of inflammatory cytokines. Kim *et al.* demonstrated that exposure of polarized intestinal epithelial cells to physiological levels of fluid shear stress leads to the formation of large vacuoles containing extracellular contents. Furthermore, they showed that shear stress-induced vacuole formation is associated with the autophagy machinery downstream from extracellular uptake. Despite vacuole formation, Caco-2 cells proliferated normally under shear stress. Thus, the presence of vacuoles was not indicative of imminent cellular senescence or cell death (Kim *et al.,* 2017). It has been reported that TNF-α plays a role in stimulating autophagy in several cell types (Qian *et al*., 2017). These findings could suggest that under rotating conditions, EcN increases TNF- mediated signaling pathways that might include autophagy in response to intracellular

vacuole formation. Most of the published studies indicate that EcN suppresses TNF-α stimulation; however, those studies are based on static conditions. Different flow environments may underlie variations in susceptibility to inflammation. Further clarification is still needed to explain the balance of pro-and anti-inflammatory cytokines that EcN could achieve in response to an infection or epithelial damage.

6.6 Cellular response of LS174T cells to incubation with EPEC strain E2348/69 and probiotic strain EcN

We have previously shown that the cellular response of the LS174T epithelial cell line to bacterial infection differed significantly from the cellular response of the HT29-MTX-E12 epithelial cells (Results 5.20). The morphology of these cell lines was examined by transmission electron and confocal laser scanning microscopy. LS174T cells were incapable of producing an organized cell layer with functional tight junctions, but instead, these cells grew in grape-like clusters (data not shown). Moreover, a disorganized development had a negative influence on cell polarization, which is already known to be very important for bacterial adhesion and invasion. A significant increase in *JAM-A* expression incubation with EPEC strain E2348/69 or probiotic strain EcN might be due to an abnormal junctional complex formation which might be repaired by the probiotic EcN. A *TLR5* response might be due to the lack of a tight monolayer that enables the bacteria to reach the basolateral side of the cells.

The mucin-release of HT29-MTX-E12 cells is similar to that of intestinal goblet cells (Halm *et al.*, 2000). In the same way, the formation of the junctional complex is functional and recapitulates the *in vivo*-like phenotype. Therefore, this epithelial cell line is an adequate model to study host-microbe interactions, also in terms of stimulation of mucin in response to bacterial infection. We can assume that the results obtained in this study are cell-line dependent. Therefore, another epithelial cell line that reproduces the tissue architecture of the colon better than the cell line LS174T is required to confirm and verify current results.

6.7 Summary and outlook

The aim of this study was to investigate host-microbe interactions in an experimental setup that is more closely related to *in vivo* conditions than the previously used common 2D cell cultures. Here, we describe host responses to probiotic *E. coli* strain EcN in comparison to EPEC strain E2348/69 with a focus on the host barrier function, represented by JAM-A expression and distribution, as well as the host immune response represented by MyD88, TLRs, and cytokine responses. Different cell culture systems were employed to compare molecular and cellular responses under different incubation conditions. We demonstrated that HT29-MTX-E12 epithelial cells grown in different cell culture systems showed distinct responses to bacterial infection. Changes in cellular responses might be due to the degree of cellular differentiation represented by tight junctional complex formation, which increased with the increasing complexity of cell culture.

Interestingly, the EPEC strain E2348/69, used as a reference to compare with the host response to the probiotic strain EcN, did not promote attaching and effacing (A/E) lesions in the mucin-secreting HT29-MTX-E12 cells. These findings might suggest that secreted mucin leads to the inhibition of the Type Three Secretion System (T3SS) of EPEC that facilitates the intimate attachment to host cells. This is consistent with very recent *in vitro* studies where it was proposed that increased mucin expression inhibits adherence of attaching and effacing organisms to intestinal epithelial cells. Taking into account the inhibitory effect of glycans within the mucin layer, it might be obvious to assume that any primary effect of probiotic or pathogenic bacteria on host cells depends, at least to some extent, on the secretion of outer membrane vesicles (OMVs) and various other bioactive components released from the bacterial cell. Under the experimental conditions chosen in this work, OMVs and cell-free supernatants from EcN and EPEC strain E2348/69 induced higher expression of *JAM-A* than the living microbe when the epithelial cells were grown in the 3D cell culture system. These findings might be due to the presence of specific factors in purified OMVs and supernatants used in this study that are not inactivated by a “taming” of bacteria within the mucus layer and the corresponding modulation of the bacterial phenotype or gene expression by the mucin glycans.

OMVs and supernatant from EcN WT might also stimulate leukocyte migration via JAM-A upregulation and phosphorylation to maintain immunological homeostasis. An upregulation of *JAM-A* expression by EPEC-derived OMVs and supernatant might be a cellular defense to epithelial damage. Since JAM-A is also involved in leukocyte trafficking, an upregulation of *JAM-A* expression in response to EPEC infection could enhance transendothelial migration of leukocytes at the site of infection to clear the pathogenic bacteria.

The expression of *MyD88* also differed when the epithelial cells were incubated with the living bacteria or secreted bacterial factors.

Furthermore, different variants from EcN, isolated from young children after two years of intestinal colonization, which carry spontaneous mutations, were used to analyze the effect of these variants on the epithelial cells. Some EcN variants upregulated *JAM-A* expression and induced higher phosphorylation of JAM-A than others. This might indicate that certain modifications in the genome of EcN may alter probiotic properties that could lead to an improvement of the epithelial barrier function. Additional studies of these variations should be done to analyze in some further detail whether these mutations in the EcN genome sequence could even improve the properties of the probiotic bacteria.

The systematic analysis of inflammation and host response-related pathways indicated that the probiotic strain EcN and its bioactive products exerted a broad pro-inflammatory effect on intestinal epithelial cells. EcN induced an increase of transcription of genes coding for pro-inflammatory cytokines, such as CXCL1, CXCL2, IL-1β, and TNF-α, which is in line with the increase in *ICAM-1* expression in internal wound healing (Sumagin *et al.*, 2016). Further validation of these observations by measuring protein levels of the secreted chemokines will be necessary. Earlier studies have shown that EcN presented more intensive pro-inflammatory characteristics compared to other probiotic strains. This means that EcN might secrete different bioactive products that differentially modulate cytokine expression, thereby contributing to intestinal health. EcN dependent "controlled inflammatory responses" may also help pathogen eradication and host survival. Comparing HT29 *vs.* HT29-MTX-E12 cells, this pro-inflammatory response was reduced by the presence of a mucus layer, again indicating the importance of the protective effect of mucin.

To mimic in a more precise way the *in vivo* tissue conditions, we employed the Rotating Wall Vessel (RWV) bioreactor as a cell culture model that facilitates the formation of cellular self-organizing 3D tissue-like aggregates. The EPEC strain E2348/69 was used to disrupt the epithelial barrier function. Besides experiments under static conditions, rotating incubation experiments with probiotic and pathogenic *E. coli* strains were performed as well. Our data showed that the presence of low-fluid shear stress modulates the cellular gene expression. Previous studies have also indicated that shear stress influences bacterial adhesion to host cells. These observations suggested the necessity to implement fluid shear stress to *in vivo*-like infection conditions in order to achieve biologically relevant cellular responses.

Another widely used model to study Inflammatory Bowel Disease (IBD) is the dextran sodium sulfate (DSS) colitis model. DSS triggers toxic effects in intestinal epithelial cells that may be related to direct cytotoxicity, interference with the regular interaction between epithelial cells, and aberrant

modulation of cellular receptors (Burgueño *et al*., 2019). The onset of this model has advantages over other various due to its simplicity, rapidity, controllability, and reproducibility (Eichele *et al*., 2017). To further analyze and simulate the probiotic effect of EcN in cell culture systems, our microscopic and gene expression analyses indicated that some kind of previous epithelial damage is necessary to observe the beneficial impact of EcN.

Finally, the data presented here showed that there is an urgent need for additional future studies that address the molecular mechanisms underlying the probiotic effects of EcN under more *in vivo*-like conditions. Along that line, experiments done using "traditional" cell culture conditions have to be looked at again carefully here. The tip of the iceberg, a link between EcN and JAM-A phosphorylation and distribution, has been identified and is currently under further investigation concerning the signaling effect on JAM-A and NF-κB induced by EcN. Studies in this field might shed additional light on the role of probiotics in mammalian host signaling and might give further insights into the restoration of a disrupted epithelial barrier during intestinal inflammation and infection for the development of potential new or more sophisticated therapies against inflammatory bowel diseases.

7. References

Abreu, M. T. (2010). Toll-like receptor signalling in the intestinal epithelium: how bacterial recognition shapes intestinal function*, Nature Reviews: Immunology, 10*(2), 131-44.

Aguilera, L., Toloza, L., Giménez, R., Odena, A., Oliveira, E., Aguilar, J., Badia, J., & Baldomà, L. (2014). Proteomic analysis of outer membrane vesicles from the probiotic strain *Escherichia coli* Nissle 1917. *Proteomics*, *14*(2–3), 222–229.

Akira, S., & Takeda, K . (2004). Toll-like receptor signalling. *Nature Reviews. Immunology, 4*(7), 499-511.

Aloisio, I., Prodam, F., Giglione, E., Bozzi Cionci, N., Solito, A., Bellone, S., Baffoni, L., Mogna, L., Pane, M., Bona, G., & Di Gioia, D. (2018). Three-Month Feeding Integration With Bifidobacterium Strains Prevents Gastrointestinal Symptoms in Healthy Newborns. *Frontiers in Nutrition*, *5*:39.

Alvarez, C.-S., Badia, J., Bosch, M., Giménez, R., & Baldomà, L. (2016). Outer Membrane Vesicles and Soluble Factors Released by Probiotic *Escherichia coli* Nissle 1917 and Commensal ECOR63 Enhance Barrier Function by Regulating Expression of Tight Junction Proteins in Intestinal Epithelial Cells. *Frontiers in Microbiology*, *7*:1981.

Arikawa, E., Sun, Y., Wang, J., Zhou, Q., Ning, B., Dial, S. L., Guo, L., & Yang, J. (2008). Cross-platform comparison of SYBR® Green real-time PCR with TaqMan PCR, microarrays and other gene expression measurement technologies evaluated in the MicroArray Quality Control (MAQC) study. *BMC Genomics*, *9*, 328.

Barrila, J., Radtke, A. L., Crabbé, A., Sarker, S. F., Herbst-Kralovetz, M. M., Ott, C. M., & Nickerson, C. A. (2010). Organotypic 3D cell culture models: Using the rotating wall vessel to study host-pathogen interactions. *Nature Reviews Microbiology*, *8*(11), 791–801.

Barrila, J., Crabbé, A., Yang, J., Franco, K., Nydam, S. D., Forsyth, R. J., Davis, R. R., Gangaraju, S., Ott, C. M., Coyne, C. B., Bissell, M. J., & Nickerson, C. A. (2018). Modeling Host-Pathogen Interactions in the Context of the Microenvironment: Three-Dimensional Cell Culture Comes of Age. *Infection and Immunity*, *86*(11).

Bazzoni, G., Martínez-Estrada, O. M., Orsenigo, F., Cordenonsi, M., Citi, S., & Dejana, E. (2000). Interaction of Junctional Adhesion Molecule with the Tight Junction Components ZO-1, Cingulin, and Occludin. *Journal of Biological Chemistry*, *275*(27), 20520–20526.

Bergstrom, K. S. B., Kissoon-Singh, V., Gibson, D. L., Ma, C., Montero, M., Sham, H., Ryz, N., Huang, T., Velcich, A., Brett Finlay, B., Chadee, K., & Vallance, B. (2010). Muc2 Protects against Lethal Infectious Colitis by Disassociating Pathogenic and Commensal Bacteria from the Colonic Mucosa. *PLoS Pathogens, 6*(5): e1000902.

Bielaszewska, M., Marejková, M., Bauwens, A., Kunsmann-Prokscha, L., Mellmann, A., & Karch, H. (2018). Enterohemorrhagic *Escherichia coli* O157 outer membrane vesicles induce interleukin 8 production in human intestinal epithelial cells by signaling via Toll-like receptors TLR4 and TLR5 and activation of the nuclear factor NF-κB. *International Journal of Medical Microbiology*, *308*(7), 882–889.

Braddock, M., Schwachtgen, J., Houston, P., Dickson, M.C., Lee, M. J., & Campbell, C. J. (1998). Fluid Shear Stress Modulation of Gene Expression in Endothelial Cells. *News in physiological sciences, 13.*

Bron, P. A., van Baarlen, P., & Kleerebezem, M. (2012). Emerging molecular insights into the interaction between probiotics and the host intestinal mucosa. *Nature Reviews Microbiology*, *10*(1), 66–78.

Burgueño, J. F., Lang, J. K., Santander, A. M., Fernández, I., Fernández, E., Zaias, J., & Abreu, M. T. (2019). Fluid supplementation accelerates epithelial repair during chemical colitis. *PLoS ONE*, *14*(4).

Cairns, M. T., Gupta, A., Naughton, J. A., Kane, M., Clyne, M., & Joshi, L. (2017). Glycosylation-related gene expression in HT29-MTX-E12 cells upon infection by *Helicobacter pylori*. *World Journal of Gastroenterology*, *23*(37), 6817–6832.

Cañas, M.-A., Fábrega, M.-J., Giménez, R., Badia, J., & Baldomà, L. (2018). Outer Membrane Vesicles From Probiotic and Commensal *Escherichia coli* Activate NOD1-Mediated Immune Responses in Intestinal Epithelial Cells. *Frontiers in Microbiology*, *9*:498.

Celli, J., Olivier, M., & Finlay, B. B. (2001). Enteropathogenic *Escherichia coli* mediates antiphagocytosis through the inhibition of PI 3-kinase-dependent pathways. *The EMBO Journal, 20*(6), 1245-58.

Cerutti, A., Chen, K., & Chorny, A. (2011). Immunoglobulin responses at the mucosal interface. *Annual Review of Immunology, 29*, 273-93.

Chassaing, B., Kumar, M., Baker, M. T., Singh, V., & Vijay-Kumar, M. (2014). Mammalian gut immunity. *Biomedical Journal*, *37*(5), 246–258.

Chu, H., & Mazmanian, S. K. (2013). Innate immune recognition of the microbiota promotes host-microbial symbiosis. *Nature Immunology*, *14*(7), 668–675.

Cordes, F., Brückner, M., Lenz, P., Veltman, K., Glauben, R., Siegmund, B., Hengst, K., Schmidt, M. A., Cichon, C., & Bettenworth, D. (2016). MicroRNA-320a Strengthens Intestinal Barrier Function and Follows the Course of Experimental Colitis. *Inflammatory Bowel Diseases*, *22*(10), 2341–2355.

Cornick, S., Kumar, M., Moreau, F., Gaisano, H., & Chadee, K. (2019). VAMP8-mediated MUC2 mucin exocytosis from colonic goblet cells maintains innate intestinal homeostasis. *Nature Communications*, *10*:4306.

Cukrowska, B., Lodínová-Žádníková, R., Enders, C., Sonnenborn, U., Schulze, J., & Tlaskalová-Hogenová, H. (2002). Specific Proliferative and Antibody Responses of Premature Infants to Intestinal Colonization with Nonpathogenic Probiotic *E. coli* Strain Nissle 1917. *Scandinavian Journal of Immunology*, *55*(2), 204–209.

Davidovich, N., Kloog, Y., Wolf, M., & Elad, D. (2011). Mechanophysical Stimulations of Mucin Secretion in Cultures of Nasal Epithelial Cells. *Biophysical Journal*, *100*(12), 2855–2864.

De Filippo, K., Dudeck, A., Hasenberg, M., Nye, E., van Rooijen, N., Hartmann, K., Gunzer, M., Roers, A., & Hogg, N. (2013). Mast cell and macrophage chemokines CXCL1/CXCL2 control the early stage of neutrophil recruitment during tissue inflammation. *Blood*, *121*(24), 4930–4937.

DeGruttola, A. K., Low, D., Mizoguchi, A., & Mizoguchi, E. (2016). Current Understanding of Dysbiosis in Disease in Human and Animal Models: *Inflammatory Bowel Diseases*, *22*(5), 1137–1150.

Deguine, J., & Barton, G. M. (2014). MyD88: A central player in innate immune signaling. *F1000Prime Reports*, *6*:97.

de Lorenzo, V., & Neilands, J. B. (1986). Characterization of iucA and iucC genes of the aerobactin system of plasmid ColV-K30 in Escherichia coli. *Journal of Bacteriology*, *167*(1), 350–355.

Demouveaux, B., Gouyer, V., Gottrand, F., Narita, T., & Desseyn, J.-L. (2018). Gel-forming mucin interactome drives mucus viscoelasticity. *Advances in Colloid and Interface Science*, *252*, 69-82.

Donnenberg, M. S., Yu, J., & Kaper, J. B. (1993). A second chromosomal gene necessary for intimate attachment of enteropathogenic *Escherichia coli* to epithelial cells. *Journal of Bacteriology, 175*(15), 4670-80.

DuPont, A. W., & DuPont, H. L. (2011). The intestinal microbiota and chronic disorders of the gut. *Nature Reviews Gastroenterology & Hepatology*, *8*(9), 523–531.

Ebnet, K., Suzuki, A., Ohno, S., & Vestweber, D. (2004). Junctional adhesion molecules (JAMs): More molecules with dual functions? *Journal of Cell Science*, *117*(1), 19–29.

Eichele, D. D., & Kharbanda, K. K. (2017). Dextran sodium sulfate colitis murine model: An indispensable tool for advancing our understanding of inflammatory bowel diseases pathogenesis. *World Journal of Gastroenterology*, *23*(33), 6016–6029.

Eichner, M., Protze, J., Piontek, A., Krause, G., & Piontek, J. (2017). Targeting and alteration of tight junctions by bacteria and their virulence factors such as Clostridium perfringens enterotoxin. *Pflügers Archiv - European Journal of Physiology*, *469*(1), 77–90.

Fábrega, M.-J., Rodríguez-Nogales, A., Garrido-Mesa, J., Algieri, F., Badía, J., Giménez, R., Gálvez, J., & Baldomà, L. (2017). Intestinal Anti-inflammatory Effects of Outer Membrane Vesicles from *Escherichia coli* Nissle 1917 in DSS-Experimental Colitis in Mice. *Frontiers in Microbiology*, *8*:1274.

Fan, S., Weight, C. M., Luissint, A.-C., Hilgarth, R. S., Brazil, J. C., Ettel, M., Nusrat, A., & Parkos, C. A. (2019). Role of JAM-A tyrosine phosphorylation in epithelial barrier dysfunction during intestinal inflammation. Molecular Biology of the Cell, 30(5), 566–578.

Fanning, A. S., & Anderson, J. M. (2009). Zonula Occludens-1 and -2 Are Cytosolic Scaffolds That Regulate the Assembly of Cellular Junctions. *Annals of the New York Academy of Sciences*, *1165*, 113–120.

Feldman, G. J., Mullin, J. M., & Ryan, M. P. (2005). Occludin: Structure, function and regulation. Advanced Drug Delivery Reviews, 57(6), 883–917.

Francino, M. P. (2016). Antibiotics and the Human Gut Microbiome: Dysbioses and Accumulation of Resistances. *Frontiers in Microbiology*, *6*:1543.

Franzosa, E. A., Hsu, T., Sirota-Madi, A., Shafquat, A., Abu-Ali, G., Morgan, X. C., & Huttenhower, C. (2015). Sequencing and beyond: Integrating molecular 'omics for microbial community profiling. *Nature Reviews. Microbiology*, *13*(6), 360–372.

Fujii, T., Kato, T., Hiraoka, K. D., Miyata, T., Minamino, T., Chevance, F. F. V., Hughes, K. T., & Namba, K. (2017). Identical folds used for distinct mechanical functions of the bacterial flagellar rod and hook. *Nature Communications*, *8*, 14276.

Fukata, M., Michelsen, K. S., Eri, R., Thomas, L. S., Hu, B., Lukasek, K., Nast, C. C., Lechago, J., Xu, R., Naiki, Y., Soliman, A., Arditi, M., & Abreu, M. T. (2005). Toll-like receptor-4 is required for intestinal response to epithelial injury and limiting bacterial translocation in a murine model of acute colitis. *American Journal of Physiology-Gastrointestinal and Liver Physiology*, *288*(5), G1055–G1065.

Gaj, S., Eijssen, L., Mensink, R. P., & Evelo, C. T. A. (2008). Validating nutrient-related gene expression changes from microarrays using RT2 PCR-arrays. *Genes & Nutrition*, *3*(3–4), 153–157.

Garrido-Urbani, S., Bradfield, P. F., & Imhof, B. A. (2014). Tight junction dynamics: The role of junctional adhesion molecules (JAMs). *Cell and Tissue Research*, *355*(3), 701–715.

Gaudet, P., Livstone, M. S., Lewis, S. E., & Thomas, P. D. (2011). Phylogenetic-based propagation of functional annotations within the Gene Ontology consortium. *Briefings in Bioinformatics*, *12*(5), 449–462.

Gaytán, M. O., Martínez-Santos, V. I., Soto, E., & González-Pedrajo, B. (2016). Type Three Secretion System in Attaching and Effacing Pathogens. *Frontiers in Cellular and Infection Microbiology*, *6*:129.

Gewirtz, A. T., Navas, T. A., Lyons, S., Godowski, P. J., & Madara, J. L. (2001). Cutting Edge: Bacterial Flagellin Activates Basolaterally Expressed TLR5 to Induce Epithelial Proinflammatory Gene Expression. *The Journal of Immunology*, *167*(4), 1882–1885.

González-Mariscal, L., Betanzos, A., Nava, P., & Jaramillo, B. E. (2003). Tight junction proteins. *Progress in Biophysics and Molecular Biology*, *81*(1), 1–44.

Guo, S., Chen, S., Ma, J., Ma, Y., Zhu, J., Ma, Y., Liu, Y., Wang, P., & Pan, Y. (2019). *Escherichia coli* Nissle 1917 Protects Intestinal Barrier Function by Inhibiting NF-κB-Mediated Activation of the MLCK-P-MLC Signaling Pathway. *Mediators of Inflammation*, *2019*.

Hafez, M., Hayes, K., Goldrick, M., Warhurst, G., Grencis, R., & Roberts, I. S. (2009). The K5 Capsule of *Escherichia coli* Strain Nissle 1917 Is Important in Mediating Interactions with Intestinal Epithelial Cells and Chemokine Induction. *Infection and Immunity*, *77*(7), 2995–3003.

Hafez, M., Hayes, K., Goldrick, M., Grencis, R. K., & Roberts, I. S. (2010). The K5 Capsule of *Escherichia coli* Strain Nissle 1917 Is Important in Stimulating Expression of Toll-Like Receptor 5, CD14, MyD88, and TRIF Together with the Induction of Interleukin-8 Expression via the Mitogen-Activated Protein Kinase Pathway in Epithelial Cells. *Infection and Immunity*, *78*(5), 2153–2162.

Halm, D. R., & Halm, S. T. (2000). Secretagogue response of goblet cells and columnar cells in human colonic crypts. *American Journal of Physiology. Cell Physiology*, *278*(1), C212-233.

Han, J. (2006). MyD88 beyond Toll. *Nature Immunology*, *7*(4), 370–371.

Hering, N. A., Richter, J. F., Fromm, A., Wieser, A., Hartmann, S., Günzel, D., Bücker, R., Fromm, M., Schulzke, J. D., & Troeger, H. (2014). TcpC protein from *E. coli* Nissle improves epithelial barrier

function involving PKCζ and ERK1/2 signaling in HT-29/B6 cells. *Mucosal Immunology*, *7*(2), 369–378.

Hesslinger, C., Fairhurst, S. A., & Sawers, G. (1998). Novel keto acid formate-lyase and propionate kinase enzymes are components of an anaerobic pathway in *Escherichia coli* that degrades L-threonine to propionate. *Molecular Microbiology*, *27*(2), 477–492.

Hirano, T., Minamino, T., Namba, K., & Macnab, R. M. (2003). Substrate Specificity Classes and the Recognition Signal for Salmonella Type III Flagellar Export. *Journal of Bacteriology*, *185*(8), 2485–2492.

Homburg, S., Oswald, E., Hacker, J., & Dobrindt, U. (2007). Expression analysis of the colibactin gene cluster coding for a novel polyketide in *Escherichia coli*. *FEMS Microbiology Letters*, *275*(2), 255–262.

Huang, H., Cruz, F., & Bazzoni, G. (2006). Junctional adhesion molecule-A regulates cell migration and resistance to shear stress. *Journal of Cellular Physiology*, *209*(1), 122–130.

Huebner, C., Ding, Y., Petermann I., Knapp, C., & Ferguson L. R. (2011). The probiotic *Escherichia coli* Nissle 1917 reduces pathogen invasion and modulates cytokine expression in Caco-2 cells infected with Crohn´s disease-associated E. coli LF82. *Applied and Environmental Microbiology, 77*(7), 2541-4.

Iden, S., Misselwitz, S., Peddibhotla, S. S. D., Tuncay, H., Rehder, D., Gerke, V., Robenek, H., Suzuki, A., & Ebnet, K. (2012). APKC phosphorylates JAM-A at Ser285 to promote cell contact maturation and tight junction formation. *The Journal of Cell Biology*, *196*(5), 623–639.

Janosch, D., Dubbert, S., Eiteljörge, K., Diehl, B. w. k., Sonnenborn, U., Passchier, L. v., Wassenaar, T. m., & von Bünau, R. (2019). Anti-genotoxic and anti-mutagenic activity of *Escherichia coli Nissle* 1917 as assessed by in vitro tests. *Beneficial Microbes*, *10*(4), 449–461.

Jayamani, E., & Mylonakis, E. (2014). Effector triggered manipulation of host immune response elicited by different pathotypes of *Escherichia coli*. *Virulence*, *5*(7), 733–739.

Jiang, Y., Kong, Q., Roland, K. L., Wolf, A., & Curtiss, R. (2014). Multiple effects of *Escherichia coli* Nissle 1917 on growth, biofilm formation and inflammation cytokines profile of Clostridium perfringens type A strain CP4. *Pathogens and Disease*, *70*(3), 390–400.

Kapałczyńska, M., Kolenda, T., Przybyła, W., Zajączkowska, M., Teresiak, A., Filas, V., Ibbs, M., Bliźniak, R., Łuczewski, Ł., & Lamperska, K. (2018). 2D and 3D cell cultures – a comparison of different types of cancer cell cultures. *Archives of Medical Science : AMS*, *14*(4), 910–919.

Kaper, J. B., Nataro, J. P., & Mobley, H. L (2004). Pathogenic *Escherichia coli*. *Nature Reviews. Microbiology, 2*(2), 123-40.

Kawasaki, T., & Kawai, T. (2014). Toll-Like Receptor Signaling Pathways. *Frontiers in Immunology*, *5*: 461.

Kennedy, E. A., King, K. Y., & Baldridge, M. T. (2018). Mouse Microbiota Models: Comparing Germ-Free Mice and Antibiotics Treatment as Tools for Modifying Gut Bacteria. *Frontiers in Physiology*, *9*:1534.

Kim, S. W., Ehrman, J., Ahn, M.-R., Kondo, J., Lopez, A. A. M., Oh, Y. S., Kim, X. H., Crawley, S. W., Goldenring, J. R., Tyska, M. J., Rericha, E. C., & Lau, K. S. (2017). Shear stress induces noncanonical autophagy in intestinal epithelial monolayers. *Molecular Biology of the Cell*, *28*(22), 3043–3056.

Kolodkin-Gal, I., & Engelberg-Kulka, H. (2009). The stationary-phase sigma factor sigma(S) is responsible for the resistance of *Escherichia coli* stationary-phase cells to mazEF-mediated cell death. *Journal of Bacteriology*, *191*(9), 3177–3182.

Kondo, Y., Higa-Nakamine, S., Maeda, N., Toku, S., Kakinohana, M., Sugahara, K., Kukita, I., & Yamamoto, H. (2016). Stimulation of Cell Migration by Flagellin Through the p38 MAP Kinase Pathway in Cultured Intestinal Epithelial Cells. *Journal of Cellular Biochemistry*, *117*(1), 247–258.

Kubori, T., Okumura, M., Kobayashi, N., Nakamura, D., Iwakura, M., & Aizawa, S. I. (1997). Purification and characterization of the flagellar hook-basal body complex of Bacillus subtilis. *Molecular Microbiology*, *24*(2), 399–410.

Kunnen, S. J., Malas, T. B., Semeins, C. M., Bakker, A. D., & Peters, D. J. M. (2018). Comprehensive transcriptome analysis of fluid shear stress altered gene expression in renal epithelial cells. *Journal of Cellular Physiology*, *233*(4), 3615–3628.

Kuo, W.-T., Shen, L., Zuo, L., Shashikanth, N., Ong, M. L. D. M., Wu, L., Zha, J., Edelblum, K. L., Wang, Y., Wang, Y., Nilsen, S. P., & Turner, J. R. (2019). Inflammation-induced Occludin Downregulation Limits Epithelial Apoptosis by Suppressing Caspase-3 Expression. *Gastroenterology*, *157*(5), 1323–1337.

Lee, H. J., & Hughes, K. T. (2006). Posttranscriptional Control of the *Salmonella enterica* Flagellar Hook Protein FlgE. *Journal of Bacteriology*, *188*(9), 3308–3316.

Lee, H.-J. (2019). Microbe-Host Communication by Small RNAs in Extracellular Vesicles: Vehicles for Transkingdom RNA Transportation. *International Journal of Molecular Sciences*, *20*(6).

Lerner, A., Shoenfeld, Y., & Matthias, T. (2019). Probiotics: If It Does Not Help It Does Not Do Any Harm. Really? *Microorganisms*, *7*(4). https://doi.org/10.3390/microorganisms7040104.

Litvak, Y., Sharon, S., Hyams, M., Zhang, L., Kobi, S., Katsowich, N., Dishon, S., Nussbaum, G., Dong, N., Shao, F., & Rosenshine, I. (2017). Epithelial cells detect functional type III secretion system of enteropathogenic *Escherichia coli* through a novel NF-κB signaling pathway. *PLOS Pathogens*, *13*(7), e1006472.

Lorenz, A., & Schulze, J. (1996). Establishment of *E. coli* Nissle 1917 and its interaction with *Candida albicans* in gnotobiotic rats. *Mikroökologie und Therapie*, *24*, 45-51.

MacFarlane, L.-A., & Murphy, P. R. (2010). MicroRNA: Biogenesis, Function and Role in Cancer. *Current Genomics*, *11*(7), 537–561.

Mack, D. R. (2005). Probiotics. *Canadian Family Physician*, *51*(11), 1455–1457.

Mack, D. R. (2011). Probiotics in Inflammatory Bowel Diseases and Associated Conditions. *Nutrients*, *3*(2), 245–264.

Maerz, J. K., Steimle, A., Lange, A., Bender, A., Fehrenbacher, B., & Frick, J.-S. (2018). Outer membrane vesicles blebbing contributes to *B. vulgatus* mpk-mediated immune response silencing. *Gut Microbes*, *9*(1), 1–12.

Mandel, L., Trebichavsky, I., Splichal, I., & Schulze, J. (1995). Stimulation of Intestinal Immune Cells By E. coli in Gnotobiotic Piglets. In J. Mestecky, M. W. Russell, S. Jackson, S. M. Michalek, H. Tlaskalová-Hogenová, & J. Šterzl (Eds.), *Advances in Mucosal Immunology: Part A* (pp. 463–464). Springer US.

Mao, M., Yu, T., Xiong, Y., Wang, Z., Liu, H., Gotteland, M., & Brunser, O. (2008). Effect of a lactose-free milk formula supplemented with bifidobacteria and streptococci on the recovery from acute diarrhea. *Asia Pac J Clin Natr: 17*(1):30-34.

Maredia, R., Devineni, N., Lentz, P., Dallo, S. F., Yu, J., Guentzel, N., Chambers, J., Arulanandam, B., Haskins, W. E., & Weitao, T. (2012). Vesiculation from *Pseudomonas aeruginosa* under SOS. *The Scientific World Journal*, *2012*: 402919.

Massip, C., Branchu, P., Bossuet-Greif, N., Chagneau, C. V., Gaillard, D., Martin, P., Boury, M., Sécher, T., Dubois, D., Nougayrède, J.-P., & Oswald, E. (2019). Deciphering the interplay between the genotoxic and probiotic activities of *Escherichia coli* Nissle 1917. *PLoS Pathogens*, *15*(9).

Moens, E., & Veldhoen, M. (2012). Epithelial barrier biology: Good fences make good neighbors. *Immunology*, *135*(1), 1–8.

Monteiro AC, Sumagin R, Rankin CR, et al. (2013). JAM-A associates with ZO-2, afadin, and PDZ-GEF1 to activate Rap2c and regulate epithelial barrier function. *Mol Biol Cell*, 24(18):2849–2860.

Monteiro, A. C., Luissint, A.-C., Sumagin, R., Lai, C., Vielmuth, F., Wolf, M. F., Laur, O., Reiss, K., Spindler, V., Stehle, T., Dermody, T. S., Nusrat, A., & Parkos, C. A. (2014). Trans-dimerization of JAM-A regulates Rap2 and is mediated by a domain that is distinct from the cis-dimerization interface. *Molecular Biology of the Cell*, *25*(10), 1574–1585.

Moon, H. W., Whipp, S. C., Argenzio, R. A., Levine, M. M., & Giannella, R. A. (1983). Attaching and effacing activities of rabbit and human enteropathogenic *Escherichia coli* in pig and rabbit intestines. *Infection and Immunity*, *41*(3), 1340–1351.

Murata, M., Kojima, T., Yamamoto, T., Go, M., Takano, K.-I., Osanai, M., Chiba, H., & Sawada, N. (2005). Down-regulation of survival signaling through MAPK and Akt in occludin-deficient mouse hepatocytes in vitro. *Experimental Cell Research*, *310*(1), 140–151.

Naik, M. U. & Naik, U. P. (2006). Junctional adhesion molecule-A-induced endothelial cell migration on vitronectin is integrin v 3 specific. *Journal of Cell Science*, *119*(3), 490–499.

Nataro, J. P., & Kaper, J. B. (1998). Diarrheagenic *Escherichia coli*. Clinical Microbiology Reviews, 11(1), 142-201.

Nougayrède, J.-P., Homburg, S., Taieb, F., Boury, M., Brzuszkiewicz, E., Gottschalk, G., Buchrieser, C., Hacker, J., Dobrindt, U., & Oswald, E. (2006). *Escherichia coli* induces DNA double-strand breaks in eukaryotic cells. *Science (New York, N.Y.)*, *313*(5788), 848–851.

Nowotny, V., & Nierhaus, K. H. (1988). Assembly of the 30S subunit from *Escherichia coli* ribosomes occurs via two assembly domains which are initiated by S4 and S7. *Biochemistry*, *27*(18), 7051–7055.

Olier, M., Marcq, I., Salvador-Cartier, C., Secher, T., Dobrindt, U., Boury, M., *et al*. (2012). Genotoxicity of *Escherichia coli* Nissle 1917 strain cannot be disssociated from its probiotic activity. *Gut Microbes*, 3, 501-509.

Otto, M. (2014). Physical stress and bacterial colonization. *FEMS Microbiology Reviews*, *38*(6), 1250–1270.

Park, S. J., Chao, G., & Gunsalus, R. P. (1997). Aerobic Regulation of the *suc*ABCD Genes of *Escherichia coli*, Which Encode α-Ketoglutarate Dehydrogenase and Succinyl Coenzyme A Synthetase: Roles of ArcA; Fnr; and the Upstream *sdh*CDAB Promoter. *Journal of Bacteriology, 179*(13), 4138-4142.

Parker, A., Lawson, M. A. E., Vaux, L., & Pin, C. (2018). Host-microbe interaction in the gastrointestinal tract. *Environmental Microbiology*, *20*(7), 2337–2353.

Peterson, L.W., & Artis, D. (2014). Intestinal epithelial cells: regulators of barrier function and immune homeostasis. *Nature Reviews. Immunology, 14*(3),141-53.

Pund, L. C. (2017). Vergleich von 2D- und 3D-Zellkultursystemen: Expressionsstudien mit HT29-Zellen nach Inkubationmit dem probiotischen *E. coli* Nissle 1917. Institute of Infectiology (ZMBE), University of Münster, Münster, Germany.

Qian, M., Fang, X., & Wang, X. (2017). Autophagy and inflammation. *Clinical and Translational Medicine*, *6*:24.

Reissbrodt, R., Hammes, W. P., dal Bello, F., Prager, R., Fruth, A., Hantke, K., Rakin, A., Starcic-Erjavec, M., & Williams, P. H. (2009). Inhibition of growth of Shiga toxin-producing *Escherichia coli* by nonpathogenic *Escherichia coli*. *FEMS Microbiology Letters*, *290*(1), 62–69.

Reuter, C., Alzheimer, M., Walles, H., & Oelschlaeger, T. A. (2017). An adherent mucus layer attenuates the genotoxic effect of colibactin. *Cellular Microbiology*, *20*(2), e12812.

Rocha, S., Carvalho, J., Oliveira, P., Voglstaetter, M., Schvartz, D., Thomsen, A. R., Walter, N., Khanduri, R., Sanchez, J.-C., Keller, A., Oliveira, C., & Nazarenko, I. (2019). 3D Cellular Architecture Affects MicroRNA and Protein Cargo of Extracellular Vesicles. *Advanced Science*, *6*(4), 1800948.

Round, J. L., & Mazmanian, S. K. (2009). The gut microbiota shapes intestinal immune responses during health and disease. *Nature Reviews. Immunology*, *9*(5), 313–323.

Sabharwal, H. (2015). Host microRNA and cytokine responses to probiotic and pathogenic bacteria. Institute of Infectiology (ZMBE), University of Münster, Münster, Germany.

Sabharwal, H., Cichon, C., Ölschläger, T. A., Sonnenborn, U., & Schmidt, M. A. (2016). Interleukin-8, CXCL1, and MicroRNA miR-146a Responses to Probiotic *Escherichia coli* Nissle 1917 and Enteropathogenic *E. coli* in Human Intestinal Epithelial T84 and Monocytic THP-1 Cells after Apical or Basolateral Infection. *Infection and Immunity*, *84*(9), 2482–2492.

Sabra, W., Lünsdorf, H., & Zeng, A.-P. (2003). Alterations in the formation of lipopolysaccharide and membrane vesicles on the surface of *Pseudomonas aeruginosa* PAO1 under oxygen stress conditions. *Microbiology (Reading, England)*, *149*(Pt 10), 2789–2795.

Sansonetti, P. J. (2004). War and peace at mucosal surfaces. *Nature Reviews Immunology*, *4*(12), 953–964.

Schlee, M., Wehkamp, J., Altenhoefer, A., Oelschlaeger, T. A., Stange, E. F., & Fellermann, K. (2007). Induction of Human β-Defensin 2 by the Probiotic *Escherichia coli* Nissle 1917 Is Mediated through Flagellin. *Infection and Immunity*, *75*(5), 2399–2407.

Schroeder, B. O. (2019). Fight them or feed them: How the intestinal mucus layer manages the gut microbiota. *Gastroenterology Report*, *7*(1), 3–12.

Schwechheimer, C., & Kuehn, M. J. (2015). Outer-membrane vesicles from Gram-negative bacteria: Biogenesis and functions. *Nature Reviews. Microbiology*, *13*(10), 605–619.

Scott, D. W., Tolbert, C. E., & Burridge, K. (2016). Tension on JAM-A activates RhoA via GEF-H1 and p115 RhoGEF. *Molecular Biology of the Cell*, *27*(9), 1420–1430.

Sender, R., Fuchs, S., & Milo, R. (2016). Revised Estimates for the Number of Human and Bacteria Cells in the Body. *PLOS Biology*, *14*(8), e1002533.

Shea-Donohue, T., Thomas, K., Cody, M. J., Zhao, A., DeTolla, L. J., Kopydlowski, K. M., Fukata, M., Lira, S. A., & Vogel, S. N. (2008). Mice deficient in the CXCR2 ligand, CXCL1 (KC/GRO-α), exhibit increased susceptibility to dextran sodium sulfate (DSS)-induced colitis. *Innate Immunity*, *14*(2), 117–124.

Smith, P. J., Wiltshire, M., & Errington, R. J. (2004). DRAQ5 labeling of nuclear DNA in live and fixed cells. *Current Protocols in Cytometry*, *Chapter 7*, Unit 7.25.

Solimando, A. G., Brandl, A., Mattenheimer, K., Graf, C., Ritz, M., Ruckdeschel, A., Stühmer, T., Mokhtari, Z., Rudelius, M., Dotterweich, J., Bittrich, M., Desantis, V., Ebert, R., Trerotoli, P., Frassanito, M. A., Rosenwald, A., Vacca, A., Einsele, H., Jakob, F., & Beilhack, A. (2018). JAM-A as a prognostic factor and new therapeutic target in multiple myeloma. *Leukemia*, *32*(3), 736–743.

Sommer, F., & Bäckhed, F. (2013). The gut microbiota—Masters of host development and physiology. *Nature Reviews. Microbiology*, *11*(4), 227–238. https://doi.org/10.1038/nrmicro2974

Sonnenborn, U., & Schulze, J. (2009). The non-pathogenic *Escherichia coli* strain Nissle 1917 - features of a versatile probiotic. Microbial Ecology in Health and Disease, 21(3-4), 122-158.

Stamatovic, S. M., Sladojevic, N., Keep, R. F., & Andjelkovic, A. V. (2012). Relocalization of Junctional Adhesion Molecule A during Inflammatory Stimulation of Brain Endothelial Cells. *Molecular and Cellular Biology*, *32*(17), 3414–3427.

Strickland, L., Dassow, G. von, Ellenberg, J., Foe, V., Lenart, P., & Burgess, D. (2004). Light Microscopy of Echinoderm Embryos. In *Methods in Cell Biology* (Vol. 74, pp. 371–409). Academic Press.

Sturm, A., Rilling, K., Baumgart, D. C., Gargas, K., Abou-ghayalé, T., Raupach, B., et al. (2005). *Escherichia coli* Nissle 1917 Distinctively Modulates T-Cell Cycling and Expression via Toll-Like Receptor 2 Signalling. *Infection and Immunity, 73*(3), 1452-65.

Sumagin, R., Brazil, J. C., Nava, P., Nishio, H., Alam, A., Luissint, A. C., Weber, D. A., Neish, A. S., Nusrat, A., & Parkos, C. A. (2016). Neutrophil interactions with epithelial-expressed ICAM-1 enhances intestinal mucosal wound healing. *Mucosal Immunology, 9*(5), 1151-1162.

Takeda, K., & Akira, S. (2005). Toll-like receptors in innate immunity. *International immunology, 17*(1), 1-14.

Tapia, R., Kralicek, S. E., & Hecht, G. A. (2017). Modulation of epithelial cell polarity by bacterial pathogens. *Annals of the New York Academy of Sciences*, *1405*(1), 16–24.

Tapia, R., Kralicek, S. E., & Hecht, G. A. (2020). Enteropathogenic *Escherichia coli* (EPEC) Recruitment of PAR Polarity Protein Atypical PKCζ to Pedestals and Cell–Cell Contacts Precedes Disruption of Tight Junctions in Intestinal Epithelial Cells. *International Journal of Molecular Sciences*, *21*(2).

Tarran, R., Button, B., Picher, M., Paradiso, A. M., Ribeiro, C. M., Lazarowski, E. R., Zhang, L., Collins, P. L., Pickles, R. J., Fredberg, J. J., & Boucher, R. C. (2005). Normal and Cystic Fibrosis Airway Surface Liquid Homeostasis. *The Journal of Biological Chemistry*, *280*(42), 35751–35759.

Thursby, E., & Juge, N. (2017). Introduction to the human gut microbiota. *Biochemical Journal*, *474*(11), 1823–1836.

Tölle, R. C., Gaggioli, C., Dengjel, J. (2018). Three-Dimensional Cell Culture Conditions Affect the Proteome of Cancer-Associated Fibroblasts. *Journal of Proteome Research, 17*(8), 2780-2789.

Tom, B. H., Rutzky, L. P., Jakstys, M. M., Oyasu, R., Kaye, C. I., & Kahan, B. D. (1976). Human colonic adenocarcinoma cells. I. Establishment and description of a new line. *In Vitro*, *12*(3), 180–191.

Tomson, F. L., Viswanathan, V. K., Kanack, K. J., Kanteti, R. P., Straub, K. V., Menet, M., Kaper, J. B., & Hecht, G. (2005). Enteropathogenic *Escherichia coli* EspG disrupts microtubules and in conjunction with Orf3 enhances perturbation of the tight junction barrier. *Molecular Microbiology*, *56*(2), 447–464.

Torres, M., Condon, C., Balada, J. M., Squires, C., & Squires, C. L. (2001). Ribosomal protein S4 is a transcription factor with properties remarkably similar to NusA, a protein involved in both non-ribosomal and ribosomal RNA antitermination. *The EMBO Journal*, *20*(14), 3811–3820.

Ukena, S. N., Singh, A., Dringenberg, U., Engelhardt, R., Seidler, U., Hansen, W., Bleich, A., Bruder, D., Franzke, A., Rogler, G., Suerbaum, S., Buer, J., Gunzer, F., & Westendorf, A. M. (2007). Probiotic *Escherichia coli* Nissle 1917 Inhibits Leaky Gut by Enhancing Mucosal Integrity. *PLoS ONE*, *2*(12).

van der Hooft, J. J. J., Goldstone, R. J., Harris, S., Burgess, K. E. V., & Smith, D. G. E. (2019). Substantial Extracellular Metabolic Differences Found Between Phylogenetically Closely Related Probiotic and Pathogenic Strains of *Escherichia coli. Frontiers in Microbiology*, *10*: 252.

van de Waterbeemd, B. van de, Zomer, G., IJssel, J. van den, Keulen, L. van, Eppink, M. H., Ley, P. van der, & Pol, L. A. van der. (2013). Cysteine Depletion Causes Oxidative Stress and Triggers Outer Membrane Vesicle Release by *Neisseria meningitidis*; Implications for Vaccine Development. *PLOS ONE*, *8*(1), e54314.

Van Itallie, C. M., Fanning, A. S., Holmes, J., & Anderson, J. M. (2010). Occludin is required for cytokine-induced regulation of tight junction barriers. *Journal of Cell Science*, *123*(16), 2844–2852.

Vieira, M. A. M., Gomes, T. A. T., Ferreira, A. J. P., Knöbl, T., Servin, A. L., & Liévin-Le Moal, V. (2010). Two Atypical Enteropathogenic *Escherichia coli* Strains Induce the Production of Secreted and Membrane-Bound Mucins To Benefit Their Own Growth at the Apical Surface of Human Mucin-Secreting Intestinal HT29-MTX Cells. *Infection and Immunity*, *78*(3), 927–938.

Vonaesch, P., Anderson, M., & Sansonetti, P. J. (2018). Pathogens, microbiome and the host: Emergence of the ecological Koch's postulates. *FEMS Microbiology Reviews*, *42*(3), 273–292.

Wang, L., Keatch, R., Zhao, Q., Wright, J. A., Bryant, C. E., Redmann, A. L., & Terentjev, E. M. (2018). Influence of Type I Fimbriae and Fluid Shear Stress on Bacterial Behavior and Multicellular Architecture of Early *Escherichia coli* Biofilms at Single-Cell Resolution. *Applied and Environmental Microbiology*, *84*(6), e02343-17.

Wagner, C. E., Wheeler, K. M., & Ribbeck, K. (2018). Mucins and Their Role in Shaping the Functions of Mucus Barriers. *Annual Review of Cell and Developmental Biology, 34*:189-215.

Wan, M. L.-Y., Chen, Z., Shah, N. P., & El-Nezami, H. (2018). Effects of *Lactobacillus rhamnosus* GG and *Escherichia coli Nissle* 1917 Cell-Free Supernatants on Modulation of Mucin and Cytokine Secretion on Human Intestinal Epithelial HT29-MTX Cells. *Journal of Food Science*, *83*(7), 1999–2007.

Werts, C., Rubino, S., Ling, A., Girardin, S. E., & Philpott, D. J. (2011). Nod-like receptors in intestinal homeostasis, inflammation and cancer. *Journal of Leukocyte Biology, 90*(3), 471-82.

Wesche, H., Henzel, W. J., Shillinglaw, W., Li, S., & Cao, Z. (1997). MyD88: An adapter that recruits IRAK to the IL-1 receptor complex. *Immunity*, *7*(6), 837–847.

Wheeler, K. M., Cárcamo-Oyarce, G., Turner, B. S., Dellos-Nolan, S., Co, J. Y., et al. (2019). Mucin glycans attenuate the virulence of Pseudomonas aeruginosa in infection. *Nature Microbiology 4*,2146–2154.

Winstanley, C., & Hart, C.A. (2001). Type III secretion system and pathogenicity islands. Journal of Medical Microbiology, 50(2), 116-126.

Yates, J. L., Arfsten, A. E., & Nomura, M. (1980). In vitro expression of *Escherichia coli* ribosomal protein genes: Autogenous inhibition of translation. *Proceedings of the National Academy of Sciences*, *77*(4), 1837–1841.

Yu, L. C.-H., Wang, J.-T., Wei, S.-C., & Ni, Y.-H. (2012). Host-microbial interactions and regulation of intestinal epithelial barrier function: From physiology to pathology. *World Journal of Gastrointestinal Pathophysiology*, *3*(1), 27–43.

Yu, S., & Gao, N. (2015). Compartmentalizing Intestinal Epithelial Cell Toll-like Receptors for Immune Surveillance. *Cellular and Molecular Life Sciences : CMLS*, *72*(17), 3343–3353.

Yu, Y., Wang, X., & Fan, G.-C. (2018). Versatile effects of bacterium-released membrane vesicles on mammalian cells and infectious/inflammatory diseases. *Acta Pharmacologica Sinica*, *39*(4), 514–533.

Yuan, C., Burns, M. B., Subramanian, S., & Blekhman, R. (2018). Interaction between Host MicroRNAs and the Gut Microbiota in Colorectal Cancer. *MSystems*, *3*(3).

Zyrek, A. A., Cichon, C., Helms, S., Enders, C., Sonnenborn, U., & Schmidt, M. A. (2007). Molecular mechanisms underlying the probiotic effects of *Escherichia coli* Nissle 1917 involve ZO-2 and PKCzeta redistribution resulting in tight junction and epithelial barrier repair. *Cellular Microbiology*, *9*(3), 804–816.

8. Appendix

8.1 Additional information

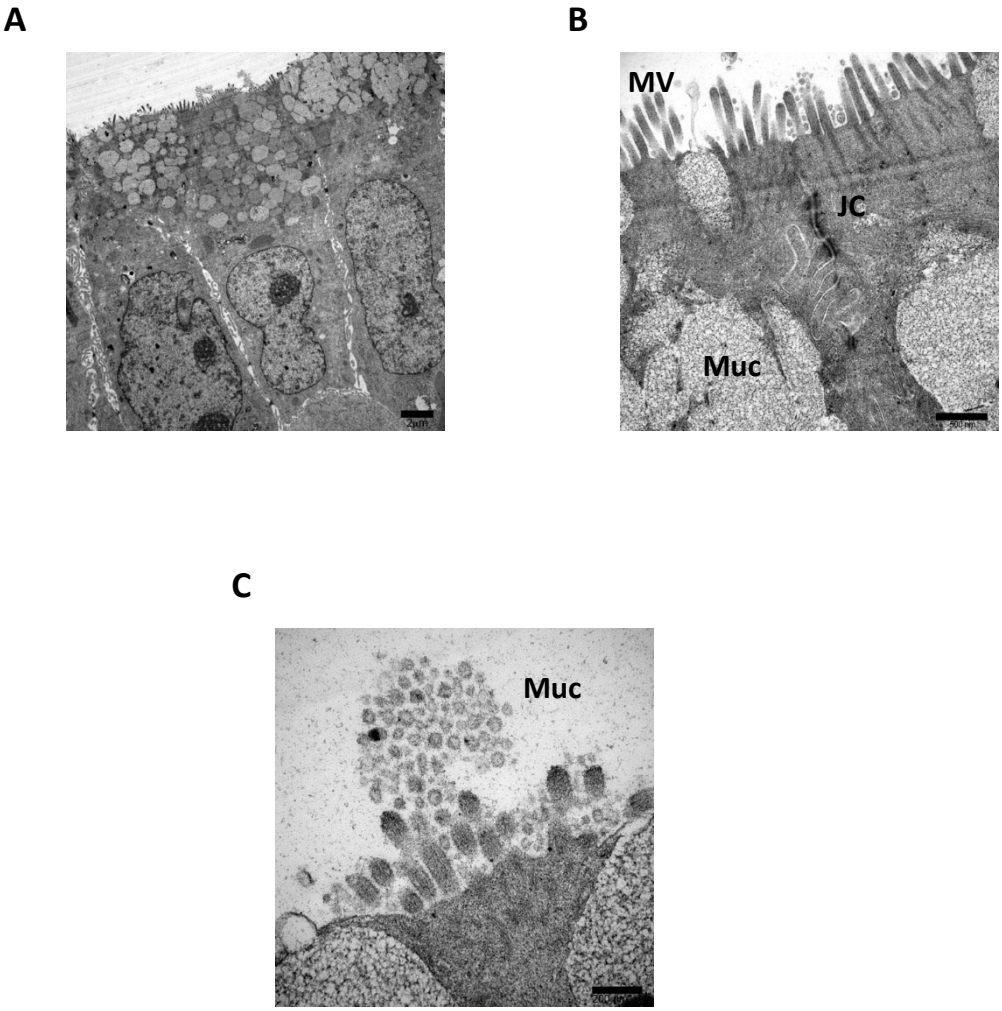

Figure 8.1.1. TEM of the physical features of HT29-MTX-E12 cells cultured in the 2.5D system (transwell filters). A) General view of the HT29-MTX-E12 cells. **B)** Cell to cell contact. There is a proper differentiation of the cells with microvilli formation, a complete tight junctional complex development, and the production of mucin. **C)** Secretion of mucin. JC: junctional complex, MV: microvilli, MUC: mucin. TEM pictures courtesy of Lilo Greune.

8.2 Scientific contribution

Oral presentations

Jessyca Gonzalez. (2020). The RWV bioreactor: a 3D cell culture model to characterize the molecular mechanisms of bacterial (probiotic *E. coli* Nissle 1917) and host interaction. 6th Joint Conference of DHGM & VAAM, Leipzig, Germany.

Poster presentations

Jessyca González, Rudolf von Bünau, Ulrich Dobrindt, Christoph Cichon. (2019). "*in vivtro"*: A 3D cell culture model to study the cellular impact of probiotic *E. coli* Nissle 1917 and Nissle variants on the host. 12th Seeon Conference. Seeon-Seebruck, Germany.

Jessyca González, Rudolf von Bünau, Ulrich Dobrindt, Christoph Cichon. (2019). "*in vivtro"*: A 3D cell culture model to study the cellular impact of probiotic *E. coli* Nissle 1917 and Nissle variants on the host. 3rd Münster Symposium on Infection Biology. Max Planck Institute for Molecular Biomedicine, Münster, Germany.

Jessyca González, Lisanne Pund, Haleluya Wami, M. Alexander Schmidt, Ulrich Dobrindt, Christoph Cichon. (2018). Getting closer to *in vivo*: a 3D cell culture model to study the molecular impact of probiotic *E. coli* Nissle 1917 on the host. 70. Jahrestagung der Deustchen Gesellschaft für Hygiene und Mikrobiologie (DGHM) e. V. Ruhr-Universität Bochum, Germany.

Jessyca González, Lisanne Pund, Haleluya Wami, M. Alexander Schmidt, Ulrich Dobrindt, Christoph Cichon. (2018). Getting closer to *in vivo*: a 3D cell culture model to study the molecular impact of probiotic *E. coli* Nissle 1917 on the host. 2nd Münster Symposium on Infection Biology, Münster, Germany.

Jessyca González, Haleluya Wami, M. Alexander Schmidt, Ulrich Dobrindt, Christoph Cichon. (2018). Getting closer to *in vivo*: A 3D cell culture model to study the molecular impact of probiotic *E. coli* Nissle 1917 and Nissle variants on the host. 11th Seeon Conference and Science Camp. Seeon-Seebruck, Germany.

8.3 Acknowledgements

Foremost, I would like to express immense and sincere gratitude to my advisor Dr. Christoph Cichon for his continuous support, patience, guidance and encouragement during my Ph.D. research. I thank him for giving me the opportunity to work under his research project and be part of it. I also thank him for being always available for discussions and for giving me the freedom to carry out my ideas.

Besides my advisor, I would like to thank my supervisors Prof. Dr. M. Alexander Schmidt and Prof. Dr. Petra Dersch, for their knowledge, insightful comments and suggestions during my studies helping me to complete this project.

My sincere thanks to my thesis committee members, Prof. Dr. Ulrich Dobrindt and Prof. Dr. Eva Liebau, for kind participation and useful discussions during my work.

I would like to thank Dr. Christian Rüter for his scientific suggestions and ideas and for helping me in the understanding of confocal microscopy. I am grateful to him.

I thank my labmates for the stimulating discussions, for the weekends we spent working together in the lab, for organizing their time to have lunch together to share with each other a bit of our free time. Many thanks to all the members of the Institute of Infectiology. Especially to Inga, Britta Lilo and Barbara for always encouraging me to talk to them in german. I appreciate the time they took to teach me and help me with the german language. I learned a lot from all of you. Thank you very much.

Thanks to Ardeypharm for financial support. Thanks to Dr. Rudolf von Bünau and Dr. Birgit Klinkert for the seminars we had during my Ph.D. These scientific meetings were very helpful and added considerably useful information to my research project.

Importantly, I want to thank my family, especially my mother and my grandma, for their unconditional support, for the long calls and advises through the phone and for cheering me up at any time. I want to thank my beloved husband José Arturo, for his braveness and effort to come with me to Germany, for accompanying me with so much love in every step and for inspiring me to give the best of me. I love you all so much.

I am grateful for the opportunity to come to Germany, I met wonderful people and I also learned incredible things about German culture.

8.4 Curriculum vitae

8.5 Eidesstattliche Erklärung

Vordruck für die Versicherung nach § 6 Abs. 3 (2)

Form for the oath pursuant to § 6 Abs. 3 (2)

Hiermit versichere ich, dass ich nicht wegen einer Straftat zu einer Strafe von mehr als einem Jahr Freiheitsentzug verurteilt worden bin, zu deren Begehung ich meine wissenschaftliche Qualifikation missbraucht habe.

I hereby declare that I have not been sentenced to more than one year imprisonment as a punishment for a crime for which I have abused my scientific qualifications.

Münster, 09.07.2020 Jessyca Gonzalez

(Unterschrift) (signature)

8.6 Eidesstattliche Erklärung

Vordruck für die Versicherungen nach § 6 Abs. 3, Nr. 5, 6, 9

Form for the oaths pursuant to § 6 Abs. 3, No. 5, 6, 9

Hiermit versichere ich, dass ich bisher noch keinen Promotionsversuch unternommen habe.

I hereby declare to not have tried to obtain a doctorate earlier.

Münster, 09.07.2020 Jessyca Gonzalez

(Unterschrift) (signature)

Hiermit versichere ich, dass ich die vorgelegte Dissertation selbst und ohne unerlaubte Hilfe angefertigt, alle in Anspruch genommenen Quellen und Hilfsmittel in der Dissertation angegeben habe und die Dissertation nicht bereits anderweitig als Prüfungsarbeit vorgelegen hat.

I hereby declare that I have produced the presented thesis by myself and without unpermitted help, that all sources and aids used are indicated, and that this dissertation has not been presented elsewhere as an examination paper.

Münster, 09.07.2020 Jessyca Gonzalez

(Unterschrift) (signature)

Hiermit erkläre ich mich mit der Zulassung von Zuhörerinnen/Zuhörern beim öffentlichen Teil der Disputation einverstanden. *

I hereby agree to admit an audience to the public part of my disputation.*

Münster, 09.07.2020 Jessyca Gonzalez

(Unterschrift) (signature)

* Auf begründeten schriftlichen Antrag der Kandidatin/des Kandidaten oder des Promotionskomitees an den Promotionsausschuss, kann die Öffentlichkeit von Vortrag und Diskussion ausgeschlossen werden. (§ 9 Abs. 8) * Upon substantiated claim that the candidate has addressed to the graduation committee the public can be excluded from the presentation and discussion. (§ 9 Abs. 8)